Control of NOx Emissions from Diesel Engines using Exhaust Gas Re-Circulation

A thesis submitted for the degree of Doctor of Philosophy

by

Roy William Horrocks

Department of Mechanical Engineering, Brunel University

March 2001

Abstract

The diesel engine currently accounts for 32 per cent of the new passenger car sales in Europe. In the US, diesel-power is responsible for 94 per cent of all freight movement. Comparing European Stage III standard petrol and diesel passenger car emissions, diesel NOx emissions are still considered a concern.

This thesis investigates the mechanisms by which oxides of nitrogen are formed during diesel combustion. It reviews the current methods of controlling NOx emissions, such as retarding fuel injection timing, exhaust gas re-circulation (EGR), water injection and exhaust after-treatment. Modelling using a phenomenological model, is used to demonstrate the extended Zeldovich mechanism and formation trends, the effects of EGR and the significance of the Zeldovich mechanism rate constants. Modified Zeldovich rate constants are proposed to improve the correlation to measured data. Clearly, EGR is currently the most effective method of reducing NOx emissions from passenger car diesel engines. The way EGR works in suppressing NOx formation is reviewed in detail.

Experimentation on a 1.8 litre inline 4-cylinder 4-valve per cylinder DI diesel with a variable nozzle turbine (VNT) turbocharger was used to demonstrate the concept of "additional" EGR on this small automotive engine. "Additional" EGR is the concept whereby a proportion of the EGR is added to the total charge, so that the volumetric efficiency increases as EGR is introduced. By using "additional" EGR, the benefits of lower NOx emissions combined with reduced particulates emissions and improved fuel consumption were clearly demonstrated at two test conditions. The reasons for achieving lower NOx emissions when using a VNT turbocharger and EGR have been explained.

Finally, several methods of calculating EGR proportion were used and compared against true mass flow. The use of a CO_2 balance was found to be the most accurate method.

In memory of my late father Frank Threapleton Horrocks

Acknowledgements

I would like to express my sincere gratitude to Professor Nicos Ladommatos and Dr Hua Zhao, without whose help and support throughout my period of study, this thesis would not have been possible.

I would like to thank Dr Suhair Abdelhalim for her help and guidance with the modelling and experimentation. Thanks are due to Mr Dionyssios Melas for his assistance with the engine testing and recording of results. I would also like to thank the Brunel Engine Laboratory staff, particularly Mr Andy Selway for his work on the engine installation and instrumentation.

I want to acknowledge those people at the Ford Dunton Engineering Centre who have helped me over the years, particularly Mr Peter Lawrence, now retired, who launched me on these studies and Mr Mike Watts who did so much to develop the Lynx Upgrade diesel engine.

I want to thank my friend Paul Davies for his advice and for proof reading some of the chapters.

I thank my family Candy, Vanessa and Frank, for their enthusiastic support and their tolerance in having to put up with papers and books around the house, and less of my time, over the past few years.

Finally, I acknowledge the financial support of the Ford Motor Company.

List of Contents

List of Figures

Chapter 1

Chapter 2

Chapter 6

Chapter 7

List of Tables

Chapter 6

Nomenclature

A	Frequency or pre-exponential factor (Arrhenius form equation)
E	Overall activation energy (J/mole [= 0.2388 cal/mole])
E_A	Activation energy (J/mole [= 0.2388 cal/mole])
EI	Emission index (g pollutants/kg fuel)
C_{mix}	Factor which depends on flow characteristics
c	Specific heat (kJ/kg K)
c_p	Specific heat at constant pressure(kJ/kg K)
c_v	Specific heat at constant volume(kJ/kg K)
k^+	Forward rate constant ($cm^3\ mol^{-1}\ s^{-1}$, $cm^6\ mol^{-2}\ s^{-1}$)
k^-	Reverse rate constant ($cm^3\ mol^{-1}\ s^{-1}$, $cm^6\ mol^{-2}\ s^{-1}$)
L	Latent heat of vaporization of a fuel (kJ/kg)
m	Mass flow rate (kg/s)
m_e	EGR mass flow rate to the engine at part load with EGR, at a given engine speed (kg/s)
m_c	Total inlet charge mass flow rate to the engine at part load with EGR, at the same speed (kg/s)
m_R	Mass of recycled exhaust gas (kg/s)
m_L	Mass air flow (kg/s)
M_{wt}	Molar mass
O_{2L}	Oxygen concentration of air
O_{2VZ}	Oxygen concentration before the cylinder
O_{2nZ}	Oxygen concentration after the cylinder
P	Pressure (Pa [=N/m^2])
Q	Heat of combustion per unit mass of fuel (kJ/Kg)
R^+, R^-	One-way reaction rates
R	Gas Constant (kJ/kmol K kJ/kmol K)
R_o	Universal Gas Constant, 8.3144 kJ/kmol K
S	Spray penetration (m)
SMD	Sauter mean diameter (μm)
St	Surface tension (N/m)

T	Temperature (K)
T_f	Stoichiometric adiabatic flame temperature (K)
T_o	Gas temperature far from a droplet (K)
V_{af}	free air volume flow rate to the engine at full load without EGR, at a given engine speed (m^3/s)
V_{ac}	free air volume flow rate to the engine at part load with EGR, at the same speed (m^3/s)
Y_{ox}^{o}	Ambient oxygen mass fraction
β	Exponent for temperature in Arrhenius type equation
ρ	Density (kg/m^3)
ν	Kinematic viscosity (m^2/s)

Subscripts

e	Equilibrium
EGR	Exhaust gas re-circulation
f	Fuel
fl	Flame
g	Gas (air)
i	Stoichiometric oxygen to fuel ratio (by mass)
ic	Intake charge
noz	Nozzle
ox	Oxygen

Abbreviations

AFR	Air/fuel ratio
API	American Petroleum Institute
ATDC	After top dead centre (degrees crank angle)
BSFC	Brake specific fuel consumption (g/kWh)
BTDC	Before top dead centre (degrees crank angle)
BMEP	Brake mean effective pressure (bar)
cal	Calorie
CO	Carbon monoxide
CO_2	Carbon dioxide
DI	Direct injection (diesel engine)
EGR	Exhaust gas re-circulation
EI	Emission index
EUDC	Extra urban drive cycle
exp	Exponential
H	Hydrogen
HC	Hydrocarbon
IDI	Indirect injection (diesel engine)
M	Molecule
N_2	Nitrogen (molecule)
NOx	Oxides of nitrogen (NO and NO_2)
NO	Nitric oxide
NO_2	Nitrogen dioxide
O_2	Oxygen (molecule)
Pm	Particulate matter
rpm	revolutions per minute
SEZM	Super-extended Zeldovich mechanism
SCR	Selective catalytic reduction
SNR	Selective non-catalytic reduction
SOI	Start of injection
T	Temperature (K)

TC	Turbocharged / turbocharger
TCI	Turbocharged and inter-cooled
VAG	Volkswagen Audi Group
VGT	Variable geometry turbocharger
VNT	Variable nozzle turbine/turbocharger

Conversions

Pressure	1 Pa (N/m^2) = 10^{-5} bar	1 bar = 10^5 Pa = 100 kPa
	1 Pa = 9.869×10^{-6} atm	1 atm = 101.325 kPa
Energy	1 J = 0.2388 cal	1 cal = 4.1868 J
Power	1 kW = 1.3596 PS	1 PS = 0.7355 kW

Chapter 1

Introduction

The diesel engine is now a true alternative power unit for European passenger cars, from the small fuel-efficient "sub-B cars" such as the VW Lupo with its 1.2 or 1.4 litre 3-cylinder diesel, to large luxury cars like the Mercedes Benz E Class with a 184kW, 4 litre V8 diesel. In the mid-sized family car segment, typified by the Ford Mondeo, the diesel share throughout Europe is 41 per cent. The overall market share of diesel passenger cars in Europe is 32 per cent; in France it is a staggering 48 per cent (Perez, 2000). The total share of diesel-powered cars sold by Volkswagen in Europe is 39.6 per cent (Anon 2000). During the first half of 2000, BMW stepped up its production of diesel engines by an impressive 53.8 per cent (Anon 2000). This increase in diesel proportion is due in part to the improvements in power and torque densities over the past 8 years, seeing specific power reaching 53kW/litre for modern high speed direct injection (DI) diesel engines. In addition, the recent achievements in refinement, with new sophisticated fuel injection systems reducing combustion noise, are giving gasoline-like in-vehicle noise and vibration levels. This is demonstrated by the premium luxury manufacturers, the likes of Audi, BMW and Mercedes Benz offering V8 diesel engines for their top of the range models.

In the US, diesel-powered trucks, trains and boats are at the core of the supply and distribution network, moving 94 per cent of all freight in the US. Each day diesel-powered equipment moves 18 million tons of freight. The inherent benefits of diesel technology – efficiency, durability and safety – have led to diesel's emergence in meeting future energy and environmental goals. However, there are challenges for the automotive and diesel industries. In December, the US EPA announced future diesel-engine emissions regulations for heavy-duty trucks and buses and plans for cleaner diesel fuel requirements that are unprecedented. The agency claims that heavy-duty vehicles will run more than 90 per cent cleaner than today's vehicles when the new rules take effect. The clean diesel engine is clearly a viable technology for the future with the

addition of cleaner fuels and exhaust treatment systems (Jost, 2001).

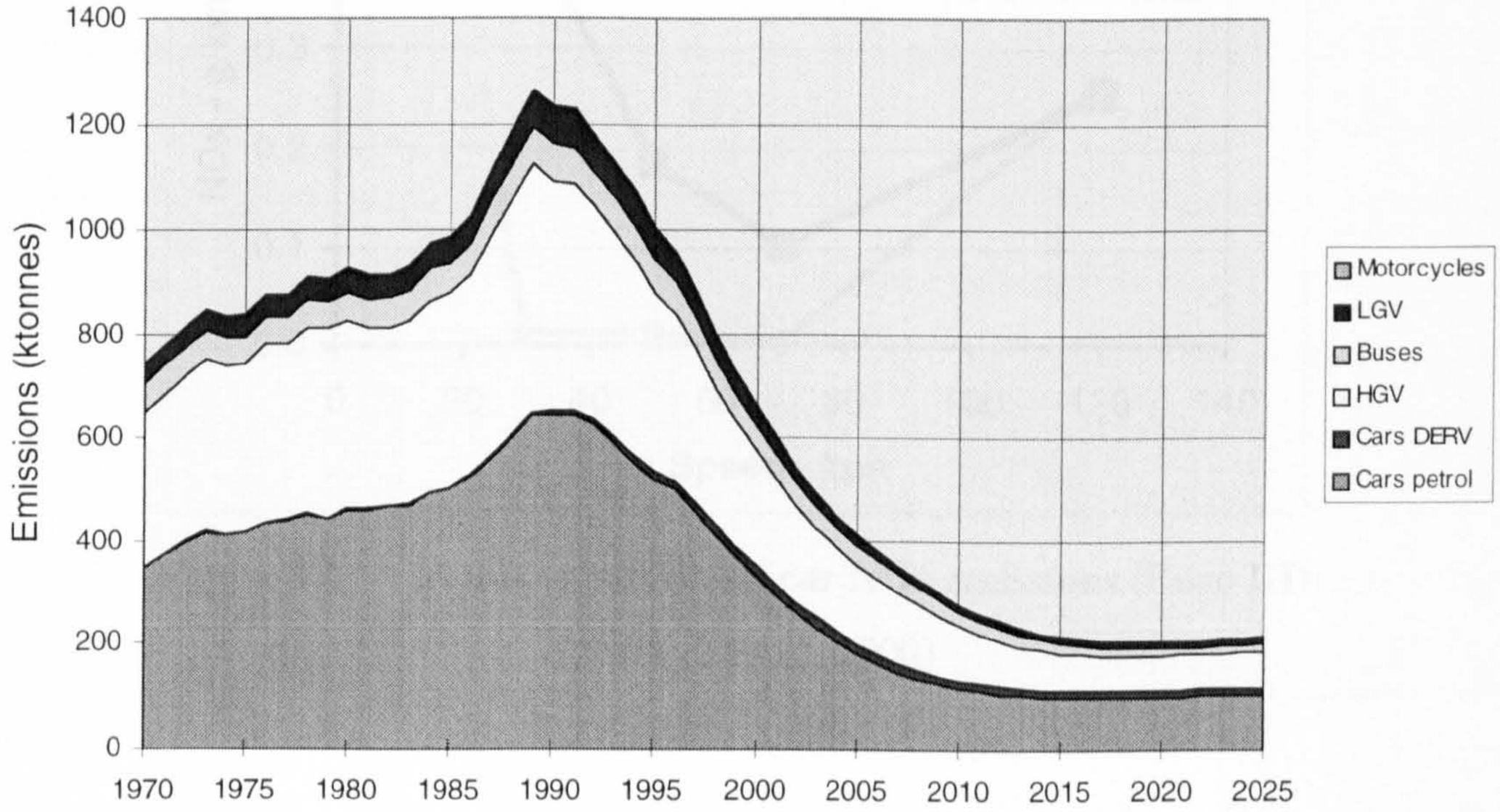

Figure 1.1 UK road transport NOx emissions (Dunne and Frost, 2000)

All internal combustion engines emit pollutants; carbon monoxide (CO), hydrocarbons (HC), oxides of nitrogen (NOx) and small particulate matter (Pm) in the exhaust gas. **Figure 1.1** shows a plot of UK road transport NOx emissions from 1970 and projected to 2025. The effect of EU regulations is dramatic, but still more is necessary (Dunne and Frost, 2000). Compared to gasoline engines with three-way catalysts, diesel engines with oxidation catalysts emit less than a third the level of CO and HC, but around three times the NOx and ten to twenty times the particulate matter. **Figure 1.2** shows a comparison of European Stage III standard petrol and diesel car NOx emissions under steady driving conditions at speeds between 25 and 120 km/h. Nevertheless, diesel cars with particulate filters can match petrol on all emissions except NOx, and are much better on CO_2. Therefore, NOx emissions from diesel cars are still considered a concern. (Dunne and Frost, 2000).

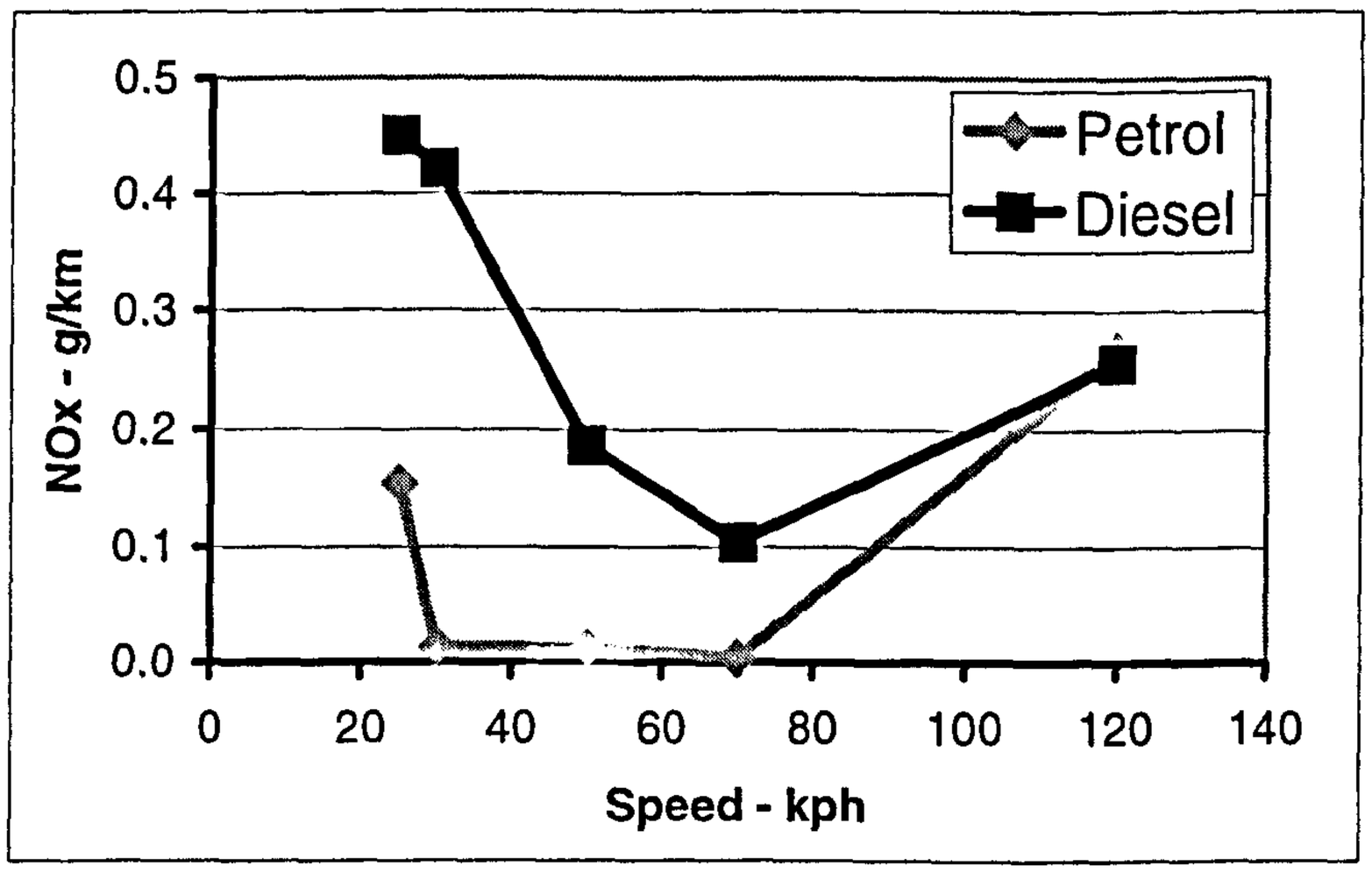

Figure 1.2 Petrol versus diesel car NOx emissions (Euro III)

(Dunne & Frost, 2000)

The oxides of nitrogen (NOx) comprise several gases including nitric oxide (NO) and nitrogen dioxide (NO_2). Nitrogen dioxide is produced both directly as a primary and indirectly as a secondary pollutant owing to spontaneous conversion of NO to NO_2 in the presence of ozone or oxygen. In the ambient air, NO_2 is probably the most important for human health, being an irritant of the airways. Secondly, NOx is involved in the formation of photochemical ozone, which results from sunlight-initiated oxidation of volatile organic compounds (VOCs) in the presence of NO and NO_2. Ozone is a highly reactive oxidising agent and is the most irritant of the common air pollutants and exposure to concentrations commonly encountered in the UK has been shown to produce inflammation of the respiratory tract. Thirdly, oxides of nitrogen and sulphur dioxide (SO_2) are the main precursors of acid deposition. In the atmosphere, NOx and SO_2 react with oxidants to form nitric and sulphuric acids during their dispersal from sources. These oxidants (OH radical, ozone and hydrogen peroxide) are formed by photochemical reactions involving NOx and VOCs (Handbook on Air Pollution and Health, 1997, Fourth Report of the Photochemical Oxidants Review Group, 1997, Third Report of the United Kingdom Review Group on Acid Rain, 1990).

The automotive industry is taking the lead in developing technologies to reduce atmospheric pollution from internal combustion engines. Continuing concern about atmospheric pollution, particularly air quality in urban areas, and the "Greenhouse"

effect, is driving more stringent emissions legislation for motor vehicles throughout the world. The lead in legislation is being taken by the EC in Europe, by California in the USA and by Japan particularly for city areas. However, the underlying priorities appear to be slightly different between Europe and the USA, as is the method of introducing new technologies. In Europe, while air quality is obviously of prime importance, "Greenhouse" gases are considered an important secondary factor and there is strong debate about carbon dioxide (CO_2) control. Moreover, the European Commission (CEC) recognises the importance of light-duty diesels for their low fuel consumption and CO_2 emissions. New technologies enabling future standards to be met are encouraged by fiscal incentives in the form of tax concessions for the owner. In the USA there appears more emphasis on ozone-forming gases and atmospheric smog aspects of air quality. Introduction of lower limits, forcing technology, is legislated by phase-in schedules for the manufacturers. The Federal Environmental Protection Agency (EPA) and Californian Air Resources Board (CARB) publish future standards and phase-in schedules much earlier, than in Europe by the EC.

To assist the European Commission in finding cost effective solutions to air quality issues relating to automotive fuels and vehicles, a tripartite initiative on air quality, emissions, fuels and engine technologies was set up. This included an "Auto/Oil" research programme known as the European Programme on Emissions, Fuels and Engine Technologies (EPEFE), run by the two industry associations ACEA (Association des Constructeurs Europeans d`Automobiles) and EUROPIA (European Petroleum Industry Association). The EPEFE programme conducted emission tests on combinations of advanced engines and fuels, to provide data to see what contributions future technology, in both engine and fuel, may bring to any required improvements in air quality.

In total, EPEFE examined 12 test gasoline with 16 gasoline powered vehicles and 11 diesel fuels in 19 light-duty vehicles and 5 heavy-duty engines. More than 2000 emission tests were run and over 0.5 million data points were generated. The EPEFE element of the European Auto Oil Programme and its preliminary report has been completed. The executive summary was issued to Member States during July 1995. The Auto Oil study has achieved the following:

- Replacement of 'Best Available Technology" by the "Cost Effectiveness" concept in new European law making.
- Avoidance of a simultaneous incentivisation of both 1996 and 2000 emission levels.
- Recognition by legislators that fuel specification is a factor influencing air quality.

The EPEFE diesel results were unfortunately fairly inconclusive, however, it was possible to conclude that a future diesel fuel having lower sulphur, density, T95 and poly-aromatics and higher cetane would be generally beneficial to diesel vehicle emissions. The programme did however establish a valuable precedent for future co-operation between the motor industry and both the oil industry and legislators.

The current European Union exhaust emission standard, known as Stage III, was introduced in January 2000 following analysis of the EPEFE results. It became mandatory for all new vehicles on 1st January 2001. The test cycle changed for this standard whereby the 40-second idling period before sampling was deleted. The next phase of legislation, Stage IV is scheduled for 2005. These standards for diesel passenger cars are shown in **Table 1.1** below, (Fraser 2001).

Table 1.1

Tailpipe Emission Standards (g/km) for Diesel Passenger Cars

Standard	Date	CO	NOx	HC+NOx	Pm
Stage II	1996	1.0	-	0.7/0.9 *	0.08/0.1 *
Stage III	2000	0.64	0.5	0.56	0.05
Stage IV	2005	0.5	0.25	0.3	0.025

* IDI/DI

From a diesel prospective the Federal Tier II standards due for model year 2004 represent a severe challenge. Not only does the durability period double from 50,000 to 100,000 miles, but the current diesel NOx waiver comes to an end and the NOx is reduced from 1.0 g/mile (0.62 g/km) to 0.2 g/mile (0.12 g/km), which at present, without NOx after-treatment technology, is a formidable task. Additionally, the

particulates standard is also reduced from 0.2 to 0.08 g/mile (0.12 to 0.05 g/km).

A further series of changes to the European Light Duty Emissions legislation is forecast for mandatory application from 2008, which will be more stringent than the Stage IV standards that will become mandatory in 2005. Particulate standards are anticipated to change at 2008, to a level that will effectively mean the fitment of a particulate filter. Followed by further severe reductions in gaseous emissions at 2010. A further NOx reduction for diesels to achieve parity with gasoline post 2010 is anticipated. Forecast diesel fuelled vehicle "Stage V" standards are shown in **Table 1.2** below, (C Hosier 2000).

Table 1.2

Forecast European Emissions Standards (g/km) for Diesel Fuelled Light-Duty Vehicles

Standard	Date	CO	NOx	HC+NOx	Pm
Stage IV	2005	0.5	0.25	0.30	0.025
Stage V phase 1	2008	0.5	0.25	0.30	0.010
Stage V phase 2	2010	0.5	0.12	0.15	0.010
Stage V phase 3	2012	0.5	0.06	0.09	0.010

The major emphasis for diesel engine emissions reduction therefore remains focused on particulates and NOx, but with lower diesel CO standards being proposed, for high speed DI engines CO now becomes a task that cannot be ignored. While the diesel industry has technology and is actively working on reduction of particulates, by further optimisation of the combustion system with even higher pressure fuel injection systems, variable geometry turbochargers and multi-valve, centralized injection nozzles, there is not the same level of hardware to address NOx emissions from combustion in the engine. There is however, a tremendous effort being put on the development of lean NOx catalysts by the automotive and catalyst industries.

Heavy-duty engine manufacturers are now considering exhaust gas re-circulation (EGR) as a means to reduce NOx for the next regulated level. Stage 4 in Europe reduces the

NOx standard to 3.5 g/kWh at 2005, and for 2008 there is a further reduction to 2.0g/kWh. In the US a level of 2.0g/hph (2.7g/kWh) will become effective in October 2002. There has historically been a reluctance to follow light-duty practice in the use of EGR because of the adverse effect on long-term durability, but the low level of the new standards means that the use of EGR is the only viable option to further reduce NOx without further worsening of fuel consumption.

Nitric oxide (NO) formation is dependant primarily upon local oxygen atom concentration and temperature. In a diesel engine NO is formed during the combustion process owing to the relatively high oxygen concentration and high temperatures. Control of NOx emissions from diesel engines is fundamentally difficult for a number of reasons, principally;

1. The high thermal efficiency of diesel cycle is synonymous with high peak temperatures.
2. The NOx-particulate trade-off; whereby suppression of NO formation has the tendency to cause an increase in particulates.
3. Excess oxygen in exhaust prevents the use of gasoline "stoichiometric three-way catalyst" technology for reduction of NOx.

This thesis focuses on the control of NOx emissions from diesel engines, principally by exhaust gas re-circulation (EGR). Brief reviews of in-cylinder NOx formation and ways to suppress formation and reduce the engine-out emissions are covered. Exhaust gas after-treatment for catalysis of NOx is also summarized in the literature survey. The work contained in this thesis demonstrates "additional" EGR and provides an insight and explanation of why lower NOx and particulate emissions can be achieved with a variable geometry turbine turbocharger.

Chapter 2

Literature Survey

2.1 NOx Formation

2.1.1 Introduction

Nitrogen oxides, nitric oxide (NO) and nitrogen dioxide (NO_2), are formed during the combustion of oil by two mechanisms; high temperature thermal fixation of molecular oxygen and nitrogen present in the combustion air and secondly, reaction of atmospheric oxygen with nitrogen containing compounds in the fuel. Both mechanisms result primarily in NO because the residence time in an internal combustion engine is too short for oxidation of NO to NO_2, even though NO_2 is thermodynamically favoured at lower temperatures. NO does, however, oxidize in the atmosphere to NO_2, which is a primary participant in photochemical smog, (Pershing and Berkau, 1973). NO and NO_2 are usually grouped together and referred to as NOx emissions.

It has generally been assumed that the thermal fixation of NO occurred according to the mechanism proposed by Zeldovich (1946).

$$O + N_2 \Leftrightarrow NO + N \qquad 2.1$$

$$N + O_2 \Leftrightarrow NO + O \qquad 2.2$$

Lavoie et al (1970) added the third reaction to the mechanism, which is often called the extended Zeldovich mechanism.

$$N + OH \Leftrightarrow NO + H \qquad 2.3$$

Analysis of the NO formation rate shows an extremely strong dependence on temperature. This strong dependence is due to the high activation energy of the forward rate constant for equation 2.1 and to the effect of temperature on the O_2 dissociation and, hence, O atom concentration. The initial NO formation rate is given by Bowman

as;

$$\frac{d[NO]}{dt} = \frac{6x10^{16}}{T^{1/2}} \exp\left\{\frac{169{,}090}{T}\right\}[O_2]_e^{1/2}[N_2]_e \qquad 2.4$$

2.1.2 Chemical Reaction Rates

Chemical processes in engines are often not in equilibrium, such as the flame reaction zone and pollutant formation mechanisms. Such non-equilibrium processes are controlled by the rates of the chemical reactions that convert reactants to products (Heywood, 1988). The rates at which chemical reactions proceed depend on the concentration of the reactants, temperature and whether any catalyst is present. This field is called chemical kinetics (Glassman, 1977).

Most of the chemical reactions of interest in combustion are binary reactions, where two reactant molecules, M_a and M_b, with capability of reacting together, collide and form two product molecules, M_c and M_d.

$$M_a + M_b = M_c + M_d \qquad 2.5$$

An example of this binary reaction is the rate-controlling step in the process by which the pollutant NO forms, in equation 2.1 above.

This is a second-order reaction since the stoichiometric coefficients of the reaction ν_a and ν_b are each unity and sum to 2.

Third-order reactions are important in combustion, for example the recombination reactions by which radical species such as H, O and OH combine during the final stage of the fuel oxidation process. For example,

$$H + H + M = H_2 + M^* \qquad 2.6$$

where M is any molecule (such as N_2) which takes part in the collision and carries away the excess energy.

In chemical reactions such as 2.1 above, the rate at which product species are produced and the rate at which reactant species are removed is controlled by concentrations of reactant species M_a and M_b. Thus, for reaction 2.1 above, the reaction rate R^+ in the forward (+) direction, reactions to products, is given by

$$R^+ = k^+[M_a][M_b] \qquad 2.7$$

If the reaction can also proceed in the (-) direction, then the backward rate R^- is given by

$$R^- = k^-[M_c][M_d] \qquad 2.8$$

k^+ and k^- are the rate constants in the forward and reverse directions for this reaction.

The rate constants k, usually follow the Arrhenius form;

$$k = A\exp\left(-\frac{E_A}{RT}\right) \qquad 2.9$$

where A is called the frequency or pre-exponential factor and may be a (moderate) function of temperature; E_A is the activation energy and R and T are the gas constant and thermodynamic temperature, respectively. The Boltzmann factor $\exp(-E_A/RT)$ defines the fraction of all collisions that have an energy greater than E_A . That is, sufficient energy to make the reaction take place. The functional dependence of k on T and the constants in the Arrhenius form, are determined experimentally.

The chemical reaction mechanisms of importance in combustion are much more complex than the above illustrations of rate-controlled processes. Such mechanisms usually involve both parallel and sequential interdependent reactions. The methodology reviewed above still holds; however, one must sum algebraically the forward and reverse rates of all the reactions that produce (or remove) a species of interest. In such complex mechanisms it is often useful to assume that (some of) the reactive intermediate species or radicals are in steady state. That is, these radicals react so quickly once they are formed that their concentrations do not rise but are maintained in steady state with the species with which they react. It follows that the net rate at which

their concentration changes with time is set equal to zero (Heywood, 1988).

2.1.3 Formation of NO in Diesel Engines

Since the overall rate of NO formation by the thermal mechanism generally is slow compared to the fuel oxidation reactions, it is often assumed, following the suggestion of Zeldovich, that the thermal NO formation reactions can be decoupled from the fuel oxidation process, (Miller and Bowman, 1989). The process of NO formation under conditions prevailing in internal combustion engines, based on previous studies, will be governed primarily by the following reactions (Lavoie, Heywood and Keck, 1970):

$$N + NO \Leftrightarrow N_2 + O + 75.0 \qquad k_1 = 2 \times 10^{-11} \qquad 2.10$$

$$N + O_2 \Leftrightarrow NO + O + 31.8 \qquad k_2 = 2 \times 10^{-11}\, e^{-7.1/RT} \qquad 2.11$$

$$N + OH \Leftrightarrow NO + H + 39.4 \qquad k_3 = 7 \times 10^{-11} \qquad 2.12$$

$$H + N_2O \Leftrightarrow N_2 + OH + 62.4 \qquad k_4 = 5 \times 10^{-11}\, e^{-10.8/RT} \qquad 2.13$$

$$O + N_2O \Leftrightarrow N_2 + O_2 + 79.2 \qquad k_5 = 6 \times 10^{-11}\, e^{-24.0/RT} \qquad 2.14$$

$$O + N_2O \Leftrightarrow NO + NO + 36.4 \qquad k_6 = 8 \times 10^{-11}\, e^{-24.0/RT} \qquad 2.15$$

where the exothermicities of the reactions (75 in the first reaction, etc) are in kcal, the exothermic rate constants k_i, are given in cm^3 per sec and the activation energies are given in kcal. The rate constants are taken from Scofield (1967) for reactions 2.10, 2.11, 2.13, 2.14 and 2.15, and from Campbell (1968) for reaction 3. Lavoie et al, did not consider the very slow reaction $2NO \Leftrightarrow N_2 + O_2$.

The Zeldovich mechanism for NO formation (Zeldovich and Raizer, 1966), shows that the rate of NO formation rises exponentially with temperature:

$$\frac{d(NO)}{dt} \approx \exp\left(-E/RT\right) \qquad \text{E/R = 123,000 deg R} \qquad 2.16$$

where the activation energy, E, is derived from the activation energy of the controlling reaction, $O + N_2 \rightarrow NO + N$, and the O_2 dissociation energy. This illustrates that the NO formation process is extremely sensitive to the local flame temperature.

Some researchers have proposed that the formation and destruction of NO in diesel engines occurs via the so-called "N_2O mechanism" (Maite and Pratt, 1974; Polifke et al, 1995 and Mellor et al, 1998). This is reviewed in Chapter 4.

Flame Temperature

The flame temperature, at the flame front where most of the NO is most likely to be formed, can be written [Williams (1965)]:

$$T_{fl} \cong \left(1 - \frac{Y^o_{ox}}{i}\right)\left[\left(\frac{Q-L}{iC_p}\right)Y^o_{ox} + T_o\right] \qquad 2.17$$

where,

C_p = specific heat (at constant pressure) of the gas

Q = heat of combustion per unit mass of fuel

L = latent heat of vaporization of the fuel,

Y^o_{ox} = ambient oxygen mass fraction

i = stoichiometric oxygen to fuel ratio (by mass)

T_o = gas temperature far from a droplet.

C_p, Y^o_{ox} and T_o will depend on the proportion of EGR.

The importance of oxygen mass fraction, intake air temperature and specific heat capacity, on flame temperature, and hence NO formation, can be seen from the above equation. The flame temperature being proportional to oxygen mass fraction and intake air temperature; and inversely proportional to specific heat. All of these parameters will be influenced by EGR. Addition of EGR will reduce flame temperature and hence NO

formation, (see later section on Effect of EGR).

Sawyer et al (1973) argued that nitrogen oxide is mainly formed in stoichiometric regions of mixture in gas turbine type combustors; therefore NOx emissions should correlate with stoichiometric adiabatic flame temperature. They plotted ln (EINOx) versus $1/T_f$ and obtained an apparent activation energy of 136,000 cal/mole. This value is close to that given by the extended Zeldovich mechanism, for the case where the NO decomposition reactions are omitted for steady-flow combustors, which yields 134 630 cal/mole (Plee et al 1981).

Plee et al (1981), experimented with an IDI diesel to examine the effects of flame temperature and chemical kinetics, without significantly affecting the air-fuel mixing process, by adding various quantities of O_2 and N_2 to the intake charge. The effect of increasing the oxygen concentration in the intake air was to rapidly increase the NOx emissions, at the three speeds tested. Various combustion chambers tested also showed similar trends.

Plee et al also argued that the majority of the NO production in diesels is expected to occur near the stoichiometric reaction zone, since only in these regions will the temperature be sufficiently high. The authors plotted the NOx emission index (EINOx) versus the inverse of the stoichiometric flame temperature ($1/T_f$), at constant fuelling. The linear correlation of ln(EINOx) with $1/T_f$ indicated that the effect of O_2 or N_2 addition on NOx is a flame temperature effect, which could be correlated with a simple Arrhenius expression, which gave an overall activation energy of -76 858 cal/mole (E/R = -38 700). The apparent activation energy obtained by these authors, was considerably lower than that derived for steady-flow combustors, but larger than that predicted by NO equilibrium. Plee et al, put forward several reasons for the difference in apparent activation energy between steady flow combustors and their diesel correlation;

1. The O-atom is not in equilibrium
2. The computed flame temperature is not representative of the actual process.
3. NO decomposition is important.

Ahmad and Plee (1983) examined the influence of flame temperature on NOx, particulate and hydrocarbon emissions from a single cylinder light-duty DI diesel

engine. The results indicated that for all loads and speeds tested, oxygen enrichment of the intake air increased NOx emissions, while it decreased gas-phase hydrocarbon, particulate carbon and volatile emissions and reduced ignition delay. Opposite emission trends were observed with addition of N_2 and EGR, both of which deplete the intake oxygen concentration. The effect of intake air composition on emissions was correlated with diffusion flame temperature. The authors selected the stoichiometric adiabatic flame temperature evaluated at TDC conditions to represent this characteristic temperature for the IDI, whilst for the DI the temperature at TDC conditions and at peak cylinder pressure were evaluated. The results agree with the expectation that an increase in diffusion flame temperature will increase the rate of NOx formation, as well as the rates of particulate and hydrocarbon oxidation, giving the characteristic NOx/particulates trade-off, whereby NOx increases and particulates and HC decrease with T_f.

Pundir et al (1985) attempted to relate NO emissions with a charge description that could probably exist in the combustion chamber of a liquid-fuelled SI engine. They make the point that during combustion of a homogeneous charge, elements burning early in the cycle attain the highest temperature and also have the largest residence time. Consequently, those burning first contribute most to NO emissions. In the case of a non-homogeneous charge, however, if the elements burning first are fuel rich, although these will attain relatively high temperature after combustion owing to a lack of oxygen, their contribution to NO emissions may not be very high. On the other hand, if elements burning first are slightly leaner than stoichiometric, their temperatures after burning will be relatively low, but due to availability of oxygen, their contribution to NO emissions could be large. The elements contributing most to NO emissions will depend on the mixture strength distribution in the combustion chamber and the instant at which these burn in the cycle. Also, an element that burns at a given instant in successive cycles, would make a varying contribution to NO emission in different cycles as its mixture strength will be different from one cycle to another. The authors studied these two effects of non-homogeneity of the charge on NO emissions by means of a combustion model and kinetic calculations of NO formation.

Oxygen concentration

The Zeldovich reaction mechanism postulates that NO formation only starts if atomic

oxygen is available. Only the oxygen atom is able to split up the strongly bound N_2 molecule at temperatures below 3000K. The thermal decomposition of N_2 to N begins at temperatures considerably above 3000K. The source of O is a two-step thermal dissociation. The dissociation of CO_2 to O_2 and CO and of H_2O to O_2 and H_2 in the first step is called primary dissociation. The dissociation of O_2 to O is the second step. The dissociation equilibrium moves to higher O concentrations at higher temperatures leading to more NO formation. An increase in the combustion products CO_2 and H_2O leads to an increase in dissociation products and therefore to higher NO formation, (Ropke et al 1995).

Ropke et al (1995) studied the effect of oxygen concentration on NOx emissions from a 1.9 litre DI diesel engine. The O_2 concentration was changed from 21 to 12 per cent by adding up to 9 per cent N_2. The side effects of the additional N_2 were considered negligible. The NOx concentration was found to decrease exponentially as the O_2 level was reduced from 21 to 12 per cent.

Iida and Sato (1988) found that nitrogen oxides increased exponentially with increasing oxygen concentration when they experimented with a single cylinder high-speed direct injection diesel engine with variations in the intake oxygen concentration, ranging from 21 to 25 per cent (by volume). Stoichiometric flame temperature was calculated utilizing the computer program developed by Olikara and Borman (1975) with initial conditions evaluated at top dead centre. Calculated stoichiometric adiabatic flame temperature estimated at top dead centre increases with oxygen concentration. Iida and Sato claimed that the linear correlation of the NOx emission index (EINOx), ln(EINOx) with the inverse of the stoichiometric flame temperature indicates that the effect of oxygen addition on NOx is a flame temperature effect, rather than a result of changes in oxygen concentration, although why this should be so is not self evident. This argument emphasises the thermal rather than chemical effect and hence the importance of local temperature on NOx formation. The correlation with stoichiometric flame temperature yielded an overall activation energy of -143,000 cal/mole for the processes.

A number of experimenters (Sawyer et al 1973, Plee et al 1981, Ahmad and Plee 1983, Iida and Sato 1988) correlated the NOx emissions index with the inverse of stoichiometric flame temperature using an equation of the Arrhenius form, similar to the

following expression;

$$EI = C_{mix} \exp (E/RT_f) \qquad 2.18$$

where

EI = emission index (g pollutants/kg fuel)

C_{mix} = factor which depends on flow characteristics

E = overall activation energy (cal/mole)

R = universal gas constant (cal/mole-K)

T_f = stoichiometric adiabatic flame temperature (K)

By plotting ln(EINOx) versus $1/T_f$, a linear characteristic can be demonstrated, giving a slope of E/R, from which the overall activation energy can be determined. **Table 2.1** lists the data from these references.

See also Section **2.3 NOx Reduction by EGR**, for further information on effect of oxygen concentration on the formation of NO.

Table 2.1

Overall activation energy derived from flame temperature correlation

Reference	Engine Type	Overall Activation Energy (note 1) cal/mole (note 2)
Sawyer et al, 1973	steady-flow combustor	-136 000
Plee et al, 1981	IDI	-152 486
Ahmad et al, 1982	0.52 L single cylinder IDI	-144 606
Ahmad et al, 1982	0.72 L single cylinder IDI	-144 606
Ahmad and Plee, 1983	0.52 L single cylinder DI	-139 090 (note 3)
Iida and Sato, 1988	1.11 L single cylinder DI	-143 000

Note 1: E in equation 1.18

Note 2: 1 cal/mole = 4.187 J/mole

Note 3: based on temperature at peak cylinder pressure

Engine design and operating parameters

Wilson, Muir and Pellicciotti took exhaust measurements of NO, soot and HC from a 2340 cc single cylinder diesel engine. Direct injection and pre-chamber configurations were assessed, as well as changes to compression ratio, swirl, thermodynamic state of the intake charge and fuel injection parameters. The main trends were:

- the pre-chamber gave lower NOx with higher fuel consumption
- increased volume ratio with pre-chamber engine gave increased NOx but reduced soot (note that volume ratios used here were 15 to 35 %, whereas modern light-duty automotive diesels with Ricardo type swirl chambers are typically 50%)
- as compression ratio was increased, NOx increased.

On the effect of load, they found that NOx peaked at an equivalence ratio of 0.3 for both DI and IDI. The characteristic reduction in NOx by injection retard for DI was evident, for example, 10 degrees giving approximately 50 per cent reduction in NOx, this was most pronounced at high loads. With the IDI a minimum NOx emission occurred at 4 deg BTDC, this was reviewed with other data and found to be peculiar to their test engine. The effect of engine speed for the DI engine was to reduce NOx with increasing speed. The pre-chamber NOx emissions behaved in the opposite way, increasing with engine speed.

Plee et al (1981), found that for the IDI engine they tested, any modification to the mixing process that lowered NOx also increased CO, and the addition of O_2 or N_2 shifted the trade-off, as it did for the NOx - particulate trade-off.

Ahmad and Plee (1983) found that for NOx emissions, the flame temperature dependence was not affected by engine type since NOx formation always occurs in the flame zone and any effects of mixing are secondary. The authors concluded that the overall activation energy for NOx from the DI engine was nearly the same as for the IDI engines, indicating that the NOx kinetics are insensitive to the combustion chamber geometry.

Duggal, Priede and Khan (1978) used a fast acting water-cooled gas-sampling valve located in the swirl chamber of a single cylinder indirect injection diesel engine. The

sampling valve could transverse horizontally across the chamber on the centre line, moving from the outer wall, downstream of the injector, to the centre. Fuel was injected through a single hole nozzle. The NO concentration profiles showed two peaks separated by a period of swirl revolution. The first peak rose rapidly following ignition, to reach a peak in 3 milliseconds and then fell gradually. The second peak was found to be considerably higher than the first. This, the authors attributed to increased air entrainment within the reaction zone, which increased the NO formed.

Aoyagi et al (1980) conducted in-cylinder gas sampling in a DI engine with measurements of local equivalence ratio and flame temperature. NO formed in the early and middle combustion periods where flame temperature and pressure were high. Temporal and spacial distributions of NO concentration became maximum when the local equivalence ratio decreased to 1.0 after which the concentration decayed over the next 30 to 50 degrees crank angle to the "frozen" exhaust level of between 1/3 to 2/3 the peak level.

2.1.4 Extended Zeldovitch Mechanism Rate Constants

Heywood (1988) explained in detail the solution of the extended Zeldovich mechanism (equations 2.1 to 2.3, Section 2.1.1). Knowledge of the rate constants is necessary for the estimation of the production rate of NO through this mechanism. **Table 2.2** lists the data required for the calculation of the rate constants for the forward reactions, while **Table 2.3** gives the corresponding data for the reverse reactions in the mechanism. Each rate constant can be calculated from the following equation:

$$k = AT^{\beta}\exp(-E/RT) \qquad 2.19$$

where the value of A,β and E/R are given in the Tables and T is in Kelvin.

Baulch, Drysdale and Horne, of the Department for Physical Chemistry, University of Leeds, published "Evaluated Kinetic Data for High Temperature Reactions" in 1973. The UK Government Department of Education and Science supported this work. This work provides a comprehensive tabulation of reaction rate data, which is critically analysed and recommends reliable values for the rate parameters. Volume 2 covers

homogeneous gas phase reactions of the H_2-N_2-O_2 system. Hanson and Salimian's Survey of Rate Constants in the N/H/O System, in Combustion Chemistry, edited by Gardiner (1984) is another, more recent, widely used reference in this field.

Rate constants for the extended Zeldovich mechanism have been determined experimentally, or calculated by a number of researchers. These are listed in **Table 2.2** for the forward reactions and in **Table 2.3** for the reverse reactions. So far as the author is aware, a comprehensive list of the rate constants, with more recent references, has not appeared in the open literature previously. Graphs of these rate constants are plotted in **Figures 2.1 to 2.6** in the form log k versus $10^4\ T^{-1}$.

Table 2.2

Extended Zeldovich mechanism rate constants

Reference	Reaction	A	β	E/R	Temperature Range
Baulch et al, 1969	$O+N_2 \rightarrow N+NO$	1.36×10^{14}	0	38 000	
Baulch et al, 1973	$O+N_2 \rightarrow N+NO$	7.59×10^{13}	0	38 000	2000 - 4000
Harris et al, 1976	$O+N_2 \rightarrow N+NO$	1.82×10^{14}	0	38 000	2120 - 2480
Blauwens et al, 1977	$O+N_2 \rightarrow N+NO$	6.03×10^{13}	0	38 000	1880 - 2350
Monat et at, 1979	$O+N_2 \rightarrow N+NO$	1.82×10^{14}	0	38 370	2380 - 3850
Seery & Zabielski, 1980	$O+N_2 \rightarrow N+NO$	1.78×10^{14}	0	38 370	2120 - 2230
Hanson & Salimian, 1984	$O+N_2 \rightarrow N+NO$	1.82×10^{14}	0	38 370	2000 - 4000
Bittker & Scullin, 1984	$O+N_2 \rightarrow N+NO$	1.8×10^{14}	0	38 433	Not stated
Heywood, 1988	$O+N_2 \rightarrow N+NO$	7.6×10^{13}	0	38 000	2000 - 5000
Mellor et al, 1998	$O+N_2 \rightarrow N+NO$	1.58×10^{14}	0	38031	1200 - 2000
Mellor et al, 1998	$O+N_2 \rightarrow N+NO$	1.63×10^{14}	0	38095	2000 - 2800
Kistiakowsky & Volpi, 1957	$N+O_2 \rightarrow NO+O$	1.99×10^{12}	0	3122	400 - 520
Kaufman & Decker, 1959	$N+O_2 \rightarrow NO+O$	1.81×10^{13}	0	3912	1500 - 1700
Clyne & Thrush, 1961	$N+O_2 \rightarrow NO+O$	8.43×10^{12}	0	3575	412 - 755
Mavroyannis & Winkler, 1961	$N+O_2 \rightarrow NO+O$	2.29×10^{12}	0	2971	420 - 620
Wray & Teare, 1962	$N+O_2 \rightarrow NO+O$	3.34×10^{13}	0	0	5000
Kretschmer & Peterson, 1963	$N+O_2 \rightarrow NO+O$	5.0×10^{7}	0	0	350
Schofield, 1967 (note 1)	$N+O_2 \rightarrow NO+O$	1.52×10^{13}	0	3924	400 - 1700
Schofield, 1967 (note 2)	$N+O_2 \rightarrow NO+O$	1.48×10^{8}	1.5	2862	400 - 5000
Baulch et al, 1969	$N+O_2 \rightarrow NO+O$	6.43×10^{9}	1	3147	Not stated
Baulch et al, 1973	$N+O_2 \rightarrow NO+O$	6.4×10^{9}	1	3150	300 - 3000
Bittker & Scullin, 1984	$N+O_2 \rightarrow NO+O$	6.4×10^{9}	1	3150	Not stated
Hanson & Salimian, 1984	$N+O_2 \rightarrow NO+O$	1.6×10^{10}	1	4470	Not stated
Heywood, 1988	$N+O_2 \rightarrow NO+O$	6.4×10^{9}	1	3150	300 - 3000
Miller & Bowman, 1989	$N+O_2 \rightarrow NO+O$	6.4×10^{9}	1	3162	Not stated
Garo et al, 1992	$N+O_2 \rightarrow NO+O$	6.4×10^{9}	1	3130	Not stated
Glarborg et al, 1992	$N+O_2 \rightarrow NO+O$	6.46×10^{9}	1	3160	Not stated
Mellor et al, 1998	$N+O_2 \rightarrow NO+O$	2.56×10^{12}	0	3226	2200 - 2900
Campbell & Thrush, 1968	$N+OH \rightarrow NO+H$	4.1×10^{13}	0	0	320
Baulch et al, 1973	$N+OH \rightarrow NO+H$	4.1×10^{13}	0	0	Not stated
Bowman, 1975	$N+OH \rightarrow NO+H$	1.0×10^{14}	0	0	300 - 2500
Bittker & Scullin, 1984	$N+OH \rightarrow NO+H$	4.0×10^{13}	0	0	Not stated
Hanson & Salimian, 1984	$N+OH \rightarrow NO+H$	2.6×10^{11}	0	0	Not stated
Heywood, 1988	$N+OH \rightarrow NO+H$	4.1×10^{13}	0	0	300 - 2500
Miller & Bowman, 1989	$N+OH \rightarrow NO+H$	3.8×10^{13}	0	0	Not stated
Glarborg et al, 1992	$N+OH \rightarrow NO+H$	3.8×10^{13}	0	0	Not stated
Mellor et al, 1998	$N+OH \rightarrow NO+H$	7.3×10^{13}	0	564	2200 - 2900

Units: cm^3, mole, s, K

Note 1: Composite of data from Kaufman & Decker, Mavroyannis & Winkler, Clyne & Thrush and Kistiakowsky & Volpi.

Note 2: Best fit data from Kaufman & Decker, Mavroyannis & Winkler, Clyne & Thrush Kistiakowsky & Volpi and Wray & Teare.

Table 2.3

Extended Zeldovich mechanism reverse reaction rate constants

Reference	Reaction	A	β	E/R	Temperature Range
Heron, 1961	$N+NO \rightarrow O+ N_2$	1.02×10^{13}	0	0	300
Clyne & Thrush, 1961	$N+NO \rightarrow O+ N_2$	3.01×10^{13}	0	100.7	476 - 755
Phillips & Schiff, 1962	$N+NO \rightarrow O+ N_2$	1.33×10^{13}	0	0	298
Lavoie et al, 1970 (note a)	$N+NO \rightarrow O+ N_2$	1.20×10^{13}	0	0	300
Hanson & Salimian, 1984	$N+NO \rightarrow O+ N_2$	2.63×10^{14}	0	0	Not stated
Heywood, 1988	$N+NO \rightarrow O+ N_2$	1.60×10^{13}	0	0	300 - 5000
Miller & Bowman, 1989	$N+NO \rightarrow O+ N_2$	3.27×10^{12}	0.3	0	Not stated
Garo et al, 1992	$N+NO \rightarrow O+ N_2$	1.60×10^{13}	0	0	Not stated
Glarborg et al, 1992	$N+NO \rightarrow O+ N_2$	3.31×10^{12}	0.3	0	Not stated
Mellor et al, 1998	$N+NO \rightarrow O+ N_2$	3.50×10^{13}	0	166	2200 - 2900
Kaufman & Decker, 1959 (note b)	$NO+ O \rightarrow N+O_2$	3.63×10^{12}	0	19900	1575 - 1665
Wray & Teare, 1962 (note b)	$NO+ O \rightarrow N+O_2$	3.13×10^{11}	0		5000
Schofield, 1967 (note c)	$NO+ O \rightarrow N+O_2$	3.19×10^{9}	1	19688	400 - 5000
Clark et al, 1969 (note b)	$NO+ O \rightarrow N+O_2$	8.91×10^{9}	0		3000
Baulch et al, 1973 (note d)	$NO+ O \rightarrow N+O_2$	1.5×10^{9}	1	19500	1000 - 3000
Hanson et al, 1974 (note b)	$NO+ O \rightarrow N+O_2$	2.34×10^{9}	1	19450	2500 - 4100
McCullough et al, 1977 (note b)	$NO+ O \rightarrow N+O_2$	1.74×10^{9}	1	19450	1750 - 2100
Hanson & Salimian, 1984	$NO+ O \rightarrow N+O_2$	3.81×10^{9}	1	20820	1500 - 5000
Heywood, 1988	$NO+ O \rightarrow N+O_2$	1.50×10^{9}	1	19500	1000 -3000
Mellor et al, 1998	$NO+ O \rightarrow N+O_2$	5.6×10^{11}	0	19317	1200 - 2000
Mellor et al, 1998	$NO+ O \rightarrow N+O_2$	5.6×10^{11}	0	19430	2000 - 2800
Bradley & Craggs, 1975 (note b)	$NO+H \rightarrow N+OH$	3.47×10^{14}	0	23940	2530 - 3020
Duxbury & Pratt, 1975 (note b)	$NO+H \rightarrow N+OH$	2.57×10^{14}	0	24560	2200 - 3250
Ando & Asaba, 1976 (note b)	$NO+H \rightarrow N+OH$	5.01×10^{13}	0	24510	2400 - 3500
Flower et al, 1977 (note b)	$NO+H \rightarrow N+OH$	2.24×10^{14}	0	25410	2400 - 4200
McCullough et al, 1977 (note b)	$NO+H \rightarrow N+OH$	1.74×10^{14}	0	24760	1750 - 2040
Hanson & Salimian, 1984 (note e)	$NO+H \rightarrow N+OH$	1.7×10^{14}	0	24560	1750 - 4200
Heywood, 1988	$NO+H \rightarrow N+OH$	2.0×10^{14}	0	23650	2200 - 4500
Miller & Bowman, 1989 (note f)	$NO+H \rightarrow N+OH$	3.8×10^{13}	0	0	Not stated
Glarborg et al, 1992	$NO+H \rightarrow N+OH$	3.8×10^{13}	0	0	Not stated
Mellor et al, 1998	$NO+H \rightarrow N+OH$	2.02×10^{14}	0	19317	1200 - 2000
Mellor et al, 1998	$NO+H \rightarrow N+OH$	1.82×10^{14}	0	19430	2000 - 2800

Units: cm^3, mole, s, K

Note a: Taken from Schofield (1967)

Note b: Taken from Hanson and Salimian, 1984

Note c: Taken from Schofield, best fit to Kistiakowsky & Volpi (1957), Kaufman & Decker (1959), Wray & Teare (1962), Mavroyannis & Winkler (1961) and Clyne & Thrush (1961).

Note d: Evaluation was based on reverse rate.

Note e: Obtained by a least-squares analysis of expressions from Duxbury & Pratt, Flower et al and McCullough et al

Note f: Is given for the forward reaction.

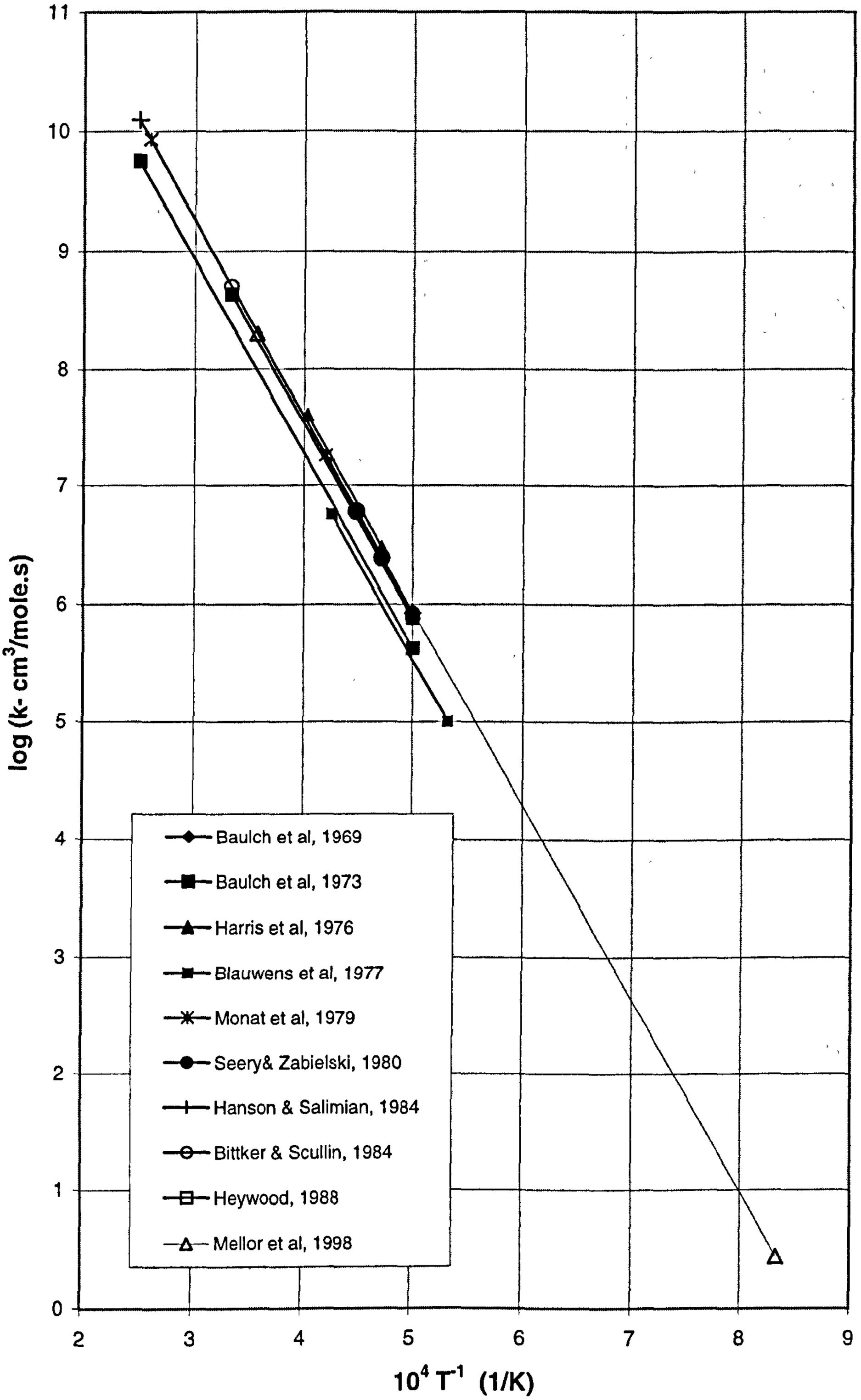

Figure 2.1 Graph of Zeldovich mechanism $O+N_2 \sim N+NO$ rate constants log k versus $10^4 T^{-1}$

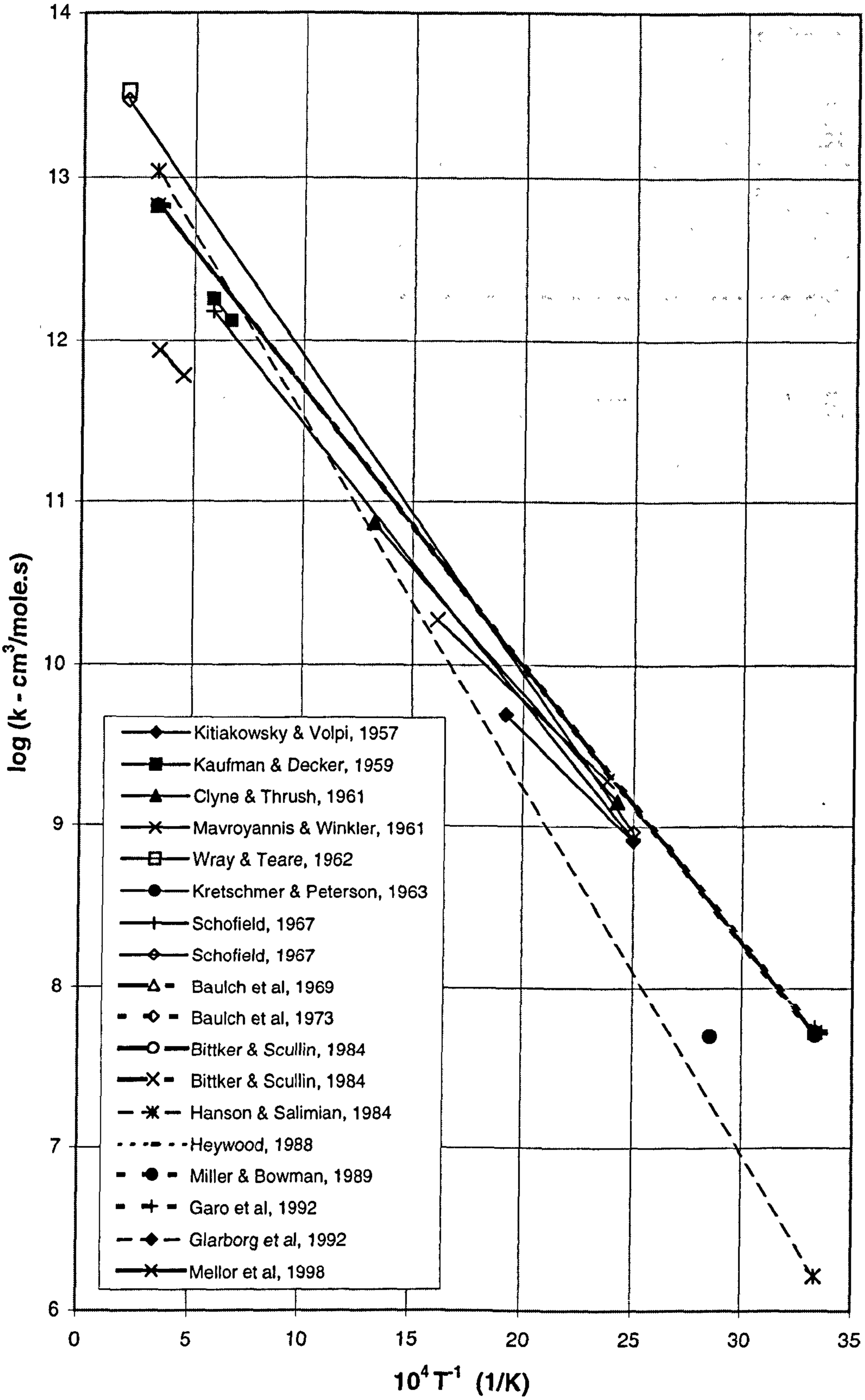

Figure 2.2 Graph of Zeldovich mechanism $N+O_2 \sim NO+O$ rate constants log k versus $10^4 T^{-1}$

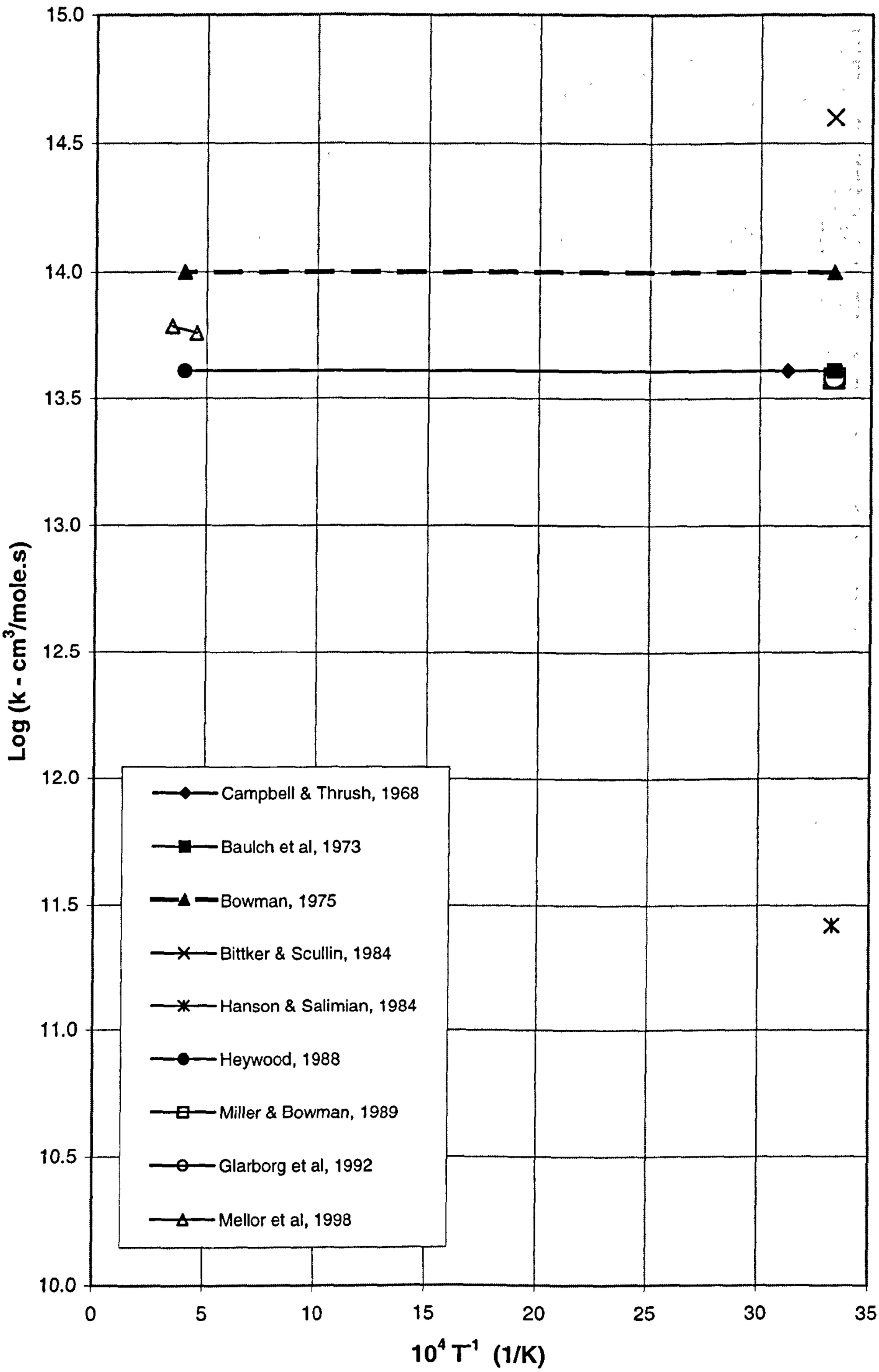

Figure 2.3 Graph of Zeldovich mechanism N+OH ~ NO+H rate constants log k versus $10^4 T^{-1}$

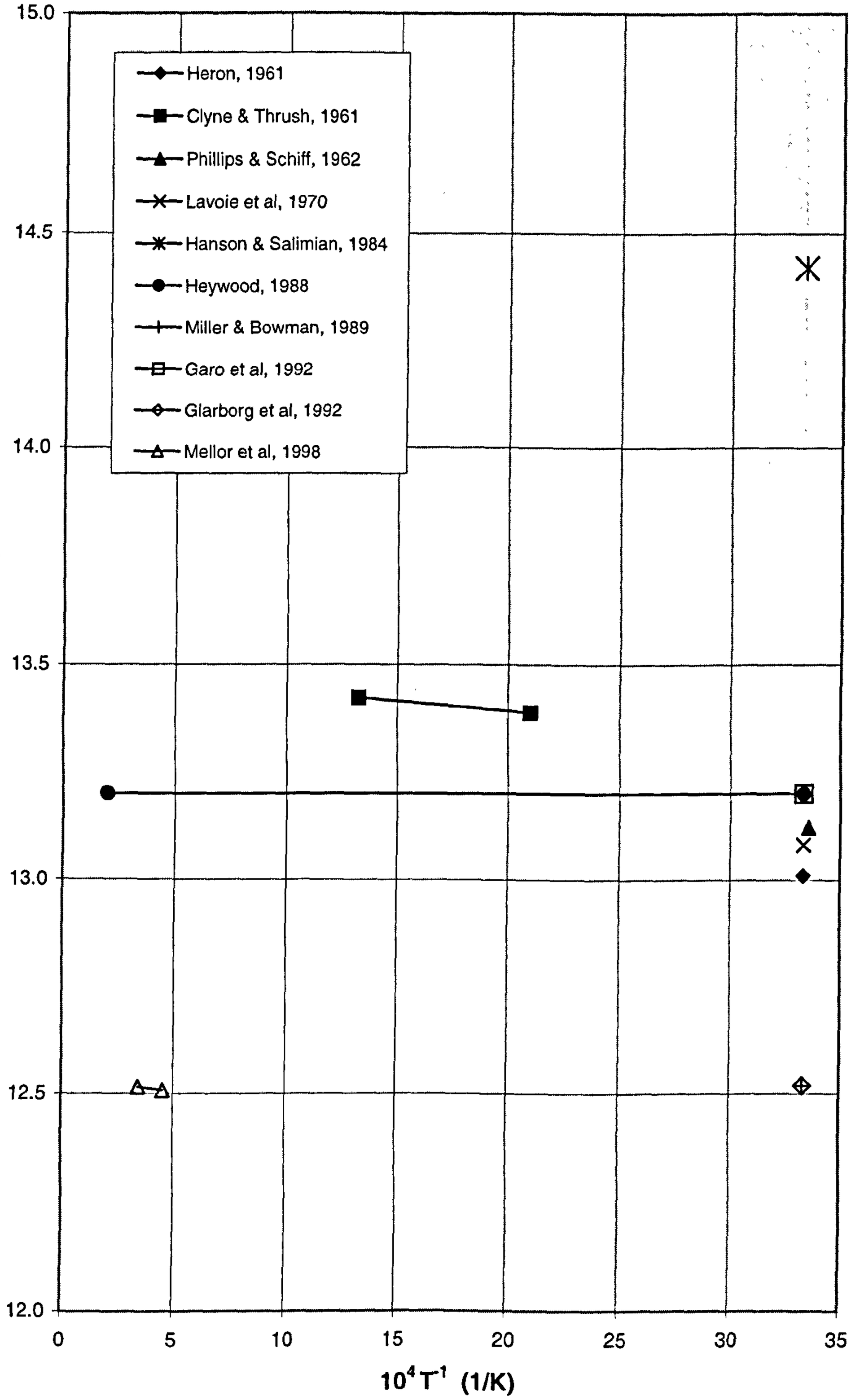

Figure 2.4 Graph of Zeldovich mechanism N+NO~O+N_2 rate constants log k versus $10^4\ T^{-1}$

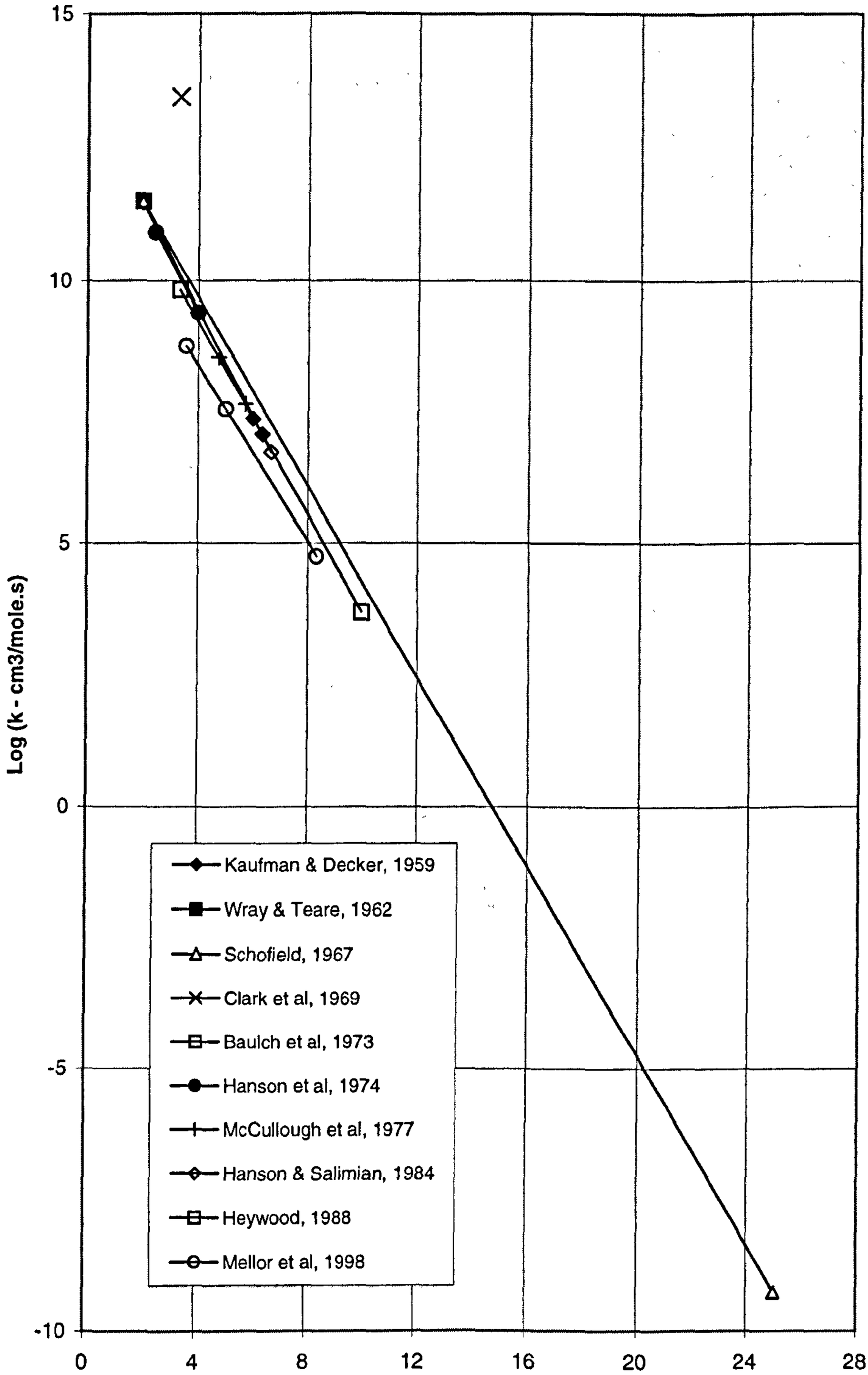

Figure 2.5 Graph of Zeldovich mechanism $NO+O \sim N+O_2$ rate constants log k versus $10^4 T^{-1}$

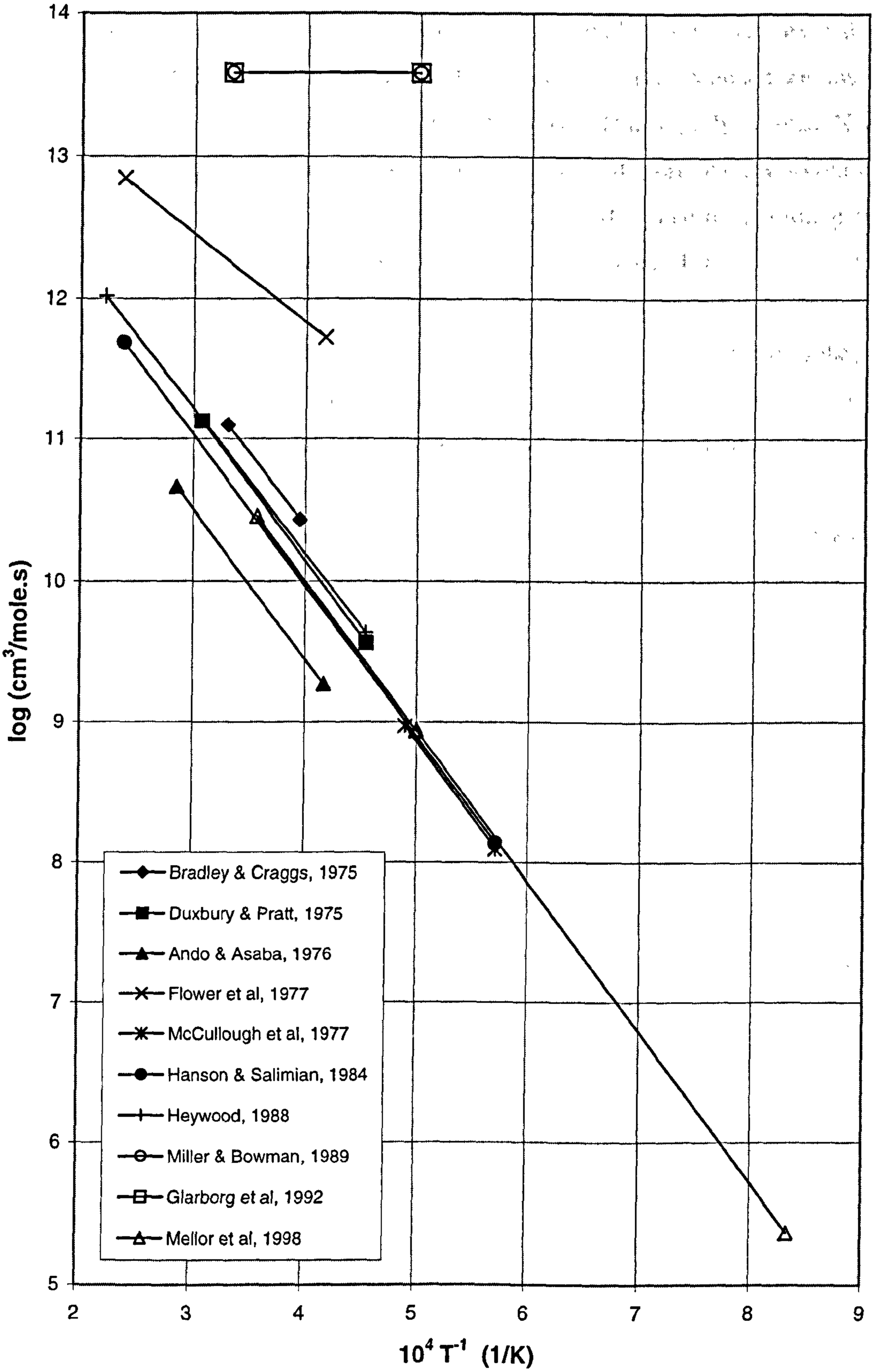

Figure 2.6 Graph of Zeldovich mechanism NO+H~N+OH rate constants log k versus 10^4 T^{-1}

2.1.5 Prompt or Rapid NO Formation

Nitric oxide formation rates in combustion of hydrocarbon fuels can exceed those attributable to direct oxidation of molecular nitrogen by the extended Zeldovich or 'thermal' mechanism, especially for rich conditions. This rapidly formed NO was termed 'prompt NO' by Fenimore (1971) since the rapid NO formation was confined to regions near the flame zone. Typical levels of prompt NO range from a few parts per million by volume to more than 100 ppmv, (Miller and Bowman 1989).

Fenimore (1971) conducted experimental studies of NO formation in atmospheric flat flames and noted a substantial amount of NO was formed very rapidly in the flame front of methane-air and ethylene-air flames, but not in CO-air or H_2-air flames. Plotting NO concentration against time for ethylene-air flames indicated a flame zone or "prompt NO" formation. In contrast, thermal NO, as predicted by the Zeldovich mechanism, is rate controlled and requires a relatively long time scale for its formation. Fenimore postulated that reactions such as;

$$CH + N_2 = HCN + N \qquad 2.20$$

may be responsible for breaking the N-N bond. Subsequent reactions of HCN and other molecules containing a single nitrogen atom could easily lead to NO.

A number of other studies have shown that prompt NO in hydrocarbon flames is formed primarily by a reaction sequence that is initiated by the rapid reaction of hydrocarbon radicals with molecular nitrogen, leading to the formation of amines or cyano compounds that subsequently react to form NO (Miller and Bowman, 1989).

Sterling and Wendt (1972) proposed a model for methane combustion, to test the Fenimore postulation, which involved the following reactions;

$CH_3 + OH = CH_2 + H_2O$	7.71 x 1014 exp (4 180 / RT)	2.21
$CH_3 + N_2 = HCN + NH_2$	4.60 x 1015 exp (19 000 / RT)	2.22
$CH_2 + N_2 = HCN + NH$	2.04 x 1015 exp (41 700 / RT)	2.23
$CH_2 + O_2 = HCO + OH$	7.38 x 1014 exp (1 700 / RT)	2.24

For the test case of isothermal burning of methane at 2100 K and 114.2 per cent theoretical air, large quantities of HCN, NH and NH_2 were produced, indicating that the Fenimore proposal could possibly be significant if the unknown reaction rates were high.

Miller and Bowman, (1989), considered the following reactions:

$CH + N_2 \Leftrightarrow HCN + N$	(Fenimore's postulation)	2.20
$CH_2 + N_2 \Leftrightarrow HCN + NH$	(Sterling and Wendt's reaction)	2.23
$CH_2 + N_2 \Leftrightarrow H_2CN + N$		2.25
$C + N_2 \Leftrightarrow CN + N$		2.26

They confirmed that the original Fenimore postulation reaction 2.20, does lead to prompt NO formation. They illustrated the steps in the process with a reaction coordinate diagram. The authors summarized that further progress in modelling prompt NO in flames requires a direct and unambiguous determination of $k_{2.19}$ at flame temperatures. They concluded from their calculations, that reaction 2.23 would be an insignificant contributor to prompt NO. But based on the rate data, the authors believed reaction 2.26 is a minor, but non-negligible contributor to prompt NO under most conditions. Moreover, because of the large endothermicity of the reaction, its importance with respect to reaction 2.20 increases with temperature. Miller and Bowman also concluded that prompt-NO formation involves 3 separate kinetic issues.

1. The CH concentration and how it is established;
2. The rate of molecular nitrogen fixation; that is, the value of $k_{2.20}$;
3. The rates of inter-conversion among fixed nitrogen fragments.

They finally concluded that additional kinetic information is needed.

An alternative explanation of prompt NO involves the rapid build up of radical species such as H, OH and O to high levels, which would cause large amounts of NO to form very quickly by the first reaction of the Zeldovich mechanism,

$$O + N_2 \Leftrightarrow NO + N \qquad 2.1$$

because of the high oxygen level.

At present there is no absolute consensus regarding the mechanism behind prompt NO, the evidence that it occurs continues to increase. Since Fenimore's report it has been observed experimentally by many others, (Pershing & Berkau 1973).

2.1.6 Formation of NO_2 in Diesel Engines

Chemical equilibrium considerations indicate that for burned gases at typical flame temperatures, NO_2 /NO ratios should be negligibly small, (Heywood 1988). The termolecular reaction;

$$2NO + O_2 \rightarrow 2NO_2 \qquad 2.27$$

is far too slow to produce any measurable NO_2 in the exhaust and NO_2 loss is in fact more likely under conditions where reduction or hydrolysis in the exhaust pipe or sample train is possible. Experimental data, however, show that NO_2 can be as high as 30 to 50 per cent of the total exhaust oxides of nitrogen from a DI diesel (Hilliard and Wheeler, 1979, Ketcher, 1997).

NO_2 may be produced from NO by reactions proposed by Merryman et al (1975)

$$NO + HO_2 \Leftrightarrow NO_2 + OH \qquad 2.28$$

$$NO + OH \Leftrightarrow NO_2 + H \qquad 2.29$$

Voiculescu and Borman (1978) used a dumping method to quickly transfer most of the cylinder contents of a 1.1 litre per cylinder DI diesel. A diaphragm and cutter system was utilized for this sampling. NO and NOx histories were obtained from the dumping data. In all cases they found the NO and NOx curves increased rapidly and then levelled off and approached the exhaust level, the rate of formation was dependent on load. They also found the NOx to NO ratio in the exhaust remained relatively constant,

ranging from 1.26 at the lowest load to 1.14 at the highest load. However, the in-cylinder ratio was higher in the rapid formation region and then decreased to the exhaust gas ratio. If NO may be converted to NO_x by small amounts of HC premixed with air in a diffusion flame, as has been suggested, the modelling of the NO_2 may be even more complex than current assumptions.

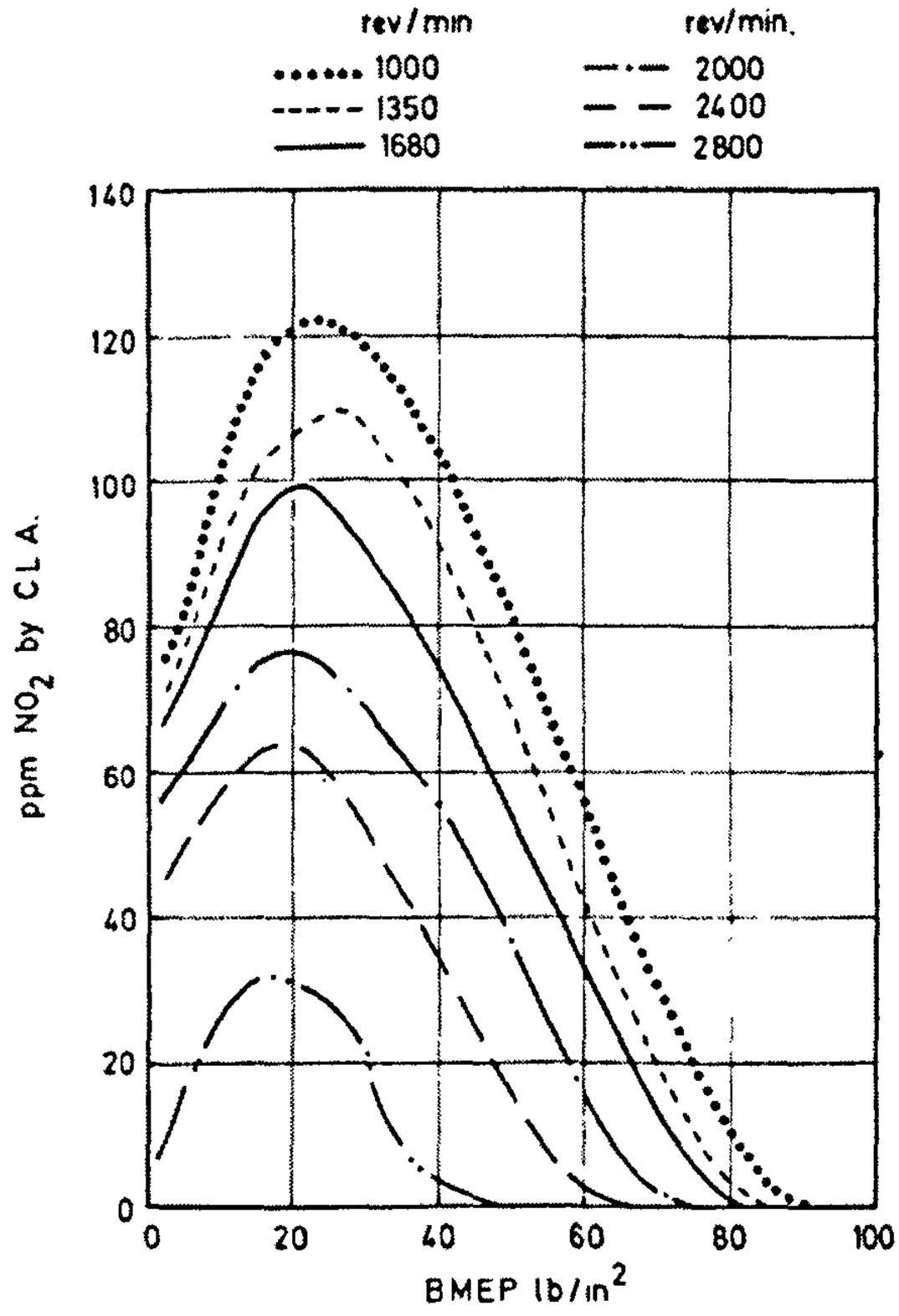

Figure 2.7 NO_2 emissions as a function of load from a 6 litre 6 cylinder naturally aspirated DI diesel engine (Hilliard and Wheeler, 1979)

Hilliard and Wheeler (1979) measured NO and NO_2, against load and speed, from DI and IDI 6 litre 6 cylinder N/A diesel engines. These results are shown in **Figures 2.7 and 2.8** which illustrate that the NO_2 component of NO_x can be high, as much as 31.5 per cent at low load and speed conditions. The heterogeneous diesel combustion is favourable to NO_2 formation and survival, at light load, because the high levels produced in the lean fringes of droplet burning have a high chance of survival by diffusing into the surrounding air, which will soon cool rapidly by adiabatic expansion. DI engines have inherently higher NO emission levels as well as lower working fluid temperatures after expansion. Both these factors would be expected to favour the

formation and survival of combustion generated NO_2. It is therefore expected that DI engines would emit more NO_2 than IDI engines under comparable conditions. Hilliard and Wheeler (1979) also recorded a 20 per cent reduction in NO_2 at the exhaust exit, which was put down to condensation or to adsorption of NO_2 on soot.

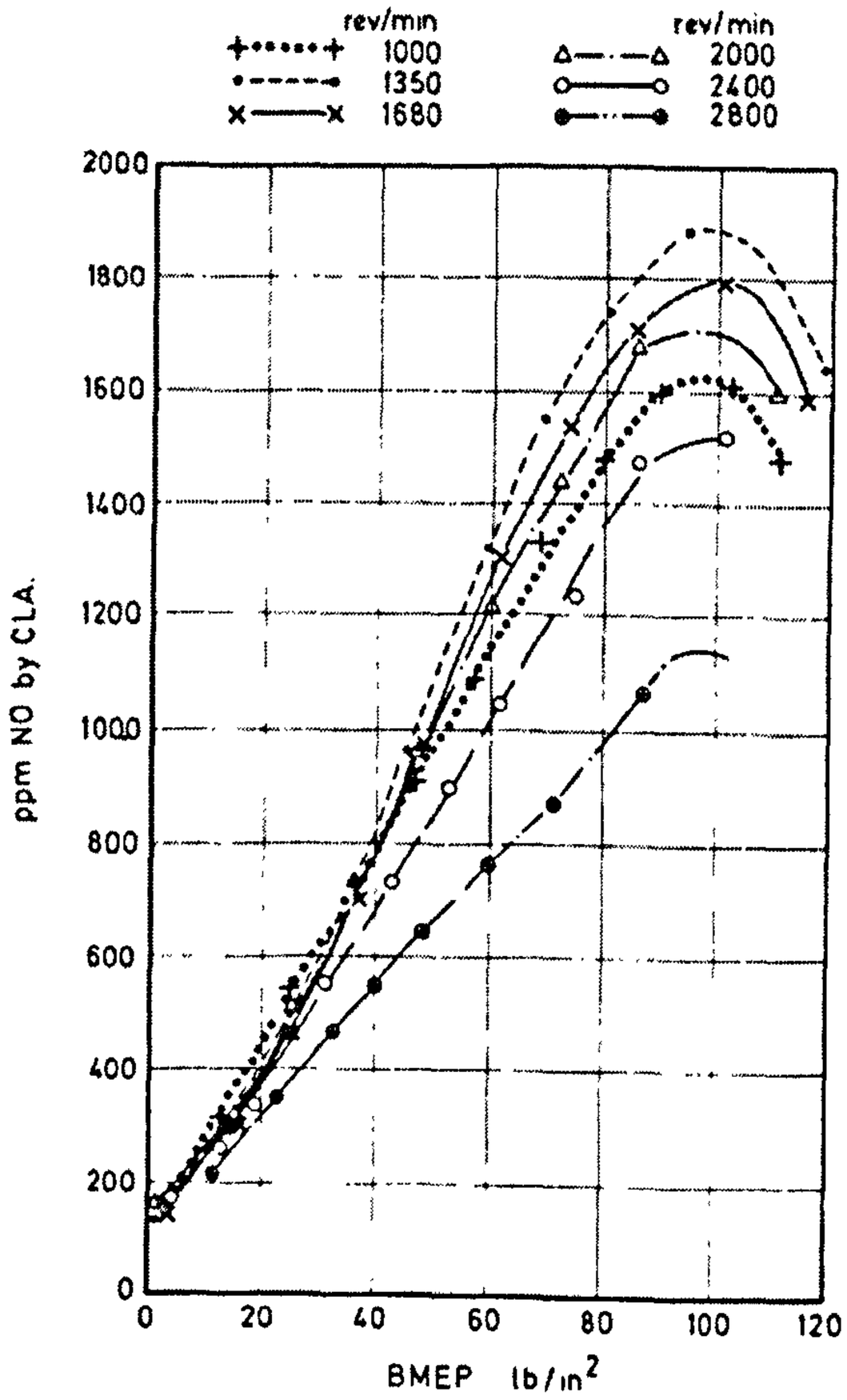

Figure 2.8 NO emissions as a function of load from a 6 litre 6 cylinder naturally aspirated DI diesel engine (Hilliard and Wheeler, 1979)

More recent work at Ford, using a Fourier Transform Infrared (FTIR) analytical bench has indicated that NO_2 levels from a turbocharged 2.5 litre high speed DI diesel in a Transit, may be as high as 50 per cent of the total NOx emissions, under the light load conditions during the ECE 15 part of the European emissions drive cycle (Ketcher 1997).

Pipho, Kittelson and Zarling (1991) reported measurements of NO and NO_2 concentrations in the combustion chamber and in the exhaust of an Isuzu 2.8L 4

cylinder DI diesel. The combustion measurements were made by total cylinder sampling, which showed that NOx begins to rise approximately 5 degrees crank angle before the start of combustion and rise steadily until about 30 degrees after TDC. An interesting result was the low level of NO_2 that remained constant after 10 degrees from the start of combustion. However, substantial differences were found between the blow-down results and exhaust readings. The highest exhaust results for the blow-down conditions had a NO_2/NO ratio of 0.03 while the late blow-downs for the same condition had ratios of approximately 0.5. In order to investigate the possibility of the sampling process forming NO_2 and the formation of NO_2 early in the combustion cycle, a simple kinetic model for premixed combustion of methane was used. The kinetic simulations indicated that the measured NO_2/NO ratio for the blow-down experiments has a strong dependence on the cooling and dilution process, which the sample undergoes. The total NOx is essentially conserved during the process but the proportions of NO and NO_2 in the cylinder cannot be determined, therefore interpretation of total cylinder sampling NO_2 data is difficult.

2.1.7 Summary

- It is generally assumed that the thermal fixation of NO occurs according to the extended Zeldovich mechanism;

$$\mathbf{O + N_2 \Leftrightarrow NO + N}$$

$$\mathbf{N + O_2 \Leftrightarrow NO + O}$$

$$\mathbf{N + OH \Leftrightarrow NO + H}$$

- From the Zeldovich mechanism rate constants, it is evident that the rate of NO formation rises exponentially with temperature. According to the Zeldovich mechanism, NO is formed by atomic oxygen, which is the result of a 2-step thermal dissociation of the primary reaction products CO_2 and H_2O. The 2-step thermal dissociation is the reason for the temperature sensitivity of NO formation.

- Extensive evidence in the literature confirms that in real diesel engines, NOx formation is indeed very sensitive to the peak flame temperature generated

during combustion. Conditions that lead to high in-cylinder temperature favour formation of higher levels of NOx, and vice versa.

- Prompt or rapid NO formation may occur in the flame zone, through the formation of hydrocarbon radicals which break down the N_2 bond to provide N radicals for NO formation.

- Oxidation of NO to NO_2 does occur in diesel engines, NO_2 emissions can be as high as 30 to 50 per cent of the total nitrogen oxides from a DI diesel at low load and speed conditions. DI engines have inherently higher NO levels than IDI diesels, as well as lower working fluid temperatures after expansion. Both these factors favour the formation and survival of combustion generated NO_2. DI engines are therefore likely to emit more NO_2 than IDI engines under comparable conditions.

2.2 NOx Formation Models and Combustion Models

2.2.1 Introduction

The internal combustion engine represents one of the more challenging fluid mechanics problems to model because the flow is compressible, low Mach number in-cylinder, turbulent, unsteady, cyclic and non-stationary, both spatially and temporally. The combustion characteristics are greatly influenced by the details of the fuel preparation process and the distribution of fuel in the engine, which is, in turn, controlled by the in-cylinder fluid mechanics. Fuel injection introduces the complexity of describing the physics of dense, vaporizing two-phase flows. Pollutant emissions are controlled by the details of the turbulent fuel-air mixing and combustion processes and a detailed understanding of these processes is required in order to improve performance and reduce emissions while not compromising fuel economy (Rutland et al, 1995).

Many models for engine combustion problems use the first law of thermodynamics as applied to either the entire cylinder contents or to sub-systems. Typically the major species of the products of combustion may be assumed to follow a shifting equilibrium process for thermodynamic purposes. For chemical kinetics calculations, many of the major species may also be assumed to be at the equilibrium concentration, (Olikara & Borman 1975). However, in practice NO formation and decomposition do not occur instantaneously, but require time to reach their equilibrium rates corresponding to the given temperature and pressure, but in an internal combustion engine, the equilibrium concentration itself changes continuously because the pressure, temperature and amounts of various species are continuously varying. The time for the NO formation process is usually comparable to or longer than the time for changes in engine conditions, so the formation process is kinetically controlled. However, for close to stoichiometric conditions at maximum pressures and burned gas temperatures, equilibrium NO concentrations may be attained (Heywood, 1988).

In principle, if the evaporation and chemical reactions are taken into account, the coupling of three-dimensional modelling of spray processes with that of fluid dynamics for the airflow, will allow the numerical calculation of the diesel combustion process.

However most of the simulation codes have not yet been validated in terms of in-cylinder spray and air motion through adequate comparison with experimental results, hence they lack reliability at present. Additionally, for spray simulation, physical processes of break-up and impingement are still unsolved. The existent fluid dynamic codes are unable to simulate accurately the turbulent characteristics in the combustion chamber, although the predictions of the average flow velocities are in reasonably good agreement with experiments. With regards to the combustion process, the formation mechanisms of particulates, consisting of soot and adsorbed soluble organic fraction, are still unclear. For the formation of NOx a number of equations have been proposed mostly expanding on the Zeldovich mechanism, but there is a large variation in the assumed rate constants, in the literature. For these reasons it is clearly not possible to make accurate predictions of heat release, heat transfer and exhaust emissions by describing the thermo-fluid dynamics as well as the chemical reactions in diesel flames (Kamimoto and Kobayashi, 1991).

Two basic types of model have been developed. These can be categorized as thermodynamic or fluid dynamic in nature, depending on whether the predominant equations are based on energy conservation or on a full analysis of the fluid motion. Thermodynamic energy-conservation-based models may be labelled as zero-dimensional, quasi-dimensional and phenomenological. Fluid-dynamic-based models are often called "multidimensional" models due to their ability to provide detailed geometric information on the flow field, based on solution of the governing flow equations (Heywood, 1988).

Several phenomenological models were proposed in the 1970s for simulating heat release and NOx formation in the combustion chamber of diesel engines. In the eighties, with the progress of multi-dimensional modelling of spray and in-cylinder air motion, a new wave of numerical simulation of combustion process started and these models have been progressively refined during the 1990s.

2.2.2 Phenomenological Models

Ahmad and Plee (1983) examined the influence of flame temperature on NOx emissions from a single cylinder light-duty DI diesel by varying the composition of the intake charge by adding either pure O_2 or N_2, at different speeds and loads. The effect of intake air composition on emissions was correlated with the diffusion flame temperature using the following expression.

$$EI = C_{mix} \exp(E/RTf) \qquad 2.18$$

where,
- EI = emission index (g pollutants/kg fuel)
- C_{mix} = factor which depends upon flow characteristics
- E = overall activation energy (cal/mole)
- R = gas constant (cal/mole-K)
- T_f = stoichiometric adiabatic flame temperature (K)

The flame temperature correlation (E/R) for EINOx obtained in an earlier study was -36,700 for both engine capacities with a divided chamber. This was consistent with the phenomenological model of diesel combustion proposed by the authors. The results from this study with the DI engines gave a correlation of -34,300 for TDC flame temperature and -35,300 with peak cycle temperature. As there was little difference between use of the flame temperature at TDC to the peak cycle temperature, (thus indicating that the NOx kinetics are insensitive to the combustion chamber geometry), the authors chose to use the former to represent this characteristic temperature.

Kyriakides, Dent and Mehta (1986) extended their earlier phenomenological model to include the prediction of soot and nitric oxide emissions. They used the Zeldovich mechanism, equations 2.1 and 2.2, for the NO formation. The Lavoie extension was not used, so the influence of C and H on the production of NO was omitted. The Zeldovich mechanism constants were taken from Danshyear and Watfa (1974). The NO model gave reasonable accuracy compared to the experimental data, despite the simplified mechanism used.

Xiaobin and Wallace (1995) presented a phenomenological model, which they claimed strikes a balance between the complexity and computational cost compared to codes such as KIVA. In their study, the phenomenological model emphasized soot oxidation. The extended Zeldovich mechanism is used for the formation of NO and additional reactions involving the formation and destruction of NO_2 are adopted from Slack and Grillo (1981). The model over predicted NOx emissions. Two possible reasons were suggested, use of the quasi-global chemical mechanism over-predicts the concentrations of radical species, which, especially in the early stage of combustion, will shift the NOx reaction in favour of higher concentrations; secondly, possible inadequate description of the mixing process.

The quasi-dimensional phenomenological model developed by Bazari (1992, 1994, 1994) was used for this study and is covered in Chapters 4 and 5.

2.2.3 Numerical Simulation Models

Despite the above comments in the introduction, there have been a number of codes written to simulate combustion processes in diesel engines. Hiroyasu and Kadota (1976) developed a mathematical model for predicting the concentration of exhaust NO, soot and other emissions in a direct injection diesel engine. NO formation was predicted via the extended Zeldovich mechanism; the calculated values of exhaust NO were higher than measured data. One reason was that the calculated flame temperature was higher than expected.

SCAN code

Benjamin et al (1980) reported results using the computer code SCAN (Stratified Charge Engine Analyzer) which includes models for calculating the movement of the flame front as it passes through the mixture and also for the controlling processes of chemical kinetics, turbulence, wall friction and heat transfer. Their predictions showed reasonable agreement with hot-wire and laser doppler anemometry measurements.

CONCHAS code

Diwkar (1982) adopted the Los Alamos CONCHAS code (Butler et al, 1979) and used more realistic submodels for wall heat transfer and wall shear stresses to obtain better agreement with experimental data for a direct injection stratified charge engine.

PICALO code

The above investigations used 2-dimensional geometry and flow conditions, which is unlikely to be true in a real engine. Duggal et al (1984) used the PICALO code to compute the in-cylinder flow field including fuel spray, droplet evaporation and combustion in a DI diesel engine. For the 3-D, 2-phase reactive flow, for evaporation and combustion, a flat bottom piston cavity was considered, which from practical terms is unrealistic. The calculated results showed that parameters such as fuel injector, computational grid and air swirl have a significant effect on the spread and evaporation of the liquid fuel spray. The former and latter are known to have a significant effect on diesel combustion from engine development results. The authors presented calculations of flame temperature distribution and cylinder pressure history, but the calculated temperatures were too high compared to measured data. This probably results from their assumption of instantaneous chemical reaction, without proper consideration for turbulence and the irregular nature of non-homogeneous combustion.

KIVA code

Amsden et al (1985) developed a comprehensive numerical code, named KIVA, that represents the spray dynamics, fluid flow, species transport, mixing, chemical reactions and accompanying heat release, that occur inside the cylinder of an engine. Since its public release in 1985, the KIVA computer program has been used for the time dependent analysis of chemically reacting flows with sprays in two and three dimensions. The new code, called KIVA-II, developed by the same group, was made public in early 1988. KIVA-II improves the earlier version in accuracy and efficiency of the physics sub-models, as well as in versatility and ease of use. The KIVA code was modified by Takenaka et al to simulate the combustion processes in a DI diesel engine with a multi-hole nozzle. The authors compared the predicted results with experimental data of time histories of chemical species, equivalence ratio and flame temperatures at various locations inside the combustion chamber. Compared to measured values, the flame temperature was found to be high, resulting in NO concentrations around 30 times measured values; also, other chemical species were seen to have different behaviours, all these discrepancies were attributed to poor prediction of the mixing process.

Ikegami et al (1984) proposed a stochastic model consisting of the spray sub-model and the combustion sub-model to describe the combustion processes in direct injection diesel engines. In each sub-model, generation of turbulence and turbulent mixing of

fuel and air are taken into account and the heterogeneity and its devolution are described using Curl's collision-redispersion model. It was shown that the model can reproduce the entire course of the rate of heat release and exhaust NO concentration fairly well for a wide range of operating conditions. Brown and Heywood (1987) evaluated a stochastic mixing model for predicting nitric oxide and soot emissions from direct injection diesel engines. The unsteady reactive flow including gas flow, spray dynamics, combustion and turbulent mixing was calculated using the KIVA code and then the flow data was used to define zones to calculate zone processes and mass flow between zones. Each of these zones was modelled next as a stochastic mixing zone whose fundamental concept was Curl's coalescence/dispersion micro-mixing. Predictions of NO and soot concentrations were compared to experimental results obtained under different engine operating conditions. The results showed excellent convergence to the measured data, demonstrating that this is an efficient and accurate method for calculating slow and complex chemistry in turbulent reactive flows. The employment of stochastic mixing concepts demonstrates the importance of consideration for turbulent mixing in slow chemistry.

Pinchon (1989) also modified the KIVA code to be applicable to very complex combustion shapes of a prechamber diesel. A k-epsilon turbulence model was used and the boundary conditions were described by the appropriate law-of-the-wall. Wall heat transfer rates were computed using a model based on a k-epsilon formulation. The spontaneous ignition was simulated by a four-step kinetics mechanism and the Magnussen eddy break-up combustion model was assumed. The complete model was applied to simulate the flow and combustion in a pre-chamber diesel engine. His calculation showed that addition of the glow plug in the pre-chamber reduces the swirl level to less than half its level without the plug. The computed flame development and global heat release are both in qualitative agreement with experiments.

Ayoub and Reitz (1995) used KIVA-II with improvements in the spray, ignition, including Cetane Number modification, combustion and emission models, to simulate diesel engine cold starting. Warm-engine computed NOx emissions were in agreement with expected trends. Fusco et al (1995) used a modified version of KIVA-3 for a divided-chamber diesel, the chamber being representative of the conditions in the piston bowl of a naturally aspirated, swirl type, high speed DI diesel. There was optical access

to the chamber for flame imaging and temperature measurements. KIVA-3 can handle complex geometries using a block-structured mesh with indirect addressing, which allows only the activated cells to be taken into account during the calculations. Additionally, a new sub model for spray (Allocca 1994) and turbulent mixing-controlled model for high temperature combustion (Magnussen, 1976) improved KIVA-3. It was concluded that computations of temperature were in qualitative agreement with the flame emissivity measurements. Rutland et al (1995) used a modified version of the KIVA code for computations of in-cylinder flow, ignition, combustion, and emissions of NOx and soot, for a heavy duty truck engine. Improved sub models were used for intake flow, combustion, unburned HC, heat transfer, wall impingement, droplet drag, droplet break-up and atomisation, crevice flow, ignition, vaporization, soot and turbulence. The extended Zeldovich mechanism (Heywood 1976) was implemented for NO formation. NOx formation has been found to be very sensitive to small changes in the computed in-cylinder gas temperature field and in previous studies (Patterson et al, 1994 and Kong et al, 1995) when a calibration factor was introduced to match predicted NOx with engine data. Rutland et al found the improved KIVA code gave accurate NOx predictions with the calibration factor close to unity. It would appear that the more accurate NOx prediction is due to the improved Renormalization Group theory (RNG) turbulence model that predicted lower peak temperatures. The updated model also successfully predicted the soot-NOx trade-off trend as a function of injection timing.

SPEED code

Gosman and Marooney (1989) outlined the features of the Imperial College SPEED code. A diesel spray version without combustion was in preparation at that time. One of the advantages of the SPEED code is the use of an unstructured mesh, which permits the easy fitting of complex engine geometries and in addition does not require any unused memory when combustion chambers with re-entrant features are present.

2.2.4 Other Numerical Models

Ishiguro et al (1988) proposed a 3-dimensional model for simulating the combustion process in a direct injection engine. The spray sub model employs a quasi-steady spray model to calculate the gas entrainment and jet penetration. The combustion sub model assumes the Magnussen's eddy dissipation concept that allows a description of the

formation of a combustible mixture due to turbulent mixing. The mixture is assumed to undergo an irreversible single-step chemical reaction. Computations show a reasonable degree of reproduction of the entire processes of heat release and flame evolution.

Raine, Stone and Gould (1995) in reporting on the refinement of the ISIS (Integrated Spark Ignition Engine Simulation) computer model, review modelling of oxides of nitrogen. They assumed the extended Zeldovich mechanism for thermal NO formation and the Miller and Bowman 'prompt' NO route. Additionally, the authors reviewed the rate coefficients for the extended Zeldovich mechanism reported in the literature by eight researchers and deduce that in view of the disagreement between rates that is apparent from fundamental chemical kinetic measurements, the choice for engine modelling work is unclear. In conclusion, NOx predictions resulting from using different reaction rates for the extended Zeldovich mechanism were compared, but the authors concluded that until comprehensive data are available for in-cylinder conditions at the start of compression, it is not possible to say which kinetic data give the best agreement.

2.2.5 Summary

- Diesel combustion represents one of the more challenging thermo-fluid mechanics problems to model because of the complex flows and presence of chemical reactions.

- The combustion process and pollutant formation are greatly influenced by air motion and fuel preparation and distribution.

- Fuel injection introduces the complexity of describing the physics of dense, vapourizing two-phase flows.

- Pollutant emissions are controlled by the details of the turbulent fuel-air mixing and combustion processes.

- The formation of NO is most commonly modelled on the extended Zeldovich

mechanism, but there is a large variation in the assumed rate constants, in the literature.

- Because of the strong temperature dependence of the NO formation rate, any errors in determining the flame temperature will have a knock-on affect on the predicted NO levels.

- Two basic types of model have been developed: thermodynamic and fluid dynamic. Thermodynamic models are zero-dimensional or quasi-dimensional and phenomenological. Fluid dynamic or "multidimensional" models can provide detailed geometric information on the flow field based on solution of the governing flow equations (Heywood).

- There have been a number of zero-dimensional and multidimensional models developed, KIVA being one of the most widely used fluid dynamic model.

- The majority of the multidimensional numerical models use the extended Zeldovich mechanism for the prediction of NO formation and emission. Some phenomological models use semi-empirical equations based on exponential expressions of a form similar to those describing the rates of chemical reactions.

2.3 NOx Reduction by Injection Retard

It is well known that retarding the injection timing of a diesel engine reduces the formation and emissions of NOx. Retarding the injection timing causes the combustion event to occur later, after the piston has passed TDC and thus the maximum cylinder pressure and peak combustion temperature are reduced. As outlined in section 2.1, the formation of NOx is very dependent on temperature and with retarded combustion the reduction in peak gas temperature reduces the formation of NOx. The drawbacks to the use of injection retard for controlling NOx emissions are the trends to increase smoke and unburned HC emissions and worsen engine efficiency, which causes an increase in fuel consumption. These disadvantageous effects can be offset by modern fast-fuel-air-mixing direct injection combustion systems that enable the engine to operate at retarded timing with less detrimental results on soot and HC emissions and fuel consumption.

Khan and Wang (1971) studied the effects of injection timing and injection rate in several DI engines. The experiments showed a significant reduction in NOx with injection retard. They found indications that an increase in the rate of fuel-air mixing reduced the sensitivity to changes in injection timing and could be used to reduce emissions of NO by operating at retarded injection timing without appreciably affecting smoke emissions. They postulated that it might be possible to retard injection timing by 10 degrees (crank) without significant sacrifice in fuel economy. The slope of the NO versus injection timing curve varied between engines, but a 10-degree retard reduced NO concentration by a factor of 1.5 to 2.5.

Yu and Shahed (1981) investigated the effects of injection retard on NOx emissions from a single cylinder DI engine. They observed the strong dependence of nitric oxide emissions on injection timing; increased emissions with advanced, and reduced emissions with retarded injection timing. Calculated histories of temperature, species concentration and nitric oxide formation illustrated that the decrease in NOx emissions at retarded injection timing was mainly due to a decrease in combustion temperature. At 8 degrees after SOC, NO formation was calculated as 1.35×10^{-4} g/deg at advanced injection timing and 0.16×10^{-4} g/deg at retarded timing. However, the local molecular oxygen concentrations were similar for both injection timings. But the local

temperatures were 2666 K with advanced injection timing and 2405 K with retarded timing. So it was concluded that a temperature increase of 261 K increased the NO formation rate by about 8 times.

Aoyama et al (1990) measured flame temperature by the two-colour method in a swirl chamber IDI and in a 2-valve DI with a re-entrant flat-bottomed combustion chamber. Combustion flame temperature distributions were examined and related to the NOx concentrations. In the IDI chamber at advanced injection timing, generating more NOx, the region of flame temperature 1900 to 2000 degrees C occurred at an early stage, and the regions above 2000 degrees C occupied a relatively wide area. At retarded timing these regions above 2000 degrees C were hardly observed. The DI engine was tested with pilot injection. With pilot and retarded main injection, NOx was reduced from 385ppm to 300ppm. By the application of pilot, the flame regions above 1900 degrees C were narrower between 4 and 12 degrees after TDC, but wider at 16 degrees after TDC, compared to the standard injection timing. Injection timing retard reduced NOx by controlling the spatial development of the localized high-temperature regions. Pilot injection delayed the development of high-temperature regions and facilitated injection retard while maintaining fuel consumption. NOx was reduced by controlling the temporal development of the localized high-temperature regions, in addition to the effects of injection retard.

Arcoumanis et al (1995) experimented with a transparent version of a production VW 1.9 litre DI diesel engine using the two-colour method to measure in-cylinder flame temperature. They used the concept of "area-averaged flame temperature" to obtain comparisons between different engine operating conditions. At an engine running condition of 2000 rpm and 2 bar BMEP, two start of injection timing settings were tested, 2° and 8° BTDC. At the later injection timing of 2° BTDC the flame image at 10° ATDC exhibited an average flame temperature of just above 2000K along the direction of three of the five sprays. At the earlier injection timing of 8° BTDC the image at 10° ATDC showed a strong increase in the areas of higher temperatures. Most of the flame core was at about 2200K with very high temperatures present at the edges of the flames. The authors concluded that advancing the time of fuel injection leads to increased overall temperatures and earlier peak temperatures at low loads

Mikulic et al (1993) conducted experiments with a single cylinder DI engine based on the Mercedes-Benz 600 series. A camshaft actuated electronically controlled unit injector was used for this study. Testing was conducted at 2000 rpm and load equivalent to 2 bar BMEP without EGR. Using a small pilot and setting the main injection timing to give the same fuel consumption as operating without a pilot, NOx emissions were reduced from 10.6 g/h to 9.0 g/h. Retarding the main injection lead to further reduction of NOx, but accompanied by an increase in fuel consumption.

2.3.1 Summary

- Retarding injection timing will reduce NOx formation by lowering peak combustion temperatures, or by controlling the spatial development of the localized high-temperature regions. But this may also cause an increase in HC and smoke emissions, as well as an increase in fuel consumption.

- Pilot injection delays the development of high-temperature regions and can facilitate injection retard while maintaining fuel consumption. Thus controlling the temporal development of the localized high-temperature regions can reduce NOx without loss of efficiency.

2.4 NOx Reduction by EGR

2.4.1 Introduction

Exhaust gas re-circulation is currently the most effective method of reducing NOx emissions from light-duty diesel engines, since it is particularly beneficial at part load conditions. These conditions characterize the duty cycle of these types of engines and form the prevalent part of the emissions test drive cycle. At part load a diesel engine is operating at a high air to fuel ratio and therefore a large proportion of the intake air charge can be replaced with exhaust gases, up to around 60 per cent by volume for a high speed DI. EGR reduces the oxygen concentration and increases the heat absorbing capacity of the inlet charge, thus reducing the peak flame temperatures to lower the formation and emissions of NOx. EGR involves, in effect, the replacement of a small quantity of oxygen and nitrogen in the inlet air to the engine with carbon dioxide and water vapour from the exhaust. Since the specific heat capacity of both CO_2 and water vapour is greater than that for oxygen, the gas temperatures within the engine cylinder during combustion are reduced (Ladommatos et al, 1996). Furthermore, by definition, EGR reduces the exhaust gas mass flow and so lowers the mass of NOx emitted per unit time or distance.

Direct injection engines will tolerate much higher levels of EGR than IDI diesels. This is because all the intake air charge is in the combustion chamber within the cylinder, so dilution of the intake air by EGR affects the nominal air/fuel ratio. In the case of the IDI, approximately half the air charge is in the swirl or pre-combustion chamber in the cylinder head, where all the fuel is injected, forming a much richer mixture at half the nominal air/fuel ratio. Hence, for the IDI, dilution of the intake air is by far more critical to the already rich mixture in the pre-combustion chamber. In addition there will be more residual combustion gases retained in the pre-combustion chamber during the induction phase.

Stawsky et al (1984) reported significant reductions in NOx with the use of EGR, ranging from 65 to 70 per cent at 20 per cent EGR. However at full load, this was accompanied by dramatic increases in CO, HC and particulates emissions. The authors

looked at combined EGR and a particulate filter to control both NOx and particulates. They concluded that further work was required owing to the increase in CO emissions.

2.4.2 Definition of EGR

The level of EGR is the amount of exhaust gas that is re-circulated into the intake charge, to replace fresh air. It is usually expressed as per cent of the normal airflow at that engine condition without EGR. This can be specified on a volumetric or mass basis. For convenience, EGR is often defined on a simple volumetric basis (Ladommatos et el, 1996, Horrocks and Robertson, 1996);

$$EGR_v\ \% = (V_{af} - V_{ac})\ 100\% / V_{af} \qquad 2.30$$

where, V_{af} = free air volume flow rate to the engine at full load without EGR, at a given engine speed

V_{ac} = free air volume flow rate to the engine at part load with EGR, at the same speed

The above definition is convenient to use because only few parameters need to be measured during engine tests. However, it relates rather poorly to the definition based on mass flow rates:

$$EGR_m\ \% = m_e\ 100\% / m_c \qquad 2.31$$

where, m_e = EGR mass flow rate to the engine at part load with EGR, at a given engine speed

m_c = total inlet charge mass flow rate to the engine at part load with EGR, at the same speed

Pittermann et al (1999) defined the exhaust re-circulation rate as:

$$X_{EGR} = m_R/(m_L + m_R) \qquad 2.32$$

Where, m_R = mass of recycled exhaust gas

and, m_L = mass air flow

In practice, the authors used the oxygen concentration before and after the cylinder, which is clearly a lot easier to measure:

$$X_{EGR} = (O_{2L} - O_{2VZ})/\{O_{2L} - O_{2nZ}\} \quad 2.33$$

where, O_{2L} = oxygen concentration of air

O_{2VZ} = oxygen concentration before the cylinder

O_{2nZ} = oxygen concentration after the cylinder

Since the mass flow rate of EGR is clearly difficult to measure directly, a crude calculation of EGR_m may be made from measured data:

$$EGR_m\,\% = \{m_a - (m_a)_{EGR}\}100\% / m_a \quad 2.34$$

where, m_a = air mass flow rate to the engine at part load without EGR, at a given engine speed

$(m_a)_{EGR}$ = air mass flow rate to the engine at part load with EGR, at the same engine speed

EGR may also be defined and measured based on the concentration of CO_2, as used by Ricardo (Needham et al 1991), Pierpont et al (1995) and more recently by the Netherlands' Ministry of the Environment (VROM) and Ricardo (Havernith, et al 1997), as shown below:

$$EGR = \frac{CO_2(inlet \sim manifold) - CO_2(ambient)}{CO_2(exhaust)} \quad 2.35$$

If CO_2 is measured with an analyser in ppm, this will provide EGR levels on a volumetric basis.

2.4.3 How EGR Works

EGR will have the following effect on the intake charge of a diesel engine (Wilson et al 1974).

1. The new mixture is warmer (less so with EGR cooling) than the air alone (by virtue of introduction of heated combustion products). Even with EGR cooling, the exhaust gas re-circulated will be hotter than the charge air and will therefore increase the bulk intake charge temperature.
2. The new mixture has a higher mean specific heat (since the combustion products H_2O and CO_2 have more degrees of freedom than air, which is diatomic).
3. The mixture has reduced oxygen concentration.

Additionally,

4. The intake air mass flow is reduced (with conventional "diesel EGR"), and hence the exhaust gas mass flow is also reduced which contributes to lower vehicle tailpipe emissions in g/km.

All the above have an effect on the flame structure, temperature and species profiles, following ignition. The reductions in nitric oxide emissions with EGR can be explained on the basis of predicted decrease in peak flame temperature in a diffusion flame. The factor dominating this suppression is the reduced oxygen mass fraction (Wilson, Muir and Pellicciotti, 1974). The authors conducted IDI and DI single cylinder engine studies to better characterise NO and soot formation in diesel flames, with respect to combustion chamber shape and compression ratio, swirl, and thermodynamic state of the intake charge and fuel injection parameters. With reference to the Zeldovich mechanism, which gives the NOx formation rate rising exponentially with temperature, the authors show that the factor dominating NOx suppression by EGR is the reduced oxygen mass fraction.

Ladommatos et al, (1996) split the effects of EGR on diesel combustion and emissions, into dilution, chemical and thermal effects. The dilution effect is the reduction in the intake charge oxygen level from that of air. The chemical effect is the dissociation at high temperatures of carbon monoxide and water vapour in the EGR gases. The

thermal effect is the increase in the specific heat capacity of the charge gas with EGR, compared to that of air.

2.4.4 Dilution Effect - Reduction of Charge Oxygen Level

Dilution is defined as the reduction in oxygen mass fraction in the inlet charge to the engine through the addition of inert gases (Ladommatos et al 1996).

It is important to note that the ambient oxygen mass fraction dominates the flame temperature. At 30 per cent EGR, by mass, C_p and T_o give rise to offsetting 2 per cent changes in flame temperature, whereas the oxygen mass fraction causes an 11 per cent suppression, (Wilson et al, 1974).

Plee et al (1982) varied the intake oxygen concentration of two single cylinder, IDI engines by adding nitrogen, argon and oxygen, while maintaining a constant start of combustion. They concluded that the major influence on NOx emissions was because of the change in flame temperature rather than the oxygen availability.

Iida and Sato (1988) reported on oxygen enrichment of the intake charge of a DI diesel engine. At fixed injection timing, this resulted in an improvement in fuel consumption, a decrease in injection delay, an increase in NOx and a reduction in particulate emissions. In a later study, Lida (1993) used the two-colour method with a single action rapid compression machine, to reveal that the increase in oxygen concentration in the surrounding gas resulted in a shorter ignition delay and an increase in flame temperature.

Mitchell et al of Pennsylvania State University (1993) experimented with an optically accessible 2-stroke DI diesel to investigate the effects of EGR. EGR was simulated using nitrogen and carbon dioxide as intake air diluents. A compressed air supply was used to simulate turbocharging and intake air temperature was maintained at 121 °C. N_2 and CO_2 were chosen to isolate the effects of specific heat and O_2 concentration of the intake gas. Keeping the start of combustion constant, four nitrogen dilution cases corresponding to 20.9, 19.0, 17.0 and 15.0 per cent O_2, by volume, were examined and three CO_2 dilution cases, as it was only possible to achieve consistent timing settings for

O_2 concentrations of 20.9, 19.0 and 17.0 per cent with CO_2 dilution. Heat release curves showed a substantial increase in premixed burn fraction with increasing dilution, because the reduced O_2 concentration, from 20.9 to 15 per cent caused an increase in ignition delay. Pressure-volume diagrams were produced to find the indicated work done during the cycle. There was no significant change in work output when using N_2 dilution. However, the work decreased by 21 per cent when the intake O_2 concentration was diluted from 20.9 to 17 per cent using CO_2, owing to the change in specific heat of the in-cylinder gas. With N_2 dilution there was no significant change in specific heat. Both N_2 and CO_2 were very effective in reducing NOx emissions see **Figure 2.9.**

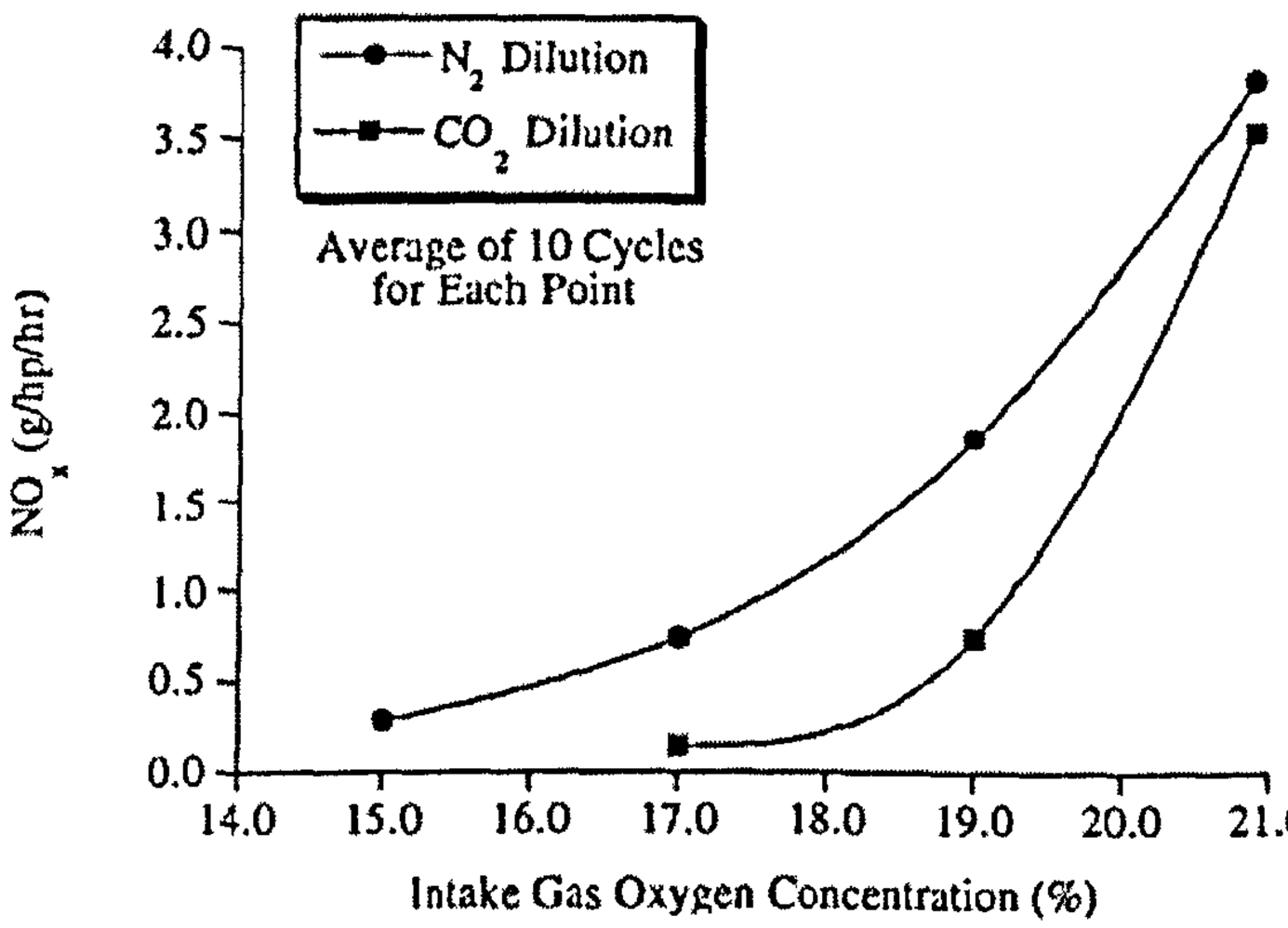

Figure 2.9 Power specific NOx emissions as a function on intake oxygen concentration, 612cc single cylinder 2-stroke DI diesel engine

(Mitchell et al, 1993)

The initial NO formation rate given by Bowman (1975)(Equation 2.36) is extremely dependent on flame temperature but only half-order dependent on O_2 concentration.

$$\frac{d[NO]}{dt} = \frac{6\times10^{16}}{T^{\frac{1}{2}}}\exp\left(\frac{-69{,}090}{T}\right)[O_2]_e^{\frac{1}{2}}[N_2]_e \qquad 2.36$$

where the subscript e indicates equilibrium concentration. In a later publication, Bowman (1992) makes a small revision to this equation, as shown below in equation 2.37.

$$\frac{d[NO]}{dt} = \frac{1.45x10^{17}}{T^{\frac{1}{2}}} \exp\left(\frac{-69{,}460}{T}\right)[O_2]_e^{\frac{1}{2}}[N_2]_e \qquad 2.37$$

The small dependence of NO formation rate on O_2 concentration in the equation cannot explain the large reduction observed in NOx production with the variation in O_2 used in the experiment. Thus the authors concluded that the reduction in NOx emissions must be due to lower flame temperatures. They plotted EINOx in g/kg fuel against inverse of calculated flame temperature shown in **Figure 2.10**, which yielded an activation energy of 73,600 cal/mole for NO formation. All the data using both diluents fell on the same line indicating the dominance of flame temperature.

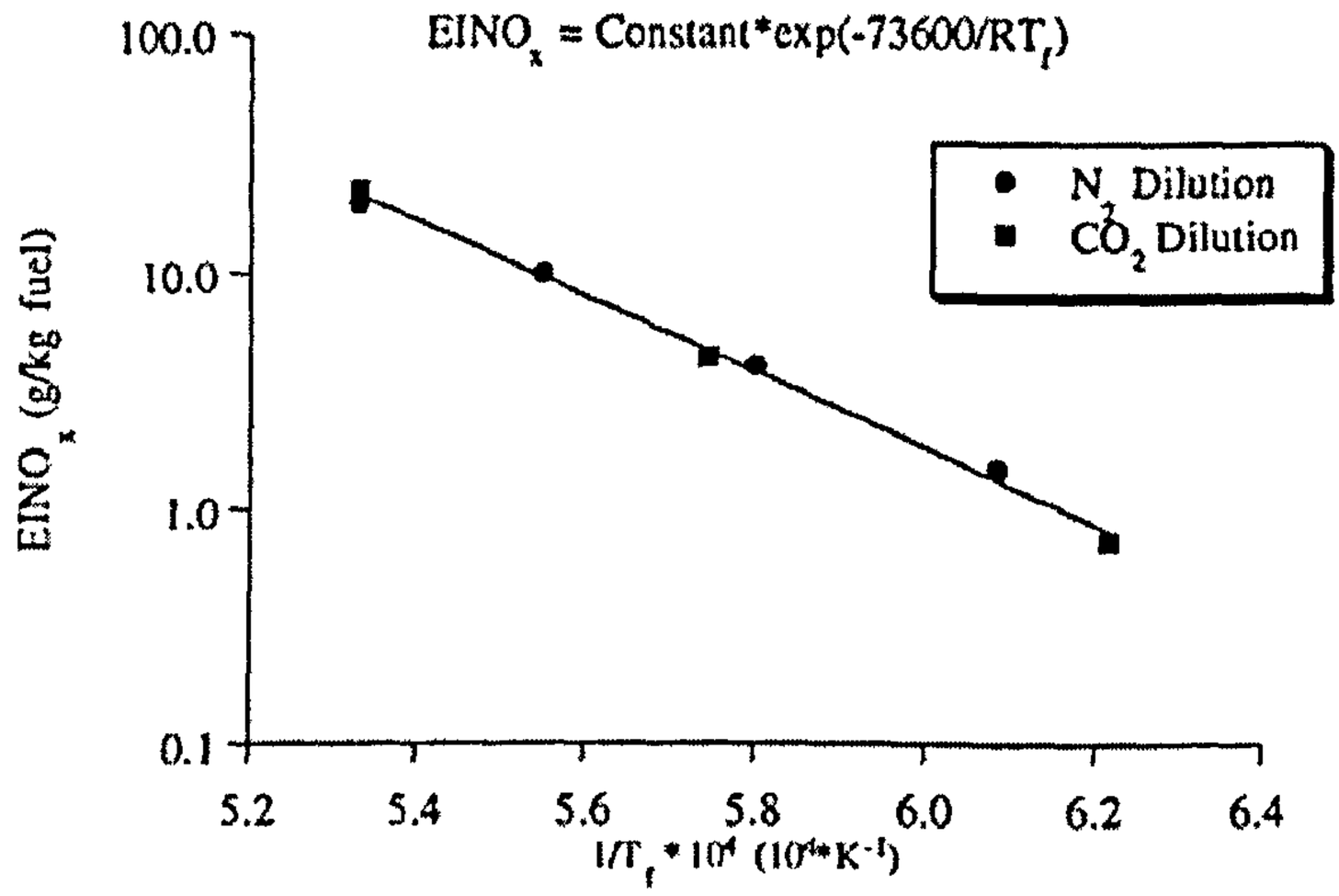

Figure 2.10 NOx emissions versus inverse flame temperature, 612cc single cylinder 2-stroke DI diesel engine

(Mitchell et al, 1993)

Ropke et al (1995) of VW studied the effect of oxygen concentration on NOx emissions from an optical 1.9 litre DI diesel engine. The O_2 concentration was changed from 21 to 12 per cent by adding up to 9 per cent N_2. The side effects of the additional N_2 were considered negligible. The NOx concentration was found to decrease exponentially as the O_2 level was reduced from 21 to 12 per cent. Engine operation below 12 per cent O_2 concentration was found to be impractical owing to incomplete combustion leading to high HC and particulate emissions. Increasing levels of EGR caused a rapid decrease in

NOx levels and correlated well with the results obtained with low O_2 concentrations. The light intensity of combustion was found to decrease rapidly with increasing EGR, as did the flame temperatures, measured by a 5-colour method. Computed NO levels, using a 2-zone model including the extended Zeldovich mechanism for the NO formation, gave a rapid reduction in NO as the O_2 concentration decreased, in agreement with the measured data. Both the measurements and computations demonstrated that the O_2 concentration of the intake charge was the main parameter influencing NO formation, through the effect on flame temperature.

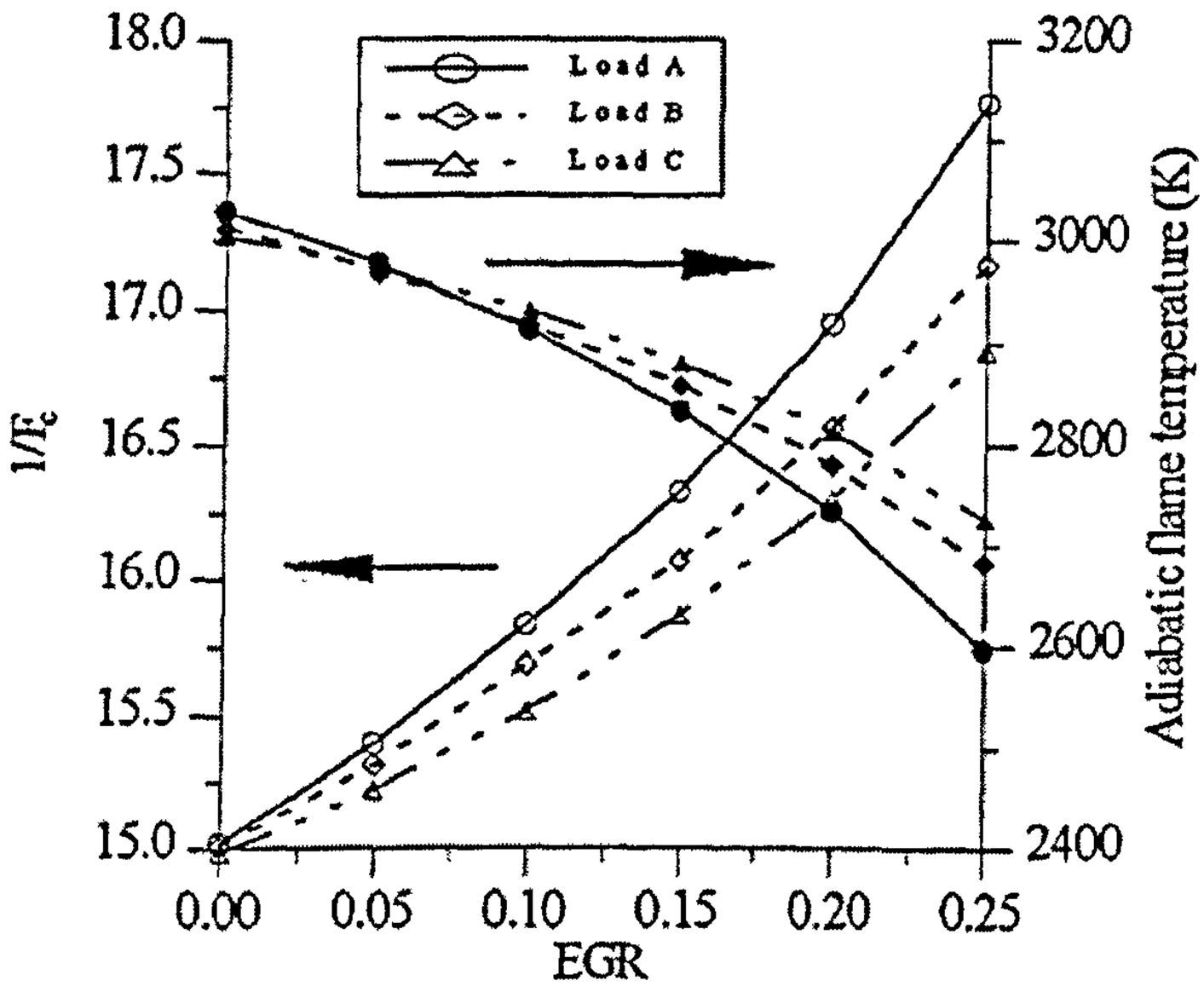

Figure 2.11 Modelled effect of EGR on the combustion equivalence ratio and on the adiabatic flame temperature, for different loads (Lapuerta et al, 1995).

Lapuerta, Salavert and Domenech (1995) concluded that the reduction of NOx emissions with EGR could be mainly explained by the reduction of the adiabatic flame temperature, which was a consequence of the lower oxygen concentration in the charge. They used a phenomenological combustion model, which had a thermodynamic sub-model to distinguish two non-spatially located zones for reactives and products of the combustion process. From the equilibrium composition obtained, the method proposed by Lavoie (1970) for the resolution of the extended Zeldovich mechanism, provided computer results of NOx emissions. The model was also used to calculate the adiabatic flame temperature and combustion equivalence ratio. Tests on a single cylinder DI

diesel engine, based on re-circulation of different amounts of exhaust gas, compared to reference tests without EGR, provided experimental data to validate the model and confirm the findings. **Figure 2.11** shows the modelled effect of EGR on the combustion equivalence ratio and on the adiabatic flame temperature, for 3 different loads. **Figure 2.12** shows experimental results for NOx against increasing levels of EGR for 3 loads and **Figure 2.13** illustrates the reduction of NOx with EGR versus oxygen concentration.

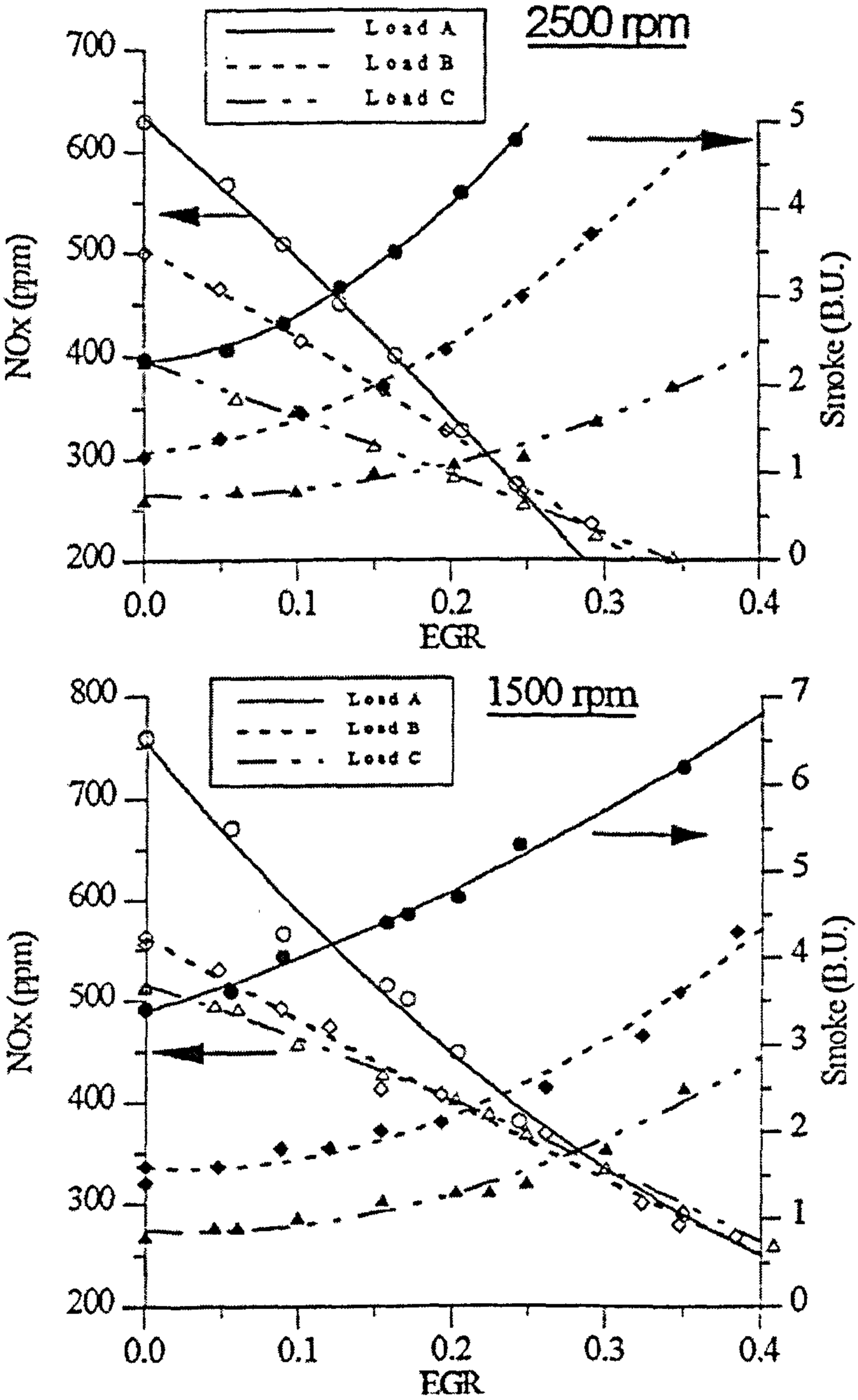

Figure 2.12 NOx and smoke (Bosch Units) measurements for different loads and EGR from a 572cc single cylinder DI diesel engine (Lapuerta et al, 1995).

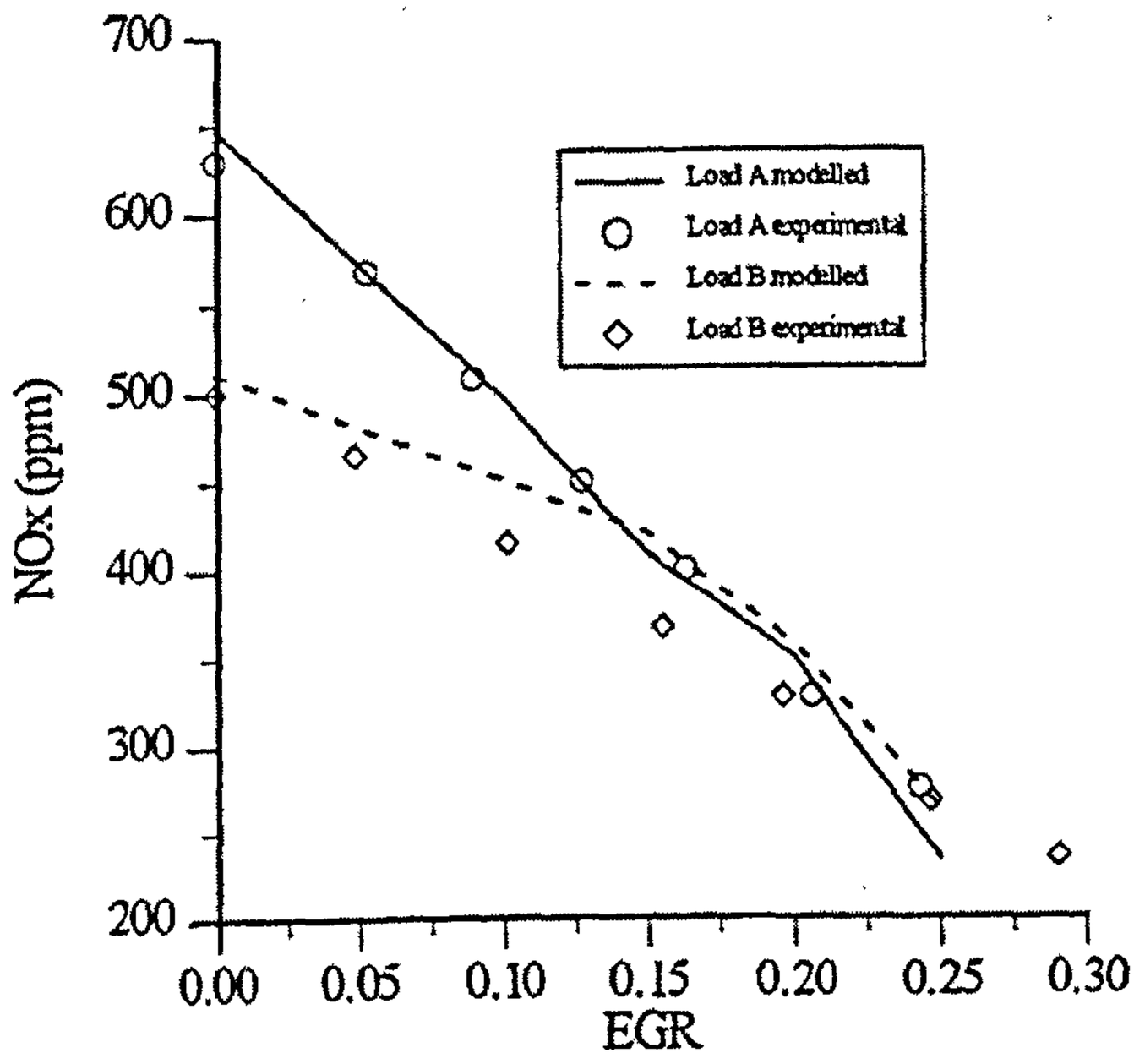

Figure 2.13 Measured and computed NOx emissions for varying EGR and loads at 2500 rpm, 572cc single cylinder DI diesel engine (Lapuerta et al, 1995).

Arcoumanis et al (1995) used the two-colour method to measure in-cylinder flame temperature in a transparent version of a VW 1.9 litre DI diesel engine. At a running condition of 2000 rpm, 2 bar BMEP and 2° BTDC SOI increasing EGR from zero to 30 per cent reduced the area of high temperature. Images at 14° and 18° ATDC showed a reduced number of areas at around 2200K compared to the zero EGR case. At 50 per cent EGR the trends were more pronounced. At 2000 rpm, 10 bar BMEP with 30 per cent EGR the flame image showed considerably lower average temperatures (2.4 per cent less) than the zero EGR case at 10° ATDC. There were also fewer areas of 2200K. At 18° ATDC the core temperature was at 2080K, down from 2240K without EGR.

Ladommatos et al (1996) conducted a number of carefully controlled engine tests to isolate the dilution, thermal and chemical effects. To isolate the dilution effect, both the thermal and chemical effects had to be eliminated. This was achieved by replacing some O_2 by a chemically inert gas, which had the same specific heat capacity as O_2. The diluted charge caused the delay period to increase. A cetane improver was added to eliminate the effect of the longer ignition delay. The inlet charge dilution resulted in a

remarkable decrease in the in-cylinder peak heat flux, and the peak cylinder gas temperature and pressure. Both NO and NOx decreased with inlet charge dilution, the

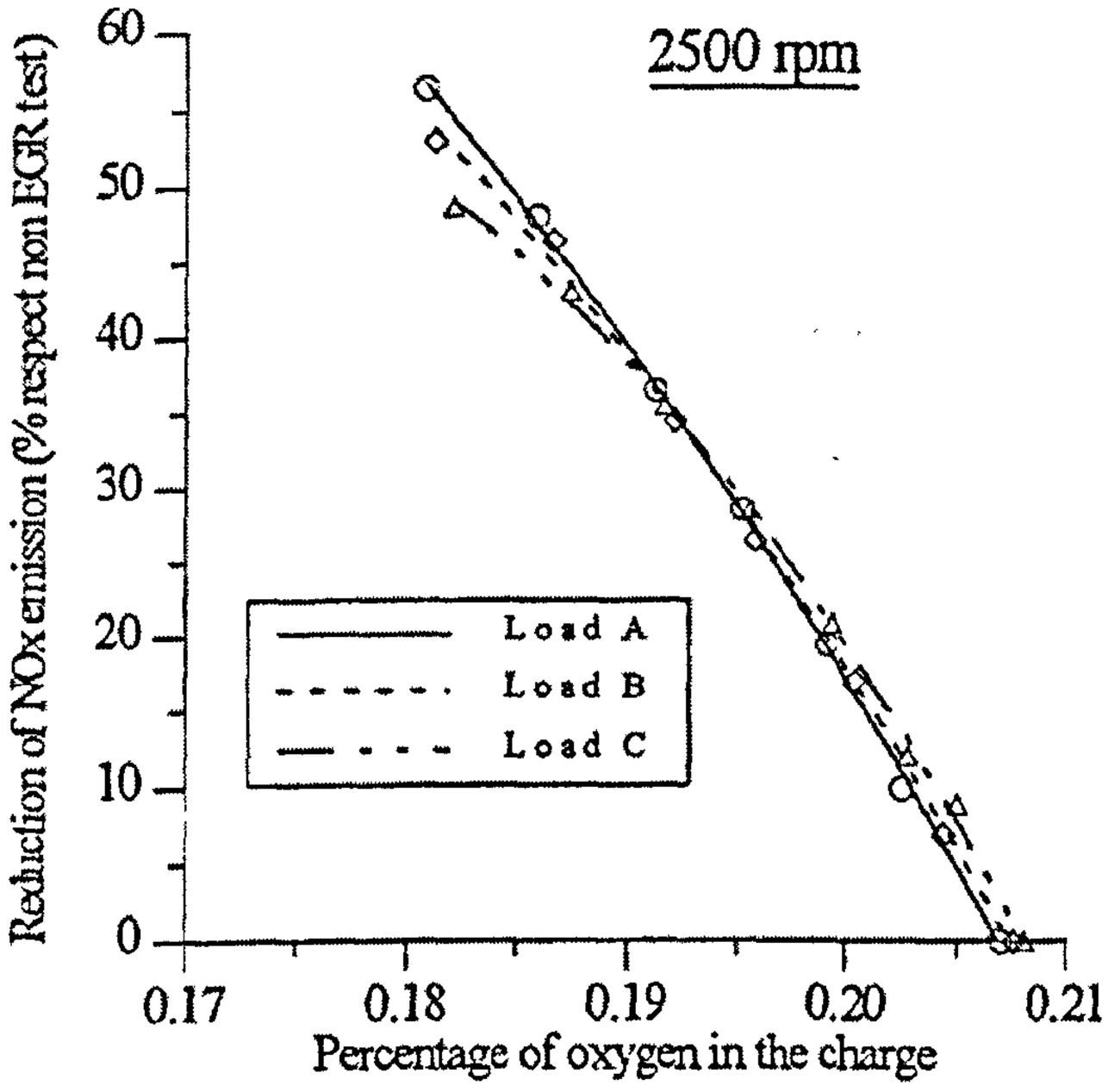

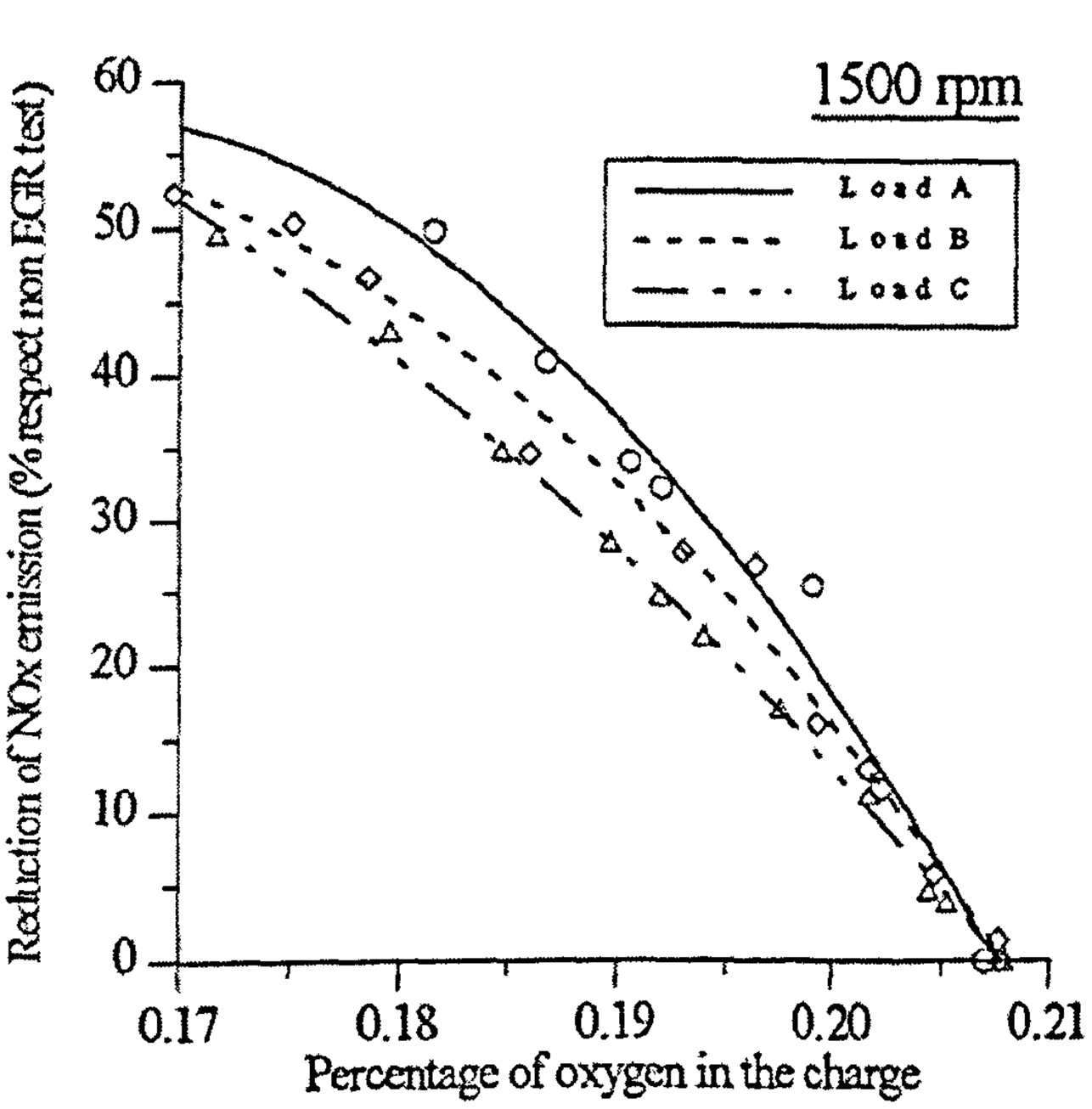

Figure 2.14 NOx reductions with EGR versus oxygen concentration in the charge, 572cc single cylinder DI diesel engine (Lapuerta et al, 1995).

influence of oxygen availability and its consequent effect on flame temperature had the dominant effect (Ladommatos et al 1996).

Ladommatos et al (1996) used, as an example, the case of a 2.5 litre DI TCI engine running at 2000 rpm, 5.6 bar BMEP, with EGR at 700°K displacing 25 per cent of the volume of the intake air at 300°K. They estimated that this resulted in a charge temperature of 360°K. The displacement of O_2 by CO_2 and H_2O resulted in a reduction in the oxygen / fuel ratio of around 7 per cent. This reduction in the O_2 concentration in the flame zone interferes with the fuel oxidation rate and reduces the flame temperature. According to Wilson et al (1974) the reduction in flame temperature owing to the lower O_2 availability is the dominant NOx suppressing mechanism. With 30 per cent EGR, Wilson et al estimated that the flame temperature would be suppressed by 11 per cent owing to the reduction in O_2 concentration and 2 per cent because of the increase in specific heat capacity of the inlet charge.

2.4.5 Chemical Effect

The chemical effect of EGR refers to the dissociation of CO_2 and H_2O and the participation of the products of dissociation in the combustion process (Ladommatos et al, 1996). Ropke et al (1995) suggested that the addition of CO_2 to the intake charge of diesel engines could lead to two-step thermal dissociation. The first step involves the dissociation of CO_2 to produce O_2 while in the second step O_2 dissociates to produce O, atomic oxygen. The atomic oxygen is essential for NO formation through the Zeldovich mechanisms. However, this source of atomic oxygen was found to be of minor importance, when applying EGR, because EGR also causes a decrease in flame temperature that lowers the rate of dissociation of CO_2.

On diluting the intake air with CO_2 and nitrogen in separate experiments, Mitchell et al (1993) found that the addition of CO_2 resulted in a substantial decrease in both NOx and soot emissions.

Ladommatos et al (1996) investigated the chemical effect of EGR. They isolated the chemical effect by keeping the O_2 concentration constant and maintaining the thermal capacity equal to air, even with an increased level of CO_2, by removing some N_2 and

adding argon to offset the higher heat capacity of CO_2. Thus the chemical effect of CO_2, a principal constituent of EGR, was investigated. Moreover, the authors compared the cumulative dilution and chemical effect test, with the dilution effect, to give the actual chemical effect of the introduction of EGR. The chemical effect of CO_2 was found to be responsible for about 10 per cent of the total reduction of NO and NOx emissions. They proposed that this could be attributable to the hydrocarbon radical reducing NOx, as reported by Miller and Bowman (1989). Additionally, CO emissions were doubled, to 2000 ppm with 6 per cent CO_2 replacing oxygen in the intake charge. The reactive CO gas could have possibly reduced NOx (Ladommatos et al 1996).

2.4.6 Thermal Effect - Specific Heat Capacity

The thermal effect is defined as the reduction in NOx owing to the increase in specific heat capacity of the intake charge with EGR, or diluent gases, to that of air. Both carbon monoxide and water vapour, which are present in exhaust gas, have higher specific heat capacities than air.

Ohigashi and Kuroda et al of Nissan Motor Company (1971) tested the hypothesis that NOx formation is primarily affected by heat capacity of the combustion gases and recycled exhaust. Tests were conducted in a spark ignition engine. Inert gases, helium, argon, nitrogen, carbon dioxide and water vapour were re-circulated, as well as exhaust gas, into the intake manifold. The authors plotted the heat capacity of the combustion gases per kg of fuel on NO levels, at A/F ratios of 13:1, 15:1 and 17:1, with varying amounts of admitted inert gases. The trend of the graphs indicated that as the heat capacity of the cylinder charge increased, the NO emissions were reduced for a given A/F ratio. They also found that increased heat capacity retarded the combustion, although they found that EGR is more effective than retarded ignition for controlling NOx emissions.

Durnholz et al (1992) advocated hot EGR for high speed DI diesel engines to reduce NOx as well as HC and particulate emissions. They sighted the decisive factor for the reduction of the adiabatic combustion temperature as the higher molar heat capacity of the re-circulated exhaust gas in comparison with air. They experimented with added gases, using nitrogen and carbon dioxide. Carbon dioxide gave a greater reduction of

NOx than nitrogen, which they attributed to the 1.6 times higher molar heat capacity compared to nitrogen. They concluded that EGR has a specific influence on the local conditions that effect the NOx formation:

- a larger amount of gas that does not participate in combustion but takes heat from the process
- by a reduced probability that fuel and oxygen molecules meet.

Durnholz et al (1992) favoured hot EGR because of the measured reduction in HC emissions, for a neutral effect on NOx, the latter being explained by the lower volumetric efficiency with hot EGR. Particulates were found to be relatively insensitive to intake temperature, because of the trade-off between soot and adsorbed hydrocarbons.

Ladommatos (1996) split the effects of EGR on diesel combustion and emissions, into dilution, chemical and thermal effects. The thermal effect is the increase in the specific heat capacity of the charge gas with EGR, compared to that of air. The authors looked at the effects of carbon dioxide (CO_2), one of the principal constituents of EGR. To isolate the thermal effect, the dilution and chemical effects were eliminated, by keeping the O_2 concentration constant and using helium to replace some N_2 , to increase the specific heat capacity of the charge. The thermal effect was found to be of minor importance in lowering NOx emissions, compared to the dilution and chemical effects.

2.4.7 Latest Developments in Use of EGR for Reduction of NOx Emissions

Apart from the wider use of electronic controls and closed loop feed-back on EGR valve lift (Ford 2.5 DI T/C in Transit) or on air mass flow, for more accurate operation of the EGR systems, in terms of effectiveness, the latest developments centre around the use of cooled EGR for HSDI diesels. Since un-cooled exhaust gases are considerably hotter than the intake air, replacing some of the intake air with EGR will cause a small increase in the overall charge temperature. This will have the tendency to increase NOx formation. The full potential of EGR in reducing NOx may be realised by cooling the EGR prior to mixing with the intake charge. Thus heating of the intake charge is minimised or the total charge may be cooled depending on the relative mass flows and temperatures. Cooling the EGR also moderates the decrease in engine volumetric

efficiency which allows a greater oxygen to fuel ratio at a given level of EGR.

2.4.8 Cooled EGR

The full potential of EGR in reducing NOx will not be realised unless the EGR is cooled. This is because the EGR is at high temperature, hotter than the intake air it replaces, which results in an increase in the overall intake charge temperature.

Cooling the EGR prior to mixing with the intake air lowers the combustion temperatures and increases oxygen to fuel ratio. The higher flow of CO_2 and H_2O into the engine with cooled EGR increases the heat absorbing capacity of the inlet charge; the lower inlet charge temperature generally reduces the combustion temperatures. The slight increase in O_2 availability may raise the flame temperature, (Wilson et al 1974), but is beneficial for soot control. Because the bulk intake charge density is higher with cooled EGR, the engine volumetric efficiency is increased compared to the case with hot EGR. This reduction in pumping work translates to an improvement in fuel consumption.

Cooling the EGR will also have a number of other complex effects, some of them undesirable. For example, it can increase the ignition delay and the amount of premixed fuel burned. This would tend to increase NOx production depending on a number of factors including injection timing. With cooled EGR, the lower inlet charge and lower compressed gas temperature can also reduce the fuel vaporization and mixing rate and lead to an increase in exhaust hydrocarbon levels (Ladommatos et al, 1996). However, in practice further significant reductions in NOx, particulates and improvements in fuel economy may be achieved with cooled EGR, compared to hot EGR.

Table 2.4

EC Passenger Car Type Approval Standards - 91/441/EEC

Diesel Engine Type	CO g/km	HC + NOx g/km	Particulates g/km
IDI diesel	2.72	0.97	0.14
DI diesel derogation (40%) until 1994	3.81	1.36	0.20

Ford introduced an EGR cooler for the 85PS turbocharged 2.5 litre DI diesel in Transit in 1995. The application of cooled EGR, with some revisions to the calibration, enabled this vehicle to meet the EC Stage 1 passenger car emission standards. The EGR cooler provided the ability to flow a greater mass of EGR. A diagram of this system is shown in **Figure 3.10** in **Chapter 3.** The earlier model introduced in 1993, without EGR cooler, met Stage 1 passenger car standards with the 40 per cent DI derogation. **Table 2.4** shows the relevant emissions levels.

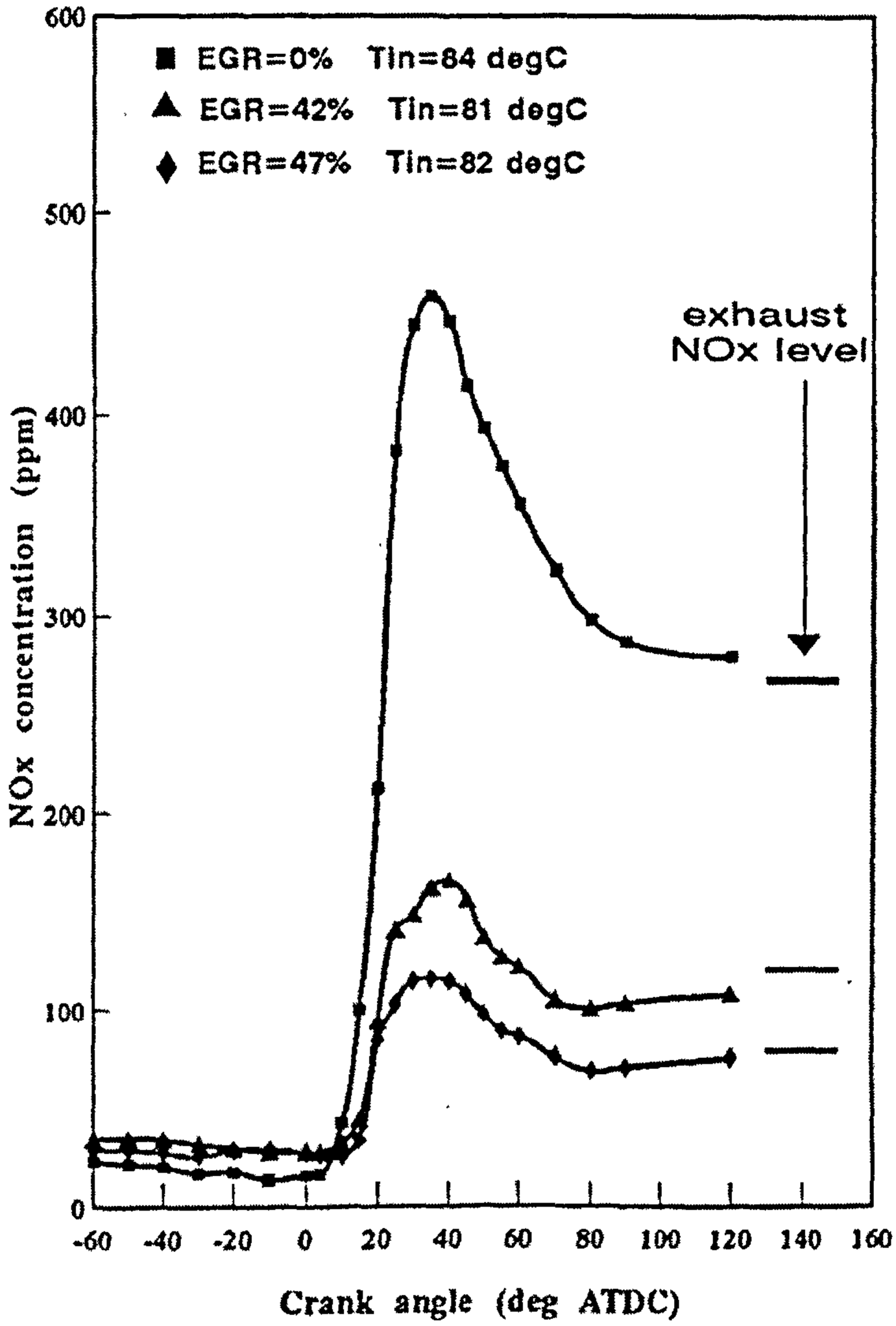

Figure 2.15 The effect on in-cylinder and exhaust NOx concentration for inter-cooling and cooled EGR, Ford 2.5 turbocharged DI diesel engine

(Ladommatos et al, 1996)

The advantages of inter-cooling and EGR cooling on NOx emissions are nicely illustrated by the in-cylinder measurements taken at Brunel University by Ladommatos et al (1996) on a Ford 2.5 litre turbocharged DI diesel. **Figure 2.15** shows in-cylinder and exhaust NOx concentrations for EGR levels of zero, 42 and 47 per cent, while maintaining an almost constant intake charge temperature of 82°C by inter-cooling and EGR cooling. The in-cylinder and tail pipe NOx levels were more than halved by 42 per cent EGR, at a similar charge temperature.

Cooled EGR was applied to a prototype 1.8 litre DI turbocharged and inter-cooled engine installed in an Escort car. The benefit the EGR cooler had on NOx emissions and fuel economy, without any deterioration in particulate emissions is illustrated in **Figure 2.16** (Hawley et al, 1998).

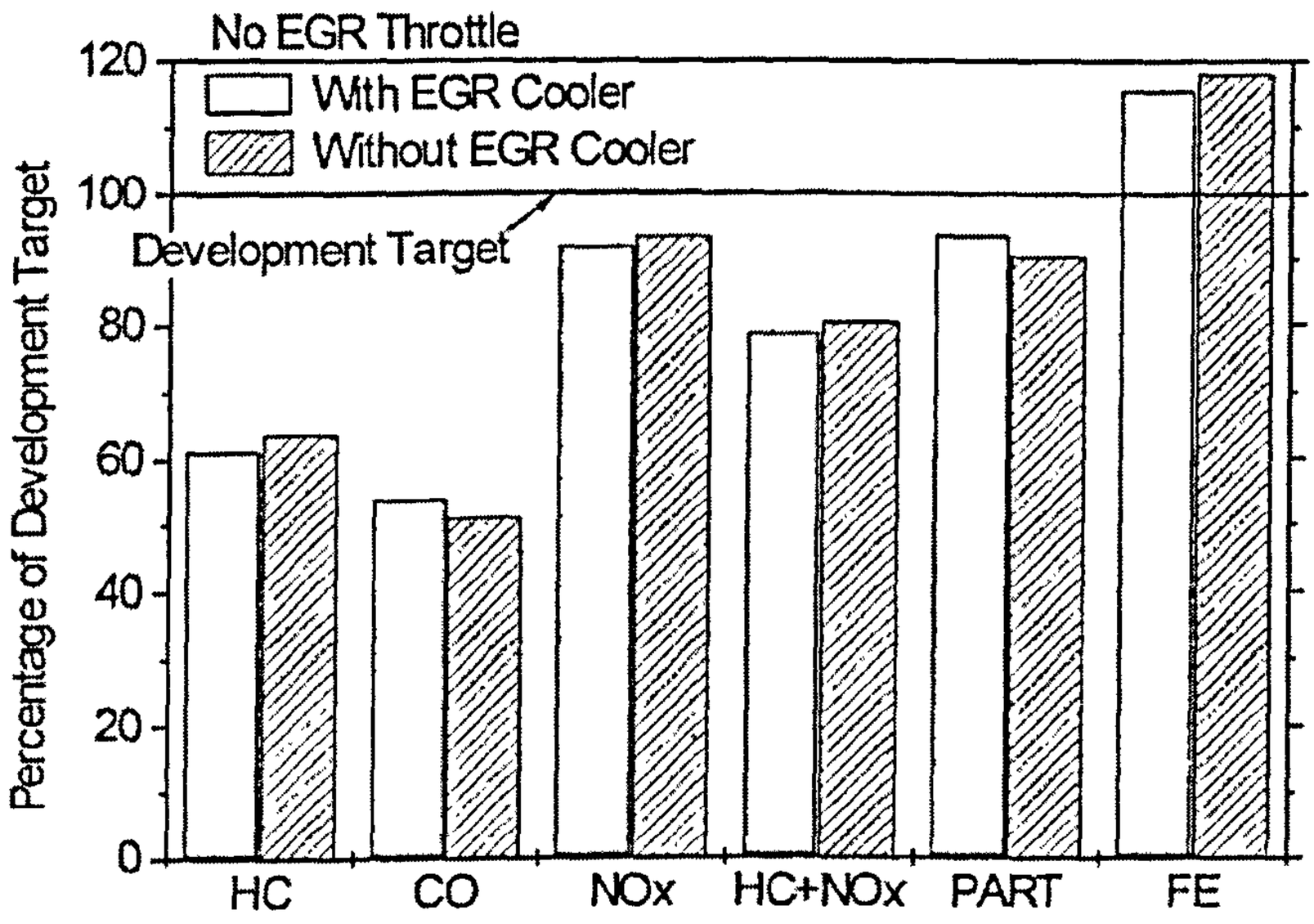

Effect of EGR cooler on vehicle emissions results

Figure 2.16 Histogram illustrating the benefit of EGR cooling on NOx and Pm emissions and fuel economy for a prototype 1.8 litre DI TCI diesel in an Escort car.
(Hawley et al, 1998)

Torpey, Whitehead and Wright of Ricardo (1971) compared emissions from a DI and IDI Ricardo E16 single cylinder engine. In general the DI emitted twice the NO emissions than the IDI at optimum injection timing, although similar amounts of

injection retard brought the peak levels much closer to the IDI. Cold EGR was found to be more effective than hot EGR in reducing NO levels from the IDI diesel. It is interesting to note that while these authors concluded that cold EGR was more effective, it was not until 1995 when Ford introduced an EGR cooler for the 2.5 diesel in Transit, that this concept was used for a production automotive engine.

Ladommatos et al (1996) conducted experiments with a 2.5 litre turbocharged DI diesel engine which demonstrated that at 2000 rpm, 3 bar BMEP, cooling EGR at a nominal volumetric rate of 48 per cent, reduced the charge temperature from 124 to 82 degrees C. This also increased the mass flow of EGR. A substantial reduction in in-cylinder NOx formation and exhaust level was achieved by keeping the start of combustion constant, by advancing the injection timing to compensate for the longer delay period with the cooler charge, see **Figure 2.17**. They compared the un-cooled and cooled EGR cases, for 25 per cent EGR by volume, at an engine speed of 2000 rpm and 5.6 bar BMEP, for a 2.5 litre T/C DI diesel. Cooling the EGR had the following effects on the intake charge:

- maintained the inlet charge at 49 g/s as opposed to 42 g/s with hot EGR
- resulted in 1.2 g/s of CO_2 and 0.5 g/s of H_2O in the inlet charge to the engine compared to 0.52 g/s of CO2 and 0.2 g/s of H_2O when EGR is hot
- resulted in 10 g/s of O_2 in the inlet charge to the engine compared to 9.13 g/s of O_2 when EGR is hot
- the inlet charge temperature was at 300 K compared to 360 K with hot EGR.

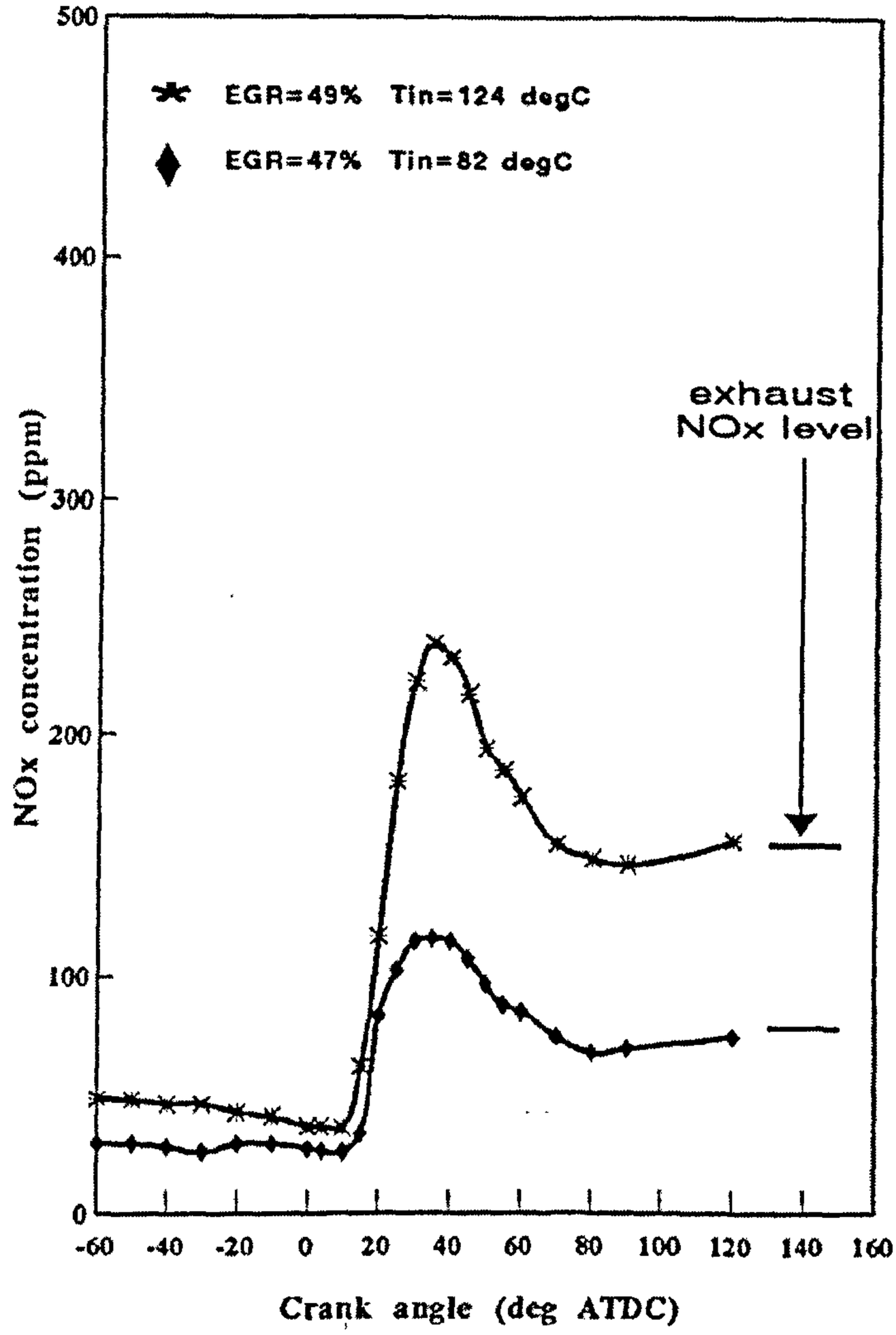

Figure 2.17 The effect on in-cylinder NOx concentration, of cooling the inlet charge with EGR at constant start of combustion, at 2000 rpm, 3 bar BMEP. Ford 2.5 DI turbocharged diesel engine (Ladommatos et al, 1996)

Horrocks and Robertson (1996) described the EGR system for a prototype 16-valve 2.5 litre high speed DI diesel. A schematic diagram of the EGR system is shown in **Figure 2.18.** An Electronic Control Unit (ECU), which, together with pump control also included the capability of modulated control of EGR valve and EGR throttle, and subsequently control of intake port de-activation. The ECU took information from a complete spectrum of engine sensors including crankshaft position, coolant temperature, air charge temperature and pressure, EGR control positional feedback, together with feedback from the pump itself. The EGR hardware consisted of an electronically controlled vacuum operated poppet type EGR valve mounted on the exhaust manifold,

the EGR gases were then cooled by passing through a Serck gas to water shell-and-tube heat exchanger, engine coolant was used for the water side cooling media. To generate sufficient pressure drop to flow the desired volume of EGR under some part load regions where EGR optimum levels for best emissions were higher than would naturally flow through the EGR valve, a throttle valve was incorporated in the induction system. This was operated when desired, such that boost pressure and air charge flow was restricted to favour the flow of exhaust gases from the EGR cooler.

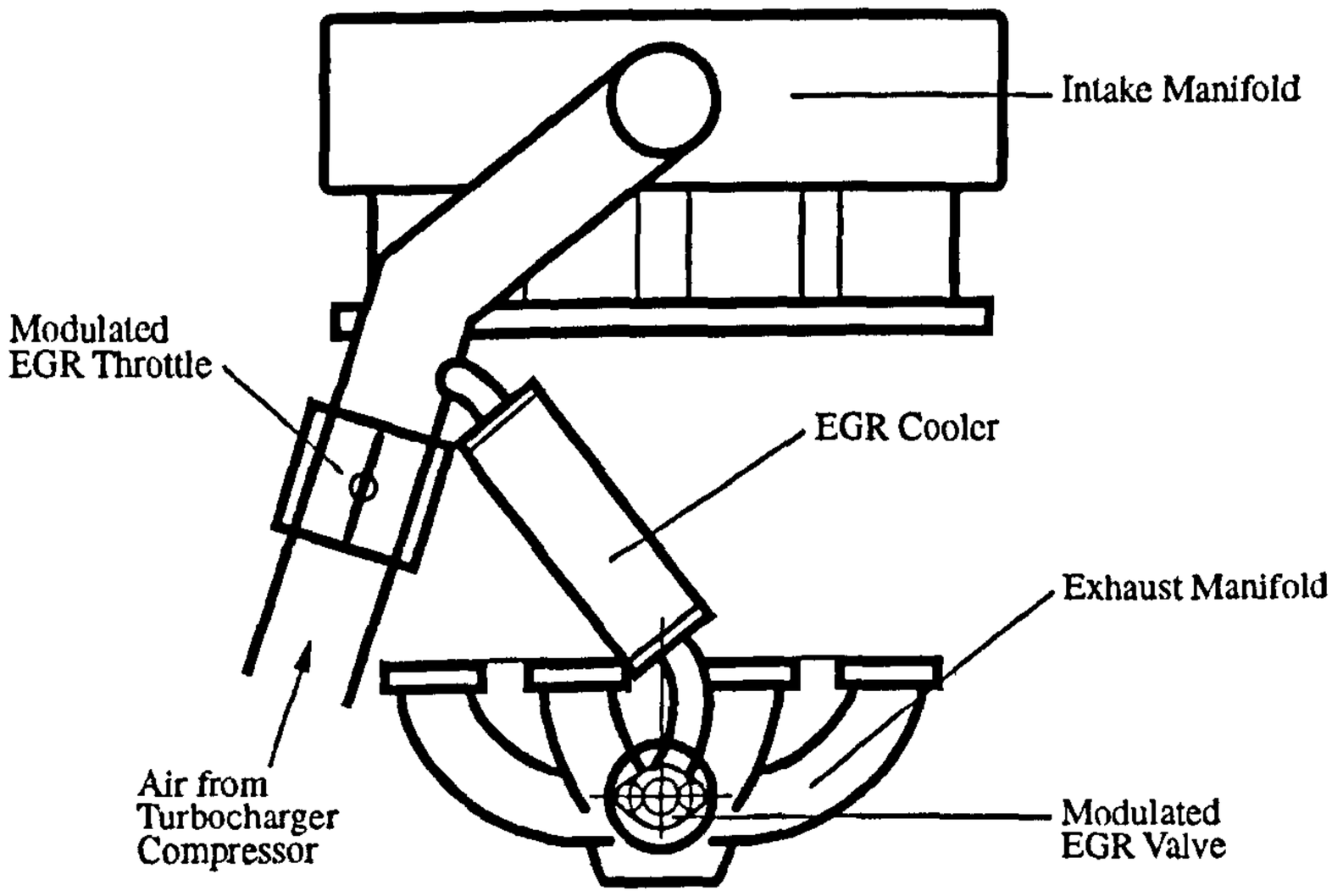

Figure 2.18 Schematic diagram of EGR system used on a prototype 16-valve 2.5 litre DI diesel engine (Horrocks and Robertson, 1996)

A review of production diesel engine EGR systems is included in **Chapter 3**.

2.4.9 Additional EGR

The conventional method of introducing EGR in diesel engines involves displacing some of the intake air with exhaust gas, causing a reduction in the air/fuel ratio, for a given engine speed and torque. If EGR could be added to the intake air charge, the air/fuel ratio would be maintained. Thus with "additional" EGR, the oxygen to fuel ratio would be maintained constant, so as not to increase significantly the soot production from the engine. The CO_2 and water vapour in the EGR then becomes

"additional" to the airflow to the engine, absorbing energy released during combustion, lowering the flame temperature and NOx formation. This method can potentially deliver large reductions in NOx with significantly less increase in particulate emissions than conventional EGR.

"Additional" EGR is best applied to a turbocharged engine with a variable geometry turbocharger and a venturi in the intake system to provide a favourable pressure difference to aid the exhaust gas flow into the intake system. Baert et al (1996) developed such a system for a 12 litre heavy-duty diesel engine. The authors' objective was a 50 per cent reduction in NOx over the ECE R49 cycle, without any increase in particulates. Thus EGR was required under full load conditions. To achieve this, the authors used a short EGR route, tapping-off exhaust gas before the turbine, cooling the gas and mixing it with the intake air by a venturi, after the compressor and intercooler. As the variable geometry turbine flow area was reduced, by closing down the vanes, pre-turbine pressure increased. When this pressure exceeded that at the venturi throat, EGR flowed. The authors were able to flow 15 per cent additional EGR over most of the engine operating range.

Ladommatos et al (1996) conducted some engine tests where an additional 1 g/s per cylinder CO_2 was added to the normal air mass flow rate of 10 g/s per cylinder. Substantial reductions in NOx emissions were recorded, in excess of 60 per cent, but this was accompanied by a 40 per cent increase in HC emissions and a 35 per cent increase in particulates. The increase in particulates was found to be entirely due to the shorter delay period. Bringing the delay period back to the baseline level with an ignition improver returned the particulates back to the baseline level as well.

2.4.10 Water Injection

Water injection may be classified into three cases (Odaka 1991):

a) in-cylinder water injection, where water is injected directly into the combustion chamber

b) injection outside the cylinder, where water is mixed with the inlet air charge in the intake system

c) water-oil-emulsion, where the water is mixed with the fuel to form an emulsion

Odaka (1991) selected to use inlet manifold water injection because of the low pressure necessary and the fact that there was no requirement to modify the combustion chamber or fuel injection system. Water was injected towards the intake port, during the induction cycle of each cylinder. Injection quantity was related to engine speed and controlled by varying the nozzle opening time. Over 40 per cent reduction in NOx was obtained at full load with 30 litre/hour water injection, this was at approximately 0.7 water to fuel weight ratio (W/F). For a given W/F ratio, the reduction in NOx was greater at higher engine loads. Emissions of HC increased at part load with the use of water injection. A slight increase in smoke was observed as the absolute humidity of the intake charge was increased. With a combination of water injection and EGR, NOx reductions of 50 to over 70 per cent were achieved, over the load range at an intermediate speed. Optimum NOx reduction was achieved with a combination of EGR and modulated water injection, which reduced water consumption to around 30 per cent of fuel flow. Corrosion and water consumption were cited as disadvantages to this method.

Torpey, Whitehead and Wright of Ricardo (1971) found water injection, into the inlet manifold, to be very effective in reducing NOx emissions levels from an IDI Ricardo E16 single cylinder engine, although the authors acknowledged that long-term effects of water injection must be investigated before it could be used as a practical method of reducing NO emissions. For automotive use there is the additional issue of storing the water on the vehicle and introducing it into the engine in a controlled manner.

Ishida and Chen of Nagasaki University (1994) investigated the effect of added water in the intake air and emulsified fuel, on NO formation. Both experimental and theoretical analyses were conducted, considering the changes in specific heat and air entrainment rate of the burned gas in the combustion chamber. The specific heat was calculated by the chemical equilibrium composition analysis considering the absolute humidity of the intake air, the amount of water added in the emulsified fuel as well as the residual gas fraction. To estimate the NO formation rate, the authors used a two-zone combustion model to calculate the burned gas temperature. Experimental engine tests showed that 0.01 kg/kg increase in absolute humidity of the intake air, corresponding roughly to 1 per cent increase in specific heat capacity, resulted in approximately 20 per cent reduction in NOx emissions. It was also shown that the NOx reduction owing to 20 per

cent water emulsified in the fuel was almost equal to that of the 1 per cent increase in specific heat capacity of the intake air.

Water vapour addition to the intake gas should have a similar effect on the NO formation as CO_2, the increased heat capacity lowering the flame temperature and reducing NO formation. Both gases are 3-atomic molecules with high heat capacity and can produce O_2 by thermal decomposition. The molar heat capacity of H_2O is, however, less than that of CO_2. Both engine measurements and computed results by Ropke et al (1995) demonstrated a significant reduction in NOx with the addition of water vapour in the intake charge.

Using water-in-oil emulsions with an ASTM-CFR engine, Cook and Law (1978) found that the optimum amount of water addition for minimum emissions was between 10 and 20 per cent.

The use of water injection, particularly with EGR, is an effective method of reducing NOx emissions from diesel engines. However, for automotive diesel engines water injection poses a number of problems that make it virtually impractical for vehicles, particularly passenger cars. Firstly, an extra storage tank on the vehicle would be required, which would need to be around a quarter the size of the fuel tank; or a similar increase in the size of fuel tank would be required in the case of water-in-fuel emulsions. Secondly, a means would be required for the controlled introduction of the water to the engine, that is, an additional metering system. If the water was combined with the fuel before the engine fuel injection pump, which would have to be in the form of an emulsion, there is the issue of corrosion of the high-pressure injection pump, pipes and injectors. There is also the additional volume of liquid to be injected by the fuel injection system. Finally, there will be a greater risk of in-cylinder corrosion.

2.4.11 Summary

- Exhaust gas re-circulation is a system whereby a proportion of the exhaust gas is diverted back into the intake system. Presently, diesel systems replace air with EGR gas, up to 60 per cent by volume.

- EGR is currently a very effective way of reducing NOx emissions at part load.

- EGR reduces NOx formation and emissions by lowering the flame temperature.

- EGR lowers the flame temperature through two effects; by dilution, reducing the oxygen mass fraction, and by a thermal effect, increasing the specific heat capacity of the charge. The dilution effect is by far the greater of the two.

- Cooling EGR prior to mixing with the intake charge provides further reductions of NOx emissions and is generally beneficial to particulates. The higher volumetric efficiency with cooled EGR leads to an improvement in fuel economy.

- Practical EGR systems consist of an EGR valve and a transfer pipe connected to the intake system, and a control system. Additional components such as an air flow meter, a throttle valve and cooler may be added to the system for improved control and effectiveness.

- Additional EGR may provide further reductions in NOx by enabling EGR to be used at full load.

- Water addition, either injected with the intake air charge, or as a water-in-fuel emulsion, will reduce NOx emissions and is more effective in combination with EGR. However it is impractical for automotive use owing to the relatively large amount of water required and problems with corrosion.

2.5 Fuel Effects on NOx Emissions

2.5.1 Introduction

Diesel fuel will affect the NOx emissions from diesel engines in two fundamental ways, by the physical and the chemical properties. It is, however, quite difficult to separate the effects of each, because the two sets of properties are to a large extent interdependent and it is hard to prepare fuels with different physical properties without affecting the chemical properties, and vice versa. Diesel fuel injection pumps effectively control the injected fuel quantity on a volumetric basis, thus the physical properties of the fuel, such as density and viscosity will affect the mass of fuel injected. The viscosity also affects the fuel spray formation and thereby, the air/fuel mixing. The viscosity of the fuel will also affect the timing control on mechanical pumps for high-speed engines and the sensitivity of injection timing to NOx emissions has been documented already. The chemical properties will affect the delay period, ignition temperature and consequently the heat release profile. It is obvious that the longer the delay period, the greater will be the amount of fuel accumulated in the combustion chamber before the start of combustion. This results in higher rates of pressure rise and maximum gas pressures and temperatures (Patterson and Henein, 1972). The relationship between increased maximum flame temperature and higher rates of NOx emissions has been well established in an earlier section.

The fuel properties reviewed under this section are those that will influence the formation of NOx; namely, density, viscosity, cetane number, volatility and the hydrocarbon type. Fuel additives for improving cetane number, NOx reduction additives and oxygenates, are also reviewed.

2.5.2 Density

Because diesel engine fuel injection pumps are in the main controlled on a volumetric basis, changes in fuel density will affect the mass of fuel injected. An increase in fuel density will therefore increase the mass of fuel injected for a given engine condition and ultimately enable the engine to produce a higher BMEP at full load. This will cause an

increase in peak pressures and temperatures leading to an increase in NOx formation and emission. If the engine has part load timing control and an EGR system which uses the fuel injection pump speed control lever as an engine load input signal, then a change in fuel density will cause an error in these controls and the level of EGR, compared to the original calibration with the reference fuel. For example, an increase in fuel density will reduce the fuel pump lever angle at part load for a given BMEP.

Burley and Rosebrock (1979) conducted engine tests using an Oldsmobile 5.7 litre IDI diesel, at 5 speed/load points with 46 experimental fuels. The fuels comprised of fuel blends, fuel additives, emulsions and heated fuels. They found that oxides of nitrogen did not correlate well with fuel characteristics. A statistical analysis indicated only slight correlation, but NOx emissions appeared related to aromatic content, specific gravity (density) and 90 per cent boiling point. They found, tentatively, that low values of these characteristics were accompanied by low NOx.

McCarthy et al (1992) demonstrated a good correlation between reducing NOx emissions with increasing American Petroleum Institute (API) gravity, that is, with lower specific gravity. This would be due to two factors, the lower fuel specific gravity would reduce full load power and secondly there was a reduction in aromatic content and hence a shorter delay period. The testing was conducted with a 1994 emission level Navistar DTA 466 heavy-duty DI diesel following the EPA transient test procedure.

2.5.3 Viscosity

Fuel dynamic viscosity will effect the mechanical operation of the fuel injection pump. High viscosity will increase the loading on the pump and the injection pressure levels, whilst low viscosity will increase leakage past the pumping elements. A change in the relationship between the speed control lever and the quantity of fuel delivered by a mechanically controlled pump, may affect the quantity of EGR if the control system relies on the speed control lever for fuel quantity input. Low viscosity may also result in increased wear of the moving components of the pump.

Miyamoto et al (1992) found that NOx emissions decreased at 3 injection timings, with increasing kinematic viscosity. This was because the higher viscosity lead to decreased

premixed combustion in a single cylinder DI naturally aspirated engine. This indicated deterioration in mixture formation with higher kinematic viscosity fuels.

2.5.4 Cetane Number

For a given number of carbon atoms, the straight-chain alkanes have the highest cetane numbers. Within this series; the larger the molecule the higher the cetane number. The best fuels for compression-ignition engines are high in alkane content, with average molecular weights greater than those of gasolines, typically a molecular weight of 170 for automotive diesel fuel compared to 110 for gasoline (Heywood 1988). Commercial kerosene is an excellent compression-ignition fuel. Isomeric compounds, double bonded alkenes and aromatics have molecules that are more resistant to pyrolosis and, therefore, have lower cetane numbers.

One of the properties of fuel that could be expected to influence NOx emissions is cetane number, because it will affect ignition delay and hence the amount of fuel mixed prior to the start of combustion. It is widely accepted that increasing the cetane number represents one option for production of cleaner burning diesel fuels. Numerous studies have demonstrated that increasing cetane number of the fuel significantly reduces all the regulated emissions, especially particulate matter and nitrogen oxide (Nandi et al, 1994). Broering and Holtman (1974) found cetane number to be the most significant fuel property affecting emissions. They reported between 23 to 25 per cent increase in NOx levels when changing from 47 to 33 cetane fuel, also that naturally aspirated engines were more sensitive than turbocharged versions. Flanigan et al (1989) reported higher NOx levels for fuel blends of pure hydrocarbons owing to longer ignition delays. From their regression analysis the production of NOx appeared dependent upon the start of combustion, which will dictate peak temperatures. Ullman et al (1990) reported NOx reduction by increasing cetane number when testing a 1991 prototype DDC Series 60 heavy-duty diesel. Their regression model predicted that increasing cetane number by 10 would reduce NOx by 3 per cent. McCathy of Amoco Oil and Slodowske et al of Navistar (1992) found that raising cetane number reduced all regulated emissions when studying the effect of fuel cetane number on emissions from a heavy-duty diesel engine which met 1994 emissions standards. They concluded that NOx reduction by raising cetane with a cetane improver is about 10 times more cost

effective than NOx reduction by reducing aromatic content alone. Heaton et al (1993) confirmed the trend of higher cetane numbers resulting in lower NOx levels when testing light-duty and heavy-duty diesel engines, with fuels ranging from 47 to 61 cetane number. Spreen et al (1995) of Southwest Research demonstrated the same effect on a prototype Navistar DTA-466 engine when testing fuels with cetane numbers ranging from 44 to 59; NOx emissions were reduced by 0.131 to 0.200 g/hp.h for a cetane increase of 10, the effect being greater for a more retarded calibration.

Bartlett et al (1992) found that DI engines showed a trend towards reducing NOx emissions with increasing cetane number, with 2 engines showing reasonable correlations. Three Ricardo Comet-type IDI engines exhibited the opposite trend. This is probably due to the higher cetane number reducing the delay period, as it will do in the DI engines, but in the case of the IDI, because of the normally retarded combustion, this will result in higher combustion pressures and temperatures leading to an increase in NOx emissions.

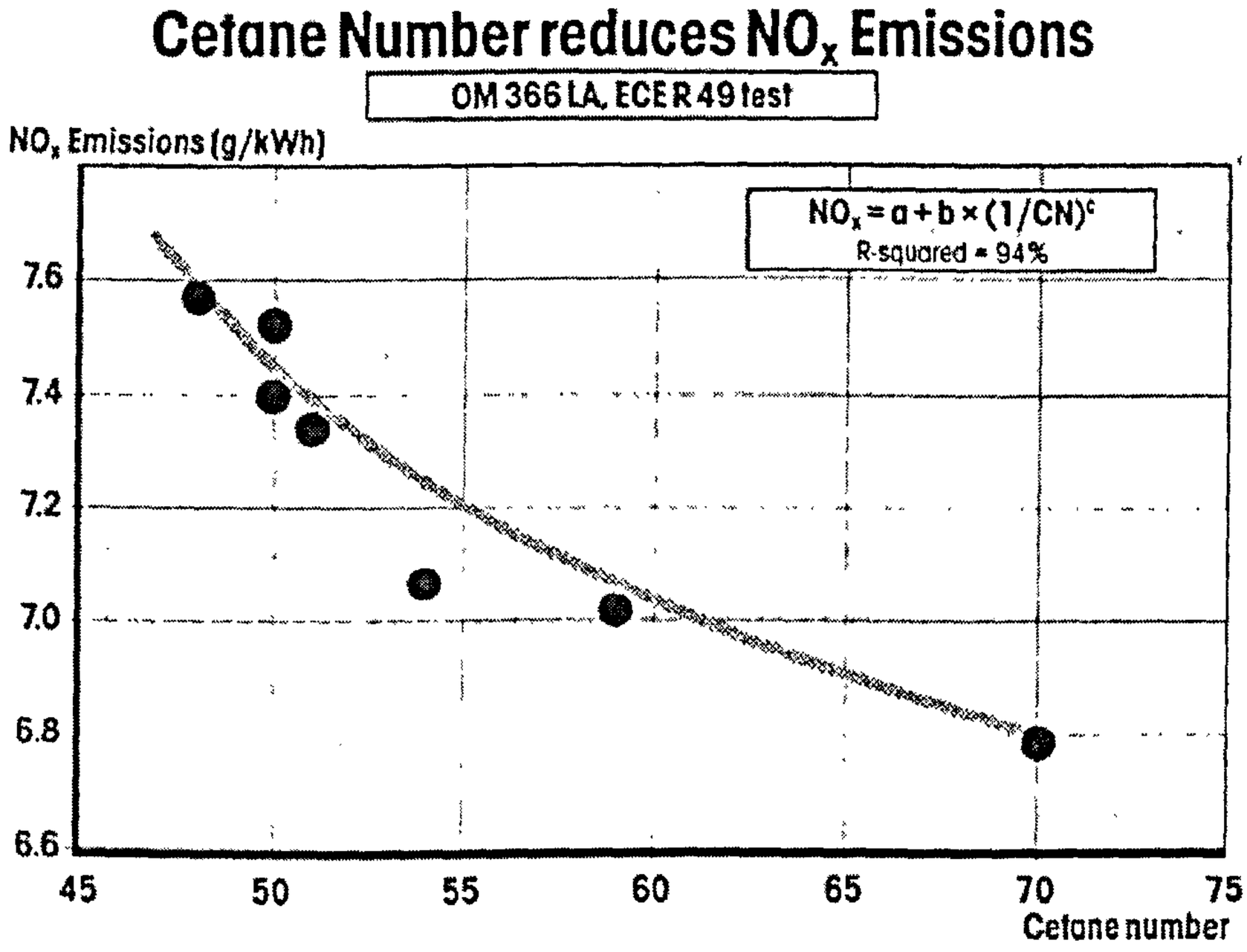

Figure 2.19 Non-linear regression model of NOx emissions versus cetane number, Mercedes-Benz OM 366LA 6 litre 6 cylinder DI diesel engine
(Lange et al, 1993)

Lange et al (1993) found no significant fuel effects on NOx emissions from a Mercedes-Benz 250D equipped with an OM 602 2.5 litre 5 cylinder pre-chamber N/A diesel. However, when testing the same 12 fuels with an OM 366LA 6 litre 6 cylinder DI turbocharged and inter-cooled diesel, there was a strong non-linear relationship with cetane number. Increasing cetane number, particularly from 45 to 55, reduced NOx emissions. Above 55 cetane there was less reduction of NOx, see **Figure 2.19.**

2.5.5 Cetane Improvers

Increasing cetane number of diesel fuel can be achieved either by lowering the aromatic content of the fuel, or by addition of chemical cetane improvers. It is generally recognised that chemical cetane improvement additives represent a low cost alternative to obtaining higher natural cetane through aromatic reduction. The use of 2-ethylhexyl nitrate as a chemical cetane enhancer is well established commercially. The commercial use of "peroxides," such as di-t-butyl peroxide (DTBP), as a cetane improvement additive is relatively new (Nandi et al 1994). It has been demonstrated in one engine and using one fuel that di-t-butyl peroxide can provide a small NOx reduction advantage compared to 2-ethylhexyl nitrate at equivalent cetane number (Liotta F J, 1993).

The effect of adding an alkyl nitrate cetane improver to increase the fuel cetane number and the consequent effect on NOx emissions when fuel nitrogen has been increased is an interesting point. Ullman et al (1990) conducted an experiment to determine whether or not the increased nitrogen level in the fuel masked the true reduction in NOx emissions, owing to the higher cetane number. Two quantities of a fuel were treated with alkyl nitrate and with ditertiary butyl peroxide to achieve the same cetane number. When both fuels were run, no differences in NOx or other emissions were observed. It can be concluded therefore that in this case, the nitrogen from the cetane improver, did not contribute to NOx emissions.

Nandi et al (1994) reported a small reduction in NOx emissions from cetane-improved fuels, compared to the base fuels. A direct comparison of heavy-duty diesel emissions from a DDC Series 60 engine was carried out with 3 different diesel fuels treated with di-t-butyl peroxide and 2-ethyhexyl nitrate to give equal cetane numbers. NOx

emissions from a low aromatic fuel containing the additives were not significantly different from the base fuel. But both additives produced 3 to 4 per cent reductions in NOx emissions in two higher aromatic fuels. The NOx emissions from the peroxide treated fuels, although not statistically significant, were lower than those from the nitrate treated fuels, in each of the base fuels. The peroxide produced about 0.5 to 1 per cent lower NOx, compared to the nitrate additive.

Andrews and Nurein (1990) evaluated Energy Plus D-2000 additive, which is almost entirely hydrocarbon in composition. This was carried out with a Petter AV1 553cc single cylinder DI diesel and A-2 diesel fuel, which had a cetane number of 47. Despite the fact that ignition delay was reduced for all engine loads, there was no significant influence of the additive concentration on the NOx emissions, although a slight reduction in NOx at high air/fuel ratios was indicated.

Ladommatos, Parsi and Knowles (1996) progressively increased the cetane number of a base fuel by the addition of an ignition improver based on ethyl hexyl nitrate to increase the cetane number from 40.2 to 62. The testing was conducted on a CFR engine. As cetane number increased, the NOx level generally decreased and this was the case for constant start of combustion and constant injection timing; although with the latter, the reduction in NOx levelled off at cetane numbers above 53. The decline in NOx concentration with increasing cetane number can be explained by decreasing cylinder gas temperature. An increase in cetane number shortens the delay period, which results in less fuel being burnt during premixed combustion, this in turn leads to lower peak cylinder gas temperatures. The reduced effect of high cetane fuel on NOx emissions when using constant start of injection is because the timing of combustion is effectively advanced, owing to the shorter delay period.

2.5.6 Volatility

Volatility will affect the rate of vaporisation of the fuel spray. The initial boiling point will be particularly significant during the delay period, prior to the start of combustion, in determining the amount of fuel mixed and the peak flame temperatures from the pre-mixed combustion. Broering and Holtman (1974) demonstrated that for the same cetane number, a "low volatility fuel," resulted in lower NOx emissions from a range of

engines over the 13-mode cycle. Burley and Rosebrock (1979) tested an Oldsmobile 5.7 litre V-8 IDI diesel on a 5-point steady-state load speed map with 46 fuels. They found that NOx did not correlate well with fuel characteristics, but appeared related to aromatic content, specific gravity and 90 per cent boiling point. They concluded that low NOx accompanied low values of these characteristics.

Lange et al (1993) found no significant fuel effects on NOx emissions from a Mercedes-Benz 250D equipped with an OM 602 2.5 litre 5 cylinder pre-chamber N/A diesel. However, when testing the same 12 fuels with an OM 366LA 6 litre 6 cylinder DI turbocharged and inter-cooled diesel, there was a strong non-linear relationship with cetane number, but no significant influence from volatility, ie T10E, T50E, T90E or final boiling point.

2.5.7 Aromatics

Aromatics are molecules containing one or more benzene rings (C_6H_6) in their structure. They have higher specific gravity and boiling points but lower cetane numbers than paraffinic molecules. Burley and Rosebrock (1979) found that NOx emissions increased with higher aromatic content in the fuel. They ran 2 series of fuel blend tests covering a range of aromatics from 2 to 65 per cent and in each case NOx emissions climbed steadily as aromatics increased. Flanigan, Litzinger and Graves (1989) blended 1-methylnaphthalene, tetralin and decalin, each to a base fuel at several concentrations. Higher NOx levels with the 1-methylnaphthalene blends were ascribed to the longer ignition delays, as were the effects of the tetralin blends. Addition of decalin to the base fuel caused no significant changes in emissions. Miyamoto et al (1992) examined mixtures of two base fuels with different cetane numbers and aromatic content. The high aromatic fuel showed slightly higher NOx emissions, owing to the longer ignition delay. The ignition delay and NOx emissions were largely equated by adding a peroxide type ignition improver to the high aromatic fuel. Taking a middle aromatic fuel and running at 3 injection timings, the authors conclude that NOx emissions are almost dominated by the ignition delay and injection timing. The effect of aromatic content on NOx emissions appears much smaller than ignition parameters.

Ullman et al (1990) when testing a 1991prototype DDC Series 60 heavy-duty diesel

found that NOx emissions responded to changes in aromatic content of the fuel. A 10 per cent lower aromatic content was estimated to reduce NOx emissions by 3 per cent. NOx emissions were also reduced by a decrease in aromatics, when McCathy of Amoco Oil and Slodowske et al of Navistar (1992) studied fuel effects on emissions from a '1994 standard' Navistar DTA 466 heavy-duty diesel engine. The cost to reduce NOx by lowering aromatic content alone was estimated to be about 10 times higher than by increasing cetane number. Decreasing aromatics by 10 per cent was predicted by Spreen et al (1995) to reduce NOx by 0.052 g/hp.h, based on their fuel study with a prototype 1994 Navistar DTA-466 engine.

2.5.8 Oxygenated Additives

The use of oxygenates to produce cleaner burning diesel fuels was initially considered over 50 years ago. Since that time, the addition of numerous oxygenated compounds to diesel fuel has been reported. Liotta of ARCO Chemical and Montalvo of Southwest Research (1993) reported on the effect of 8 oxygenates on exhaust emissions from a DDC Series 60 heavy-duty DI diesel engine measured over the EPA transient test cycle. Based on fuel blending properties, the authors chose 3 glycol ethers, an aromatic alcohol, an aliphatic alcohol and polyether polyol. Some of the oxygenated additives used produced a slight decrease of 1 to 2 in cetane number. This was attributed to the chain branching present. Oxygenates that lacked branching, such as diglyme (an ether), were either cetane neutral or produced a small increase in cetane number of the base fuel. To compensate for the reduction in cetane number, they added small amounts of 2-ethylhexyl nitrate to treat the oxygenated blends, to minimise the effect of cetane number on engine emissions. The addition of the oxygenated additives to the fuel produced small increases in NOx emissions. At the lower additive treatment levels, less than 5 per cent, the increased NOx emissions from the oxygenated fuels were not significant, within the limits of their evaluation. At typical use levels, 2 per cent or lower, the use of oxygenated additives would be expected to have little or no effect on NOx emissions. The authors also looked at a fuel with both oxygenated and cetane improvement additives to produce a fuel that would give lower particulates and NOx emissions, compared to the base fuel. A fuel blend was prepared containing 2 per cent glycol ether C and sufficient peroxide to raise the cetane number from 43 to 53. Particulates were reduced by 8 per cent and NOx by nearly 3 per cent compared to the

baseline.

2.5.9 NOx Reduction Additives

In 1986, Perry and Siebers (1986) introduced the RAPRENOx exhaust after-treatment process for reduction of NOx, using cyanuric acid, (see After-Treatment Section later in this chapter). Researchers at Texaco Research Laboratories have proposed a scheme to incorporate the isocyanic acid into the fuel. Caton and Siebers (1989, 1990) determined that the most effective temperatures for the RAPRENOx process were between 1100 and 1300°K. Since this temperature range will be traversed twice during diesel combustion, the Texaco researchers incorporated the isocyanic acid into a thermally stable carrier that would allow it to survive until the expansion stroke. Tree of Cummins Engine and Bower et al of the University of Wisconsin-Madison (1993) investigated the feasibility of this approach with a single cylinder DI diesel engine in which standard diesel fuel and fuel in which the cyanuric acid based additive, Texaco Diesel Additive (TDA), had been added. A 5 per cent by weight, addition of TDA was successful in reducing NOx by approximately 40 per cent at two load conditions, $\Phi \approx 0.5$ and $\Phi \approx 0.3$, at 1500 rpm. The ISFC and HC and CO_2 emissions, were unchanged by the additive. From their heat release analysis, it appeared that the reduction in NOx could not be accounted for by differences in combustion, although the 5 per cent TDA case exhibited a slightly larger and slower premixed burn with a smaller and slower diffusion burn. However, reproduction of these results was not accomplished. Over twenty different additive blends were tested with varying results, ranging from engine instability to increased NOx, to varying amounts of reduction. These data indicate that variability and stability of the TDA additive is an issue.

Ethanol has a lower flame temperature than diesel and hence its addition to diesel fuel in the form of a blend will reduce the peak combustion temperatures and hence reduce NOx emissions. Andrews and Salih (1990) investigated 5 to 20 per cent ethanol in diesel blends, the lower concentration could be considered as a fuel additive. With every litre of blended fuel 35cc of naptha was added to prevent the two liquids separating. Testing was carried out with a Petter AV1 553cc DI diesel engine running at 1500 rpm. The NOx emissions were reduced at all equivalence ratio and power settings. However, the extent of the reduction was very variable both with equivalence

ratio and with proportion of ethanol, at constant load. At low powers there was a reasonable correlation between the NOx reduction and the ethanol concentration. At full load the reduction in NOx was small at 5 to 10 per cent and was independent of the proportion of ethanol. This is because the lower heating value of the ethanol blends means that a richer mixture has to be used, for the same power, which generates more NOx. Moreover, ethanol lengthens the ignition delay which extends premixed burning and increases NOx formation. Where ethanol is available, it would appear to be a viable additive for diesel fuel to reduce NOx and other emissions without a significant fuel economy penalty (Andrews & Salih, 1990).

2.5.10 Summary

- The physical and chemical properties of diesel fuel will affect NOx emissions from diesel engines, but it is difficult to separate the effects of each.

- A density increase will enable an engine to produce higher BMEP at full load, causing greater peak pressures and temperatures leading to increased NOx formation and emissions. A good correlation exists between lower density and reduced NOx emissions for DI engines, but only a slight one in the case of IDI diesels.

- Numerous studies have demonstrated that increasing cetane number of the fuel significantly reduces all the regulated emissions, especially particulate matter and nitrogen oxide, from DI diesels. Ricardo Comet swirl chamber type IDI engines may exhibit the opposite trend, giving an increase in NOx emissions. This is due to the shorter delay period leading to higher combustion pressures and temperatures, because of the normally retarded combustion.

- Cetane improvers will generally give the same benefit as a high cetane fuel, compared to a low cetane fuel.

- Fuel volatility does not have a first order influence on NOx emissions from diesel engines. Nevertheless, there is some evidence that a "low volatility fuel"

will result in lower NOx emissions; this would be a second order effect.

- High aromatic fuels will typically give higher NOx emissions, compared to low aromatic fuels, because of the longer ignition delay.

- The addition of oxygenated additives to diesel fuel will give a small or no increase in NOx emissions, this is because of a slight decrease in cetane number with oxygenates.

- The addition of isocyanic acid in a thermally stable carrier has been successful in reducing NOx emissions, but the variability and stability of the additive is an issue in reproducing the results.

- Ethanol, where it is available, would be a viable additive for diesel fuel to reduce NOx and other emissions without significant fuel economy penalty.

2.6 NOx Reduction by Exhaust After-Treatment

2.6.1 Introduction

Diesel exhaust contains between 5% and 15% excess oxygen which makes the removal of NO_x much more difficult than for gasoline exhaust from a stoichiometric mixture. The three-way catalysts that are capable of reducing 90% of the NO_x in gasoline exhaust do not reduce NO_x in diesels. New types of catalyst, called lean NO_x catalysts, are being developed for diesel applications, one of which promotes the selective reduction of NOx under lean conditions by reaction with hydrocarbons, as opposed to the 3-way catalyst which promotes the reduction of NOx near stoichiometric conditions only, primarily through reactions with H_2 and CO. Three strategies have been investigated to remove NOx from diesel exhaust (Perry & Siebers 1986, Horrocks 1994):

a) selective catalytic reduction (SCR),

b) catalysed thermal decomposition,

c) selective non-catalytic reduction (SNR), or chemical reduction or "Thermal DeNOx."

In the SCR technique, NO selectively reacts with reducing species from the gas stream in the presence of a catalyst, even under overall oxidizing conditions. The reducing species may initially be present in the exhaust stream, such as some HC species, or be injected from an on-board source such as ammonia or urea. A number of catalysts have been researched: two of the most widely studied include various metal ion exchanged zeolites and the use of precious metal as the active sites, and which often incorporate some HC storage. Also, vanadium and molybdenum formulations have been evaluated.

The metal exchange zeolite technology operates at a temperature window of around 300°C upwards, but currently has very poor high temperature stability, with activity falling to zero in a few hours at 700°C.

The precious metal catalysts currently achieve NOx conversions over a very narrow temperature window, typically from 180°C to 250°C, with a peak conversion of approximately 50% at around 210°C. The theoretical conversion over the European test

cycle, given an ideal strategy and fuel delivery system, would be 30 to 35%.

Catalysed thermal decomposition of NO into N_2 and O_2 is a catalytic decomposition reaction without the need for any other chemical species to be present. This method has advantages of simplicity and innocuous reaction products. At present, results suggest that pure thermal decomposition of NO with copper-ZSM-5 zeolite catalysts is impractical for automotive exhaust treatment since conversion efficiencies are extremely low at space velocities (see below) utilized during vehicle operation. Moreover, the conversion rate reduces with the presence of water vapour.

Cyanuric acid has been proposed by a number of researchers, as an alternative chemical process for NOx reduction, though there are drawbacks that include low space velocity requirements (see below) and toxicity issues.

In addition to NO_x control, diesel catalysts must also reduce HC, CO and particulate matter (PM). HC control is particularly important because European standards have separate NO_x and HC+NO_x standards. If HC emissions are too high or have high deterioration, then NO_x emissions must be correspondingly lowered.

As a measure of the exhaust gas residence time in the catalytic converter and a means of determining the required size of a catalyst, the industry uses a term called "space velocity." This is defined as the exhaust gas volumetric flow in m^3/h, divided by the catalyst volume in m^3, giving a space velocity unit of h^{-1}. Therefore, space velocity is the number of times per hour that the gas contained in the catalyst is renewed. Generally catalyst performance, in terms of conversion efficiency and light-off temperature, improves with lower space velocities, in other words with bigger catalysts and therefore greater residence time. But this has to be weighed against the size and cost of the catalyst for a commercial application. Packaging of catalysts in modern passenger cars is not an easy task, with the pressure for reduced vehicle weight and maximising space for the occupants. For diesel oxidation catalysts, the space velocity will typically be in the range of 40,000 to 60,000 h^{-1}, as an average, over the current European drive cycle (ECE-15 plus EUDC).

The light-off temperature is defined as the exhaust gas temperature at which 50 per cent

conversion is attained (Held et al, 1990). At present this creates a problem for lean NOx catalysts since most of them do not achieve 50 per cent conversion.

2.6.2 Selective Catalytic Reduction

Burgler, Herzog and Zelenka of AVL reported some early non-selective NOx catalyst results in 1992. A 20 per cent reduction at an exhaust temperature of 260 °C dropped to 5 per cent at 180 °C. They concluded that the catalysts have to be developed further for improved conversion rates at low exhaust gas temperatures and improved conversion rates in the presence of low CO and HC emissions. The authors postulated that Non-selective Catalytic Reduction (NCR) would be more cost effective for light-duty vehicles, since there would not be the requirement for the onboard dosing system. However, the conversion efficiencies are not high enough to make these catalysts viable, so development is focused on selective catalytic reduction.

Selective catalytic reduction (SCR) is recognized as the most effective commercial technology to control NOx emissions from chemical plants and stationary power sources (Heck 1994).

The selective catalytic reduction (SCR) method normally involves the injection of a reducing species that then selectively reacts with NO, even in the presence of excess oxygen. The reducing species may initially be present in the exhaust stream or might be injected from an on-board source. Thus there are two types of lean NO_x catalyst system, passive and active systems. The passive system stores and then uses engine-out HC to reduce the NO_x, and the active system uses diesel fuel injected in front of the catalyst, or an alternative media such as ammonia or urea, injected from an on-board source.

The hydrocarbon to NOx ratio (C_1 /NOx) must be approximately 0.5 in order to meet the stoichiometric requirements for the NO reduction reaction shown as the equation below.

$$(\text{-}CH_2\text{-}) + 2NO + {}^1/_2O_2 \rightarrow CO_2 + H_2O + N_2 \qquad 2.38$$

Diesel exhaust has typically lower C_1 /NOx ratios than the stoichiometric, thus it is expected that hydrocarbons will have to be added to the exhaust, probably in the form of diesel fuel. Unfortunately the Cu/ZSM-5 and Pt catalysts are so poorly selective in their use of the added hydrocarbon that about 90 per cent of the hydrocarbon is oxidized to CO_2 and H_2O, which is a waste of hydrocarbon, and translates into an unacceptable fuel economy penalty. Furthermore, the exothermic reaction leads to high bed temperatures with resultant conversion of sulphur containing fuel compounds to sulphates, which contribute to particulate emissions, (Deeba et al, 1995).

Deeba et al, of Engelhard summarized the status of lean NOx catalysts very well in their 1995 SAE paper. Two materials that have attracted great attention, as lean NOx catalysts are Cu/ZSM-5 and Pt based. Cu containing ZSM-5 is active for lean NOx reduction at temperatures above 350 °C, provided sufficient hydrocarbons are present as reductants. Deeba et al (1995) also point out some serious limitations of Cu/ZSM-5 based catalysts, which are likely to prevent their use in mobile applications; namely, poor hydrothermal stability, owing to the presence of water vapour, low hydrocarbon selectivity, and sensitivity to sulphur poisoning. The Pt based catalysts are active in a narrow temperature range of 200 - 300 °C, which is considerably narrower than the target range of 150 - 350 °C for light-duty diesel engines.

Copper ion-exchanged ZSM-5 Zeolite Catalysts

Held et al (1990) and Konno et al (1992) have independently reported that copper ion-exchanged ZSM-5 zeolite is able to reduce NOx in the presence of oxygen with hydrocarbons as the reducing agent. However, Held et al, reported only a 15 per cent NOx conversion from diesel exhayst, at a low space velocity of 15,000 h^{-1}, even when adding 4,700 ppm ethylene, with a copper exchanged ZSM-5 catalyst. Much higher conversions were achieved using urea as the reduction agent. Work at Ford has shown that this type of catalyst can give an initial NO conversion of 45 per cent, but that deactivation is likely to occur owing to water vapour and SO_2 in the exhaust gases, and ageing (Montreuil and Gandhi, 1992). M Konno et al of Hokkaido University tested a copper ion-exchanged ZSM-5 zeolite catalyst on a diesel engine and reported a NOx reduction efficiency of about 25 per cent at the maximum activation temperature of 400 °C, moreover, this improved to nearly 80 per cent by increasing the hydrocarbon concentration with the addition of light oil to the 'dry' exhaust. However, like other

researchers, the existence of water vapour in the exhaust was found to decrease catalyst activity. The adverse effect of water vapour is a major issue for the practical application of Cu-ZSM-5 zeolite catalysts for diesel engine exhaust after-treatment.

Copper Catalysts

NOx reduction evaluation by hydrocarbons such as cyclopropane [C_3H_6], normal-heptane [C_7H_{16}], normal-cetane [$C_{16}H_{34}$] and diesel fuel when used in conjunction with copper deposited on a base of γ-alumina catalysts was carried out by Muramatsu et al (1993) at Riken Corporation. Diesel engine tests showed on average a 10 to 15 per cent reduction in NOx over a temperature range of 350 to 550 °C, using a supplemental spray system for $C_{16}H_{34}$ and diesel fuel at a HC/NO mass ratio of 4 (compared to 0.32 for equation 2.38). Clearly, this level of NOx conversion would not be viable for a commercial system and no mention was made of other pollutant reduction performance. Moreover, at a diesel fuel/NOx mass ratio of 4, the fuel economy penalty would be higher than desirable.

Platinum Catalysts

Deeba et al (1995) reported on a catalyst of Pt supported on γ-alumina (γAl2O3) at a precious metal loading of 70 g/ft^3 as a reference and two proprietary HTC-1 Engelhard catalysts, made of the same components but with some variation in composition. The temperature range of NOx reduction for the new catalyst was shown to be between 180 and 350 °C and comprised of two regions. The first region had a maximum NOx conversion of about 45 per cent at 200 °C and the other region with maximum NOx reduction of about 55 per cent at 300 °C, clearly a broader range than the Pt/γAl_2O_3 reference catalyst. An interesting feature of the HTC-1 material is its ability to store HC species that can be used as a highly selective reductant for the NOx around 200 °C, which is the mechanism responsible for the first low temperature NOx reduction peak. Coupling this unique lean-NOx formulation with a diesel oxidation catalyst resulted in 4-way capability for simultaneous removal of NOx, CO, HC and the SOF portion of particulates from diesel exhaust.

Leyrer, Lox and Strehlau of Degussa (1995) reported on a novel high temperature NOx formulation devoid of copper, with a platinum loading. As a reference, a first generation Pt-zeolite type sample was used. One interesting feature they found was

improved effectiveness by increasing the catalyst diameter, for a constant precious metal loading of 2.47 g/l (70 g/ ft^3). Conversion levels of 93 per cent for CO, 52 per cent for HC, 35 per cent for NO and 35 per cent for particulates were achieved over the US FTP-75 cycle with a 1.9 litre IDI T/C diesel passenger car. The amount of secondary fuel corresponded to a 2 per cent increase of fuel consumption. Catalyst loading of 2.47 g/l (70 g/ ft^3) was recommended to prevent hydrocarbon slip, even though 1.76 g/l (50 g/ ft^3) gave relatively high CO and NOx conversions. Thirty hour diesel engine bench ageing demonstrated almost no deterioration.

Ammonia and Urea Reductants

Selective catalytic reduction of NOx with ammonia was first discovered and patented by Dr Gunther Cohn at Engelhard (Cohn et al, 1961).

Ammonia is widely used as the reduction agent for catalytic reduction of NOx at stationary power plants and such systems can achieve very high efficiencies (Lueders et al, 1995). Catalytic reduction of NOx by means of injecting urea or ammonia has been applied to line-haul locomotives and ferries, respectively.

Temperature is the single most important variable in NOx SCR. Three general classes of catalysts have evolved into commercial use: precious metals for operation at temperatures between 175 and 290°C, base metals for operation at temperatures between 260 and 450°C and zeolites for operation at high temperatures. The balance between the SCR and ammonia oxidation reactions determines the operating temperature range for low temperature SCR catalysts. At low temperatures the SCR reaction dominates, but as temperature increases, NOx conversion increases with increasing temperature. Eventually as temperature increases further, the destruction of ammonia and generation of NOx via the oxidation reactions causes overall NOx conversion to reach a plateau and finally decreases with increasing temperature. Most commercial SCR catalyst formulations are those comprising of V_2O_5 supported on TiO_2 (V/Ti) operating in the medium temperature range. Ingredients such as tungsten and molybdenum may be added to diminish SO_2 oxidation activity and improve operation above 425°C but the basic formulation remains generally the same. These catalysts operate best in the 260 to 450°C temperature range. High temperature zeolite catalysts for SCR above 450°C were first used in the 1970s (Pence and Thomas 1980).

Ford, with FEV, demonstrated this technology applied to a diesel Transit vehicle (Lueders et al, 1995). A eutectic aqueous solution of urea was chosen for this exercise because it can achieve similar performance to ammonia and as such is non poisonous and does not present a fire hazard. The catalyst consisted of a vanadium-titanium substrate with a cell density of 200 cells per square inch (CPI) and the catalyst volume was optimised at 7.4 litres. Injection of the urea solution into the exhaust was controlled by a microprocessor. NOx conversion efficiencies of 65 and 83 per cent were achieved on the European and FTP-75 cycles, respectively. A reductant tank capacity of 40 litres would be required for the 2.5 litre diesel Transit to operate between the 15,000 km service interval. This tank would therefore need replenishing at each service. Issues with this system concern operation at low ambient temperatures, the size of catalyst and the practicability of an emission related reductant carried additionally on board the vehicle (Lueders et al, 1995).

Havenith of the Netherlands Ministry of Environment and Verbeek et al of TNO reported on the development of a urea deNOx catalyst concept for heavy-duty diesel engines in November 1995 (Havernith et al 1995). Three SCR catalysts and one oxidation catalyst were used with a total volume of 70 litres for a 12 litre TCI engine. An aqueous urea solution (40 per cent urea by mass) was injected with an air blast nozzle about 1 meter upstream of the catalysts. Urea injection was controlled by microprocessor. The maximum space velocity in the SCR catalysts was 28,000 h^{-1}. The system gave a 71 per cent reduction in NOx over the ECE 13-mode emissions cycle. One observation from this work was that the SCR system produced relatively high N_2O emissions, about 10 times higher than normally expected. Ammonia emissions were below 11mg/kWh.

2.6.3 Catalysed Thermal Decomposition

Although the most promising system is selective catalytic reduction (SCR), it is possible to remove NO under lean operating conditions by catalysed thermal decomposition of NO into N_2 and O_2. M Iwamoto et al at the Myazaki University, Japan, has been active in the area of NO decomposition, focusing on zeolites that have been ion-exchanged with various metal cations. Their investigation of a variety of zeolites has resulted in

the discovery that certain zeolites, particularly those which have been exchanged with Cu(II), exhibit NO decomposition activities which remain stable over protracted periods of time (Iwamoto et al, 1986). The catalyst yielding the most promise consists of a type ZSM-5 zeolite, ion exchanged with Cu(II). Maximum NO conversion efficiencies of 70 to 90 per cent have been reported for steady-state reactors (Montreuil, 1992, Iwamoto et al, 1986). However, Montreuil at Ford, has demonstrated that at high space velocities, typical of automotive catalysts, the thermal decomposition is extremely small and that reaction rates were drastically reduced with the introduction of water vapour which would be present in diesel exhaust. The work at Ford concluded that unless the rate of conversion kinetics could be increased by an order of magnitude or more, this approach to NO removal from vehicle exhaust will be impractical (Montreuil, 1992, Montreuil and Gandhi, 1992).

Yoshikawa H et al (1994) used a surface treated carbon fibre felt for adsorption and reaction of NO, one sample was treated with hydrogen nitrate, which was shown to enhance the NO reduction process. The principal concept of NO reduction with the use of the carbon fibre felt is that C atoms on the surface adsorb O atoms of NO and then react in the high temperature to form CO_2 or CO. The remaining dissociated nitrogen atoms are converted into N_2. On a test rig using pure NO gas, no N_2O was detected by gas chromatography. Testing on a small single cylinder diesel engine the authors report NO reductions of up to around 80 per cent with 300g of the treated carbon fibre felt. A chemical analysis of the carbon fibre felt did show a reduction in carbon and an increase in nitrogen and oxygen, together with a reduction in weight over a period of time. The authors did not attempt to identify a size or mass of felt required for a practical application, or any service replenishment requirements.

2.6.4 Chemical Reduction or "Thermal De-NOx"

Perry and Siebers (1986) proposed a new chemical process capable of completely removing NOx from the products of combustion. They demonstrated the method by eliminating NOx from a portion of the exhaust from a single cylinder diesel engine. The proposed scheme was based on addition of isocyanic acid (HNCO) to the exhaust stream. Isocyanic acid is formed from the decomposition of cyanuric acid (HOCN) when cyanuric acid is heated above approximately 330 °C.

$$(HOCN)_3 \rightarrow 3HNCO \qquad 2.39$$

When HNCO is mixed with an exhaust gas stream at temperatures = 400 °C, a series of reactions occur that result in the loss of HNCO and NO. This is because the NCO radicals formed from the photolysis of isocyanic acid (HNCO) react very rapidly with nitric oxide (Perry 1985). A continuous sample of exhaust gas from a small single cylinder diesel engine was drawn at a rate of 1 l/min over a 256 cc cyanuric acid bed followed by a 31 cc packed bed with a surface area of 1,630 cm^2. For cyanuric acid bed temperatures above 360 °C the NOx was essentially eliminated (Perry & Seibers, 1986).

For a practical application to a light-duty diesel vehicle there are immediately a number of issues. Scaling up the cyanuric acid bed volume for a typical diesel passenger car engine size of 1.8 to 2.0 litres would give an impractically large size. Secondly, for efficient conversion, the bed temperature would have to be maintained at 360 °C, which would mean heating it for an extended period of time, when the engine is operating at part load. Thirdly, there is also the problem of useage of cyanuric acid, storage, and top up over the life of the vehicle.

2.6.5 Summary

- Three-way "stoichiometric" gasoline catalysts will not reduce NOx in "lean" diesel exhaust. Lean NOx catalysts are being developed for diesel application. Three strategies have been investigated:
  a) selective catalytic reduction (SCR),
  b) catalysed thermal decomposition,
  c) selective non-catalytic reduction (SNR), or chemical reduction or "Thermal De-NOx."

- The most promising type is SCR using a Pt based catalyst on an alumina washcoat. Conversion efficiencies of up to slightly over 50 per cent have been achieved at between 200 and 300 °C, depending on the formulation. However, this only translates into 30 to 35 per cent reduction over the European drive cycle.

- With all the zeolite and precious metal alumina SCR systems, an improvement in NO conversion efficiency of around 3 times, was achieved by the addition of further hydrocarbons. This means that injection of diesel fuel into the exhaust upstream of the catalyst will be necessary to achieve the best efficiency for a practical automotive system. But this results in a fuel economy penalty in the order of 2 per cent.

- The highest conversion efficiencies have been demonstrated with urea injection and a vanadium-titanium catalyst, 65 and 83 per cent were achieved on the European and FTP-75 cycles, respectively. However, this system requires an additional storage tank for the reactant, which would need replenishing over the life of the vehicle.

- Catalysed thermal decomposition and chemical reduction do not appear to be viable for automotive use.

2.7 Conclusions

- There is wide consensus that the Zeldovitch mechanism can be used to predict NO from Diesel engines and other combustion systems; the values of the activation energy used by various workers for the calculation of the rate constants are generally in good agreement.

- The rate of NO formation rises exponentially with temperature, this has been demonstrated experimentally and is confirmed by the Zeldovitch rate equations. Prompt or rapid NO formation may occur in the flame zone.

- Oxidation of NO to NO_2 does occur in diesel engines; NO_2 emissions can be as high as 30 to 50 per cent of the total NOx emitted from DI diesels.

- Retarding injection timing will reduce NOx formation by lowering combustion temperatures; this may also cause an increase in HC and smoke emissions, as well as an increase in fuel consumption.

- Pilot injection delays the development of high-temperature regions and can facilitate injection retard while maintaining fuel consumption.

- EGR remains the most effective way of controlling NO formation along with more traditional techniques such as retarded injection timing.

- EGR reduces NOx formation and emissions by lowering the flame temperature through two effects; by dilution, reducing the oxygen mass fraction, and by a thermal effect, increasing the specific heat capacity of the charge. The dilution effect is by far the greater of the two.

- Cooling EGR prior to mixing with the intake charge provides further reductions of NOx emissions and is generally beneficial for particulates. The higher volumetric efficiency with cooled EGR leads to an improvement in fuel economy.

- Water addition, either injected with the intake air charge, or as a water-in-fuel emulsion, will reduce NOx emissions and is more effective in combination with EGR. However it is impractical for automotive use.

- The physical and chemical properties of fuel affect NOx emissions from diesel engines, but it is difficult to separate the effects of each. An increase in fuel density will enable an engine to produce higher BMEP at full load, causing greater peak pressures and temperatures leading to increased NOx formation and emissions. A good correlation exists between lower density and reduced NOx emissions for DI engines, but only a slight one in the case of IDI diesels.

- Numerous studies have demonstrated that increasing fuel cetane number significantly reduces all the regulated emissions, especially particulate matter and nitrogen oxide, from DI diesels. Ricardo Comet swirl chamber type IDI engines may exhibit the opposite trend, giving an increase in NOx emissions. This is due to the shorter delay period leading to higher combustion pressures and temperatures, because of the normally retarded combustion. Cetane improvers will generally give the same benefit as a high cetane fuel, compared to a low cetane fuel.

- New exhaust after-treatment technologies such as SCR NOx catalyst systems offer important additional scope that will help engine manufacturers meet emission legislation during the next five to ten years and bring the diesel NOx emissions closer to those of gasoline engines fitted with 3-way catalysts.

Chapter 3

Diesel Engine EGR Systems

3.1 EGR System Description

Diesel engine EGR systems comprise of a number of different components, each with a different function, which connect the exhaust to the intake system. These may include;

- EGR valve
- Throttle valve
- Venturi
- EGR cooler
- EGR tube

The primary role of the EGR valve is to regulate the flow of re-circulated exhaust gas. The vast majority of valves in production today have an inward opening poppet valve operated by a vacuum actuator, like the valve shown in **Figure 3.1**.

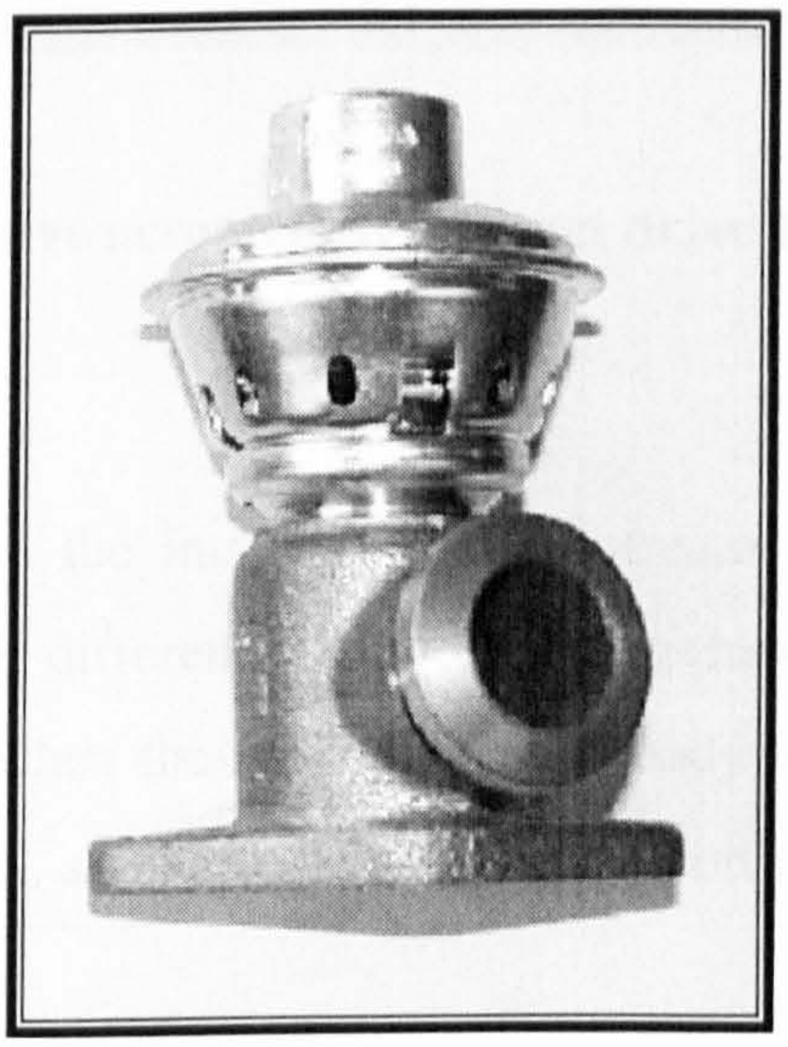

Figure 3.1 A pneumatic EGR valve (Courtesy of SAGEM SA)

Electric actuators are beginning to come on to the market. These may have inward or outward opening poppet valves depending on the type of actuator. Linear solenoids, stepper motors or torque motors are types of electric actuators being developed by

various component suppliers. These offer the advantage of faster and more precise operation compared to a conventional vacuum motor system. **Figure 3.2** shows a direct drive DC torque motor actuated EGR valve.

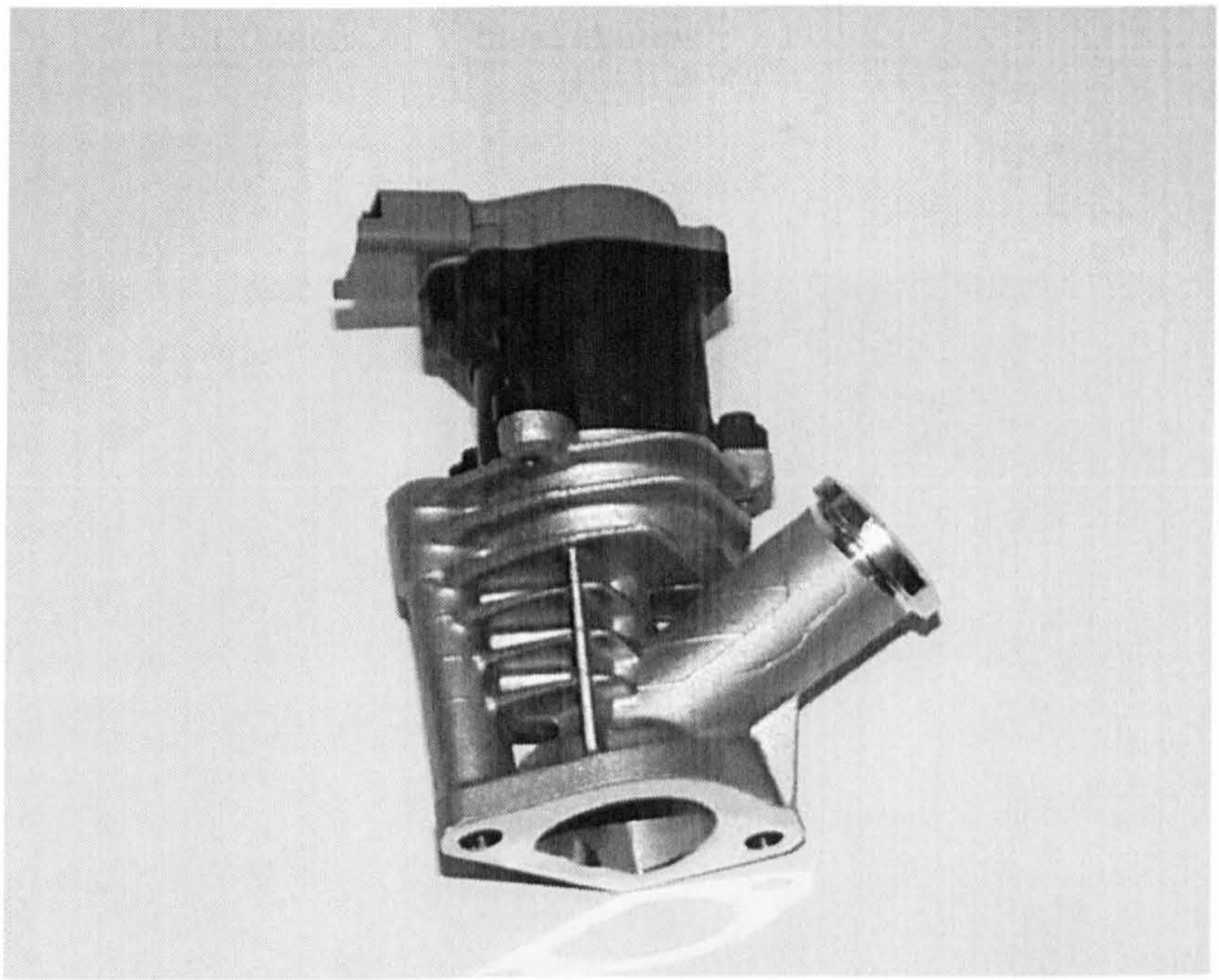

Figure 3.2 An EGR valve actuated by a direct drive DC torque motor (Courtesy of SAGEM SA).

Throttle valves are used in the intake system, upstream of the EGR entry point, to provide a greater pressure difference between the exhaust and intake manifold, to increase the flow of EGR when the EGR valve is already fully open. These valves are traditional "butterfly" valves, similar to petrol engine throttles.

A venturi is sometimes used to provide a higher pressure differential between exhaust and intake manifolds, to assist the flow of EGR into the air charge. A venturi is normally used instead of a throttle valve, in order to get better pressure recovery.

The EGR cooler cools the exhaust gas before it is introduced into the air charge stream. The majority are of tube and plate construction in stainless steel, generally vacuum

brazed together. Engine coolant is passed through the EGR cooler to provide the cooling medium.

EGR tube is a thin wall stainless steel tube that is used to connect the various system components together, to allow flow from the exhaust to intake manifolds. Connections are usually by two-bolt flanges or V-band clamps.

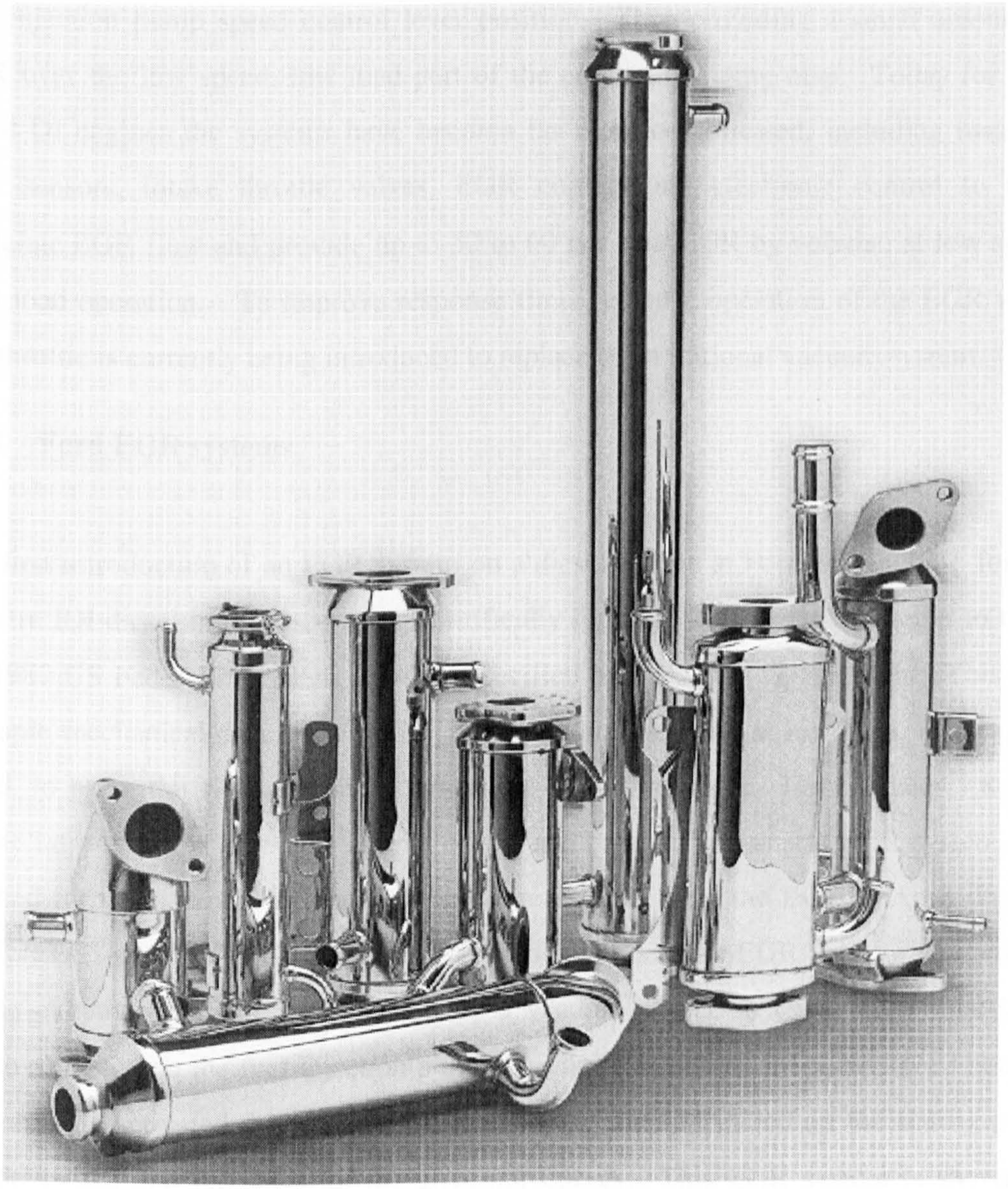

Figure 3.3 **A selection of EGR coolers** (Courtesy of Serck Heat Transfer Ltd).

3.2 Production EGR Systems

Automotive diesel engine EGR systems were introduced from the mid to late-1980s in order to meet stricter NOx emissions regulations, such as the 1987 US Federal emissions standard introduced by some non-EC countries in January 1986, and the EC "5th Amendment" which came into force for passenger cars over 2.0 litres capacity in October 1989. Up until that time, either there were no emissions standards for diesel vehicles, or the severity was such that they could be met without recourse to EGR. The early systems applied to IDI engines were simple on-off EGR valves, controlled by the fuel injection pump speed control lever position. Thus providing a small amount of EGR over the low speed, low load part of the engine-operating map. Today for high speed DI engines the systems have become far more complicated, including mass air flow sensors, intake throttle valves, EGR coolers and electronic control to fully modulate EGR flow and provide up to 50 to 60 per cent EGR by volume, at low speed light load operation. To improve response times, electric operation of the EGR valve and throttle is currently being introduced to replace the traditional vacuum system.

3.2.1 Ford EGR systems

The first introduction of an EGR system on a diesel engine at Ford was in 1986 for the 1.6 litre IDI diesel in the Escort car, specifically for the Swiss market, in order to meet the 1987 US Federal emissions standard specified by the Swiss Government. This was a simple mechanical/pneumatic on-off EGR system operating at low load, low engine speed, to bring the NOx emissions below the 87 US standard. For the later 1.8 litre engine introduced in 1989, the simple on-off mechanical/ pneumatic EGR system was retained for the naturally aspirated version, in order to meet the EC "5th Amendment" (88/76/EEC) and 1987 US Federal emissions standards. The EGR valve was mounted on the exhaust manifold and operated by a vacuum source that was controlled by a switch mounted on the fuel injection pump. A cam attached to the pump speed control lever spindle activated this switch. EGR coverage thus depended on the setting point for the switch and the shape of the governor curves. This EGR system is shown in **Figure 3.4** and the EGR coverage is shown in **Figure 3.5.**

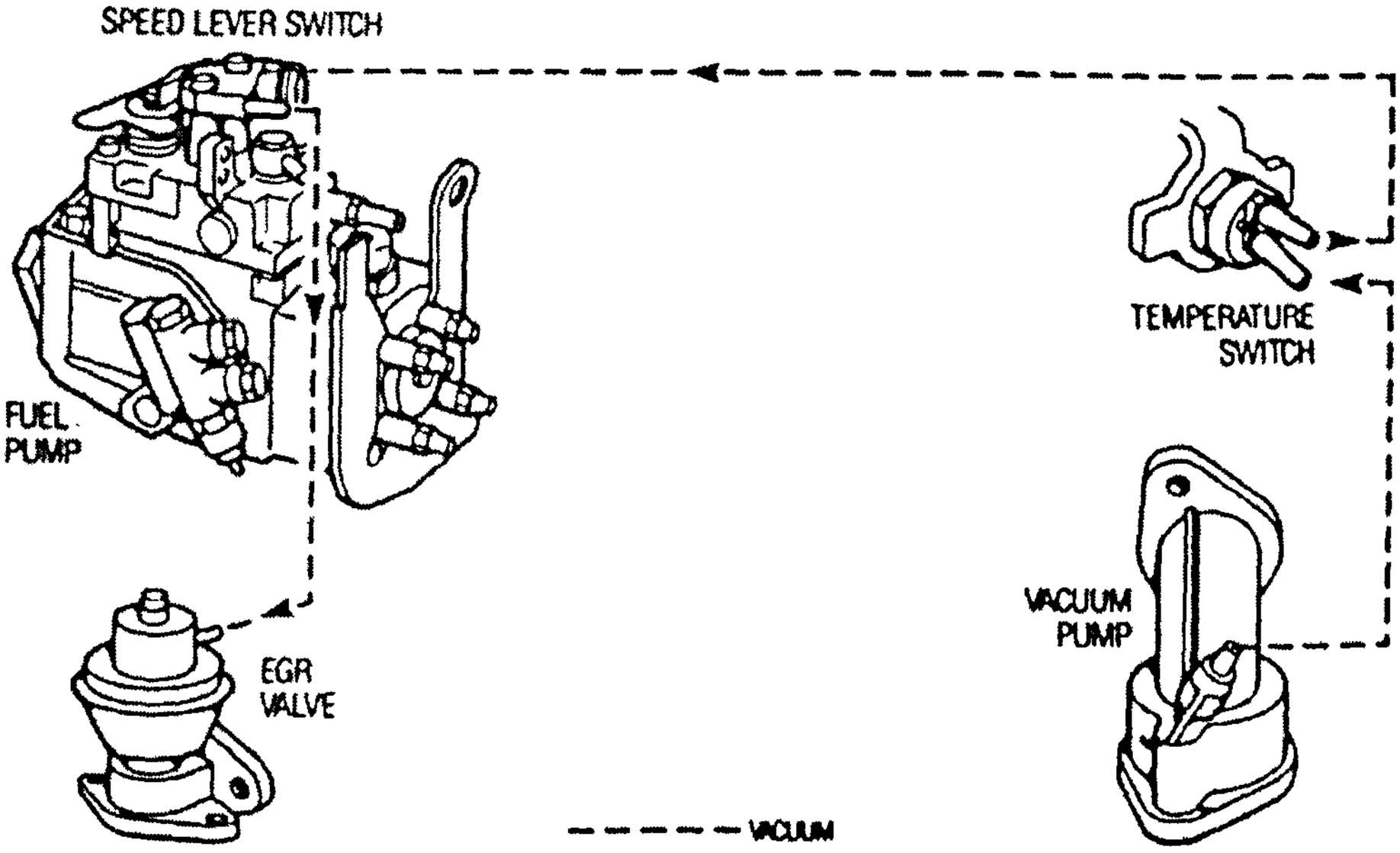

Figure 3.4 Schematic diagram of simple on/off EGR system for the Ford 1.8 litre naturally aspirated IDI diesel engine (Lawrence et al, 1989)

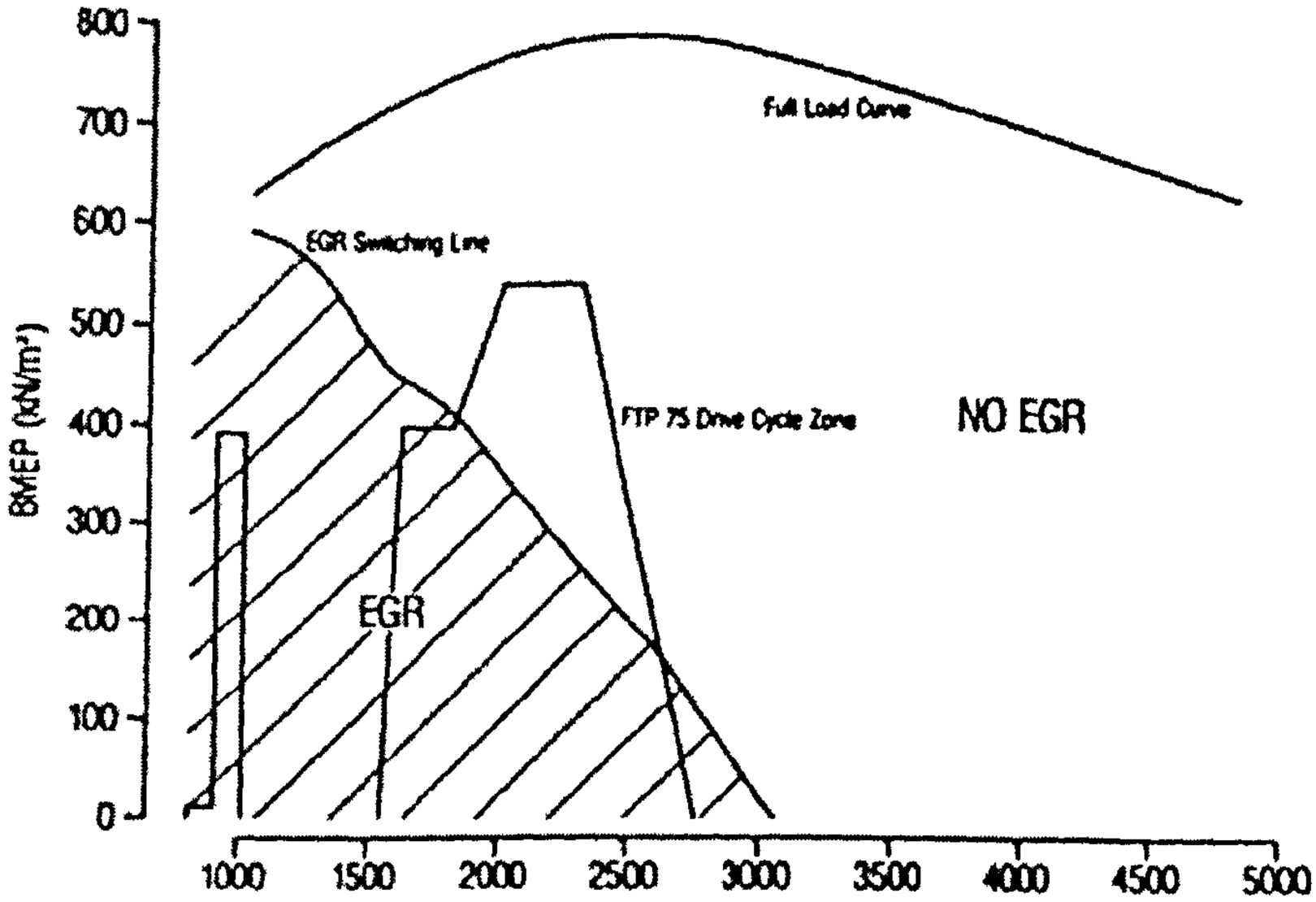

Figure 3.5 EGR coverage related to BMEP and speed for the Ford 1.8 litre naturally aspirated IDI diesel engine (Lawrence et al, 1989)

An open loop electronically controlled EGR system was specified for the 1.8 litre

turbocharged diesel engine fitted in the Sierra car, which was introduced for the 1989 model year. The electronic control unit (ECU) received signals from the alternator, for engine speed, and from a potentiometer on the fuel injection pump speed lever, for engine load. The ECU processed these signals and modulated the EGR level via a current to vacuum transducer (CVT) that altered the vacuum signal received by the EGR valve. The EGR valve lift and the engine exhaust and intake manifold pressures, determined the level of EGR. A schematic diagram of this electronically controlled EGR system is shown in **Figure 3.6.** The EGR coverage for this engine as installed in the Sirerra car to meet the EC "5th Amendment" and 1987 US Federal emission standards is shown in **Figure 3.7** (Lawrence et al, 1989, Lawrence and Evans 1990).

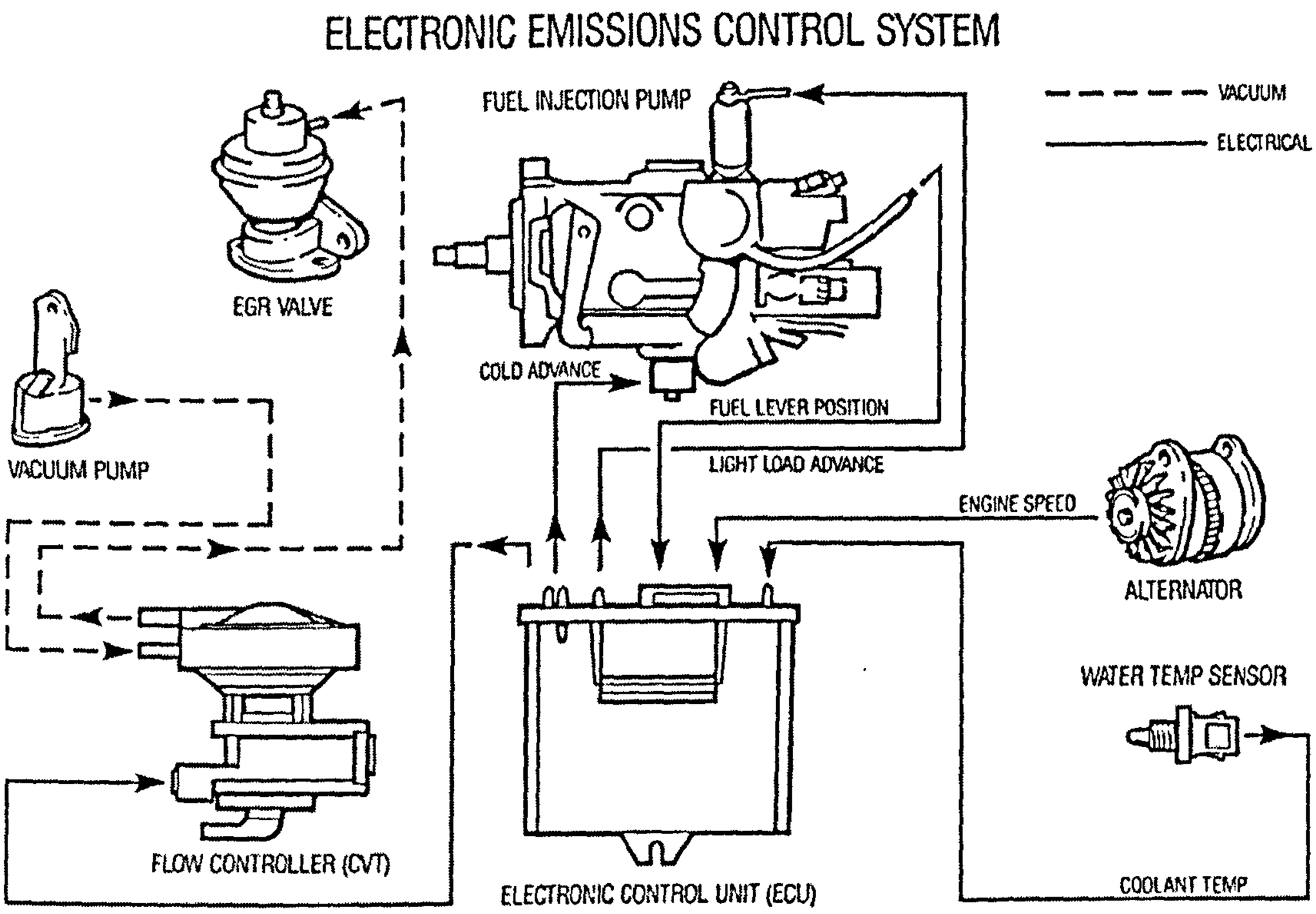

Figure 3.6 Schematic diagram of electronically controlled EGR system for Ford 1.8 litre turbocharged IDI diesel engine (Lawrence et al, 1989)

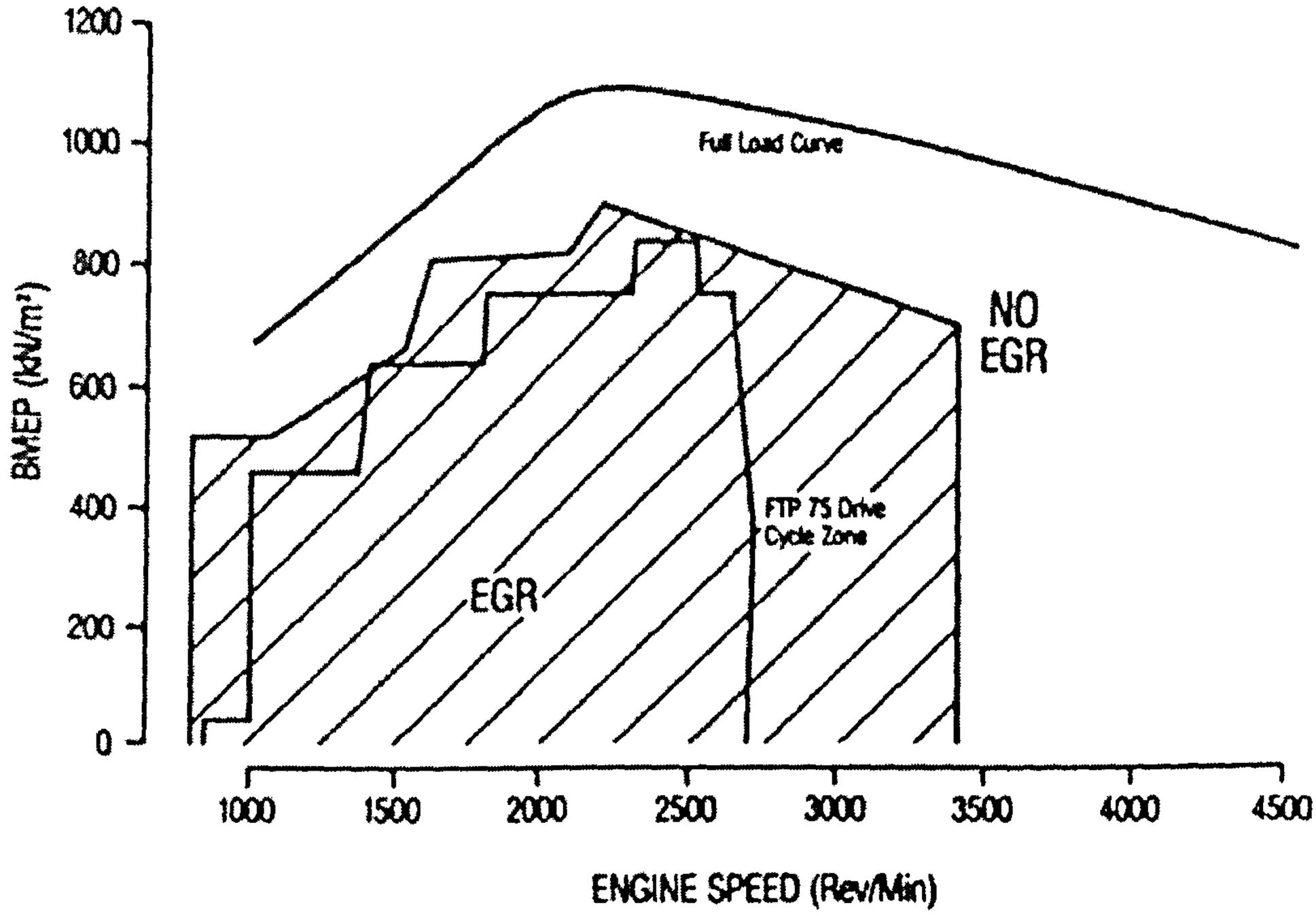

Figure 3.7 **EGR coverage related to BMEP and engine speed for Ford 1.8 litre turbocharged IDI diesel engine** (Lawrence et al, 1989)

At the same time, the truck engine team developed a mechanically modulating EGR system for the 2.5 litre direct injection diesel engine used in the Transit commercial vehicle. This was required to control NOx emissions in order to meet US Federal emissions standards required by some non-EC countries, and the forthcoming EC '5th Amendment' emissions legislation. Although the direct injection (DI) diesel engine was inherently more fuel efficient, it also emitted higher NOx levels than its IDI counterpart. The saving grace for this engine was the fact that at part load the average air to fuel ratio in the combustion chamber was far leaner than in the pre-chamber of the IDI engine. It was thus feasible to use far higher levels of EGR to reduce NOx emissions, than in the IDI engine. However, this meant that a fully modulating EGR system was required. In order to keep the additional cost to a minimum a simple, yet ingenious mechanically controlled EGR system was devised and developed for this engine. This utilised the Bosch VE mechanical fuel injection pump speed lever position for engine speed and load information, which was mechanically translated via a cam to a butterfly valve in the intake system, upstream of the EGR tube from the EGR valve. Restriction of the intake charge by the butterfly valve caused an increased depression in the intake

manifold. A connection from the higher depression side of the butterfly valve to the upper side of a diaphragm-operated EGR valve, caused the EGR valve to open. Thus exhaust gas flowed from the exhaust manifold to the intake manifold. The amount of EGR was controlled by the cam, from the movement of the pump speed lever, thus setting the butterfly valve position to give the depression in the intake manifold to lift the EGR valve and draw in exhaust gas from the exhaust manifold. This system was found to be very effective in modulating EGR to control NOx emissions and is covered by a Ford patent, following the invention by Messrs C P Davies and K Ewen. Test results, without and with EGR using this system are shown in **Table 3.1** below. Note that the NOx emissions were more than halved, and also because of the reduced exhaust gas flow, reductions of the other gaseous and particulate emissions were achieved with EGR (Horrocks, 1992).

Table 3.1

1989 Model Year 2.5 DI Transit Federal Emissions results

2040 kg inertia, 5.14:1 rear axle ratio (Horrocks 1992)

Test Condition	US Federal Emissions – g/km			
	CO	HC	NOx	Pm
Without EGR	0.94	0.28	2.78	0.22
With EGR	0.83	0.19	1.22	0.17
Reduction with EGR	12%	32%	56%	23%

The first fully electronic diesel engine management system ("drive-by-wire") used by Ford was developed for the 2.5DI turbocharged diesel that was launched in 1992, for the Transit vehicle. This took the Lucas EPIC system that had full electronic control of the fuel and EGR systems. The EGR system consisted of an EGR valve mounted on the exhaust manifold that was connected directly to a throttle body housing, downstream of the throttle. This throttle valve downstream of the compressor outlet was found to be necessary to impart a sufficient pressure drop between exhaust manifold and intake system in order to flow high levels of EGR at low loads. The throttle body was bolted to a 'cross-over' tube that transported the exhaust gas over the top of the engine to the intake manifold. This engine has a cross-flow arrangement, with intake and exhaust

manifolds on opposite sides of the cylinder head. The EGR valve and throttle received the same vacuum signal, via a current to vacuum (CVT) transducer. Both valves, therefore moved in unison, the EGR valve to open exhaust gas flow before it entered the turbine, thus also reducing boost pressure, and the throttle valve to further reduce boost, and therefore promoted exhaust gas re-circulation. The EGR valve lift position was measured with a potentiometer and the signal used for feedback to the Lucas EPIC controller, where the valve lift was mapped against speed and load.

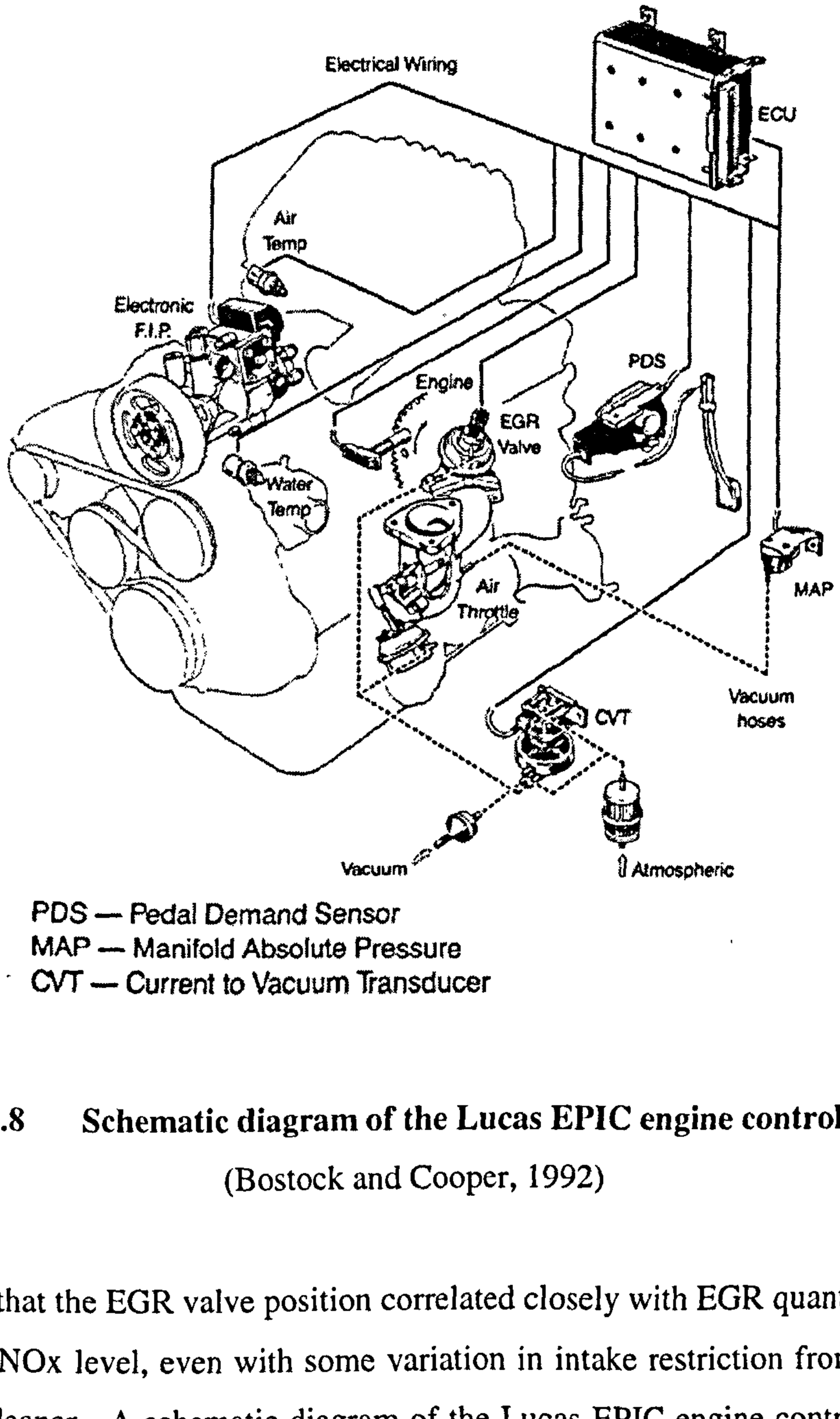

Figure 3.8 Schematic diagram of the Lucas EPIC engine control system

(Bostock and Cooper, 1992)

It was found that the EGR valve position correlated closely with EGR quantity and with the resulting NOx level, even with some variation in intake restriction from a partially blocked air cleaner. A schematic diagram of the Lucas EPIC engine control system is shown in **Figure 3.8** and **Figure 3.9** shows the induction and EGR system for the 1992

model year 2.5 litre engine. **Figure 3.10** shows the EGR rate map for this engine (Bostock and Cooper, 1992).

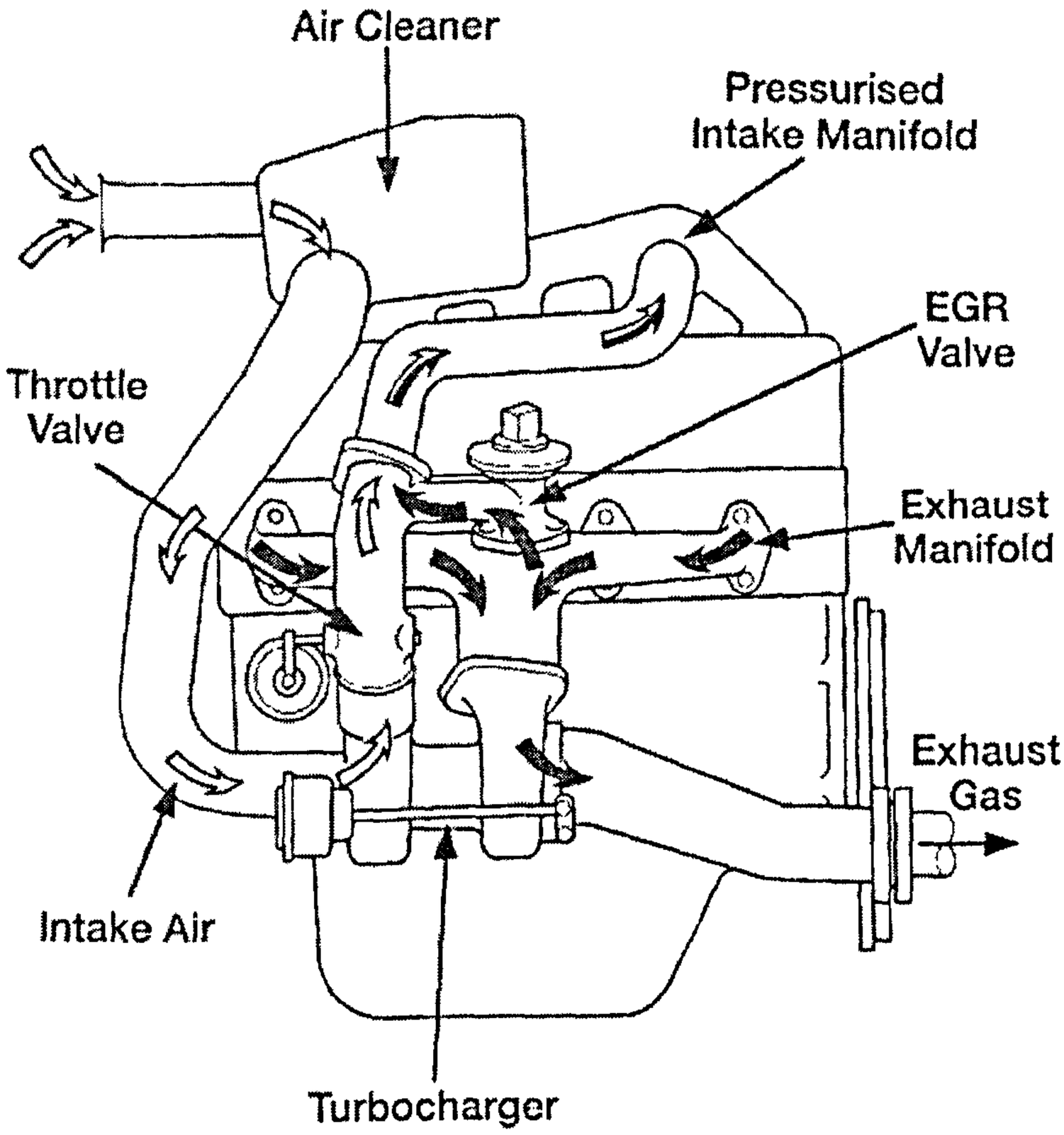

Figure 3.9 Induction, exhaust and EGR system for the Ford 2.5 litre turbocharged DI diesel engine (Bostock and Cooper, 1992).

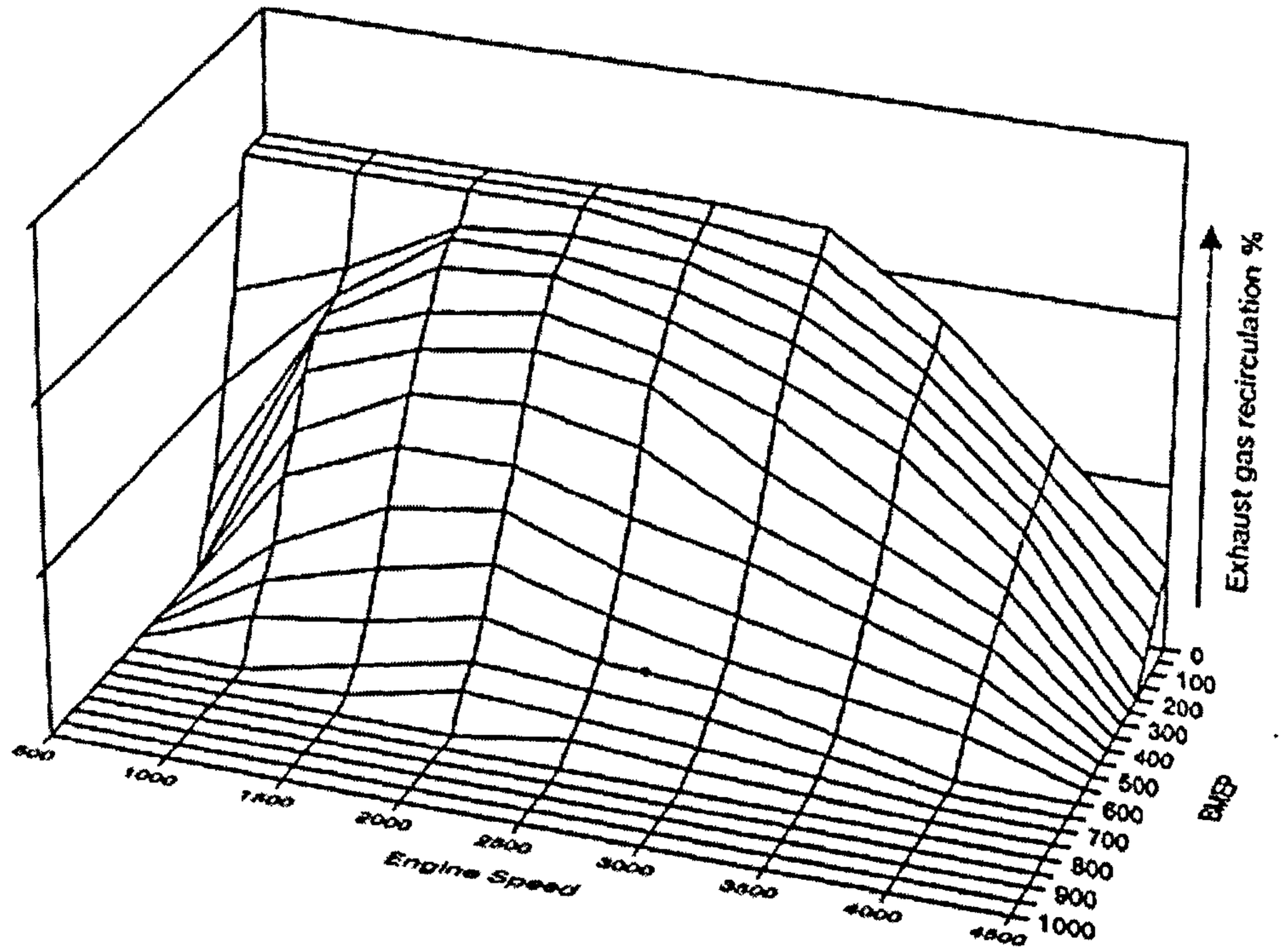

Figure 3.10 EGR map for the Ford 2.5 litre turbocharged DI diesel engine, (Bostock and Cooper, 1992).

In 1993, the 1.8 litre IDI turbocharged engine was inter-cooled to give a power of 65kW for the Mondeo car. The EGR system was improved by incorporating a mass airflow sensor, which was used as a feedback for electronic closed loop EGR control. Air mass flow, measured by a mass airflow (MAF) sensor was used as feedback for EGR control. The fuel injection pump remained the Lucas mechanical DPC, so engine load information was taken from the pump lever position and engine speed was measured from the flywheel by a crankshaft speed sensor. This information was processed by the ECU to set the EGR level to a mapped value by opening the EGR valve until the correct air mass flow was achieved for that particular engine speed and load. A schematic diagram of this control system is shown in **Figure 3.11** (Carnochan and Horrocks, 1993).

1. Electronic diesel control module
2. Crankshaft speed sensor
3. Fuel lever position sensor
4. Coolant temperature sensor
5. Mass airflow sensor
6. Exhaust gas recirculation valve
7. Current to vacuum transducer
8. Light load advance solenoid
9. Cold advance solenoid
10. Catalyst
11. Turbocharger
12. Air cleaner
13. Vacuum pump
14. Injection pump
15. Injector
16. Intercooler

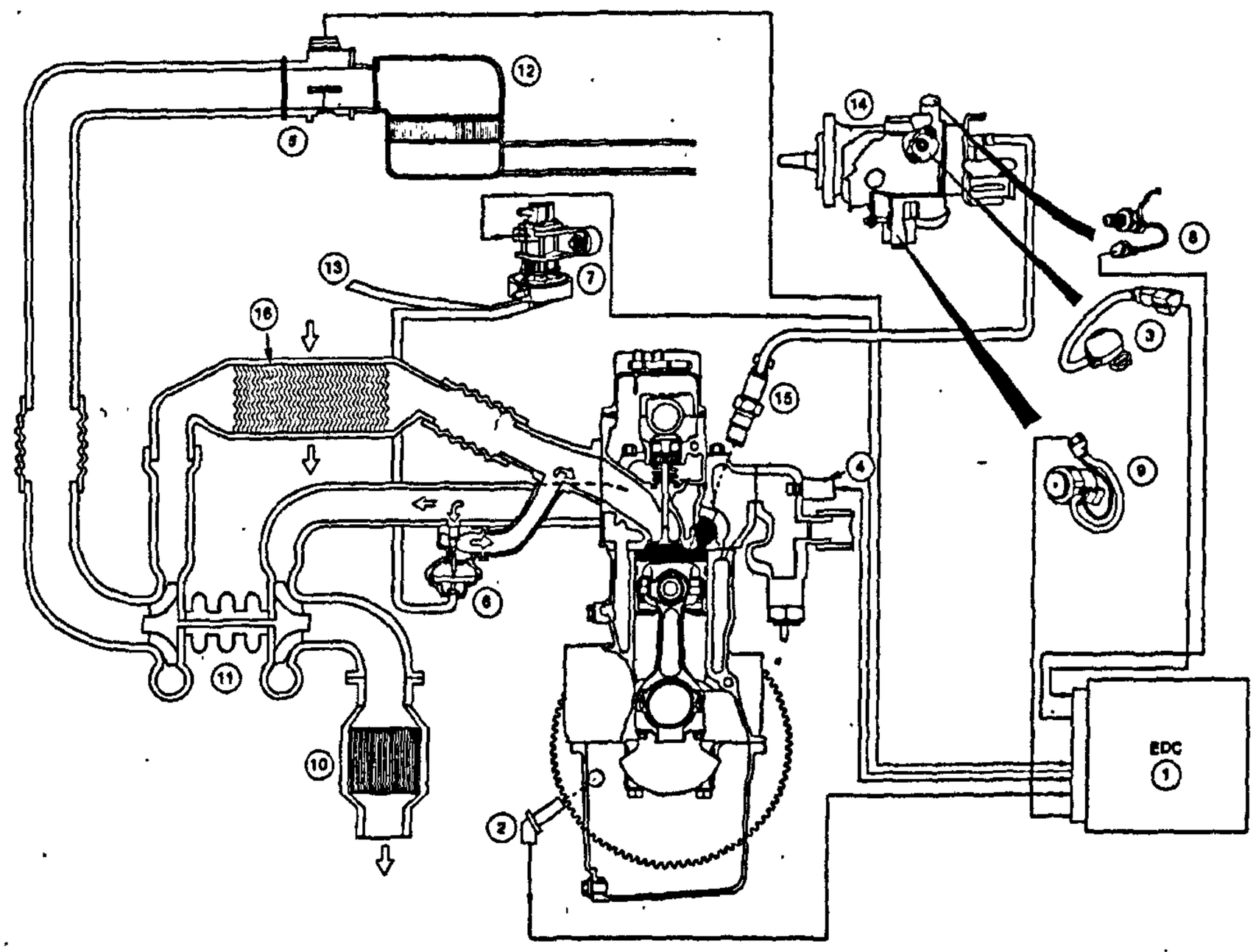

Figure 3.11 Schematic diagram of electronic control system for Ford 1.8 litre turbocharged IDI diesel engine in Mondeo car (Carnochan & Horrocks, 1993).

For the 1997 model year, the EGR valve was integrated with the intake manifold, to reduce the system complexity, weight and cost to give a high value modular component. This part is shown in **Figure 3.12.**

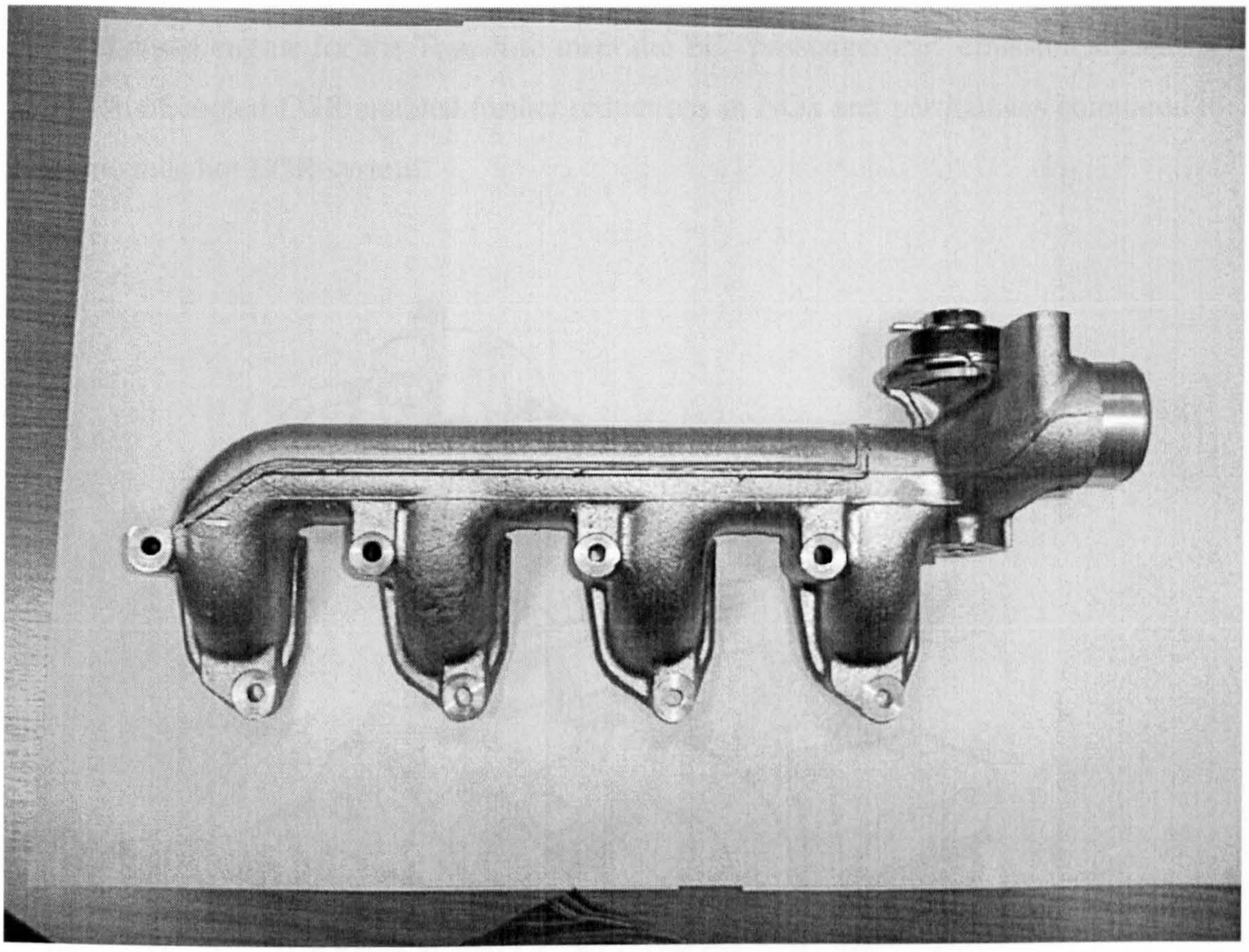

Figure 3.12 Ford 1.8 litre IDI diesel intake manifold and integrated EGR valve.

The different philosophies of EGR system design and control strategy, between the IDI and DI groups at Ford, can be explained in part by the inherent control aspects of each system. Mass airflow feedback control, while being a more expensive system, ensures the correct air-fuel ratio for in-cylinder combustion without excessive smoke levels, which had been a concern with the IDI engine. Thus any alterations in intake or exhaust system pressures, owing to a dirty air filter or a soot loaded silencer, did not influence the air-fuel ratio of the cylinder charge, because the EGR level was controlled on intake charge air flow mass. For the DI engine, being more tolerant to EGR level, precise air-fuel ratio control was not such a strong priority, and the lower cost EGR valve lift feedback system was the best value solution. In summary, while both EGR systems are aimed at controlling NOx emissions, the MAF system also inherently ensures smoke level control. The EGR valve feed-back system, on the other hand, ensures NOx control under all conditions, since the EGR valve will always open the correct amount, for a given engine condition.

Ford introduced the concept of cooled EGR for the 1993 model year 85PS 2.5 litre DI turbocharged engine for the Transit to meet the EC "passenger car" emission standards. The use of cooled EGR enabled further reductions in NOx and particulates compared to the previous hot EGR system.

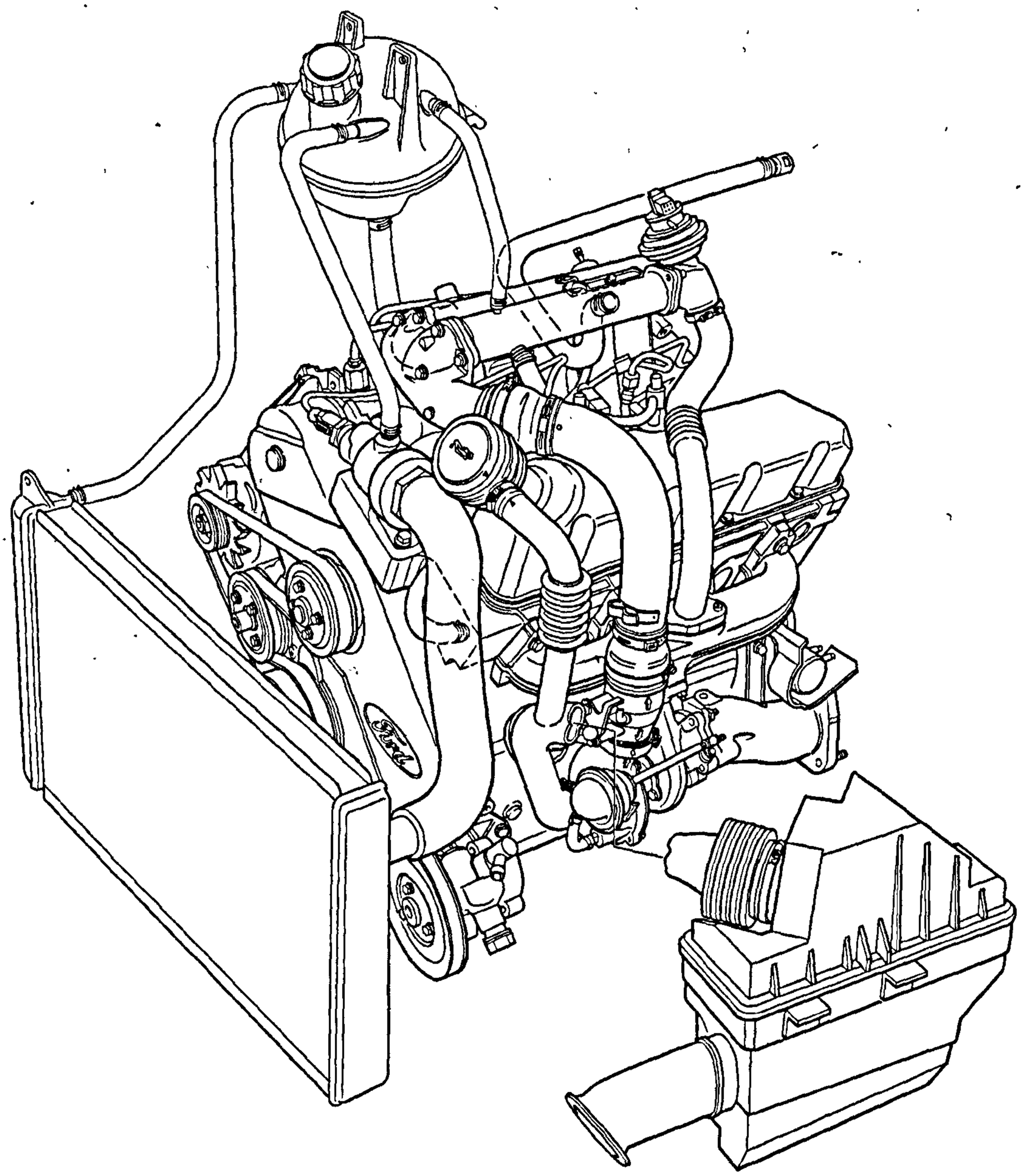

Figure 3.13 1993 model year 85PS 2.5 litre DI turbocharged engine for the Transit

Figure 3.13 shows a diagram of the 1993 model year 85PS 2.5 litre DI turbocharged engine for the Transit. The EGR cooler was installed above the engine parallel to the

crankshaft axis, adjacent to the intake manifold plenum. EGR was taken from the exhaust manifold by a pipe up to the EGR valve that was attached to the end of the cooler. The gases were therefore cooled before mixing with the charge air at the outlet of the cooler and flowing to the plenum of the intake manifold, as can be seen in **Figure 3.13.**

Ford's new 1.8 litre Endura DI diesel engine for the Focus, a further development of the Dagenham 1.8 litre diesel, has a modern EGR system incorporating the latest technical features. The system is shown in **Figure 3.14.** Exhaust gas is re-circulated from the exhaust manifold, before entry to the turbocharger turbine, via a cooler and EGR valve to the intake manifold. This engine has a "U" flow arrangement, thus the exhaust and intake manifolds are on the same side of the cylinder head. The EGR flow rate is controlled by the vacuum actuated valve that is directly integrated into the intake manifold for reduced component complexity, cost and improved package efficiency, this module is shown in **Figure 3.15**. A stainless steel shell and tube EGR cooler is packaged at the exhaust manifold to cool the exhaust gas before it is re-circulated via the valve into the intake manifold. Using coolant from the engine, exhaust gas temperature is reduced by up to 200 degrees C. The reduction in EGR gas temperature and consequent increase in density both reduces inlet charge temperature and allows higher levels of EGR to be used therefore giving greater NOx emissions reductions. The combination of higher EGR and density air not only helps lower NOx, but also ameliorates the increase in smoke emissions that usually accompany increased EGR levels. The cooler has the additional benefit of improving cabin heater performance as additional heat energy is added to the engine coolant system during cold start and warm up, (Lawrence 1998).

The EGR valve seat incorporates a "conical" profiled seat for improved flow control at low valve lift. In addition to the main valve diaphragm, a secondary rolling stem seal is present to prevent oil in exhaust and vent gases migrating past the valve and bush arrangement, improving long term reliability.

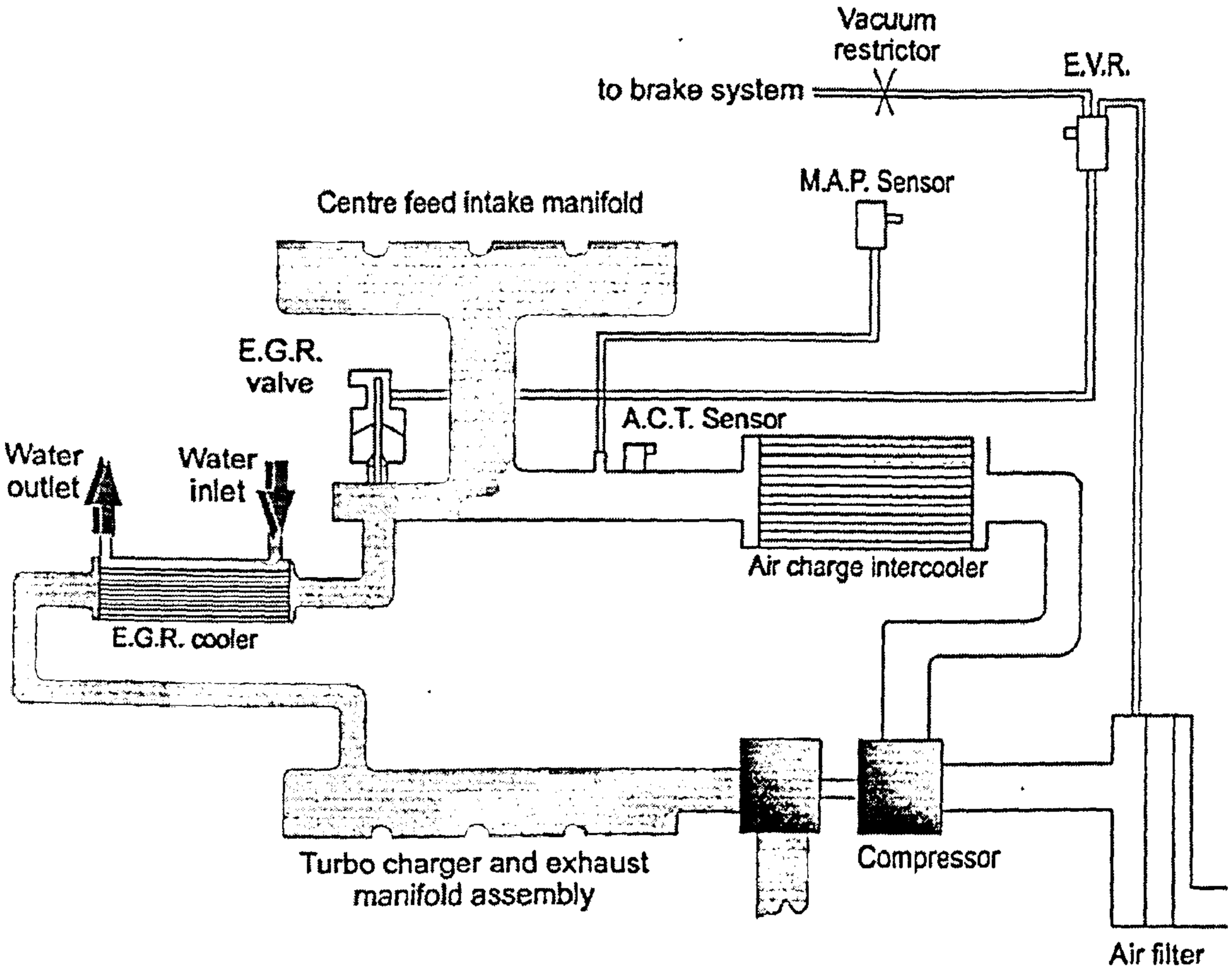

Figure 3.14 Schematic of EGR system for Ford 1.8 litre Endura DI diesel engine for the Focus car (Lawrence 1998).

The intake manifold has a central entry, where the charge air and EGR are introduced, this feature gives good EGR distribution between the cylinders, an essential feature to maximise the use of EGR to high levels. EGR valve position and hence flow, is controlled by the engine management system, the Ford EEC V module, with closed loop feed-back of valve position by a potentiometer fitted on the EGR valve. The vacuum level to open the EGR valve is set by the ECU using an EVR current to vacuum regulator. It is interesting to note that mass airflow (MAF) control of EGR, used on the earlier IDI engines in Mondeo, has been dropped in favour of EGR valve feedback. This will be discussed in more detail under EGR Control (Lawrence, 1998).

Figure 3.15 Ford Endura DI diesel intake manifold and integrated EGR valve

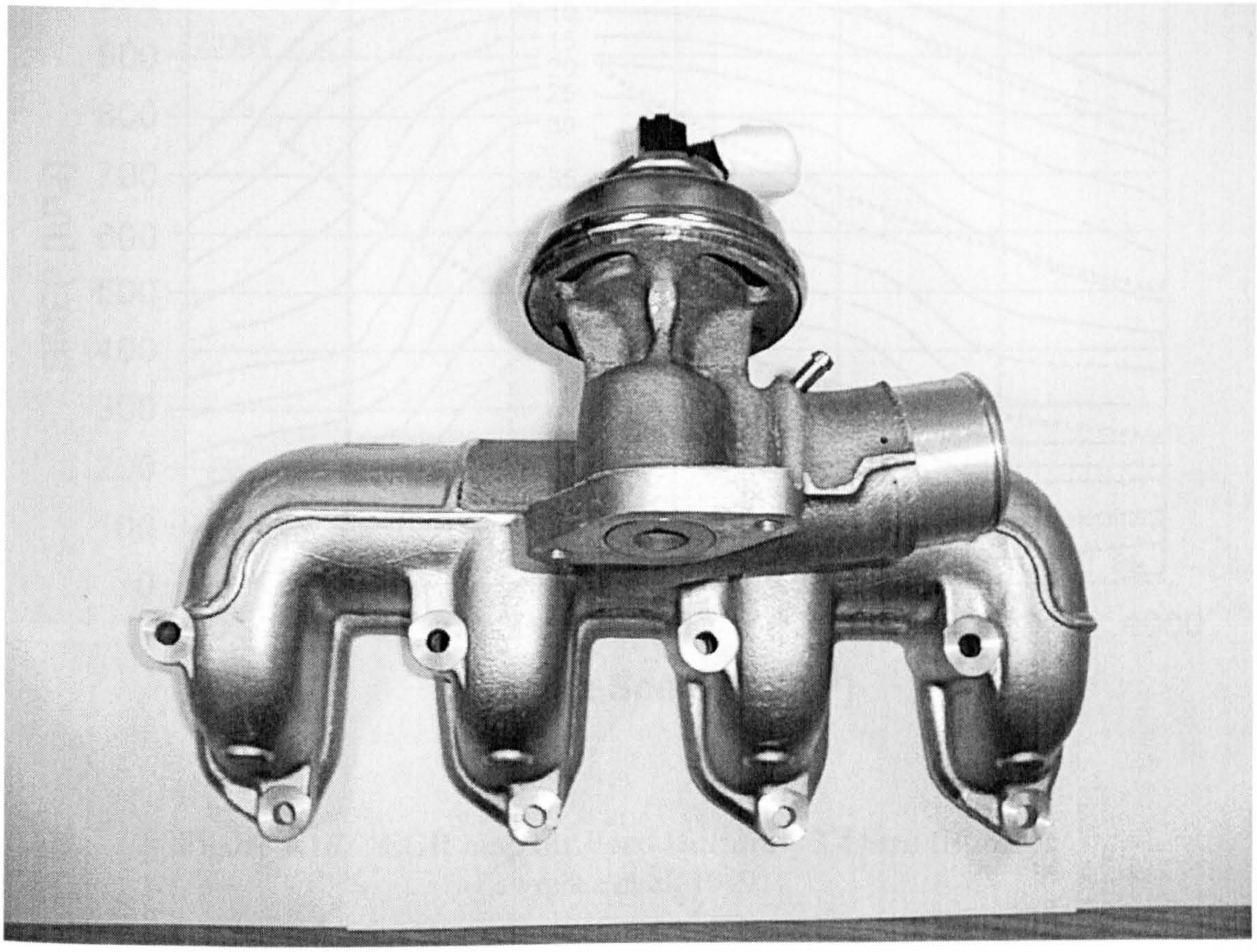

The new Duratorq 16-valve 2.4 litre DI diesel, for the new Transit, has a typical modern EGR system. A vacuum-actuated valve that incorporates a pintle design to improve controllability at low valve lifts, regulates the rate of EGR. Control of this valve is by the engine management system, via an electro-vacuum regulator. Closed-loop feedback of valve position is achieved using a valve lift potentiometer. An EGR cooler is used for the 66kW and 88kW variants. This increases the effectiveness by reducing the EGR temperature by up to 200°C. Thus reducing intake charge temperature, for a constant EGR mass, and allowing higher EGR rates to achieve substantial NO_x reductions. The EGR map for this engine is shown in **Figure 3.16**, **Figures 3.17 and 3.18** show the Duratorq EGR system layout and components (Lawrence et al, 2000).

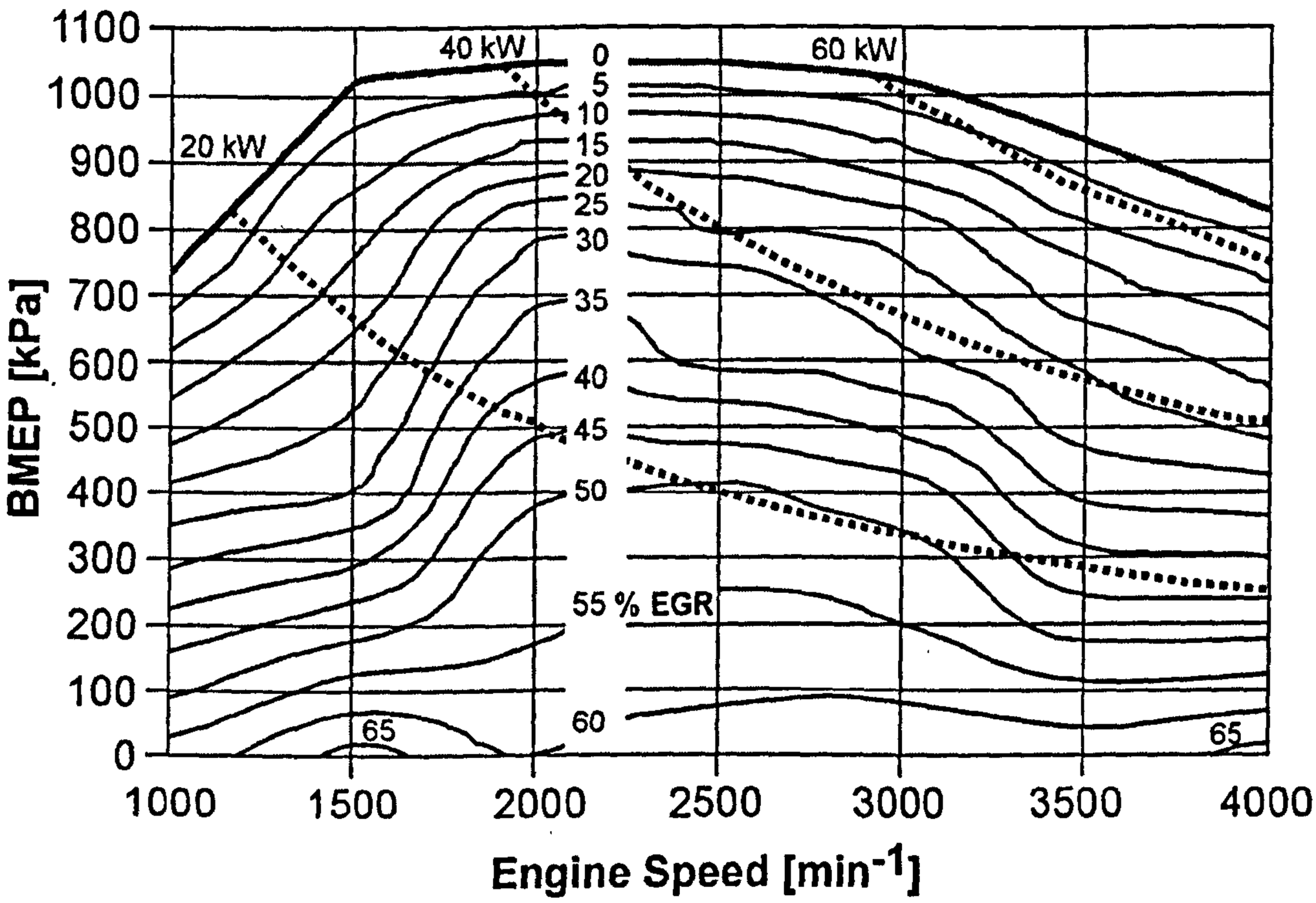

Figure 3.16 EGR map for Ford Duratorq 2.4 litre DI diesel
(Lawrence et al, 1999)

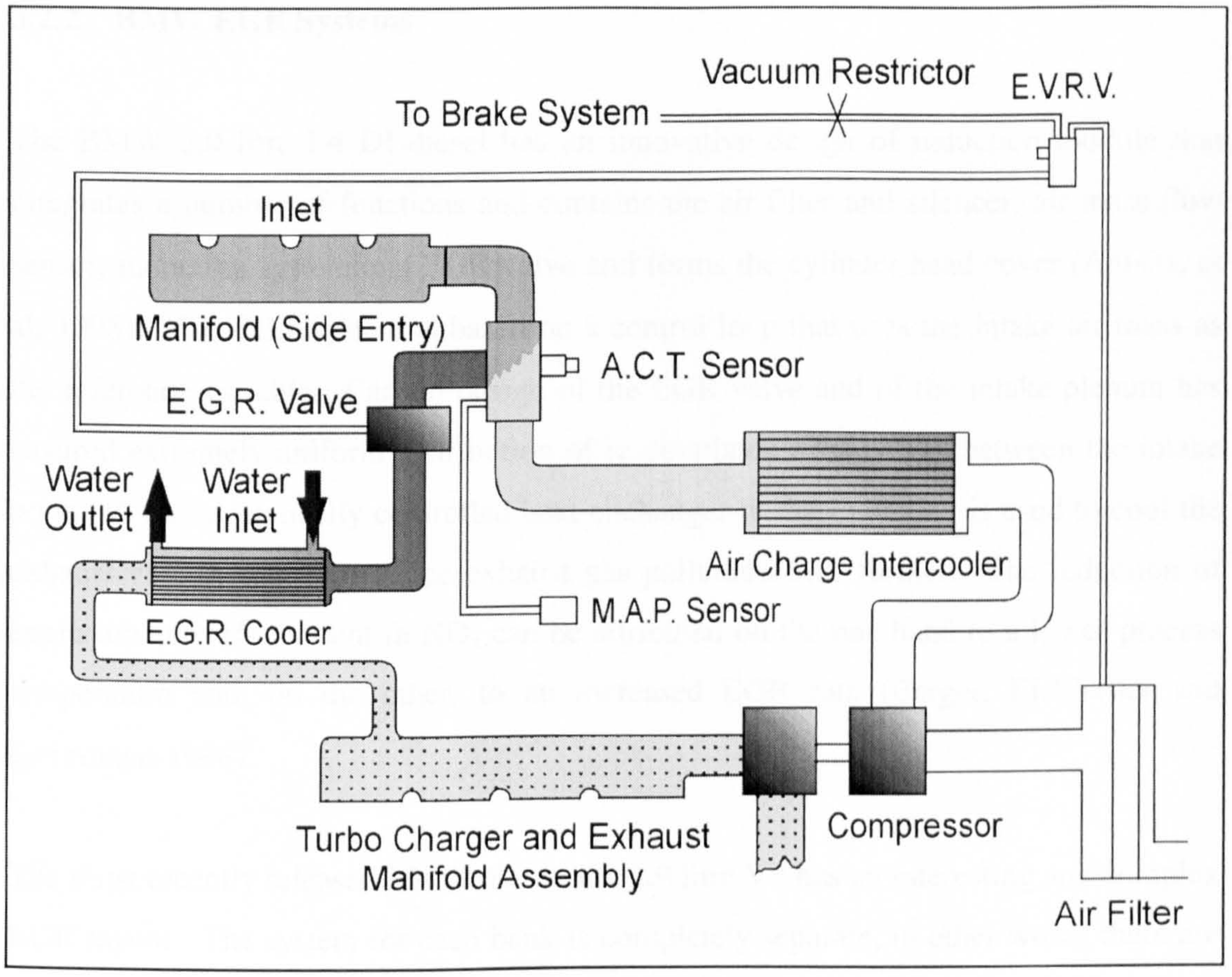

Figures 3.17 and 3.18 Ford DURATORQ diesel EGR System layout and components (Lawrence et al, 1999)

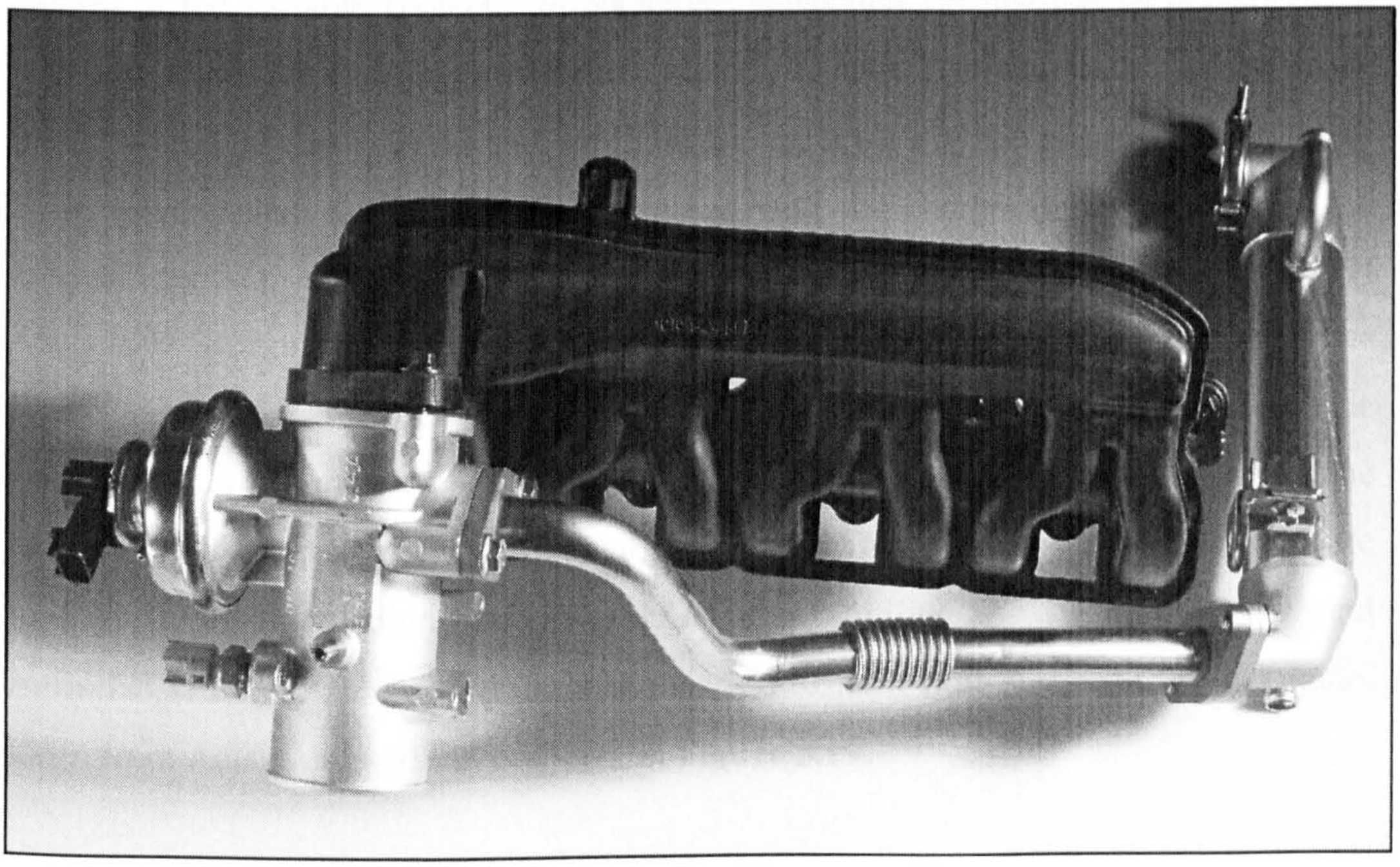

3.2.2 BMW EGR Systems

The BMW 2.0 litre I-4 DI diesel has an innovative design of induction module that integrates a number of functions and contains the air filter and silencer, air mass flow sensor, induction system and EGR valve and forms the cylinder head cover (Anisits, et al, 1998). The EGR system is based on a control loop that uses the intake air mass as the reference variable. Careful design of the EGR valve and of the intake plenum has ensured extremely uniform distribution of re-circulated exhaust gas between the intake ports. A thermostatically controlled heat exchanger in the EGR line is used to cool the exhaust gas, in order to reduce exhaust gas pollutants still further. The reduction of approximately 15 per cent in NO_x can be attributed on the one hand to a lower process temperature and, on the other, to an increased EGR rate (Berger, Eichlseder and Steinmayr, 1998).

The most recently released BMW diesel, the 3.9 litre V8 has an interesting and complex EGR layout. The system for each bank is completely separate, in other words there are two systems, one for each bank of cylinders. The intake and exhaust systems are also separate for the two banks. This is reported by Ansits et al (1999) to give very precise control of the variable geometry turbocharger vanes and exhaust gas recirculation. A duct cast at the rear of the cylinder heads takes the exhaust gas from the outside to inside the 'V' where the gas goes through an EGR cooler, cooled by the engine coolant, to the EGR valve, where the exhaust gas is mixed with the charge air. Interestingly, the exhaust gas from one bank is fed back into the other. In a presentation at RWTH Aachen, Dr Borgmann explained that this layout was simply expedient plumbing. The intake manifold is divided horizontally into two levels. In the upper level, the compressed air is mixed with the re-circulated exhaust gas; in the lower level, the mixture is distributed to the individual cylinders. This design is reported to ensure uniform EGR distribution and good EGR compatibility (Ansits et al, 1999 and Nefischer et al, 1999). A diagram of the air and exhaust flow systems for this engine, taken from Anisits et al (1999) is shown in **Figure 3.19.**

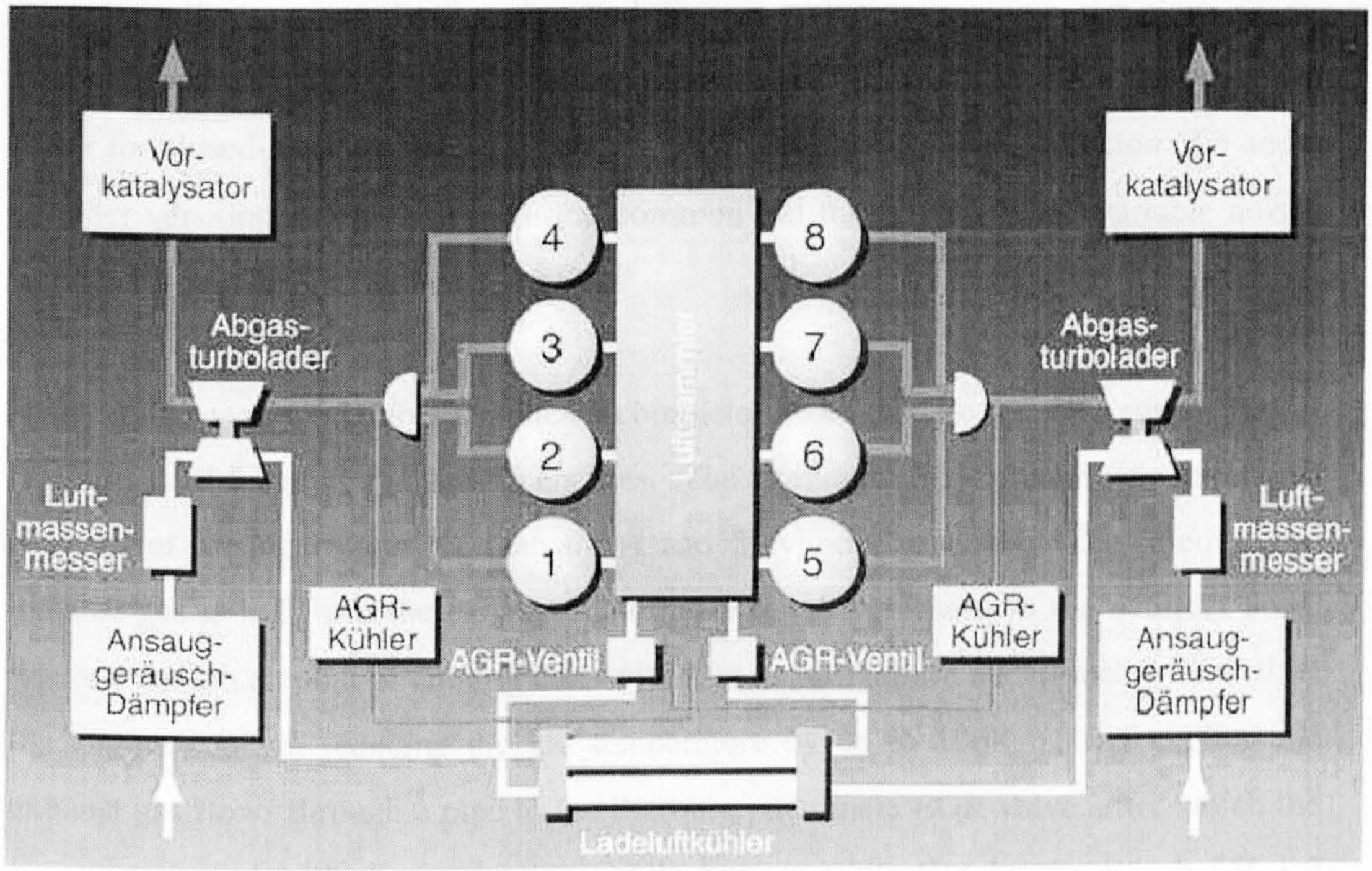

Figure 3.19 BMW V8 air intake and exhaust gas flow system (Anisits et al, 1999)

3.2.3 Mercedes-Benz EGR systems

The Mercedes A class has two variants of a 1.7 litre 4-valve DI diesel with Bosch common rail (OM668). EGR gas is taken from the opposite end of the exhaust manifold from the turbocharger, in a stainless steel pipe, to an aluminium pipe, which also acts as a support bracket for the intake module, to the EGR valve, after which the exhaust gas is introduced and mixed with the intake air charge. Upstream of the EGR mixing point is a throttle valve that is used to increase the pressure gradient between the air charge and exhaust. Thus EGR and intake charge throttle valves control the flow of EGR, both units are vacuum operated and controlled by the ECU. A hot wire air mass flow meter is integrated into the intake pipe to measure the intake mass airflow (Brueggeman and Wamser, 1997).

The C220 turbo-diesel, introduced in 1997 with a new 2.2 litre engine (OM611), featuring 4-valves per cylinder and common rail fuel injection equipment, had a pneumatically operated EGR valve and throttle valve to regulate the flow of re-circulated exhaust gas, which was controlled by the ECU using a hot-wire mass air flow meter for closed-loop control. This engine was revised with the introduction of 5 and 6 cylinder versions in 1999, all featuring common rail fuel injection and variable nozzle turbochargers, (Peters and Puetz, 1997).

Mahle Filter-systeme GmbH supplies a complete intake module for the new 4 cylinder (OM611) and 5 cylinder (OM612) engines. The integrated EGR system was developed as a set of identical parts for both the 4 and 5 cylinder modules. The re-circulated exhaust gas is fed from the exhaust manifold through a passage in the cylinder head, where a certain amount of cooling takes place, to an aluminium duct which is cooled by the engine coolant, reducing the gas temperature by up to 100K. After cooling the exhaust gas flows through a pipe to the Pierburg pneumatic EGR valve, after which the gases are mixed with the intake air. EGR flow is controlled by the Bosch CR 1.0 control unit using feed-back on air mass flow, a mass air flow sensor being mounted in the clean air pipe before the turbocharger, Elsaesser A, Braun and Jensen (2000), Klingmann Flick and Brueggemann (1999). The 6-cylinder engine (OM613) has a separate stainless steel EGR cooler, rather than the water-cooled aluminium duct used on the 4 and 5 cylinder engines. Also, the larger manifold of the 6-cylinder engine is made of aluminium, (Klingmann et al, 1999).

The latest diesel engine in the Mercedes-Benz stable is the 4.0 litre V-8 that was released in 2000. This has the same major dimensions as the 4, 5 and 6 cylinder engines and shares many of the technical features. The two VNT turbochargers have electric actuators and the intake air filtering system has two hot-film mass airflow meters, in order to equalise the air mass flow to each bank of cylinders. Two EGR valves are combined in one casting with two separate electrical actuators, these are located in the "V" of the banks, upstream of the single EGR cooler. The exhaust gas is introduced to the intake charge at a throttle located after the air/water intercooler. The throttle is also electrically actuated. Electric actuation was chosen because of the speed of response and the in-built position feedback. Moreover, electric actuation of the turbine vanes

provides the option of open-loop control of the turbochargers in the EGR zone. In this way it is possible to reduce pumping work and to decouple boost pressure control from air mass flow control, Brueggemann et al (2000).

3.2.4 Volkswagen Audi (VAG) EGR systems

VAG introduced its 1.9 litre TDI engine for the 1992 model year in the Audi 80 car. This engine was equipped with an EGR system controlled by the Bosch MSA6 electronic diesel engine management system, which controlled the Bosch VP34 fuel injection pump and EGR systems. To achieve high EGR flows at low loads, exhaust gas was taken from the exhaust manifold upstream of the turbocharger and returned to the intake downstream of the charge-air cooler. This control system used an air mass flow meter to modulate the EGR valve lift and hence flow rate, to achieve a nominal mapped value for air mass flow versus engine speed and fuel flow, Rhode et al (1991). Later developments of this system were to incorporate the EGR valve into the aluminium intake manifold, creating a modular unit.

The Audi 2.5 litre V6 diesel engine is equipped with a single VNT turbocharger located at the rear of the 'V.' This sits on a cast iron manifold, located at the rear of the engine in the middle of the 'V' that joins the two exhaust pipes from the manifolds on each bank. It is from this central manifold that the EGR is taken upstream of the turbocharger. A vacuum motor controls the VNT turbocharger turbine vanes. An EGR pipe takes the gas to a pneumatic EGR valve, which is connected via another EGR pipe to an aluminium charge-air pipe that connects to the two intake manifolds, one for each bank.

The new Audi 3.3 litre V8 is equipped with two VNT turbochargers located on the exhaust manifold of each bank. EGR is taken from each manifold via thin walled stainless steel tubes to EGR valves, both of which are located on the intake manifold module positioned in the middle of the bank. This module contains the air to water intercooler and the EGR cooler which is also water-cooled. Both charge air and EGR are water cooled in this unit. The EGR is then introduced to the charge air in the plenum of the intake manifold on top of the cooler, within this unit. The two EGR valves are pneumatically operated, (Bach et al, 1999).

Table 3.2 Automotive DI Diesel Engine EGR Systems Summary

Engine	Air flow meter	Air intake throttle	EGR valve location	EGR valve actation	EGR cooler	EGR thru' cylinder head	Turbo type
Audi 2.5 V-6	Yes	No	One – "hot" side	Vacuum	No	No	VNT
Audi 3.3 V-8	Yes - 2	Yes (1)	Two - "hot" side	Vacuum	Yes (2)	No	VNT – 2
BMW 2.0 I-4	Yes	No	"Cold" side attached to intake manifold	Vacuum	Yes	No	VNT
BMW 2.9 I-6	Yes	No	"Cold" side attached to intake manifold	Vacuum	Yes	No	VNT
BMW 3.9 V-8	Yes – 2	No	Two "cold" side attached to intake manifold	Vacuum	Yes - 2	Yes	VNT – 2 (3)
Fiat 1.9 I-4 JDT	Yes	No	"Hot" - located on exhaust manifold	Vacuum	No	No	W/G
Fiat 2.4 I-5 JDT	Yes	No	"Hot" - located on exhaust manifold	Vacuum	No	No	VNT
GM 2.0 I-4 Ecotec	Yes	No	Incorporated in intake manifold	Vacuum	No	Yes	W/G TC
Mazda 2.0 I-4	Yes	No	Mounted on intake manifold	Vacuum	No	No	VNT
Mercedes SMART CDI	No (4)	No	Mounted on intake manifold	Electric	No	No	W/G TC
Mercedes 1.7 I-4, OM668	Yes	Yes	Mounted on intake manifold	Vacuum	No	No	W/G TC
Mercedes 2.2 I-4, OM611	Yes	No	"Cold" side mounted on intake manifold	Vacuum	Yes (5)	Yes	VNT
Mercedes 2.7 I-5, OM612	Yes	No	"Cold" side mounted on intake manifold	Vacuum	Yes (5)	Yes	VNT
Mercedes 3.2 I-6, OM613	Yes	No	"Cold" side mounted on intake manifold	Vacuum	Yes	Yes	VNT
Mercedes 4.0 V-8, OM628	Yes – 2	Yes-1(3)	Two, "hot" side	Electric	Yes- 1	No	VNT – 2 (3)
Nissan 2.0 I-4	Yes	No	Mounted on intake manifold	Electric stepper motor	No	No	VNT
PSA 2.0 I-4	Yes	No	"Hot" - located on exhaust manifold	Vacuum	No	No	W/G TC
Renault 1.9 I-4	Yes	No	On intake manifold	Vacuum	No	No	W/G TC
Rover Storm 2.5 litre I-5	Yes		"Hot" mounted on exhaust manifold	Vacuum			W/G TC
Toyota 2.0 I-4	No (4)	Yes	"Cold" side mounted on intake manifold	Vacuum	Yes	No	W/G TC
VW 1.4 I-3	Yes	Yes (1)		Vacuum	No	No	W/G TC
VW 1.9 I-4	Yes	No	Mounted on intake manifold	Vacuum	No	No	W/G TC

Note (1) Used for engine shut-off.
Note (2) Part of the air to water intercooler module located in the "V" of the engine.
Note (3) Electric actuators
Note (4) EGR controlled by EGR valve lift feed-back.
Note (5) Cooling occurs through the cylinder head and further cooling occurs in a water-cooled aluminium combination manifold.

Table 3.3 Automotive DI Diesel Engine EGR Systems References

Engine	Reference
Audi 2.5 V-6	Bauder et al (1999)
Audi 3.3 V-8	Schiller and Ruegheimer (1999), Bach et al (1999)
BMW 2.0 I-4	Anisits et al (1998), Berger et al (1998), Ford Competitive Analysis (1999)
BMW 2.9 I-6	Anisits et al (1998), Anisits et al (1999)
BMW 3.9 V-8	Anisits et al (1999)
Fiat 1.9 I-4 JDT	Piccone and Rinolfi (1997)
Fiat 2.4 I-5 JDT	Piccone and Rinolfi (1997)
GM 2.0 I-4 Ecotec	
Mazda 2.0 I-4	Ford internal data
Mercedes SMART CDI	Thiemann et al (1999), Dietz (1999)
Mercedes 1.7 I-4, OM668	Brueggemann (1997), Ford Competitive Analysis (1999)
Mercedes 2.2 I-4, OM611	Klingmann, et al (1999)
Mercedes 2.7 I-5, OM612	Klingmann, et al (1999)
Mercedes 3.2 I-6, OM613	Klingmann, et al (1999)
Mercedes 4.0 V-8, OM628	Brueggemann et al (1999), Brueggemann et al (2000), Jost (2001)
Nissan	Mase et al (1998)
PSA 2.0 I-4	
Renault 1.9 I-4	
Rover Storm 2.5 I-5	Rover Press Information
Toyota 2.0 I-4	Toyota Press Information (1997)
VW 1.4 I-3	Neumann et al (1998)
VW 1.9 I-4	Rhode et al (1991)

Table 3.2 shows a summary of automotive DI diesel EGR systems and **Table 3.3** provides the references. The range of EGR components fitted to these engines can be reviewed. Clearly the majority of engines use airflow meters, while only a small number use air throttles. The valve location is of interest, ranging from the "hot" side mounted on the exhaust manifold, to the "cold" side after the cooler. Approximately half the engines use EGR coolers and a small number route the EGR through the cylinder head. Just over half the engines use VNT turbochargers. A brief history of VNT turbochargers is given in **Appendix 4** on page 270.

3.2.5 EGR Valve Position, "Hot" versus "Cold" Side

The review of current production automotive diesel engine EGR systems shown in **Table 3.2**, demonstrates a range of EGR valve positions; varying from a "hot" position on or near the exhaust manifold, to a "cooler" position on the intake manifold, or a "cold" location at the cold side of the EGR cooler. Apart from packaging constraints, the position of the EGR valve is determined by the peak temperatures it will withstand, and the effect on its operation. **Table 3.4** below summarises the advantages and disadvantages of the alternative positions.

Table 3.4 EGR Valve Position, "Hot" versus "Cold" Side

Valve Position	Advantages	Disadvantages
Hot-side	▪ Minimizes carbon and lacquer build-up, and formation of sulphuric acid	▪ Larger valve diameter ▪ Requires isolation or water cooling for electric actuator ▪ Special materials ▪ Higher cost valve
Cold-side	▪ Smaller valve ▪ Lower cost materials ▪ Lower cost valve assembly ▪ Reduced EGR gas volume to intake system	▪ Increased susceptibility to fouling and condensate formation

With the trend towards electric actuation of EGR valves, there will also be a move towards "cold" side valves owing to the temperature limitations of the electric components. The potential danger of a cold side valve is a build-up of lacquer on the valve stem, which can cause the valve to stick. There may also be a greater build-up of soot and heavy-hydrocarbon deposits on the valve, as well as a higher possibility of condensate formation, which may well be acidic.

3.2.6 Heavy-Truck EGR systems

Heavy-duty engine manufacturers are now considering EGR as a means to reduce NOx for the next regulated level. Stage 4 in Europe reduces the NOx standard to 3.5 g/kWh at 2005, and for 2008 there is a further reduction to 2.0g/kWh. In the US a level of 2.0g/hp hour will become effective in October 2002. There has historically been a reluctance to follow light-duty practice in the use of EGR because of the adverse effect on long-term durability, but the low level of the new standards means that the use of EGR is the only viable option to further reduce NOx without further worsening of fuel consumption.

Until now, NOx reductions have been achieved by retarding injection timing. However, engine design experts at all of the engine manufacturers say the 2002 limit is beyond the point where further retardation would suffice. EGR is the technology that will have to be used. The good news is that EGR is so efficient in controlling NOx, when it is cooled before its return to the engine, that engine designers expect to be able to advance injection timing which will both reduce soot and improve fuel economy (Fetterman and Shank, 2000).

One of the major concerns about using EGR with high-output diesel engines stems from this need to cool the exhaust gases. Typically, US diesel fuel contains some 300-400 ppm sulphur, which, on combustion, can form SO_x. Other combustion products include NO_x and predominantly, water. If the exhaust gases are hot, all of these components remain gaseous. However, when the EGR stream is cooled before it is returned to the engine, the mixture drops below its dew point. Water condenses out, reacts with the NO_x and SO_x and forms a mist of nitric and sulphuric acids in the EGR stream. This is then fed back into the engine where it can cause catastrophic increases in piston and ring wear (Fetterman and Shank, 2000). Experience on European light-duty engines has not shown this to be an issue; generally the EGR gases are not cooled below the dew point under normal engine operation.

MAN, the German truck and engine manufacturer has become the first to go for EGR to reduce NOx emissions. All the company's Euro 3 engines have some sort of EGR. Dr

Klaus Schubert, MAN Chairman and former technical director concedes that there is a crucial trade-off between NOx, particulates and fuel consumption. Using EGR to cut NOx allows injection timing to be advanced which brings down particulates and helps fuel economy. To incorporate EGR across the entire engine range MAN has come up with a low-cost version for the smaller units, using a modest 4 to 5 per cent by closing the exhaust valve 25 degrees early, to increase the residual fraction and provide "internal" EGR. The bigger engines adopt a more typical system, bleeding 10 to 12 per cent from the exhaust manifold back via an EGR cooler to the intake. There is no electronic control, but a butterfly valve built into the cooler is used to cut out EGR for starting and at high loads. Electronic controls will come in the third quarter of 2001 with second generation Bosch common rail fuel injection equipment (Anon, 1999).

In the United States, Cummins Engine Company, Inc. produces a version of its 5.9 litre B-series DI diesel engine with non-cooled EGR. The engine was developed to meet the stringent Californian Transitional Low Emissions Vehicle (TLEV) standards for heavy-duty engines. EGR is controlled electronically in response to throttle demand and ambient conditions. The EGR system is subject to on-board diagnostic requirements for emission controls. The Cummins TLEV automotive engine uses a form of open-loop control of EGR. EGR is drawn from the exhaust manifold upstream of the turbocharger turbine and transferred to the intake manifold via a flow control orifice and a vacuum actuated EGR valve. The EGR valve is used to close the EGR path during start-up and during periods when the engine coolant is below a prescribed value. The venturi is used to increase the available pressure differential between the exhaust and intake manifolds, which can be limited on efficiently turbocharged engines. A schematic diagram of this system is shown in **Figure 3.20**. The EGR rate schedule with engine speed and load is determined by the natural characteristics of the EGR and air-handling systems (Charlton, 1998).

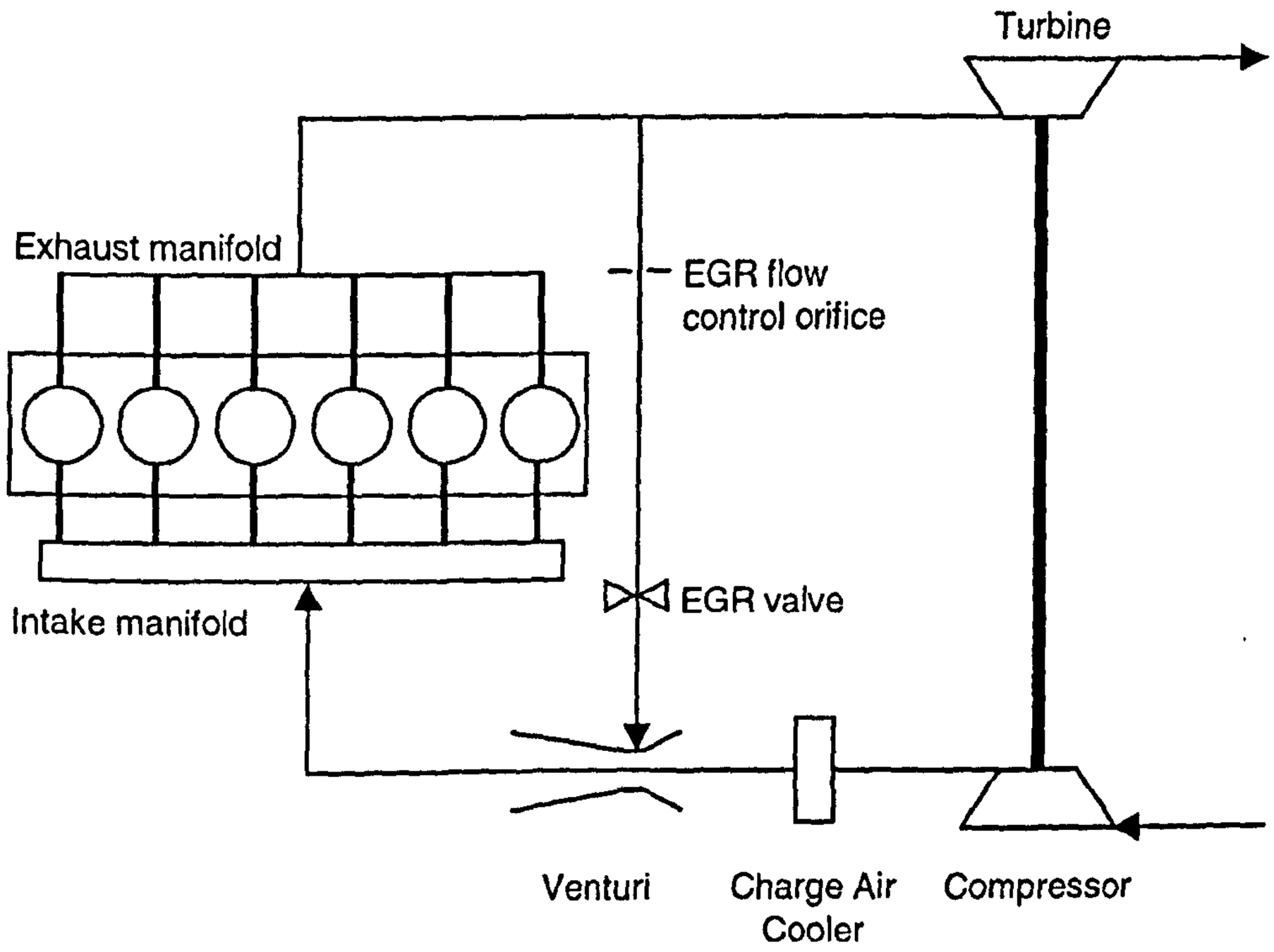

Figure 3.20 Schematic diagram of Cummins TLEV diesel engine EGR system (Charlton, 1998).

3.3 Experimental EGR Systems

In the late 1970s Ford management was concerned about the impact of potential forthcoming legislation to limit NOx emissions; there was a fear that it might limit the sales of light-duty diesel vehicles. Accordingly, a joint project was set up with Robert Bosch GmbH to establish what magnitude of reduction might be possible if a sophisticated EGR system was to be applied to the 2.36 litre IDI diesel engine then in production. The proposed system made use of the Bosch "Jetronic" petrol injection hardware to create an air/fuel ratio based method of control. Unfortunately the secrecy surrounding the exercise severely limited the distribution of the data generated. (Bosch insisted that any vehicle tests should not be conducted on Ford property and that at no time would the engine or vehicle be left in Ford hands without Bosch personnel being present). In the event the results were such as to convince the Ford management that it was commercially possible to cope with the worst levels of future NOx legislation that

could be foreseen at that time. Subsequently, and many years later when Ford did have a need to introduce a fully modulated EGR system, a much simpler and cheaper system was adopted for the 2.5 litre DI diesel. As far as is known, Bosch never did make use of the Jetronic hardware in a commercial diesel EGR application (Davies, 2001).

An EGR system for a Ford prototype 16-valve 2.5 litre engine was reported by Horrocks and Robertson (1996) and Horrocks (1997). This consisted of an electronically controlled vacuum operated poppet type EGR valve mounted on the exhaust manifold. A Serck gas to water heat exchanger cooled the EGR gases; engine coolant was used for the waterside cooling media. To generate sufficient pressure drop to flow the desired volume of EGR under some part load regions where EGR optimum levels for best emissions were higher than would naturally flow through the EGR valve, a throttle valve was incorporated in the induction system. This was operated when desired such that boost pressure and air charge flow were restricted to favour the flow of exhaust gases from the EGR cooler. A schematic diagram of the EGR system is shown in **Figure 3.21.** EGR loops, demonstrating the high tolerance to EGR, in terms of low smoke and significant reduction in NOx emissions for the 16-valve 2.5 litre engine are shown in references Menne et al (1994) and Horrocks et al (1995).

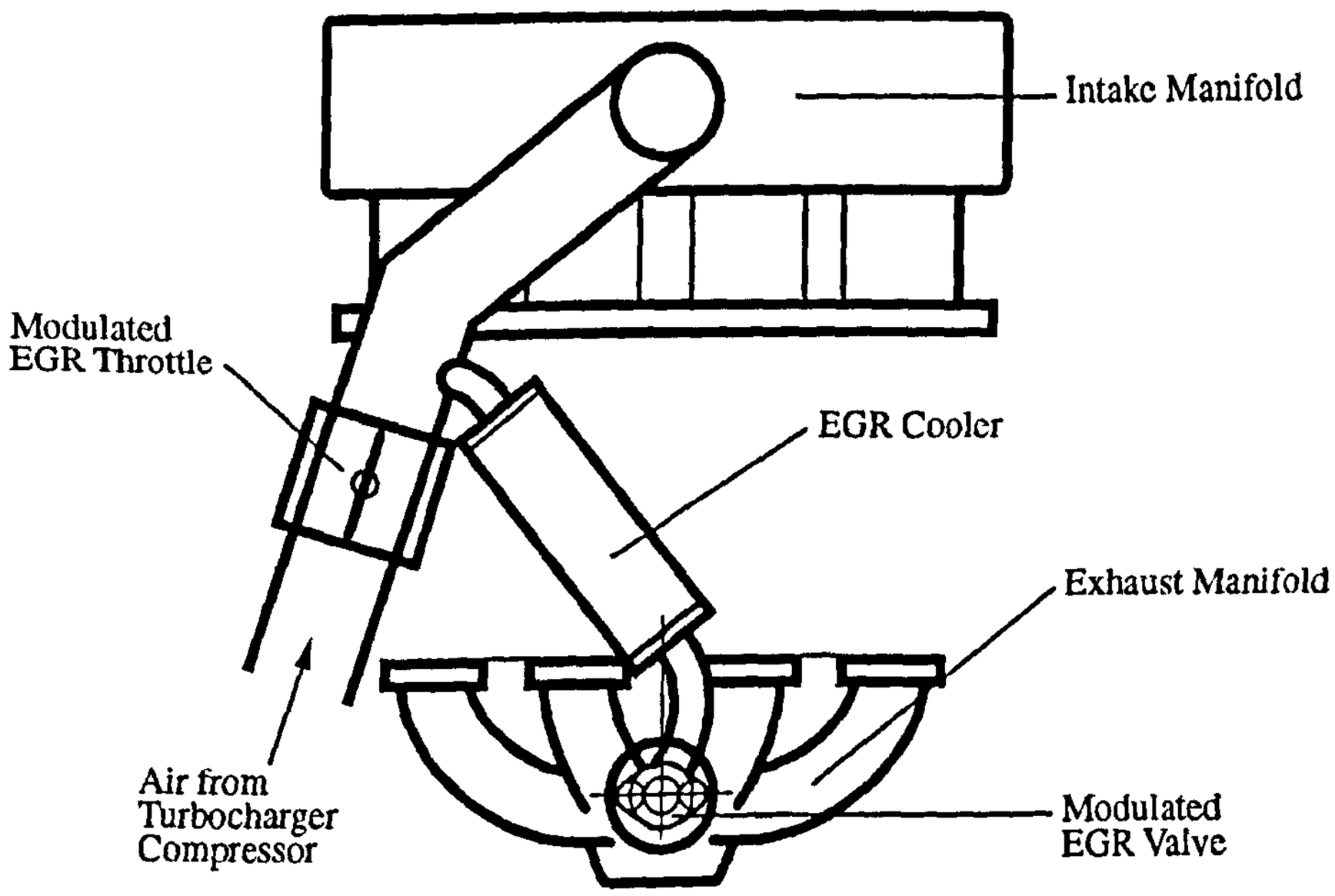

Figure 3.21 Schematic diagram of EGR system used on a prototype 16-valve 2.5 litre DI diesel engine (Horrocks, 1997)

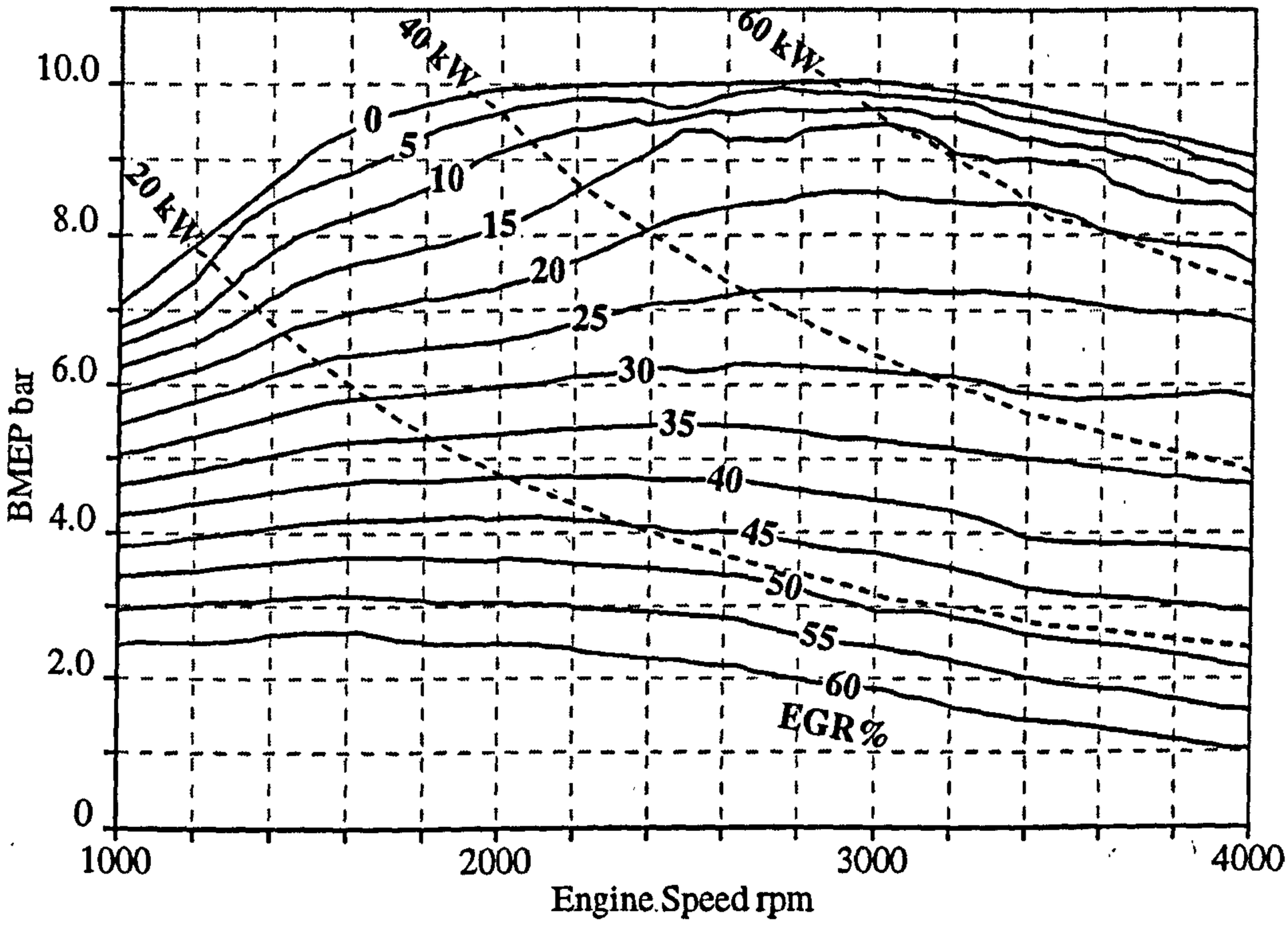

Figure 3.22 EGR map for prototype 16-valve 2.5 litre DI diesel engine

(Horrocks, 1997)

The final EGR map is shown in **Figure 3.22.** As can be seen in **Figure 3.22**, EGR levels of up to 60 per cent were achievable at low load and small amounts of EGR could be introduced up to 9 bar BMEP, above speeds of 1700 rpm. Thus EGR could be used over a significant area of the engine operating range, providing substantial reductions in NOx emissions. Electronic control of fuel injection and EGR provided accurate calibration throughout the engine operating range. This particular engine never went into production, but it was the fore runner of a family of modern 4-valve per cylinder high speed DI diesel engines deigned and developed at Ford.

Honeywell Turbocharging Systems have proposed two methods for introducing EGR for highly turbocharged heavy-duty truck engines, where the intake manifold pressure usually exceeds that of the exhaust manifold. The first system uses a VNT turbocharger to increase the exhaust manifold pressure, above that of the intake charge. This is the same system that has been used experimentally for the work reported in this thesis, on a

light-duty automotive engine, and similar to that proposed by TNO (Baert et al, 1996), reported earlier in section 2.3.10. The second system also uses a VNT turbocharger, but this has a double-sided compressor wheel which acts as an integral EGR pump. Thus one side of the compressor boosts the charge air, while the other side further compresses the EGR gas. The proposed system takes the EGR gas through a cooler before it enters the compressor. An EGR valve located on the turbine housing regulates the level of EGR (Shahed and Waszkiewicz, 2000).

3.4 EGR Control Systems

The majority of EGR systems in production currently use intake air mass flow as the reference variable, for the electronic control system. For a given engine speed and fuel demand under hot operating conditions, the EGR valve lift is adjusted to achieve a pre-mapped value of air mass flow. Under cold operating conditions it is normal to reduce the level of EGR because of white and blue smoke concerns before the combustion chamber has warmed. This is done by a temperature off-set map, which reduces the level of EGR while the coolant temperature is below a pre-determined level.

A small number of manufacturers, notably Ford, Mercedes and Toyota, use closed-loop feedback on the EGR valve lift, which is pre-mapped in the engine control unit. This requires a linear movement sensor to be an integral part of the EGR valve, in order to sense and feedback the valve lift.

With the use of variable nozzle turbochargers (VNT) it is necessary to use an air mass flow meter. This is owing to the fact that air flow is affected by not only the level of EGR but also by the turbocharger vane position, which in turn effects the level of EGR because of the influence on pressure drop across the engine.

The quantity of exhaust gas returned must be precisely metered for emissions reasons and to prevent response faults and visible soot. Control must be fast and must be highly accurate and constant over long periods. This is achieved with a regulated EGR system, shown in **Figure 3.23** below. The data are stored in performance maps in the engine control unit (ECU). The EGR valve is actuated via an electro-pneumatic transducer,

which is supplied with pulses by the ECU. Re-circulation rates are at most circa 50 per cent (Bauder at al, 1997).

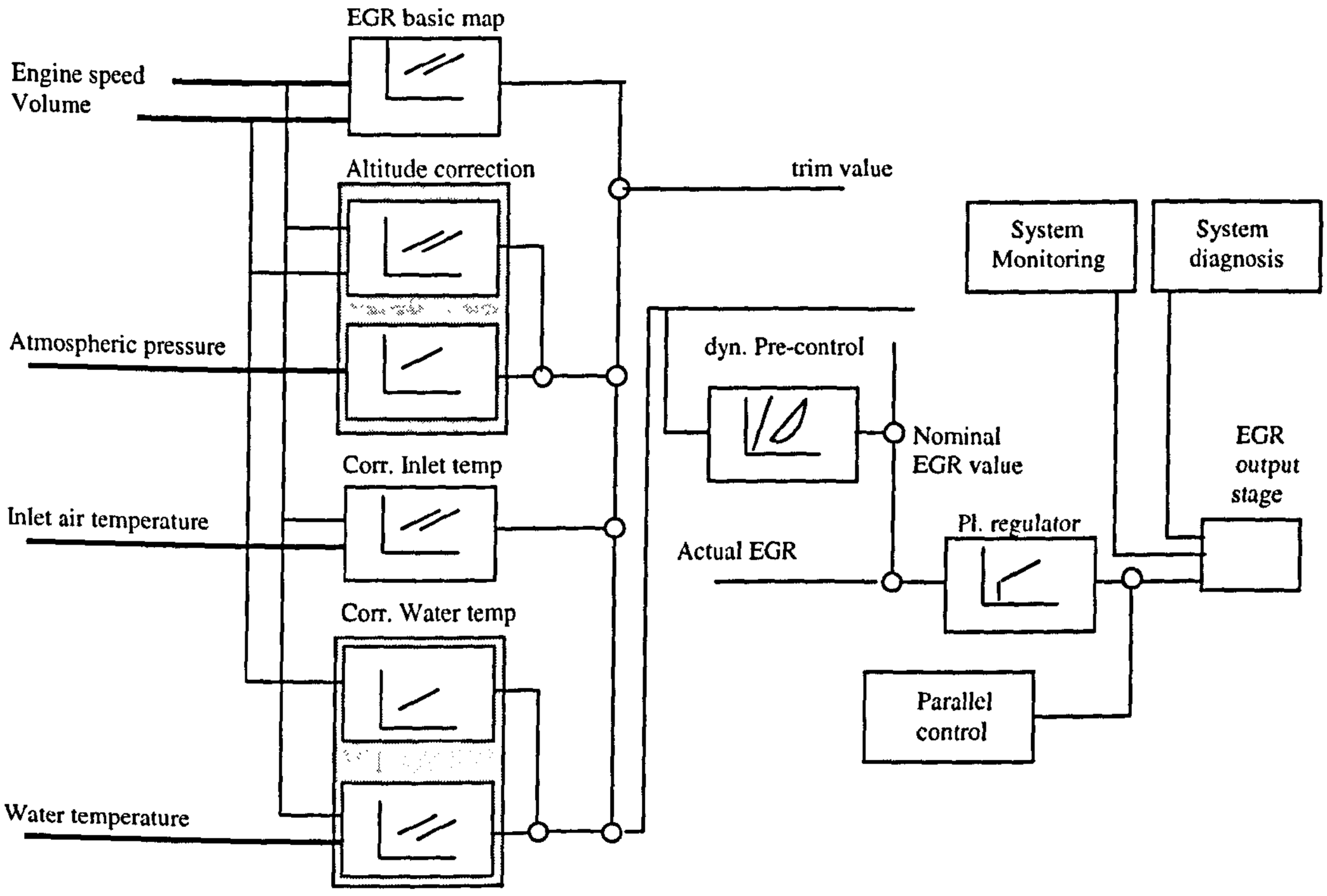

Figure 3.23 Diagram of Audi 2.5 litre V-6 EGR control circuit

(Bauder et al ,1997)

EGR holds further potential for stricter emission levels of the future thanks to improved dynamic response and more precise proportioning, which can both be achieved with the help of electronically operated EGR valves. The electronic EGR valve is incorporated into the engine management system and is operated directly by the ECU. In comparison to conventional pneumatic EGR systems, electric EGR systems display a number of advantages, such as greater accuracy owing to more precise proportioning as well as much better dynamics, and thus enable greater potential for NOx reduction (Anon 1998).

3.5 Future EGR Systems

Future EGR systems will incorporate all the features covered in the previous sections, including a mass air flow sensor, intake throttle valve, EGR cooler, EGR valve and electronic control to accurately fully modulate EGR flow. For quick response times, the EGR valve and throttle will be electrically operated. The component suppliers are developing three types of electric actuators; proportional solenoid valves, DC stepper motors and 4-pole rotary actuators or torque motors. The solenoid and torque motor actuators bring the response time down to within 50 to 100ms, compared to typically 200 to 300ms for a vacuum system. The whole system will most likely be integrated into a module with the intake system to improve the installation on the engine, the assembly at the build plant and reduce the overall piece cost.

3.6 Conclusions

- EGR has been used on production automotive diesel engines since the mid- to late-1980s for reducing NOx emissions.

- EGR is currently used on all high-speed automotive DI diesel engines for reduction of NOx emissions in order to meet European Stage 2, Stage 3 and Stage 4 standards.

- EGR will continue to be the major engine feature to control NOx emissions.

- The use of an EGR cooler is becoming more widespread, in order to meet the stricter Stage 3 and Stage 4 emissions standards.

- Some engines use an intake throttle to generate the necessary pressure drop to meet the required EGR flow, under all engine operating conditions.

- Vacuum operation of the EGR valve and throttle, where fitted, is the most widespread actuation method at present.

- Electric operation of the EGR valve is being introduced, to improve the response time.

- The use of EGR for reduction of NOx emissions is being introduced on heavy-truck engines.

Chapter 4

NOx Modelling

4.1 NOx Formation Model

4.1.1 Merlin Combustion-Emissions Model (Lloyd's Register DEEPC)

This is a quasi-dimensional phenomenological model and is based on a multi-zone combustion modelling concept. It takes into consideration, on a zonal basis, details of fuel spray formation, droplet evaporation, air-fuel mixing, spray wall interaction, swirl, heat transfer, auto-ignition and rate of reaction. The emissions model uses the chemical equilibrium, as well as the kinetics of fuel, NO, CO and soot reactions in order to calculate the pollutant concentrations within each zone and the whole of the cylinder.

The thermal NO formation, NO formed due to the atmospheric nitrogen in the high temperature combustion gases, is modelled based on the extended Zeldovich mechanism taking into account the kinetics of NO formation. The fuel-bound nitrogen is assumed to be converted to NO directly during the course of combustion development. The prompt NO mechanism is not taken into account.

The extended Zeldovich mechanism uses the following reactions as documented in Chapter 2.

$$O + N_2 \leftrightarrow NO + N \qquad k_1, k_{-1} \qquad 2.1$$

$$N + O_2 \leftrightarrow NO + O \qquad k_2, k_{-2} \qquad 2.2$$

$$N + OH \leftrightarrow NO + H \qquad k_3, k_{-3} \qquad 2.3$$

By assuming that NO formation is not directly coupled to combustion and by approximating the concentrations of O, O_2 , OH, H and N_2 by their equilibrium values, it can be shown (Heywood, 1988) that:

$$d[NO]/dt = 2R_1(1- \beta^2)/(1+ \beta R_1/(R_2 + R_3)) \qquad 4.1$$

where:

$\beta = [NO]/[NO]_e$

$R_1 = k_1[O]_e[N_2]_e = k_{-1}[NO]_e[N]_e$

$R_2 = k_2[N]_e[O_2]_e = k_{-2}[NO]_e[O]_e$

$R_3 = k_3[N]_e[OH]_e = k_{-3}[NO]_e[H]_e$

k_1 = forward rate constant for equation 1 $\{7.6 \times 10^{13} \exp(-38000/T)\}$ $cm^3\ mol^{-1}\ s^{-1}$

k_{-1} = reverse rate constant for equation 1 $\{1.6 \times 10^{13}\}$ $cm^3\ mol^{-1}\ s^{-1}$

k_2 = forward rate constant for equation 2 $\{6.4 \times 10^9\ T \exp(-3150/T)\}$ $cm^3\ mol^{-1}\ s^{-1}$

k_{-2} = reverse rate constant for equation 2 $\{1.5 \times 10^9\ T \exp(-19{,}500/T)\}$ $cm^3\ mol^{-1}\ s^{-1}$

k_3 = forward rate constant for equation 3 $\{4.1 \times 10^{13}\}$ $cm^3\ mol^{-1}\ s^{-1}$

k_{-3} = reverse rate constant for equation 3 $\{2.0 \times 10^{14}\ T \exp(-23{,}650/T)\}$ $cm^3\ mol^{-1}\ s^{-1}$

and [ ] denotes the species concentrations and $[\ ]_e$ denotes the equilibrium concentration, in moles/cm^3. The rate constants shown above are taken from Heywood, who in turn took them from Bowman (1975), originally published by Baulch et al (1973).

In Chapter 2 the extended Zeldovich mechanism and the reported rate constants were reviewed. It is clear from the literature that the reactions are reversible with forward rate and reverse rate constants. In-cylinder NOx measurements from a firing 2.5 litre DI diesel engine carried out at Brunel University (Balian, 1992, 1995) show that the

concentration of NO rises very rapidly following the start of combustion and reaches a peak at around 2.5 to 3.5 ms after the start of combustion. The concentration then falls off as the temperature drops, until it "freezes" towards the end of the combustion period, which establishes the exhaust level. The reduction in NO concentration during the diffusion phase of combustion indicates that the reverse reactions are taking place at a greater rate than the forward reactions. Thus the forward and reverse reactions are both important in predicting the final levels at exhaust valve opening, and subsequently in the bulk exhaust.

For the NO sub-routine, the Merlin DEEPC emissions model assumes the following reaction rate equations, with reference to equation 4.1.

$$R_1 = k_{-1}[NO]_e[N]_e \qquad 4.2$$

$$R_2 = k_2[N]_e[O_2]_e \qquad 4.3$$

$$R_3 = k_3[N]_e[OH]_e \qquad 4.4$$

Hence the code uses the reaction rate constants k_{-1}, k_2 and k_3, that is, the first reverse reaction and the second and third forward reaction rate constants. It is assumed this was done to minimise the number of calculations for species equilibrium concentrations.

The values of the rate constants used in the code are taken from Heywood (1988), which were originally published by Baulch, et al (1973) and are listed in **Table 4.1.**

Table 4.1

Extended Zeldovich Rate Constants used in Merlin-DEEPC code

Rate Constant	Value cm^3/mole.s (K)
k_{-1}	1.6×10^{13}
k_2	$6.4 \times 10^9 T \exp[-3150/T]$
k_3	4.1×10^{13}

The rate of formation of NO is then given by:

$$d[NO]/dt = 2R_1(1- \beta^2)/(1+ \beta R_1/(R_2 + R_3)) \qquad 4.5$$

where:

$$\beta = [NO]/[NO]_e$$

$$R_1 = 1.6 \times 10^{13}[NO]_e[N]_e$$

$$R_2 = 6.4 \times 10^9 \, T \exp\{-3150/T\}[N]_e[O_2]_e$$

$$R_3 = 4.1 \times 10^{13}[N]_e[OH]_e$$

From the above, it will be noted that it is only R_2 in the above equation that is dependent on temperature, that is the formation of NO, owing to the temperature dependence of k_2. The reverse reaction k_{-1} is not temperature dependent and so will occur throughout the cycle, as will the forward reaction k_3, depending, of course on the species equilibrium concentrations.

Although researchers have had some success in using only the thermal-equilibrium-O (Zeldovich) mechanism to predict NO emissions in the past and in many cases the one step mechanism is sufficient to estimate NOx emissions, our current understanding of NO production shows that the situation is indeed more complex (Turns 1996). The basic premise behind the use of the Zeldovich is that the NOx chemistry is much slower than the combustion chemistry; thus the O- and OH- atom concentrations have time to reach equilibrium. This assumption of uncoupled combustion and NOx formation chemistry breaks down, however, when O- and OH- atoms are formed via the Zeldovich reactions much more rapidly than if O atoms were in equilibrium.

4.1.2 Potential Improvements in the NOx Prediction Model

Super-extended Zeldovich mechanism

Miller et al (1998) have proposed a "super-extended" Zeldovich mechanism (SEZM) that predicts NOx formation levels to a greater accuracy than the established "extended Zeldovich" mechanism, when compared to gasoline test data. The reactive chemistry

mechanism includes 67 reactions and 13 chemical species. The SEZM incorporates O, O_2, OH, H, N_2, NH, N_2O, NO_2 and NO. The 67 reactions, which were found to dominate thermal NOx formation for dilute (fuel-lean and EGR operation) and fuel-rich operation in internal combustion engines, are listed in SAE paper 980781.

The SEZM kinetics were solved in a similar manner to the Zeldovich mechanism. Formation and destruction time scales for N, NH, NH_2, NH_3, HNO, N_2O and NO_2 are shorter than that of NO but longer than those of the O_2, N_2, O, and OH radicals. Therefore, N, NH, NH_2, NH_3, HNO, N_2O and NO_2 concentrations were obtained by assuming partial equilibrium (Miller 1997, Lavoie 1973). Consequently, NO was determined by solving one non-linear differential equation (non-linear kinetic equation) for NO, while solving 7 algebraic equations (partial equilibrium) for N, NH, NH_2, NH_3, HNO, N_2O and NO_2 while assuming the radicals were in equilibrium, Miller et al (1998).

Because the predicted NOx levels were still in excess of the experimental data by more than 20 per cent, Miller et al, incorporated an empirical parametric variation of equation 4.1, by modifying the rate constant with a pressure coefficient:

$$O + N_2 \leftrightarrow NO + N \qquad 2.1$$

$$k_{1M} = C_p\ 1.8x10^{14}\exp(-38370/T)$$

where C_p has the value shown in the **Table 4.2** below and P is the instantaneous in-cylinder pressure in atmospheres.

Table 4.2

Empirical parametric factor for modifying k_1 for pressure variation

(Miller et al, 1998)

C_p	P
1.00	<15
0.7	15-20
0.48	20-25
0.31	25-30
0.25	30-35
0.20	>35

Miller et al found that this modification of k_1 with pressure, giving a factor of 5 decrease in the reaction rate, produced accurate NOx predictions as a function of load.

N_2O pathway to NO formation

Mellor et al (1998) looked at a skeletal mechanism to model NO formation in diesel engines. This entailed considering all the pathways of NO formation and decomposition. The significant pathways were determined through kinetic analysis. At high pressures, formation of N_2O can occur, some of which is converted to NO through further reactions with free radicals, such as O and H atoms (Malte and Pratt, 1974, Polifke et al, 1995).

Malte and Pratt developed the original N_2O mechanism based on work at low pressures (0.5 to 1.0 atm).

$$N_2O + O \Leftrightarrow 2NO \qquad 4.6$$

$$O + N_2 + M \Leftrightarrow N_2O + M \qquad 4.7$$

$$N_2O + H \Leftrightarrow N_2 + OH \qquad 4.8$$

$$N_2O + O \Leftrightarrow N_2 + O_2 \qquad 4.9$$

At higher pressures, which are of interest for diesel combustion, Polifke et al (1995) observed that NO formation through the N_2O mechanism is simplified.

$$N_2O + H \Leftrightarrow NO + NH....\Rightarrow 2NO \qquad 4.10$$

Mellor and co-workers believe that NO formation through the N_2O mechanism becomes increasingly significant since the forward rate of the three-body reaction (equation 4.8) is pressure sensitive. At pressures in the order of 60 atm and above, the N_2O mechanism makes an important contribution to the NO formation process at all stoichiometric temperatures of interest. In addition, at typical diesel operating conditions, NO decomposition in the zone of burnt gases surrounding the burning zone, is dominated by the reverse N_2O mechanism (Mellor, 1998).

Modelling of NO_2 formation

A potential area for improvement to the prediction of total NOx, relates to the formation of NO_2 . In Chapter 2 it was reported that DI diesel engines emit NO_2 levels that can be as high as 50 per cent of the total NOx, during part load operation. Since NO_2 is formed from NO, the modelling of its formation would not add to the accuracy of the total NOx model. However, a model for the formation of NO_2 would provide the split between NO and NO_2, which would be of use for the application of diesel NOx and particulate after-treatment.

Hilliard and Wheeler (1979) and Lenner et al (1982) have reported considerable proportions of NO_2 in the NOx emissions from diesel engines at moderate loads. Lenner (1986) reported on NO_2 emissions from an IDI turbo diesel powered car, with EGR, and without EGR, but with a particulate trap. He also took measurements from a 9.6 litre truck engine. The passenger car with EGR yielded NO_2 fractions in the range 15 to 35 per cent, peaking at 0.75kW (1 hp) load. The NO_2 fractions from the car when the particulate trap was fitted were very much lower, less than 3 per cent except at idling. This may well be because the NO_2 was converted to NO as part of the particulate oxidation process. Cooper and Thoss (1989) found that NO_2 concentrations

between 200 to 800 ppm, promoted the oxidation of diesel particulates at 300°C. The truck engine emitted up to 25 per cent of the NOx as NO_2 at mid-speed.

Possible reactions for the formation of NO_2 are as follows:

$$2\,NO + O_2 \rightarrow NO_2 + NO_2 \qquad \text{(formation)} \qquad 4.11$$

Merryman et al (1975) proposed the following 2 reactions. Hori et al (1992) conducted chemical kinetic reactions, where it was found that the NOx is conserved during the reaction, and that the dominant reaction of the conversion of NO to NO_2 is the "HO_2 mechanism" (the conversion of NO to NO_2 by the HO_2 radical) shown in reaction 7 below.

$$NO + HO_2 \rightarrow NO_2 + OH \qquad \text{(formation)} \qquad 4.12$$

$$NO_2 + H \rightarrow NO + OH \qquad \text{(destruction)} \qquad 4.14$$

Additionally (Turns, 1996),

$$NO_2 + O \rightarrow NO + O_2 \qquad \text{(destruction)} \qquad 4.14$$

where the HO_2 radical is formed by the three-body reaction (Turns, 1996)

$$H + O_2 \Leftrightarrow HO_2 + M \qquad 4.15$$

$$NO + O + M \rightarrow NO_2 + M \qquad \text{(formation)} \qquad 4.16$$

Pipho et al (1991) of the University of Minnesota, investigated NO_2/NO ratios during total cylinder sampling from an operating diesel engine and compared measured values with those from a simple kinetic model. They proposed that the reactions responsible for most of the NO_2 formation following the dilution processes were:

$$NO + HO_2 \Leftrightarrow NO_2 + OH \quad \text{(formation)} \qquad 4.17$$

$$NO + O + M \Leftrightarrow NO_2 + M \quad \text{(formation)} \qquad 4.18$$

with the reverse of reaction 7 and the reactions

$$NO_2 + O \Leftrightarrow NO + O_2 \quad \text{(destruction)} \qquad 4.19$$

$$NO_2 + H \rightarrow NO + OH \quad \text{(destruction)} \qquad 4.20$$

responsible for removal of NO_2. Dilution similar to their simulated process does occur during the diesel combustion process.

$2\,NO + O_2 \rightarrow NO_2 + NO_2$

Heywood (1988) states that this reaction is too slow to produce any measurable NO_2 in the exhaust.

Baulch et al (1973) recommended the following rate constant:

$$k_6 = 1.2 \times 10^9 \exp\{530/T\} \qquad cm^6\,mol^{-2}\,s^{-1}$$

within the temperature range 273 - 660 K. The authors make the point that if the mechanism is complex, in particular if more than one mechanism is operative in the conversion of NO to NO_2 - it would be unreasonable to expect the rate constant to obey a simple Arrhenius expression over a wide range of temperatures. The available data suggest a curved Arrhenius plot over the temperature range 140 - 800 K. However, if the data below 273 K are ignored, then the above expression describes the most reliable data in the temperature range 273 - 660 K to within 50 per cent.

$NO + HO_2 \rightarrow NO_2 + OH$

Bowman (1992) refers to this as the principal NO_2 formation reaction.

Baulch et al (1973) make no recommendation for the rate constant for this reaction. The only experimental determination of k appears to be from unpublished work by Zafonte, which is referred to by Johnston (1970/1). Heywood refers to it as a plausible mechanism for the persistence of NO_2, NO formed in the flame zone can be rapidly converted to NO_2 via this reaction, but subsequent conversion back to NO occurs via

$$NO_2 + O \rightarrow NO + O_2 \qquad 4.21$$

unless the NO_2 formed in the flame is quenched.

Glassman (1996) refers to this reaction as the significant step, in the formation of NO_2 , pointing out that there can be appreciable amounts of HO_2 in the early parts of a flame. In low temperature regions of flames, HO_2 is relatively stable and it can react with NO formed in low temperature regions (Bowman 1992). The appearance of NO_2 is supported by the fact that this reaction (3.7) is two orders of magnitude faster than reaction (3.9).

A later section will cover the role of fuel on the conversion of NO to NO_2.

$NO_2 + H \rightarrow NO + OH$

Bowman (1992) refers to this as the principal NO_2 removal step. Turns (1996) also sites this as a reaction responsible for the destruction of NO_2. Baulch et al (1973) make the following recommendation for the rate constant for this reaction.

$$k_8 = 3.5 \times 10^{14} \exp(-740/T) \quad cm^3\ mol^{-1}\ s^{-1}$$

in the temperature range 298 - 630 K

Baulch et al (1973) state that the reverse reaction, between nitric oxide and OH to give NO_2 , ($NO + OH \rightarrow NO_2 + H$) has never been studied directly. The rate constant could be calculated from the recommended expression for k, but it could not be recommended for use above 630 K.

$NO_2 + O \rightarrow NO + O_2$

The reaction of NO_2 with oxygen is extremely fast (Baulch et al, 1973). Baulch et al recommend the following rate constant.

$$k_9 = 1.0 \times 10^{13} \exp\{-300/T\} \quad cm^3\ mol^{-1}\ s^{-1}$$

within the temperature range of 300 to 550 K. These authors report that there is no experimental data for the reverse reaction. Using calculations for the reverse reaction and thermodynamic data, they recommend a rate constant of:

$$k_{-9} = 1.7 \times 10^{12} \exp\{-23400/T\} \qquad cm^3\ mol^{-1}\ s^{-1}$$

for use in the temperature range 300-550 K. The authors state that this reaction is insignificant relative to other reactions oxidizing NO at nitric oxide concentrations above 10-77 mol cm^{-3} and temperatures below 1000 K.

$NO + O + M \rightarrow NO_2 + M$

Baulch, et al (1973) recommend the following rate constants for this reaction:

$$k_{11} = 1.1 \times 10^{15} \exp\{940/T\} \quad cm^6\ mol^{-2}\ s^{-1} \quad (M = O_2, Ar)$$

(200-500 K)

$$k_{-11} = 1.1 \times 10^{16} \exp\{-33000/T\} \quad cm^3\ mol^{-1}\ s^{-1} \quad (M = Ar)$$

(1400-2400 K, M = Ar)

The reverse reaction rate constant is so small, in comparison to the other reactions, that this can be ignored.

The role of fuel on the conversion of NO to NO_2

From various studies, (Bromly et al, 1988 and 1992, Hori et al, 1992 and Taylor et al, 1998) it appears that the effect of fuel on the conversion of NO to NO_2 is an important factor controlling NO_2 exhaust emissions.

Ratios of NO_2/NO far in excess of the appropriate equilibrium values were found to be due to the presence of oxidation intermediates of hydrocarbons, assumed to be hydroperoxyl radicals and other peroxides, in relatively high concentrations during tests conducted with flow-through reactors (Bromly et al, 1988).

Hori et al (1992) conducted experimental and fundamental chemical kinetic calculations for NO_2 formation. The fundamental chemical mechanism of NO_2 formation is called the "HO_2 mechanism" (the conversion of NO to NO_2 by the HO_2 radical). Recent data suggest that the conversion of NO to NO_2 is affected by the presence of fuels. Hence the concentration and species of hydrocarbons in exhaust gas may be an important factor controlling NO_2 exhaust emissions.

From calculations it was found that the total NOx level was conserved during the reaction and that the dominant reaction for the conversion of NO to NO_2 was NO + HO_2 = NO_2 + OH even in the presence of fuel. The fuels that easily decomposed to produce active species and consequently produced high HO_2 concentrations achieved a higher conversion of NO to NO_2. The effectiveness of promotion strongly depends on the type of fuel. The experiments showed a trend where the effectiveness increased as $H_2 < CH_4 < C_2H_6 < C_2H_4 < C_3H_8 < i\text{-}C_4H_{10} < n\text{-}C_4H_{10}$. The kinetic calculations confirmed these trends, and a lower conversion was predicted for C_3H_6.

Table 4.3

Summary of NO_2 formation and destruction reactions, and rate constants;

$k = AT^{\beta} \exp(-E/RT)$

Equ. No	Reaction	A	β	E/R	Temperature Range	Reference
4.6	$2\,NO + O_2 \rightarrow NO_2 + NO_2$	1.2×10^{9}	0	-530	273 - 660	Baulch et al, 1973 (Note α)
4.7	$NO + HO_2 \rightarrow NO_2 + OH$	2.1×10^{12}	0	-240	1000-2000	Hanson & Salimian, 1984
4.8	$NO_2 + H \rightarrow NO + OH$	3.5×10^{14}	0	740	298-630	Baulch et al, 1973 (Note β)
4.9	$NO_2 + O \rightarrow NO + O_2$	1.0×10^{13}	0	300	300-550	Baulch et al, 1973 (Note γ)
4.11	$NO + O + M \rightarrow NO_2 + M$	1.0×10^{15}	0	-940	200-500	Baulch et al, 1973 (Note Δ)

Units: moles, cm^3, s, K

Note α: k is defined by $^1/_2 d[NO]/dt = -d[O_2]/dt = k[NO]^2[O_2]$. Baulch et al suggest an error limit of +/- 50% in the temperature range quoted, no high temperature data available. Units $cm^6\ mol^{-2}\ s^{-1}$.

Note β: Baulch et al suggest an error limit of +/- 50% at 298 K increasing to a factor of 2 at 633 K, no high temperature data available.

Note γ: Baulch et al suggest an error limit of +/- 25% in the temperature range quoted, limited high temperature data available.

Note Δ: Baulch et al suggest an error limit of +/- 20% in the temperature range quoted, no high temperature data available. Units $cm^6\ mol^{-2}\ s^{-1}$.

The rate of formation of NO_2 is given by:

$$d[NO_2]/dt = k_6[2NO][O_2] + k_7[NO][HO_2] - k_8[NO][OH] - k_9[NO][O_2] + k_{11}[NO][O][M] \qquad 4.22$$

Where [ ] denotes the species concentrations in moles/ cm^3.

However, all the rate data have been obtained at relatively low temperatures, as shown in **Table 4.3**. Chemical equilibrium considerations indicate that for typical flame temperatures (T>1500K), $(NO_2)/(NO)$ ratios are negligible. Nevertheless, significant NO_2 concentrations have been measured in gas turbine exhausts (Johnson and Smith 1978), in turbulent diffusion flames (Schefer and Sawyer 1977, and Cernansky and Sawyer, 1975) and more recently in a small high speed DI diesel engine (Ketcher, 1997).

Modelling prompt NO formation

Prompt NO chemistry is thought to dominate over thermal NO production for fuel rich conditions, as well as for ultra lean conditions, where the combustion temperatures are extremely low, resulting in a minimal contribution from the thermal mechanism (Miller and Bowman, 1989).

Miller et al (1997) found that prompt NO contributed less than 1 per cent to the total NO production, for normal engine conditions, with the bulk of the NO production being attributed to thermal NO which is produced in the adiabatic region behind the flame front. However, HCN production might still occur in this rich combustion and if it does it is likely that the fixed nitrogen would be released as NO at the diffusion flame, (Miller and Kee 1986, Miller and Bowman 1989).

Miller and Bowman (1989) considered the following reactions.

$$CH + N_2 \Leftrightarrow HCN + N \qquad 2.20$$

(Fenimore's postulation, equation 2.20 in Chapter 2)

$$CH_2 + N_2 \Leftrightarrow HCN + NH \qquad 2.23$$

(Sterling and Wendt's reaction, equation 2.23 in Chapter 2)

$$CH_2 + N_2 \Leftrightarrow H_2CN + N \qquad 2.25$$

(Equation 2.25 in Chapter 2)

$$C + N_2 \Leftrightarrow CN + N \qquad 2.26$$

(Equation 2.26 in Chapter 2)

Their calculations showed that equations 2.23 and 2.25 (Chapter 2) were insignificant contributors to prompt NO. Reaction 2.26 was considered to be a minor, but non-negligible, contributor to prompt NO under most conditions. Because of the large endothermicity of the reaction $C + N_2 \rightarrow CN + N$, its importance with respect to reaction 2.20 (Chapter 2) increases with increasing temperature. Miller and Bowman confirmed Fenimore's postulation that reaction 2.20 does lead to prompt NO. Table 4.4 lists a range of rate coefficients proposed for reaction $C + N_2 \rightarrow CN + N$.

Table 4.4

Rate coefficient expression for the reaction $C + N_2 \rightarrow CN + N$)

Rate coefficient (cm^3/mol-sec) k (T)	**k (2000K)**	**Reference**
1.44×10^{10} *	1.44×10^{10}	Morley (1976)
$8.0 \times 10^{11} \exp(-11000/RT)$	5.0×10^{10}	Blauwens et al (1977)
$4.0 \times 10^{11} \exp(-13600/RT)$	1.3×10^{10}	Matsui and Nomaguchi (1978)
$1.0 \times 10^{12} \exp(-19200/RT)$	8.0×10^{10}	Roth and Ibreighith (1984)
$1.2 \times 10^{12} \exp(-13600/RT)$	3.9×10^{10}	Matsui and Yuuki (1985)
$4.2 \times 10^{12} \exp(-20400/RT)$	2.5×10^{10}	Dean et al (1988)
$3.0 \times 10^{11} \exp(-13600/RT)$	9.8×10^{10}	Miller and Bowman (1989)

* Temperature range 2000 K < T > 2560 K

From the table above, taken from Miller and Bowman (1989), it is clear that further progress in modelling prompt NO in flames requires a direct and unambiguous determination of the rate coefficient at flame temperatures, for the Fenimore reaction,

$$C + N_2 \rightarrow CN + N. \qquad 2.26$$

Miller and Bowman also concluded that prompt-NO formation involves 3 separate kinetic issues:

1. the CH concentration and how it is established;
2. the rate of molecular nitrogen fixation; that is, the value of $k_{2.20}$; the reaction rate coefficient for equation 2.20;
3. the rates of interconversion among fixed nitrogen fragments.

Up to an equivalence ratio of approximately $\phi = 1.2$ the HCN and N produced by reaction 2.20 are converted rapidly to NO principally by the mechanism discussed by Miller et al (1984).

$$HCN + O \leftrightarrow NCO + H \qquad 4.23$$

$$HCN + O \leftrightarrow NH + CO \qquad 4.24$$

$$NCO + H \leftrightarrow NH + CO \qquad 4.25$$

$$NH + H \leftrightarrow N + H_2 \qquad 4.26$$

$$N + OH \leftrightarrow NO + H \qquad 4.27$$

$$N + O_2 \leftrightarrow NO + O \qquad 4.28$$

Beyond $\phi = 1.2$, several factors combine to cause the NO concentration to decrease relative to HCN:

(a) the conversion of HCN by the above mechanism is no longer rapid;

(b) the recycle of NO to HCN begins to inhibit NO production;

(c) the reaction $N + NO \leftrightarrow N_2 + O$, shifts directions from reverse to forward.

At $\phi = 1.4$ the peaks in the CN and total fixed nitrogen concentrations occur simultaneously. Beyond $\phi = 1.4$ the fixed nitrogen concentration is limited by the

availability of the chain carriers, H and OH, required for producing CH from methane. Also, reaction

$$CH_3 + N = H_2CN + H \qquad 4.29$$

appears as a competitor for nitrogen atoms, competing favourably with reaction.

$$N + OH \leftrightarrow NO + H. \qquad 4.30$$

Calculations and experiments show little prompt NO produced at equivalence ratios above 1.8, (Glarborg et al 1986, Miller and Bowman 1989).

Miller et al (1998) modelled prompt NO production in their SEZM mechanism, using the empirical correlation as suggested by Lavoie and Blumberg (1973),

$$[NO]_{flamefront} = f(\phi)P^{1/2}[NO]_{Equilibrium} \qquad 4.31$$

which accounts for equivalence ratio and pressure dependencies on flame front NO. Prompt NO chemistry is typically restricted to regions near the flame front where HCN and hydrocarbon fuel concentrations are sufficiently large to be considered important in the total NO production.

4.2 Summary and Conclusions

The extended Zeldovich mechanism for thermal NO formation is the mechanism responsible for the vast majority of NO formed in premixed and diffusion combustion of hydrocarbon fuels at elevated pressures and temperatures. It is the basis for all modelling of NOx formation in combustion where elevated temperatures are experienced. Additionally, there are a number of other reactions responsible for the formation of NO during diesel combustion. These are, 'prompt NO' formation, conversion of N_2O to NO, and NO formed from fuel bound nitrogen, but these only contribute a small proportion of the total NOx formation.

A large number of reaction rate constants have been proposed by a number of researchers, for the Zeldovich mechanism. A selection of these has been assessed and will be reviewed in the next chapter.

A number of refinements to the Zeldovich mechanism have also been proposed. In a super-extended Zeldovich mechanism, reported by Miller et al (1998), NO was determined by solving one non-linear differential equation (non-linear kinetic equation) for NO, while solving 7 algebraic equations (partial equilibrium) for N, NH, NH_2, NH_3, HNO, N_2O and NO_2 while assuming the radicals were in equilibrium. Additionally by modifying the rate limiting reaction, $O + N_2 \leftrightarrow NO + N$, with an empirical coefficient to incorporate the influence of pressure, the accuracy of the model was improved for a gasoline engine.

At high pressures, formation of N_2O can occur, some of which is converted to NO through further reactions with free radicals, such as O and H, (Malte and Pratt, 1974, Polifke et al, 1995)

Another refinement for the prediction of total NOx is modelling of prompt NO formation. Prompt NO formation contributes to total NO levels under rich conditions, as well as ultra lean air/fuel ratios. Fenimore's postulation that $CH + N_2 \Leftrightarrow HCN + N$ leads to prompt NO has been confirmed by other researchers, Miller and Bowman (1989). However, there is a wide range of rate coefficients proposed for the Fenimore reaction.

Lavoie and Blumberg suggested an empirical correlation:

$$[NO]_{flamefront} = f(\phi)P^{1/2}[NO]_{Equilibrium} \qquad 4.32$$

which accounts for equivalence ratio and pressure dependencies on flame front NO.

However, there is debate about how much NO formation is attributable to the prompt reaction.

A further refinement for the prediction of NOx is establishing the proportion of NO_2, or the ratio NO/ NO_2. There are a number of possible reactions leading to the formation of NO_2, but the most important are:

$$NO + HO_2 \rightarrow NO_2 + OH \qquad 4.18$$

$$NO + O + M \rightarrow NO_2 + M \qquad 4.19$$

While the following two reactions are responsible for the removal of NO_2, converting it back to NO.

$$NO_2 + O \rightarrow NO + O_2 \qquad 4.20$$

$$NO_2 + H \rightarrow NO + OH \qquad 4.21$$

As can be seen from the above reactions, NO_2 is formed from NO, so the modelling of its formation would not add to the accuracy of the total NOx model. However, a model for the formation of NO_2 from the above reactions would provide information on the split between NO and NO_2, which would be of use for the application of diesel NOx and particulate exhaust after-treatment, where the level of NO_2 is important for the respective reactions.

Chapter 5

Engine Simulation with EGR

5.1 Emissions modelling using the MERLIN-DEEPC code

The Merlin-DEEPC code was developed by the Performance Technology Department at Lloyd's Register, under funding from the UK Government Department of Transport and the Diesel Engineering Department of Ford Motor Company Ltd.

The phenomenological combustion and exhaust emissions model is a multi-zone quasi-dimensional, diesel engine exhaust emissions predictive capability code, with the acronym, DEEPC. It takes into consideration, on a zonal basis, details of fuel spray formation, droplet evaporation, air-fuel mixing, spray wall interaction, swirl, heat transfer, self-ignition and rate of reaction. The emissions model uses chemical equilibrium, as well as the kinetics of fuel, NO, CO and soot reactions, in order to calculate the pollutant concentrations within each zone and the whole of the cylinder.

The combustion process in a DI diesel engine is modelled as a complex sequence of overlapping and interacting events, which are completed in a short period of time. Injected fuel is assumed to be characterised in the form of intermittent pockets of fuel being emitted from the nozzle hole during each calculation time step, thereby making segments of fuel as injection proceeds. All the droplets in a spray segment are assumed to have the same Sauter mean diameter. Allowance is made for droplet size variation from one segment to the next. At the start of atomisation, each spray segment is divided into a definite number of combustion zones. Air entrainment rate depends on the physical position of each zone, with centreline zones receiving least and edge zones receiving the most air. Swirl affects the shape of the spray and the rate of entrainment and is accounted for by modifying spray angle and penetration. Spray-wall impingement is assumed to take place when the moving zone reaches the nearest wall. Ignition is assumed to start at the vapour phase in each zone. The ignition delay is

measured from the point of atomisation and is related to zone temperature and air-fuel ratio through known correlations. Heat transfer is modelled on a zonal basis and both convective and radiation heat transfers are modelled. Zone temperature, volume and mass for a fixed cylinder pressure are calculated from the energy equation in conjunction with mass conservation and an equation of state is solved iteratively for each zone, (Bazari 1992).

Thermal NO formation is based on the Zeldovich mechanism taking into account the kinetics of NO formation (reviewed in Chapter 2).

$$O + N_2 \Leftrightarrow NO + N \qquad 2.1$$

$$N + O_2 \Leftrightarrow NO + O \qquad 2.2$$

$$N + OH \Leftrightarrow NO + H \qquad 2.3$$

By assuming that NO formation is not directly coupled to combustion and by approximating the concentrations of O, O_2, OH, H and N_2 by their equilibrium values, Heywood (1988) showed that:

$$d[NO]/dt = 2R_1(1-\beta^2)/(1+\beta.R_1/(R_2+R_3)) \qquad 5.1$$

where

$$\beta = [NO]/[NO]_e$$

$$R_1 = k_1^+ [O]_e[N_2]_e$$

$$R_2 = k_2^+ [N]e[O_2]_e$$

$$R_3 = k_3^+ [N]_e[OH]_e$$

$$k_1^+ = 7.6 \times 10^{13} \exp(-38000/T)$$

$$k_2^+ = 6.4 \times 10^9 \, T \exp(-3150/T)$$

$$k_3^+ = 4.1 \times 10^{13}$$

Chemical equilibrium within each zone is calculated by the method outlined by Olikara and Borman (1975).

The fuel-bound nitrogen is assumed to totally convert to NO directly during the course of combustion.

The EGR process is modelled by considering the mass percentage EGR and the degree of cooling on the re-circulated gas. The inlet manifold temperature and composition are calculated from the exhaust gas temperature and composition by assuming perfect mixing of the EGR and intake air. The inlet manifold temperature and composition, and the degree of scavenging, will determine the trapped gas temperature and composition, (Bazari 1992).

The input required to run the program is:

- Measured fuel delivery
- Measured fuel line pressure, as a function of crank angle
- Measured dynamic start of injection
- Injector nozzle opening pressure
- Injector nozzle geometry, hole diameter and length, and number of holes
- Swirl ratio, a fixed value of swirl is assumed.

5.1.1 Calibration of the MERLIN-DEEPC model

The following correlations were used in the DEEPC code for the modelling of the Lynx Upgrade engine.

1. Spray penetration correlation, Dent (1971)

$$\text{Spray penetration, } S = 3.07(\Delta P_{noz}/\rho_g)^{0.25} \{d_{noz}.t\}^{0.5}.(294/Tg)^{0.25}$$

Where, ΔP_{noz} ~ pressure drop across nozzle, N/m^2

ρ_g ~ air density in cylinder, kg/m^3

d_{noz} ~ nozzle hole diameter, m

t ~ time, s

Tg ~ gas temperature, K

2. Spray angle correlation, Abramowich (1963)

$\tan(\theta/2) = 0.13\ (1 + \rho_g/\rho_f)$ where, ρ_g ~ air density in cylinder, kg/m^3

ρ_f ~ fuel density, kg/m^3

3. Fuel droplet Sauter mean diameter correlation, Elkotb (1982)

Sauter mean diameter, $SMD = 308500.\ \rho_f^{0.385}\ .\ \nu_f^{0.737}\ .st_f^{0.737}\ .\ \rho_g^{0.06}\ .\ \Delta P_{noz}^{-0.54}$

Where, ρ_f ~ fuel density, kg/m^3

ν_f ~ fuel kinematic viscosity, m/s

st_f ~ fuel surface tension, N/m

ρ_g ~ air density in cylinder, kg/m^3

ΔP_{noz} ~ pressure drop across nozzle, N/m^2

4. Ignition delay correlation, Wolfer (1938)

Ignition delay, $\tau_p = 0.44\ P^{-1.19} \exp(4650/T)$

τ_p ~ ms

P ~ atmospheres absolute

T ~ K

The correlations described above were chosen, based on previous experience in DI diesel engine modelling at Ford, because they aligned predicted results more closely to experimental data than other alternative published correlations that were available.

For the initial calibration of the model to the experimental data, a priority order of certain basic parameters was scheduled, these were:

1) fuel mass flow
2) air mass flow
3) BMEP
4) boost temperature
5) peak cylinder pressure

To achieve a close correlation with the experimental data a number of coefficients and constants were adjusted in the code. Predicted fuel mass flow was correlated with the experimental measurement by adjustment of the injector nozzle discharge coefficient, the final value used was 0.732. The simulated air mass flow was calibrated to the experimental result by adjusting a number of parameters in the program; such as heat transfer coefficients for the exhaust plenum and turbine volute, and the simulated blow-by.

Once the fuel and air mass flows correlated to the experimental data, the predicted BMEP was finally tuned by adjustment of the simulated injection timing. The experimental reading was taken at 10 per cent needle lift, whereas the model simulates injection timing when the line pressure equates to the injector opening pressure. The line pressure data therefore had to be adjusted from a timing point of view, relative to crank angle, to give the correct injection timing to fine-tune the BMEP.

5.1.2 Engine operating condition

One engine operating condition was selected for the modelling exercise to examine the accuracy of the Zeldovich mechanism in predicting exhaust NOx concentrations. In order to investigate the effect on the predicted mode result, and the relative accuracy of the rate constants, a selected number of published rate constants were used for the simulation. Also, the sensitivity of the Zeldovich rate constants was assessed.

The European standard for measuring exhaust emissions from light-duty vehicles is a vehicle drive cycle that consists of two parts. Part One, the urban ECE-15 cycle is made

up of four elementary urban cycles. Each elementary urban cycle comprises fifteen phases, idling, acceleration, steady speed, deceleration and idling again, repeated three times. The average speed for this part is 19 km/h, the effective running time is 13 minutes and the distance covered over the 4 cycles is 4.05 km. Part Two, the extra urban drive cycle (EUDC) comprises 13 phases of idling, acceleration, steady speed and deceleration. This is a faster drive cycle with an average speed of 62.6 km/h with a maximum speed of 120 km/h. It lasts 6 minutes and 40 seconds and covers a theoretical distance of 6.955 km. This drive cycle is shown in **Figure 5.1.** During the test the exhaust gases are diluted and a proportional sample collected in one or more bags. The exhaust gases are sampled and analysed, and the total volume of the diluted exhaust is measured. Carbon monoxide, hydrocarbons, oxides of nitrogen and particulate emissions are analysed for diesel engines, with the corrected measurements expressed as g/km.

A block diagram of the Merlin model of the Lynx Upgrade engine is shown in **Appendix 1** on page 265.

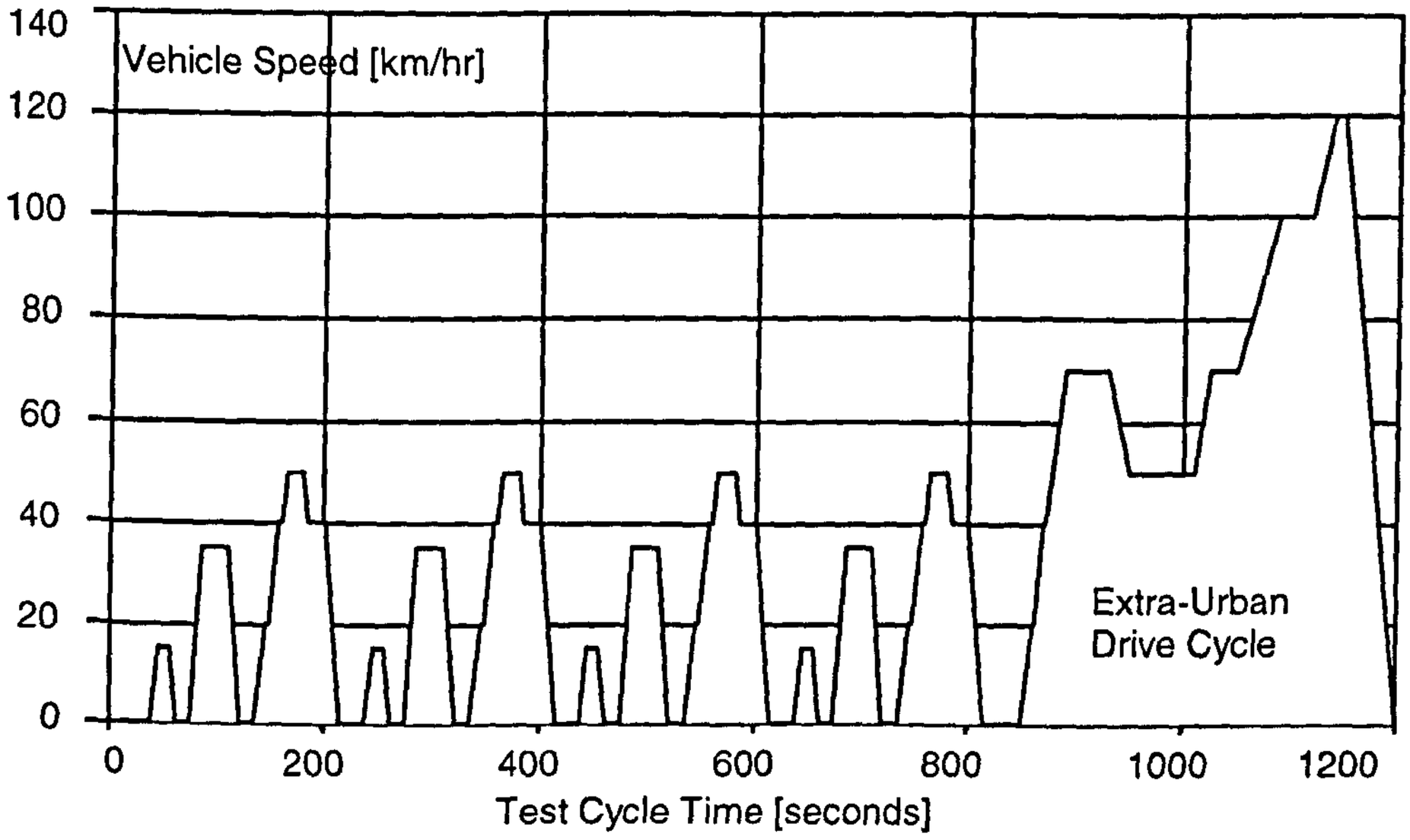

Cycle Analysis

Distance Travelled

ECE-15 cycle	1.013 x 4	= 4.052 km
EUDC cycle		= 6.955 km
Total		= 11.007 km

Maximum Speed

ECE-15 cycle	50 km/h
EUDC cycle	120 km/h

Average Speed

ECE-15 cycle	19 km/h
EUDC cycle	62.6 km/h
Acceleration	21.6% of cycle
Deceleration	13.8%
Idle	35.4%
Steady speed	29.3%

Figure 5.1 European emissions vehicle drive cycle.

In order to develop diesel engine combustion and fuel injection systems it is normal practice within the automotive industry to develop steady-state mini-mapping points to represent the vehicle drive cycle. These are used for initial fuel injection system and combustion optimisation, and calibration on a steady-state dynamometer test bed prior to testing on a transient dynamometer or in a vehicle on a chassis rolls. These mini-

mapping points can be obtained by computer prediction methods, such as the Ford Corporate Vehicle Simulation Program (CVSP). This program simulates the legislative drive cycle for a particular engine-transmission-vehicle combination. It takes into account the transmission ratios, tyre rolling radii, vehicle rolling resistance and aerodynamic drag. By using a high number of discreet load speed points from the engine-operating map for brake specific fuel consumption (BSFC), the program predicts the total cycle fuel consumption. It is also possible to reduce the number of engine speed / load points to a relatively small number, and to weight their importance by assessing the time spent at, or near, that particular operating mode, for steady-state dynamometer testing. A 14-mode steady-state engine speed / load mini-mapping cycle has been used for the 1.8 litre diesel in the Escort car for a number of years; this is shown in **Table 5.1.** More recently this has been modified for the 1.8 litre Endura DI diesel in the new Ford Focus.

Table 5.1

14 Mode Steady-State Simulation of European Drive Cycle

For 1.8 Diesel in Escort Car

Mode No	Engine Speed rpm	BMEP bar	Torque Nm	Weighting
1	800	0	0	27.7
2	1000	1.0	14	4.0
3	1150	4.4	61.4	2.7
4	1500	4.0	55.8	2.4
5	1800	0.8	11.2	8.9
6	1800	2.0	27.9	6.0
7	1800	3.0	41.9	8.9
8	**1900**	**5.8**	**81.0**	**4.2**
9	2150	4.1	56.6	2.6
10	2300	6.0	83.7	3.3
11	2400	0.9	12.6	12.9
12	2600	3.9	54.4	3.4
13	**2700**	**8.0**	**111.7**	**2.0**
14	3200	5.0	69.8	0.9

One of these modes, mode 13, which is 2700 rpm and 8 bar BMEP, was chosen for this exercise.

5.1.3 Comparison between experimental results and MERLIN-DEEPC predicted NOx emissions for a Lynx Upgrade engine operated at 2700rpm, 8 bar BMEP.

Figures 5.2 to **5.9** show comparisons of the predicted engine performance parameters of air mass flow, fuel mass flow, BMEP, boost temperature and pressure, peak cylinder pressure and exhaust temperature, plotted against the experimental data taken from the engine with increasing levels of EGR. These figures clearly illustrate close correlation

for, air mass flow, fuel mass flow and BMEP. At low levels of EGR, boost temperature was modelled accurately, but as the EGR level increased above 20 per cent, the modelled temperature did not follow the experimental rise in boost temperature, leading to an error of 48 K at 40 per cent EGR. Boost pressure and therefore peak cylinder pressures were less accurately modelled, although the trend was correctly represented. The modelled value was lower by 0.18 bar with no EGR, and got progressively lower with increasing EGR. A similar situation occurred with peak cylinder pressure, although the relative accuracy was better, with a 4 per cent error at zero EGR which doubled to an 8 per cent error at 40 per cent EGR.

The emissions predictions are shown in **Figures 5.10** to **5.15**. **Figure 5.10** shows CO emissions plotted in g/kg_{fuel} and here the correlation to the experimental data was not good, the modelled results were about a third of the experimental value. Carbon dioxide emissions are plotted in **Figure 5.11** and here, the predicted values were higher than the experimental results, an error of 10 per cent occurred at zero EGR, but this increased to 42 per cent at 40 per cent EGR. Clearly the DEEPC code was not modelling CO_2 correctly at high EGR levels. Unburned hydrocarbon levels from a diesel engine are very low, less than 2 g/kg_{fuel} and the model had difficulty in predicting accurate values, as can be seen from **Figure 5.12**. Prediction of smoke emissions was good up to an EGR level of 20 per cent, but the model did not predict the upturn in smoke at higher levels of EGR, as seen in **Figure 5.13**. The prediction of particulates is relatively good and accurately determined the trend over the range of EGR levels, although the accuracy falls off at high EGR levels.

The NOx results are plotted in **Figure 5.15**; as expected there was almost a linear fall in the experimental measurements of NOx emissions with increasing levels of EGR. The predicted NOx levels follow a similar trend, although they were initially higher at zero and 10 per cent EGR, but converged with the experimental results at 20 per cent EGR, and then crossed-over to give lower values at 30 and 40 per cent EGR. The over-prediction at zero EGR represented an error of 17 per cent compared to the experimental measurement, a 25 per cent error at 10 per cent EGR, converged to within 3 per cent at 20 per cent EGR. The modelled result diverged at 30 per cent EGR giving an under-predicted error of 52 per cent at 30 per cent and 66 per cent at 40 per cent EGR.

The accuracy of the predicted NOx results relies on a number of assumptions. Firstly, it is assumed that the Zeldovich mechanism is the predominant method for the formation of NOx. Moreover, the Zeldovich mechanism relies on the prediction of concentrations of NO, N, O_2 and OH as well as the local temperature. It is not known how accurate these constituents were modelled, as they were not been measured. It may therefore be that these quantities were less accurately modelled during engine operation at high levels of EGR. It has already been illustrated in **Figure 5.10** that the prediction of CO, for example, was not particularly accurate. There is also the fundamental assumption that the levels of NO, N, O_2 and OH have achieved equilibrium values. With regards to in-cylinder temperature prediction, boost temperature was modelled fairly accurately up to 20 per cent EGR, the predicted values then diverged from the experimental as EGR was increased, **Figure 5.5**. Boost pressure, **Figure 5.6**, on the other hand was under-predicted throughout the EGR loop, by 10 to 13 per cent up to 20 per cent EGR, diverging to a 22 per cent error at 45 per cent EGR. Peak cylinder pressure was under-predicted throughout the EGR loop by 4 to 8 per cent, except at 45 per cent EGR where the error was 14 per cent, as shown in **Figure 5.8**. Exhaust temperature, however, was slightly over-predicted by around 7 per cent throughout the loop, so it is very difficult to assess whether in-cylinder zonal temperatures were accurately predicted for the Zeldovich mechanism.

Despite the prediction errors, the model does demonstrate the correct trends, and the level of accuracy at the low EGR rates is not untypical of combustion models at the present time. For routine simulation exercises and for extensive parametric studies of engine performance and emissions, the phenomenological models are generally favoured (Wahab 1998). This is mainly because of the ease of modelling; the lesser computer facilities required, and the shorter turn around time compared to three-dimensional CFD modelling.

5.1.4 Comparison between experimental results and MERLIN-DEEPC predicted NOx emissions using different chemical kinetic rates for Lynx Upgrade engine operated at 2700rpm, 8 bar bmep.

In the standard version of DEEPC the rate constants were taken from Heywood (1988), who referenced Bowman (1975). Bowman took the rate data from Baulch et al (1973) who conducted a critical review of published data and recommended rate constant expressions for these reactions. The results previously discussed from this prediction with the standard version were then compared with alternative rate constants for k_{-1}, k_2 and k_3, taken from the literature survey. Schofield (1967) recommended a k_{+2} expression that includes a 1.5 'ß' term, this was used with the standard rate values for k_{-1} and k_3. Hanson and Salimian (1984) proposed rate constants which were one to two orders of magnitude different to those of Baulch et al, and rate constants from Glarborg et al (1992) which are similar to those of Baulch et al, with the exception that k_{-1} has a 0.3 'ß' term. **Table 5.2** summarizes the rate constants used for the prediction work.

Table 5.2

Extended Zeldovitch mechanism rate constants used in MERLIN-DEEPC predictions

$$k = AT^{\beta} \exp(-E/RT)$$

Reference	Reaction	Const	A	β	E/R	Temperature Range
Hanson & Salimian, 1984	$N+NO \rightarrow O+ N_2$	k_{-1}	2.63×10^{14}	0	0	
Heywood, 1988	**$N+NO \rightarrow O+ N_2$**	k_{-1}	**1.60×10^{13}**	**0**	**0**	
Glarborg et al, 1992	$N+NO \rightarrow O+ N_2$	k_{-1}	3.31×10^{12}	0.3	0	
Schofield, 1967 (note 2)	$N+O_2 \rightarrow NO+O$	k_2	1.48×10^{8}	1.5	2862	400-5000
Baulch et al, 1973	**$N+O_2 \rightarrow NO+O$**	k_2	**6.4×10^{9}**	**1**	**3150**	**300 - 3000**
Hanson & Salimian, 1984	$N+O_2 \rightarrow NO+O$	k_2	1.6×10^{10}	1	4470	
Heywood, 1988	**$N+O_2 \rightarrow NO+O$**	k_2	**6.4×10^{9}**	**1**	**3150**	**300 - 3000**
Glarborg et al, 1992	$N+O_2 \rightarrow NO+O$	k_2	6.46×10^{9}	1	3160	
Baulch et al, 1973	**$N+OH \rightarrow NO+H$**	k_3	**4.1×10^{13}**	**0**	**0**	
Hanson & Salimian, 1984	$N+OH \rightarrow NO+H$	k_3	2.6×10^{11}	0	0	
Heywood, 1988	**$N+OH \rightarrow NO+H$**	k_3	**4.1×10^{13}**	**0**	**0**	
Glarborg et al, 1992	$N+OH \rightarrow NO+H$	k_3	3.8×10^{13}	0	0	

Units: **A - cm^3/mole.s when $\beta = 0$; T- temperature in Kelvin**

Note 2: Best fit data from Kaufman & Decker, Mavroyannis & Winkler, Clyne & Thrush, Kistiakowsky & Volpi and Wray & Teare.

These comparisons are shown in **Figure 5.16**. Here experimental and predicted NOx emissions in g/kg fuel were plotted against the level of EGR. This plot clearly demonstrates that the Heywood/Baulch rate constants were the best. However, the

Glarborg rate constants, although grossly over-predicting at the zero and low EGR levels, did converge with the experimental measurements at the high EGR levels. The 'Schofield' result was almost identical to the Heywood/Baulch result which indicated that the final NOx concentration prediction was insensitive to the 1.5 'ß' term for k_{+2}. A sensitivity study was therefore conducted, whereby the rate constants were factored by a range of constants to establish the effect on the final calculation of the NOx concentration.

Figure 5.17 shows the results of the initial sensitivity study on the rate constants, where the standard Heywood/Baulch constants were each in turn multiplied by a factor of 2.0. It can be seen from **Figure 5.17** that the doubling of k_{-1} had the most effect, particularly when there was no EGR, so the highest in-cylinder temperatures would occur with high levels of excess oxygen; here, the predicted value increased from 49 to 81 g/kg of fuel. As the amount of EGR was increased, the modelled result with double k_{-1} converged towards the standard result, but was closer to the experimental values at 30 and 40 per cent EGR. Doubling k_2 and k_3 had virtually no effect on the predicted result, as shown by the plotted results in the figure, these results were virtually on top of the standard values. It is interesting to note that all the predictions during the EGR loop, over-predicted NOx levels at zero and low levels of EGR and under-predicted at high levels of EGR.

Using the information from the sensitivity study, the standard Heywood/Baulch rate constants were modified in order to obtain a better fit to the experimental results. **Figure 5.18** shows the measured data and standard MERLIN-DEEPC predictions as in previous figures, with the predictions using the modified rate constants that gave an improved correlation to the experimental results from the EGR loop. However, there remained a degree of under-prediction at the high EGR rates. The rate constants used for these calculations are shown in **Table 5.3** below.

Table 5.3

Modified Rate Constants for Extended Zeldovich Mechanism in Merlin-DEEPC code

Rate Constant	Value cm^3/mole.s
k_{-1}	3.2×10^{13}
k_2	5.12×10^8 T exp[-3150/T]
k_3	3.28×10^{12}

The Merlin-DEEPC code with the standard and modified rate constants for the Zeldovich mechanism were next used to model NOx emissions for an injection timing swing at the same engine condition of 2700 rpm and 8 bar BMEP, with 30 per cent EGR. These results again in the form of g/kg fuel burned, were plotted against injection timing in degrees crank angle BTDC and can be seen in **Figure 5.19**. The predictions show the correct characteristic, but the model, with both sets of rate constants under-predicts compared to the experimental data across the range of the injection timing swing. It is also somewhat unfortunate that the measured NOx emissions from the timing swing, which was a different test to the EGR loop, were higher, as shown on **Figure 5.19** for the 5°BTDC timing point, which was the injection timing used during the EGR loop.

5.2 Summary and Conclusions

- All the thermal NOx simulations using the Zeldovich mechanism in the Merlin/DEEPC code during the EGR loop, over-predicted NOx levels at zero and low levels of EGR and under-predicted at high levels of EGR. The reason for these inaccuracies and the trend with varying levels of EGR is not clear. Inaccuracies may arise for the following reasons.

1. It was assumed that the Zeldovich mechanism was the predominant method for the formation of NOx, for example modelling of prompt NO

was not included.

2. The Zeldovich mechanism relies on the prediction of concentrations of NO, N, O_2 and OH.
3. The Zeldovich mechanism relies on the prediction of local temperature.
4. The modelling is based on the fundamental assumption that the concentration levels of NO, N, O_2 and OH have achieved equilibrium values.

- Comparing the predicted NOx results using Schofield's rate constant with a 1.5 'ß' term for k_{+2} demonstrated that the final NOx prediction was insensitive to the 1.5 'ß' term for k_{+2}, since the result was almost identical to the Heywood/Baulch result which did not have a 'ß' term.

- The sensitivity study conducted by individually doubling the Zeldovich rate constants demonstrated that the first equation, $O + N_2 \leftrightarrow NO + N$, is by far the most important for the formation of NO. The final NO level predicted by the Zeldovich mechanism was sensitive to the value of the first reaction rate constant.

- The modified rate constants gave a small improvement in the accuracy of modelling NO, compared to the standard rate constants for different EGR levels and injection timings.

- Despite the prediction errors, the model does demonstrate the correct trends, and the level of accuracy at the low EGR rates is not untypical of combustion models at the present time. For routine simulation exercises and for extensive parametric studies of engine performance and emissions, the phenomenological models are generally favoured (Wahab 1998). This is mainly because of the ease of modelling, the lesser computer facilities required, and the shorter turn around time compared to three-dimensional CFD modelling.

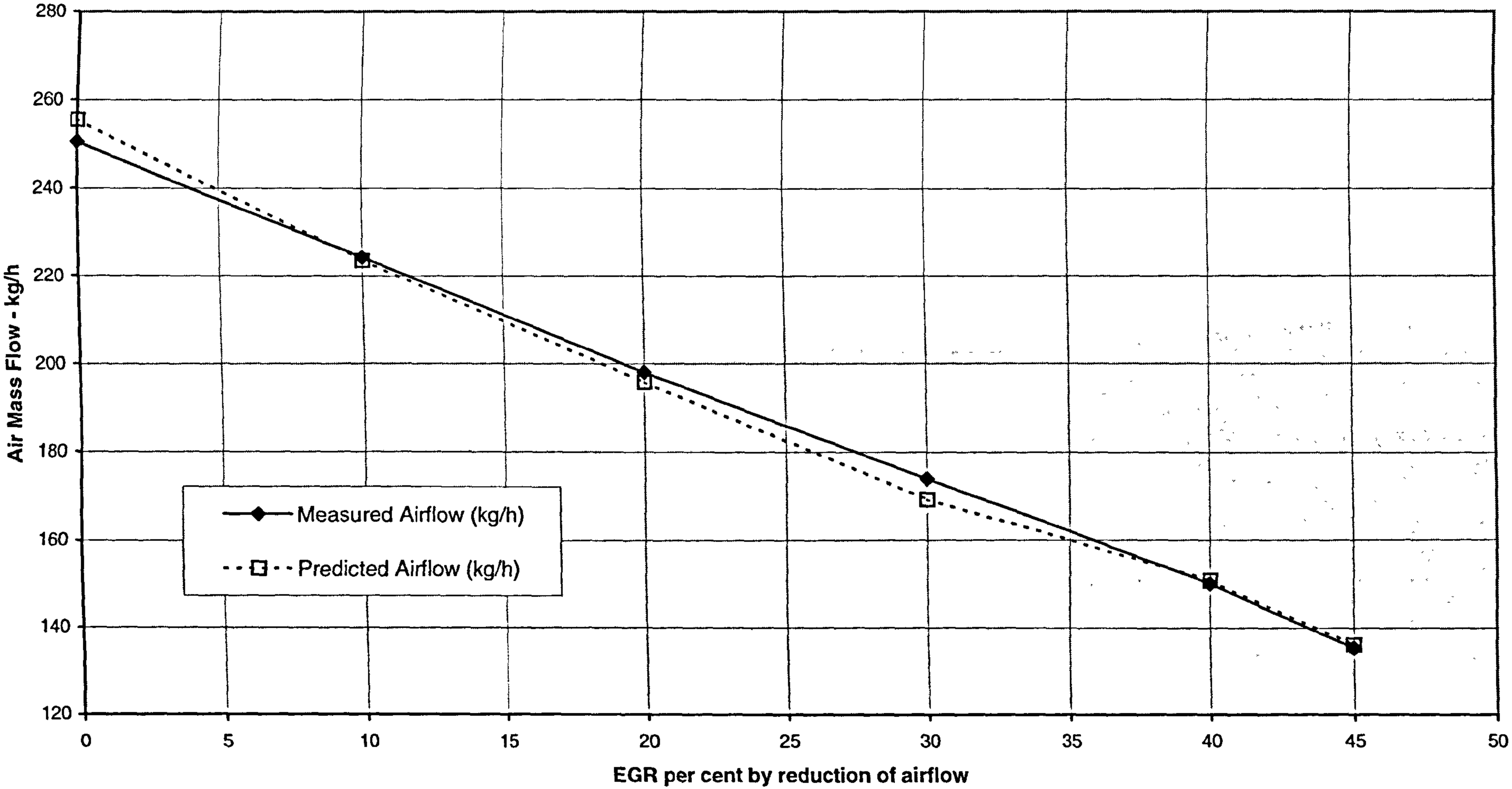

Figure 5.2 Comparison of experimental results and predicted air mass flow, versus EGR per cent at 2700 rpm 8.0 bar BMEP

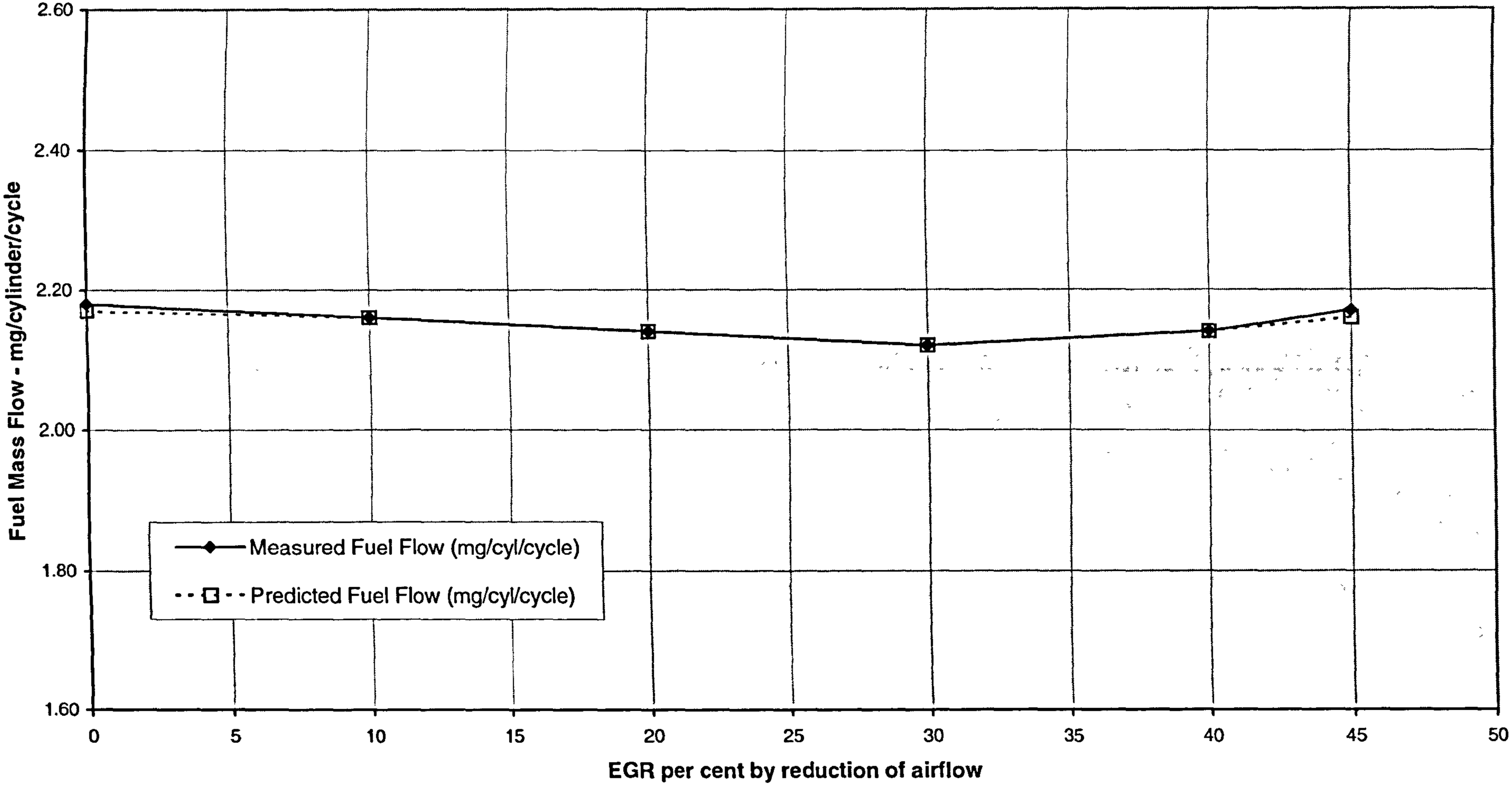

Figure 5.3 Comparison of experimental results and predicted fuel mass flow versus EGR per cent at 2700 rpm 8.0 bar BMEP

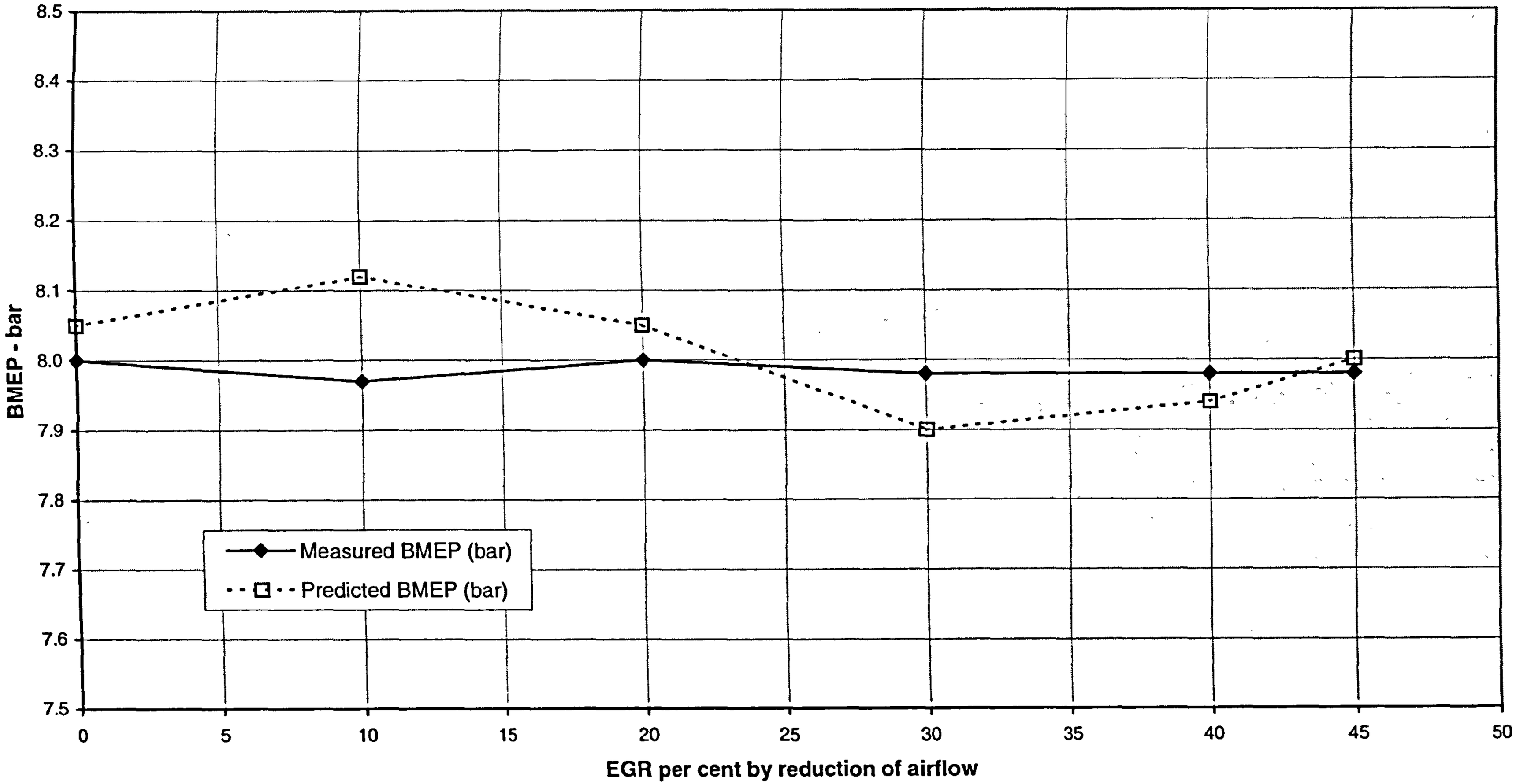

Figure 5.4 Comparison of experimental results and predicted BMEP versus EGR per cent at 2700 prm 8.0 bar BMEP

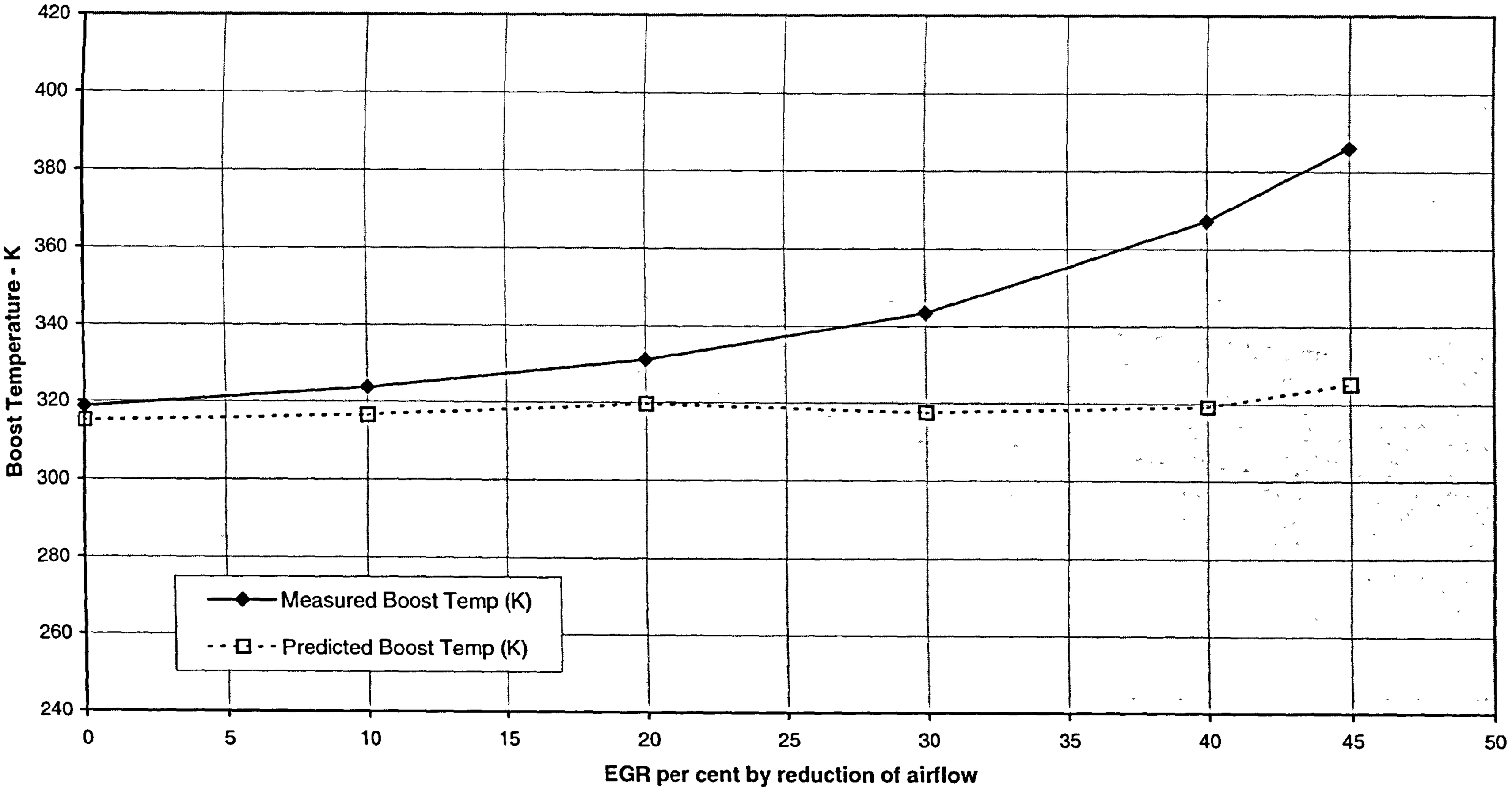

Figure 5.5 Comparison of experimental results and predicted boost temperature versus EGR per cent at 2700 rpm 8.0 bar BMEP

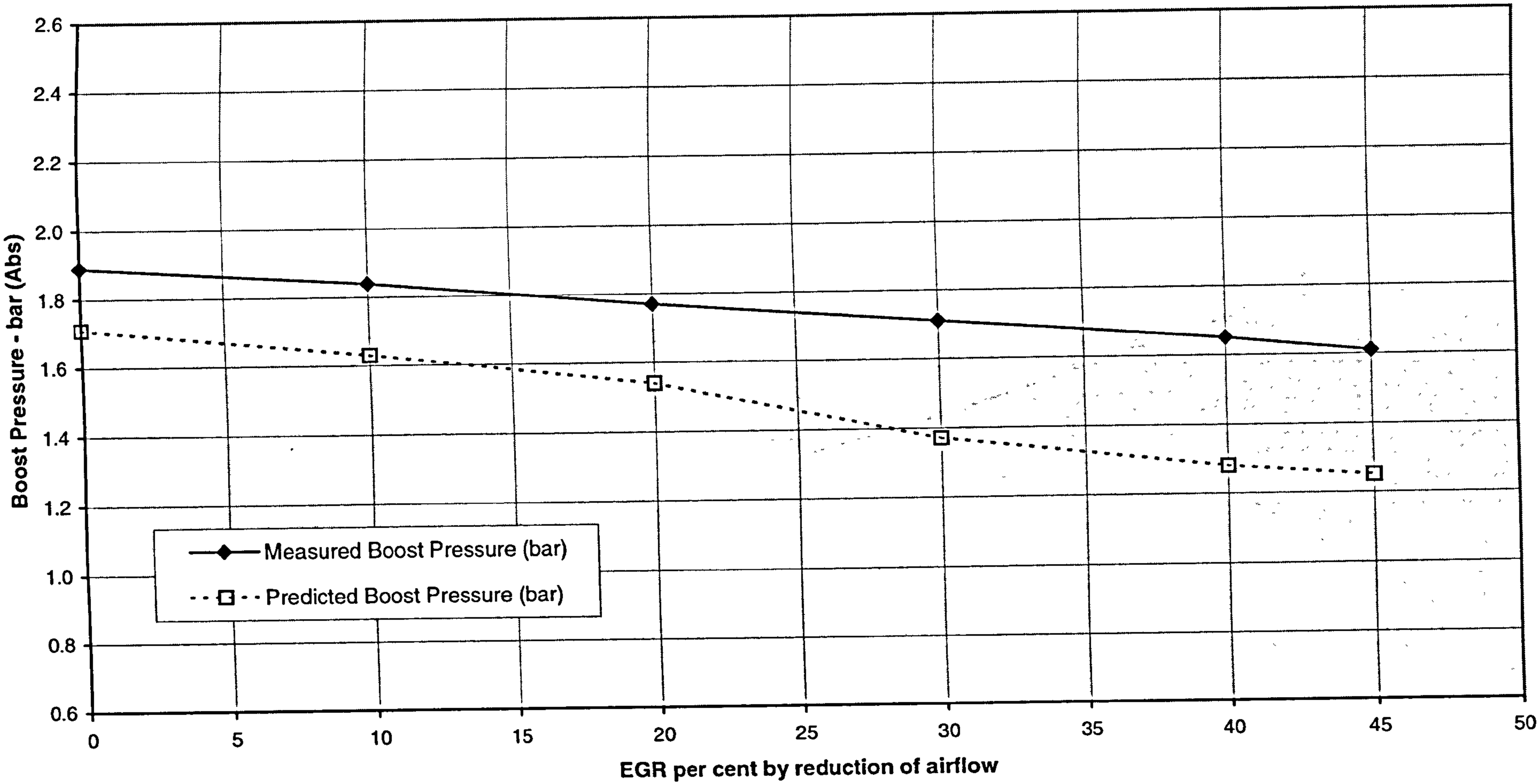

Figure 5.6 Comparison of experimental results and predicted boost pressure versus EGR per cent at 2700 rpm 8.0 bar BMEP

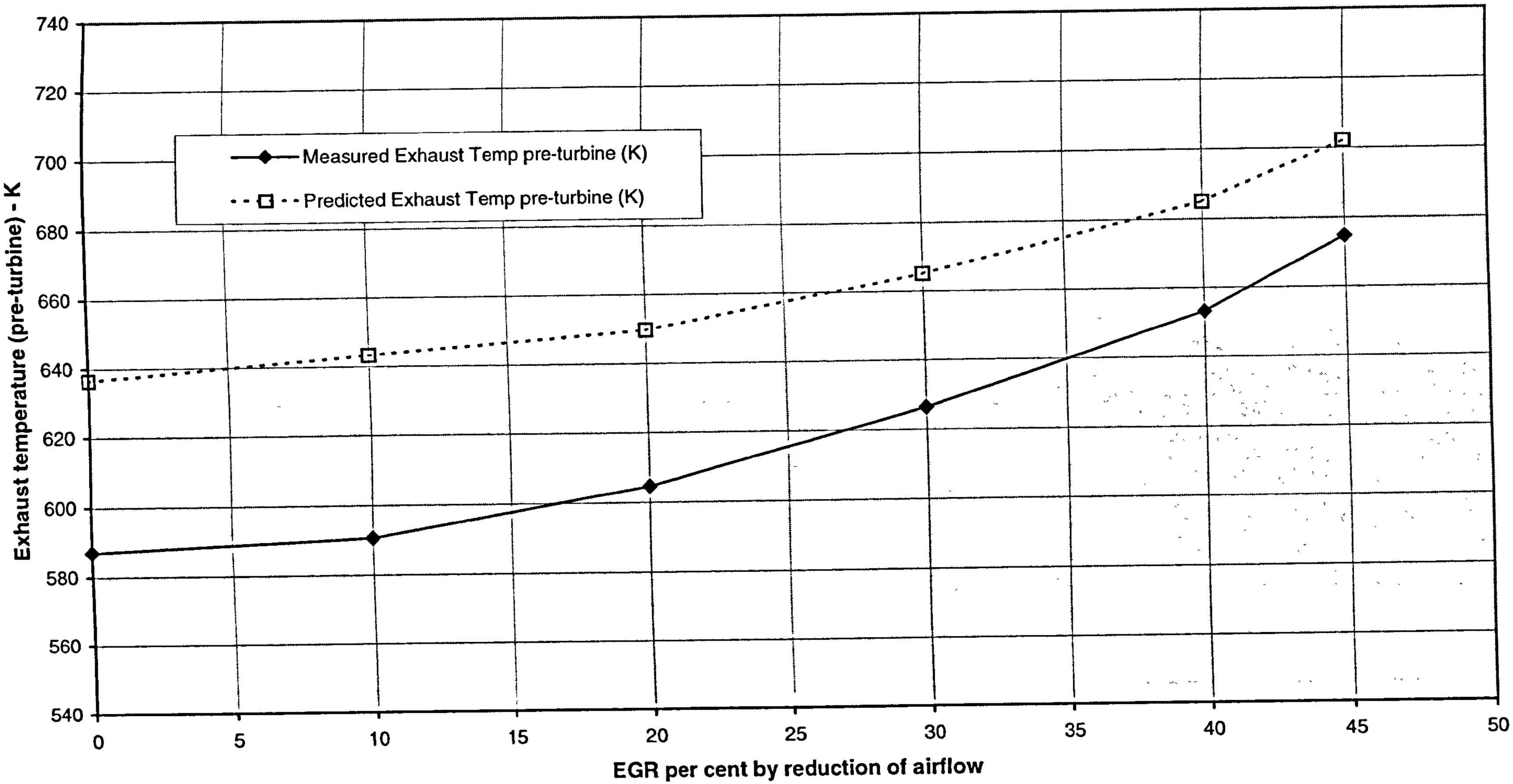

Figure 5.7 Comparison of experimental results and predicted exhaust temperature versus EGR per cent at 2700 rpm 8.0 bar BMEP

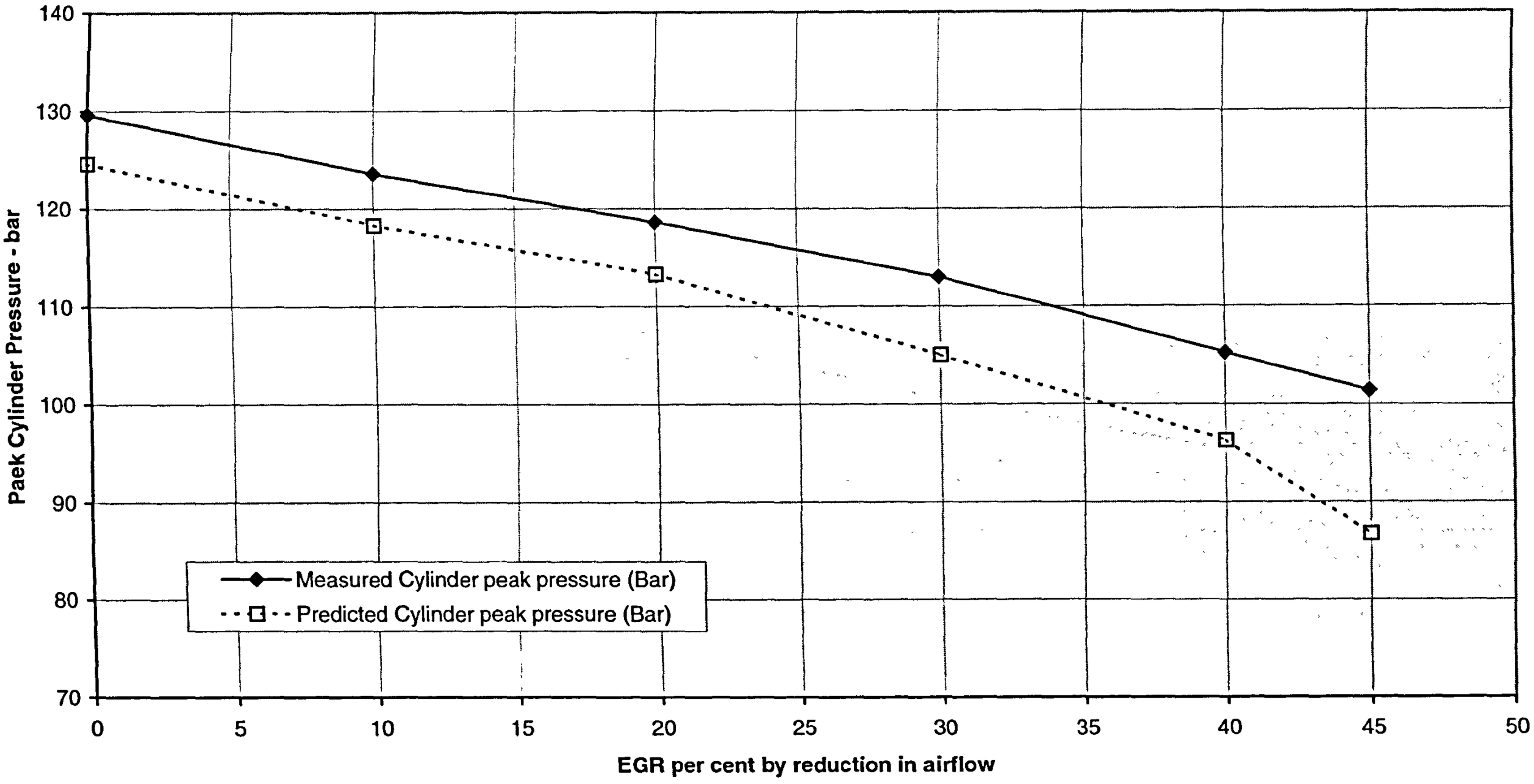

Figure 5.8 Comparison of experimental results and predicted peak cylinder pressure versus EGR per cent at 2700 rpm 8.0 bar BMEP

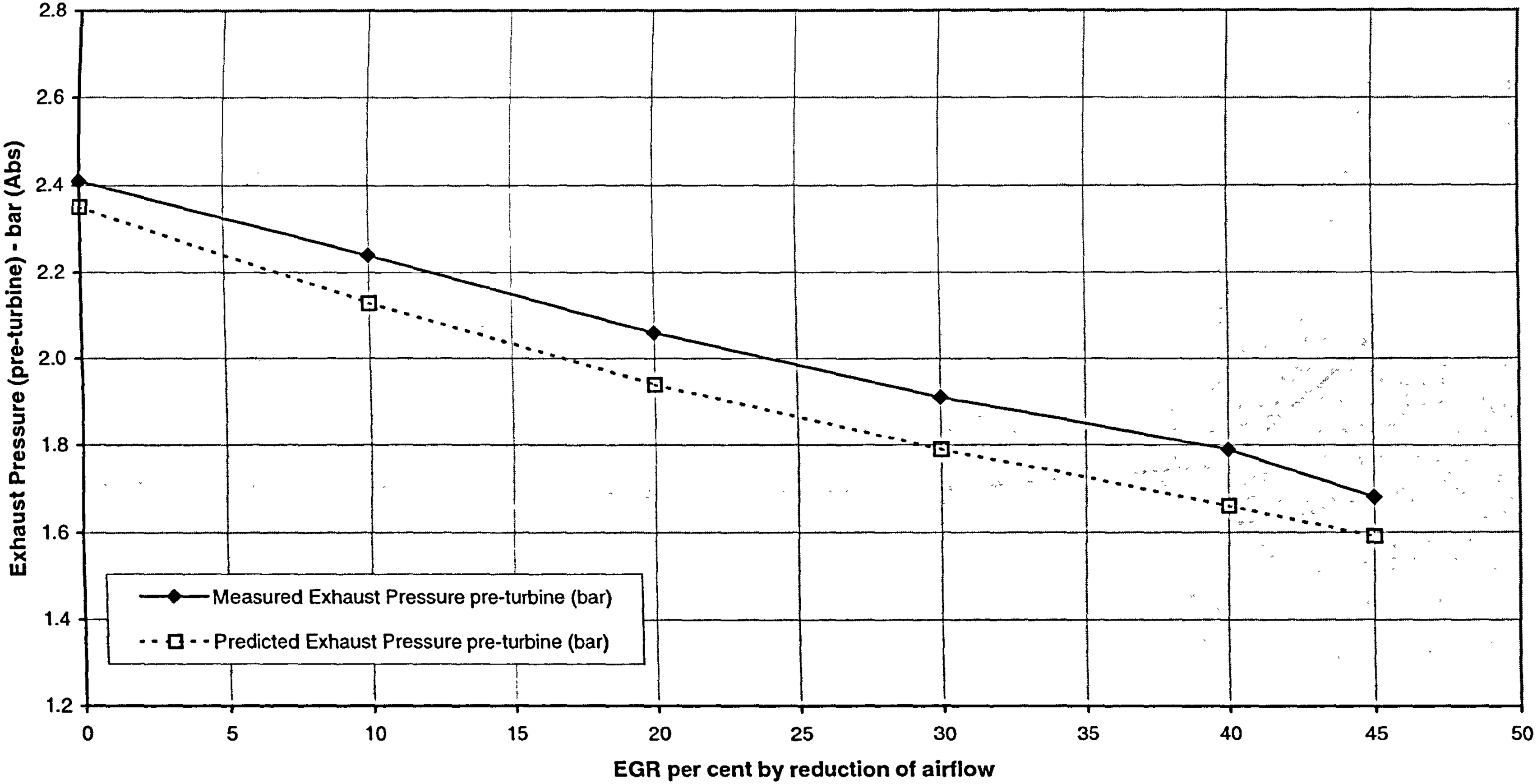

Figure 5.9 Comparison of experimental results and predicted exhaust pressure versus EGR per cent at 2700 rpm 8.0 bar BMEP

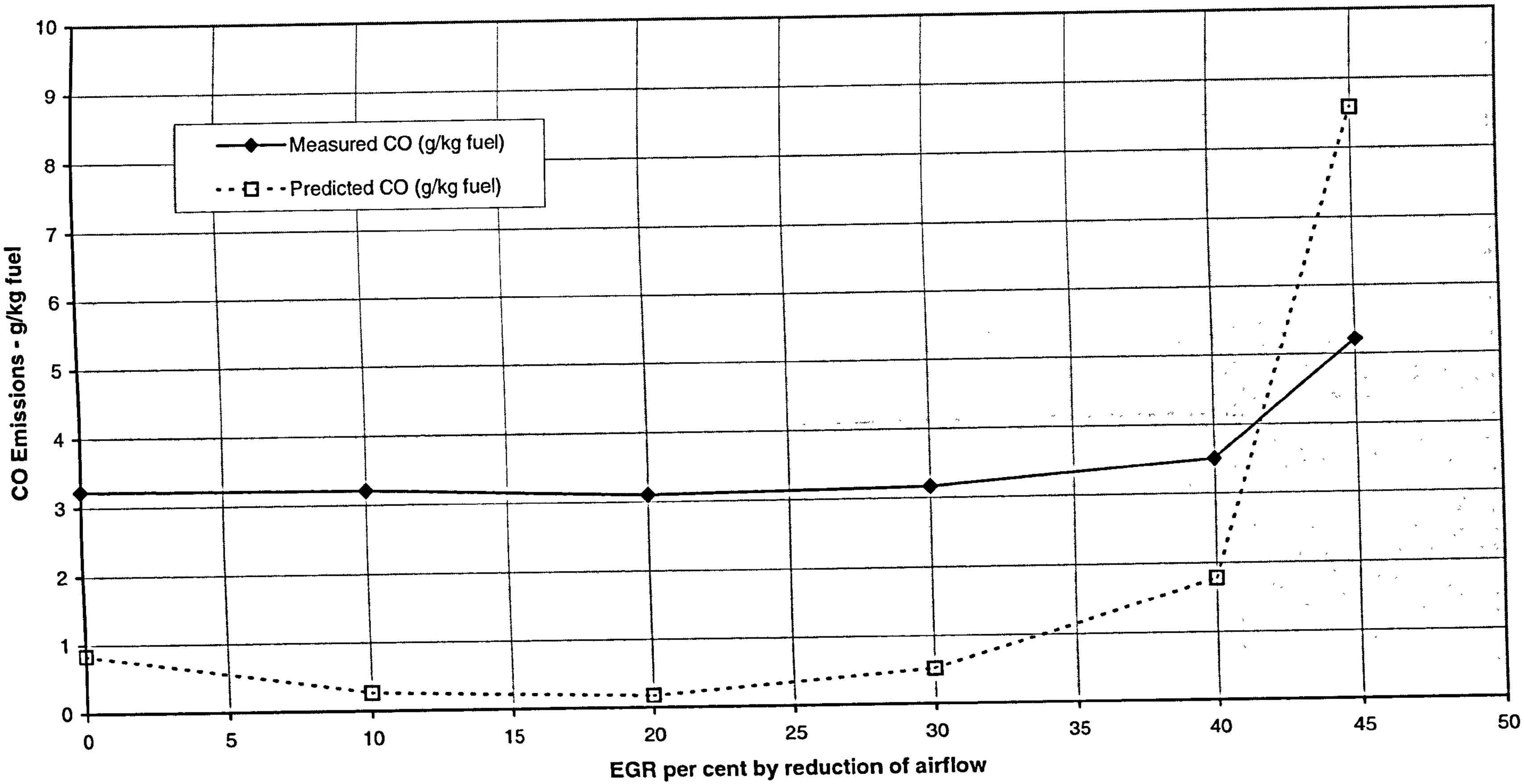

Figure 5.10 Comparison of experimental results and predicted CO emissions versus EGR per cent at 2700 rpm 8.0 bar BMEP

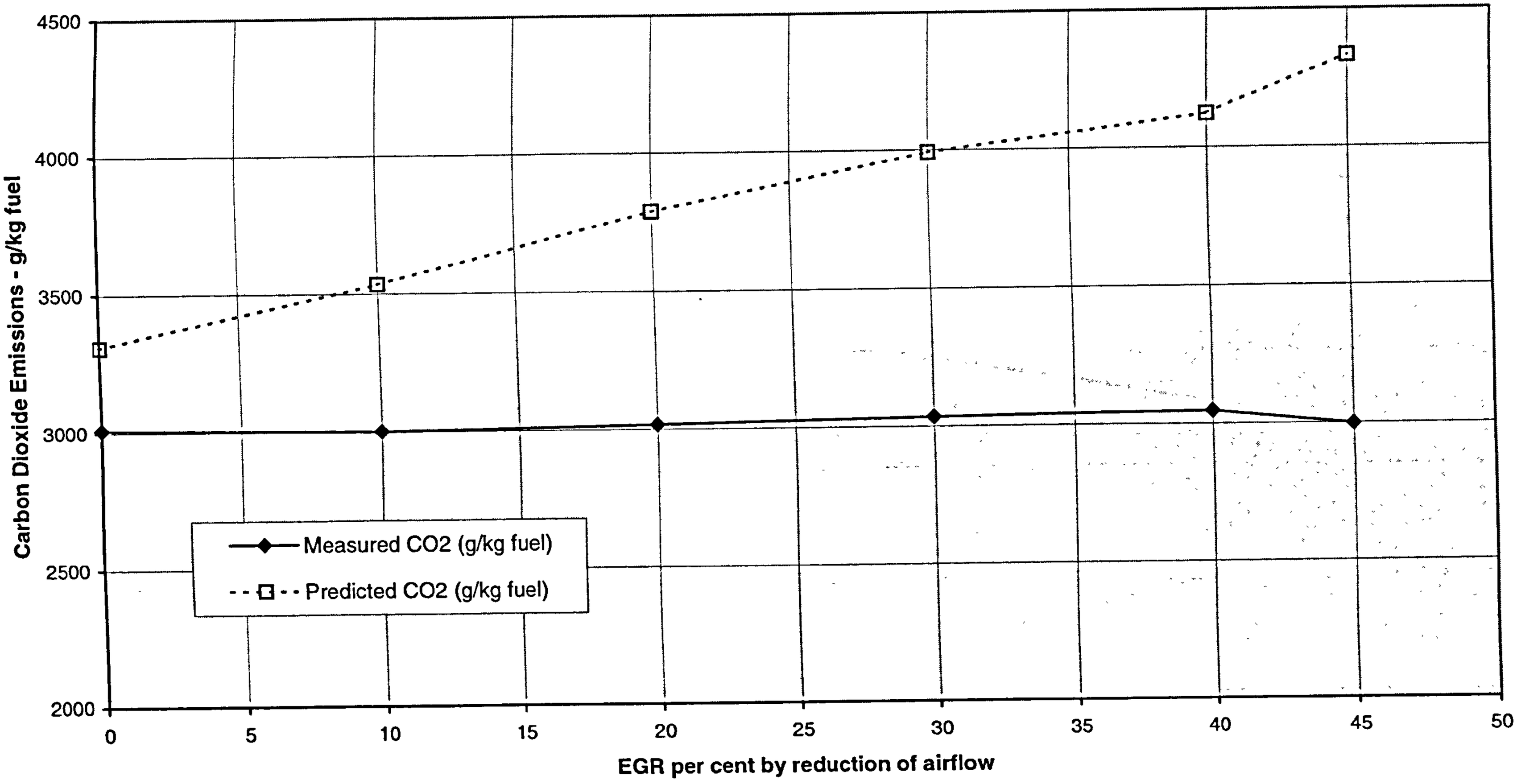

Figure 5.11 Comparison of experimental results and predicted carbon dioxide emissions versus EGR per cent at 2700 rpm 8.0 bar BMEP

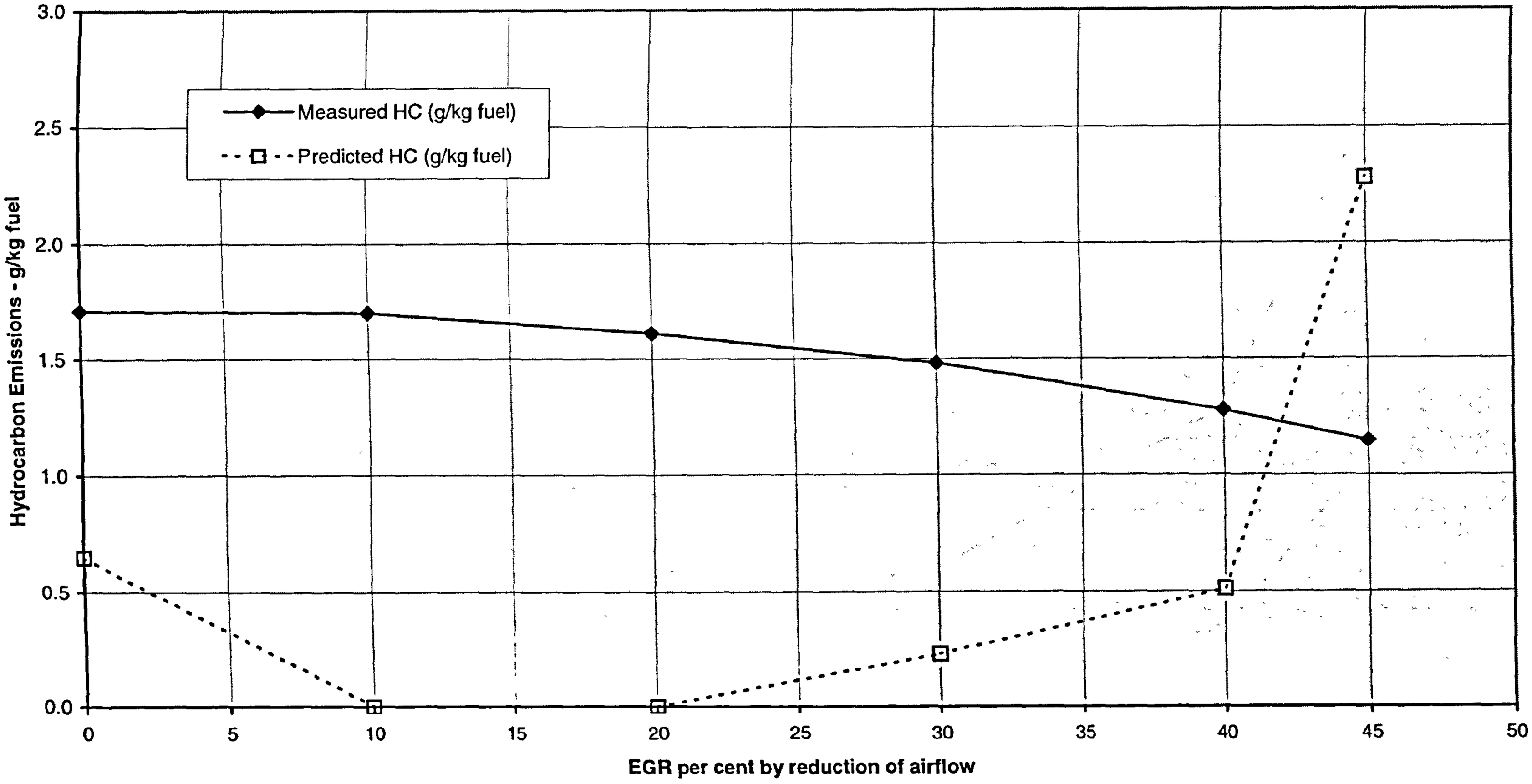

Figure 5.12 Comparison of experimental results and predicted hydrocarbon emissions versus EGR per cent at 2700 rpm 8.0 bar BMEP

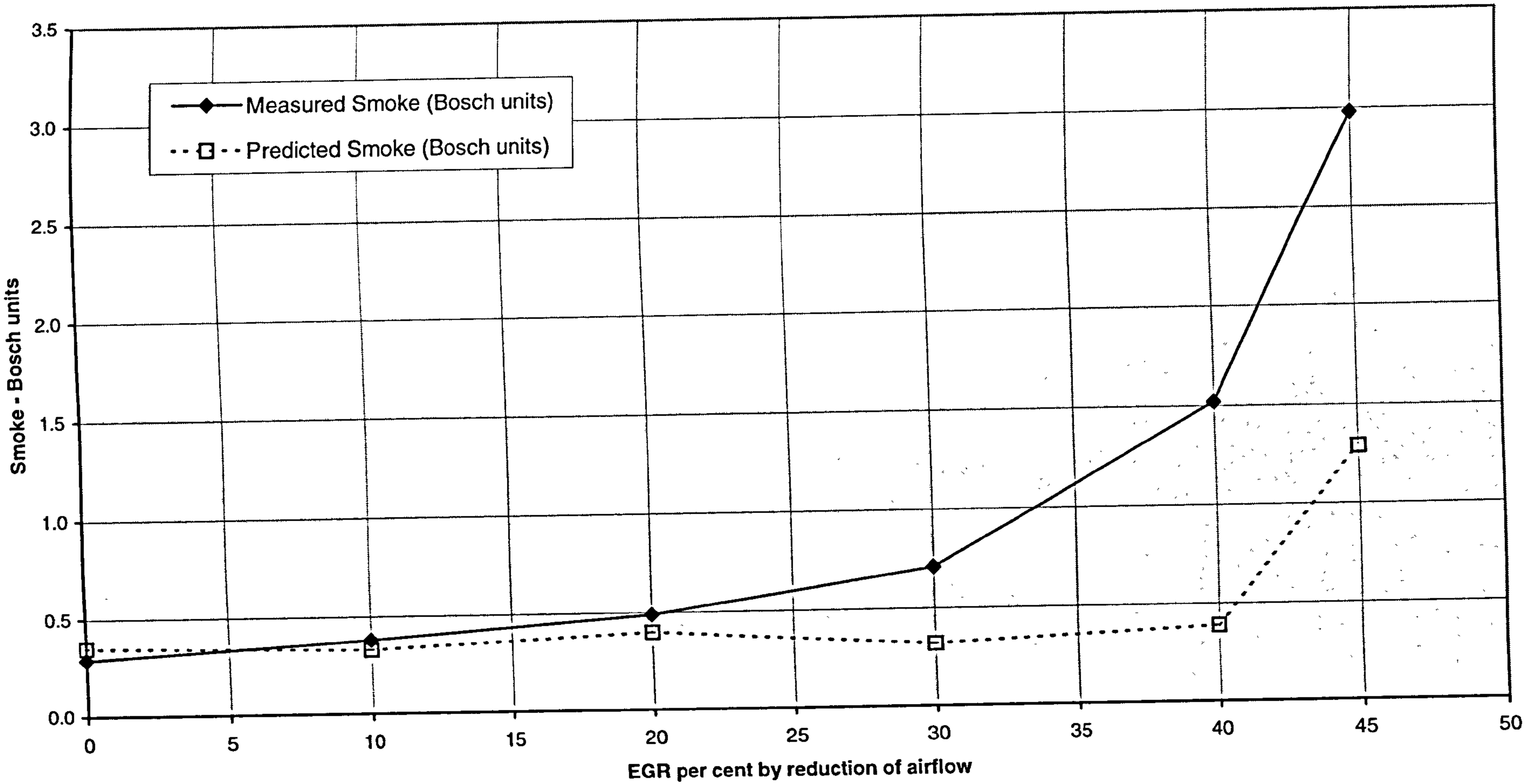

Figure 5.13 Comparison of experimental and predicted smoke versus EGR per cent at 2700 rpm 8.0 bar BMEP

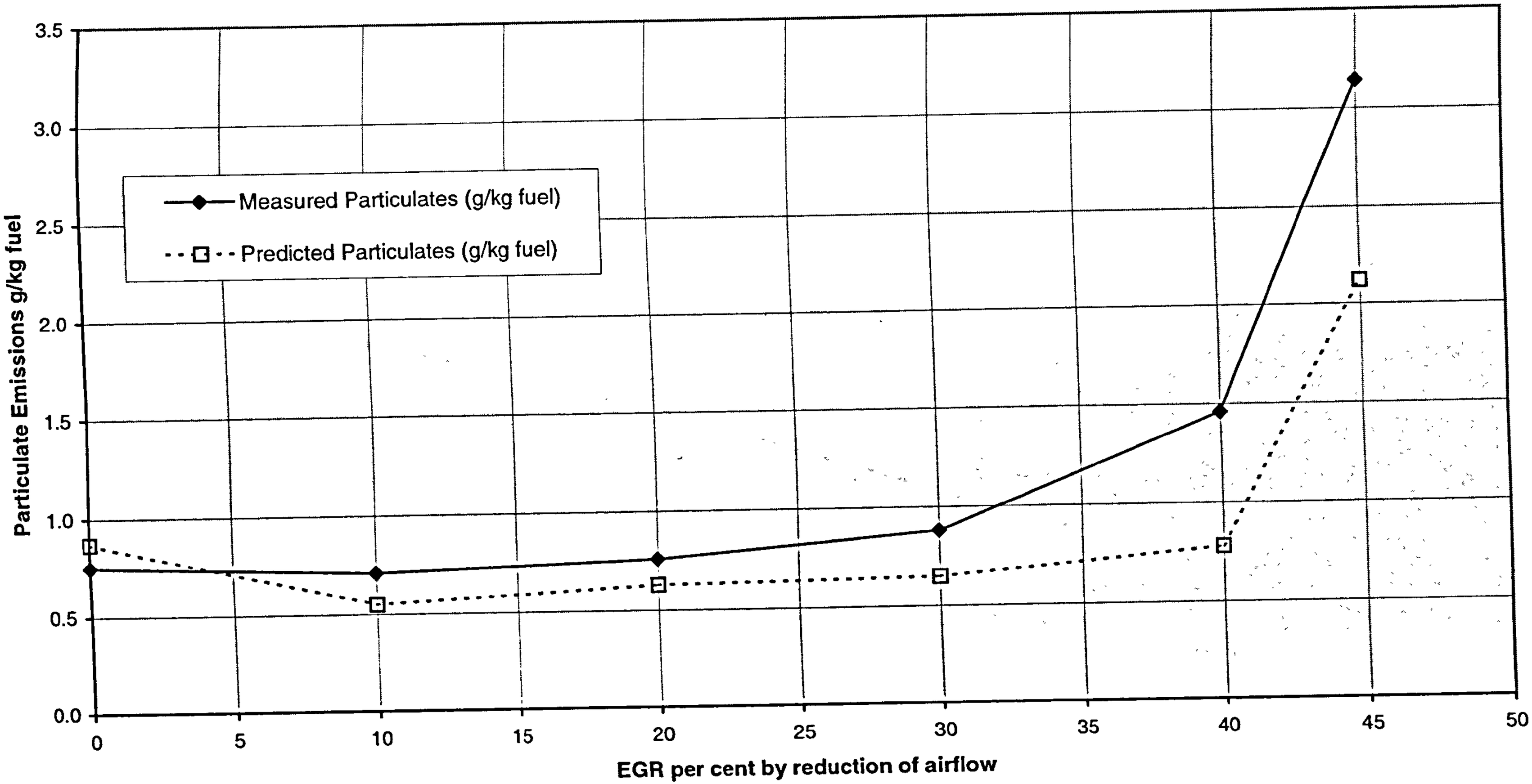

Figure 5.14 Comparison of experimental results and predicted particulates emissions versus EGR per cent at 2700 rpm 8.0 bar BMEP

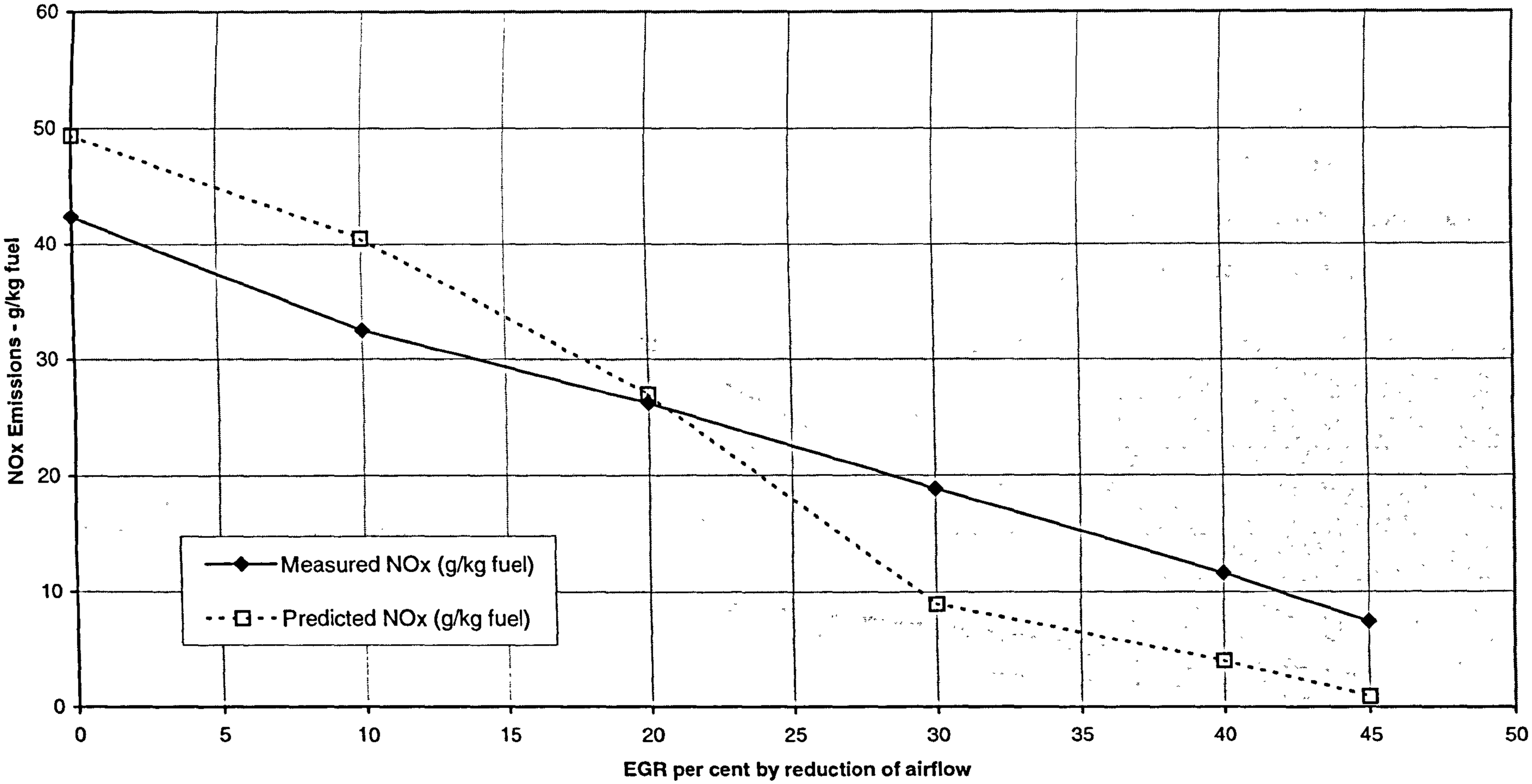

Figure 5.15 Comparison of experimental results and predicted NOx emissions versus EGR per cent at 2700 rpm 8.0 bar BMEP

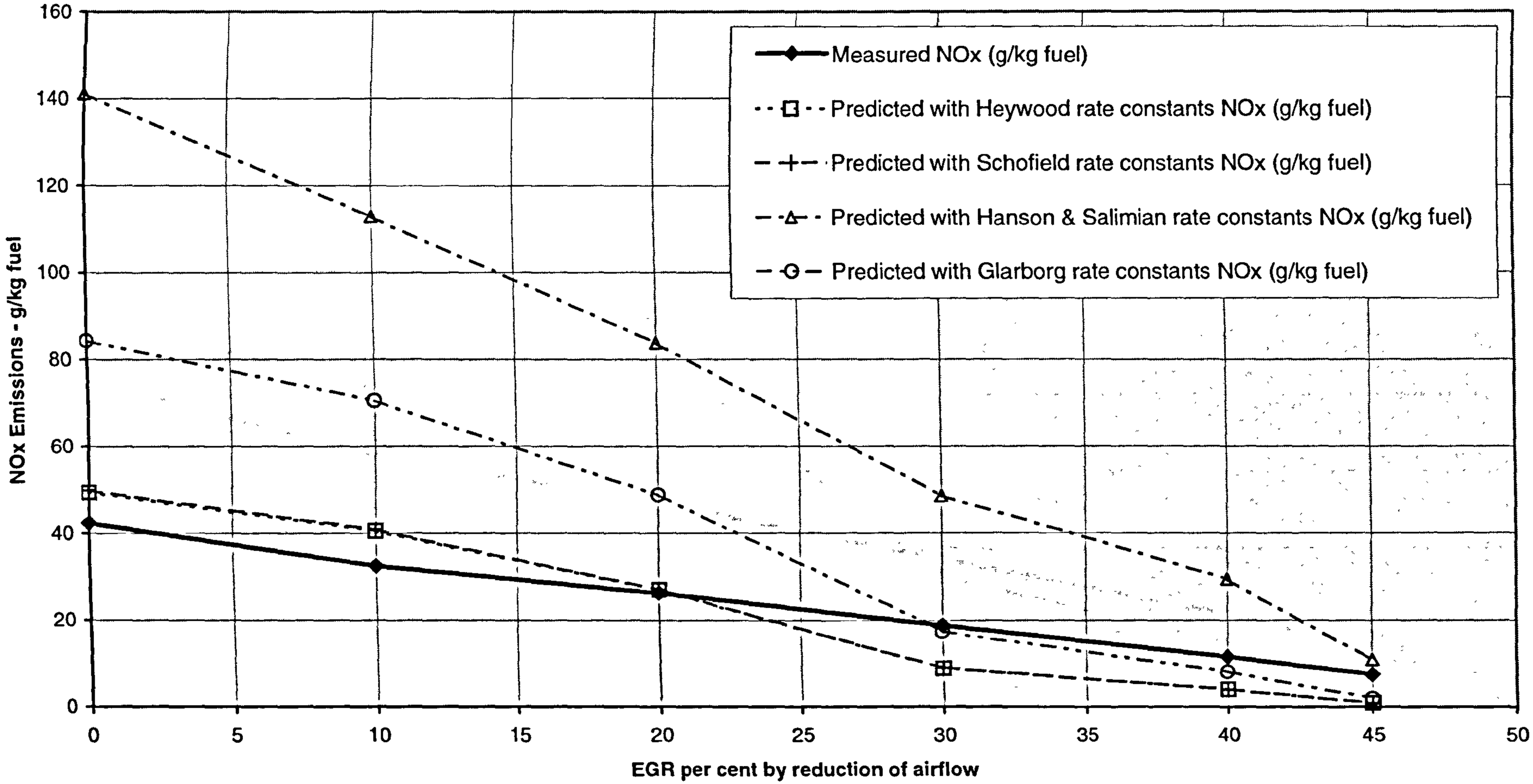

Figure 5.16 Comparison of experimental results and predicted NOx emissions using different rate constants, versus EGR per cent at 2700 rpm 8.0 bar BMEP

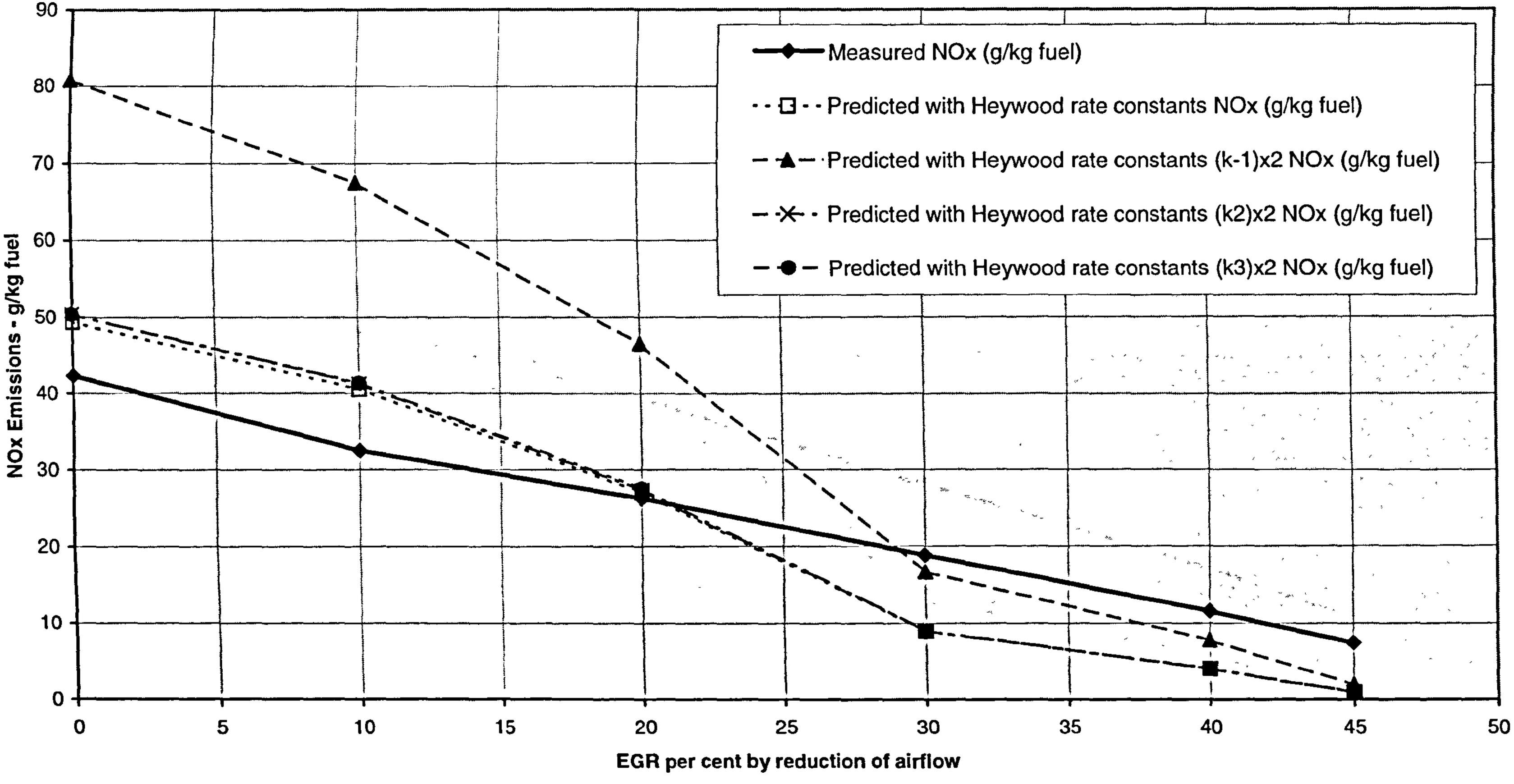

Figure 5.17 Sensitivity study of Zeldovich rate constants, versus EGR per cent at 2700 rpm 8.0 bar BMEP

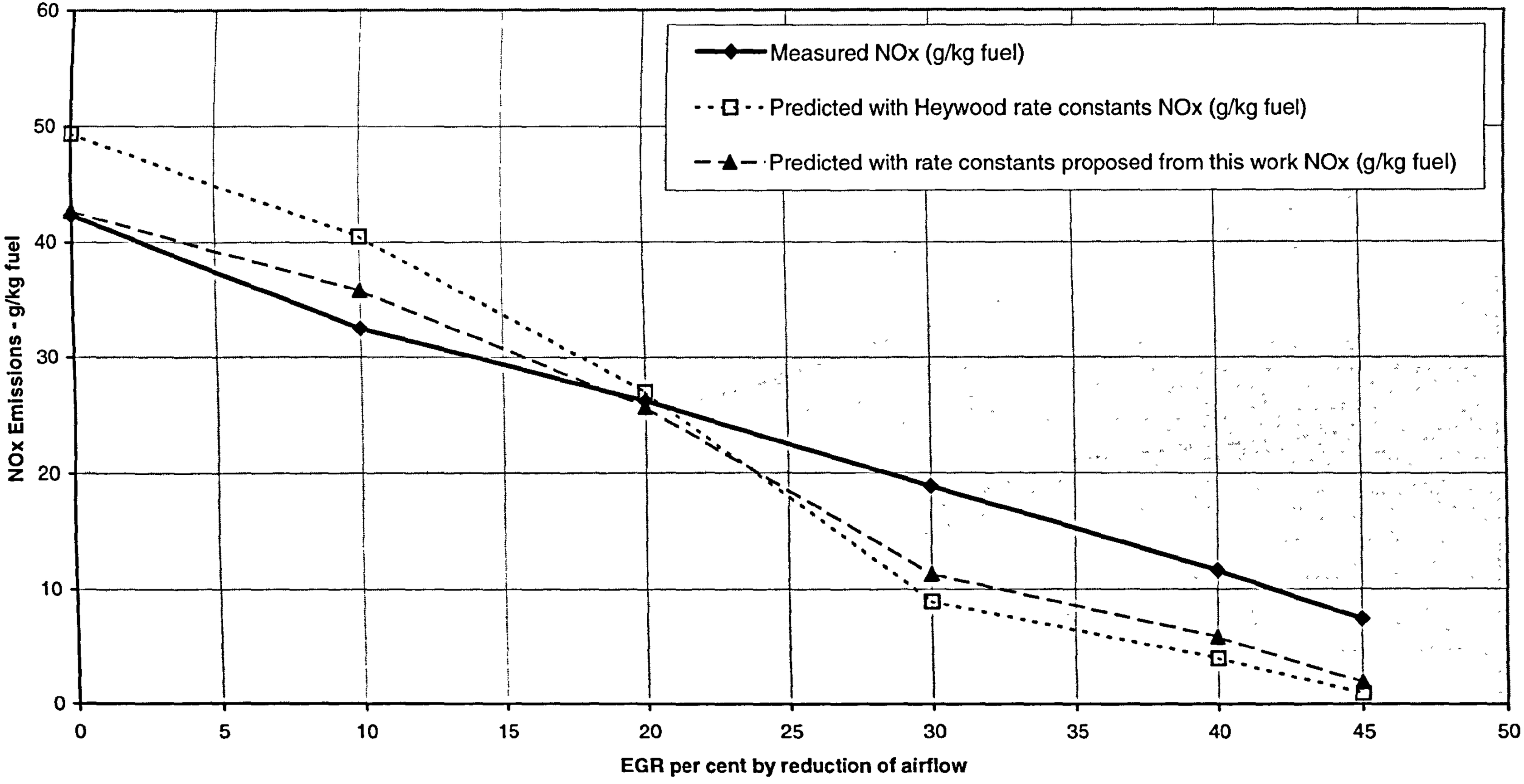

Figure 5.18 Comparison of experimental results and predicted NOx emissions using proposed rate constants, versus EGR per cent at 2700 rpm 8.0 bar BMEP

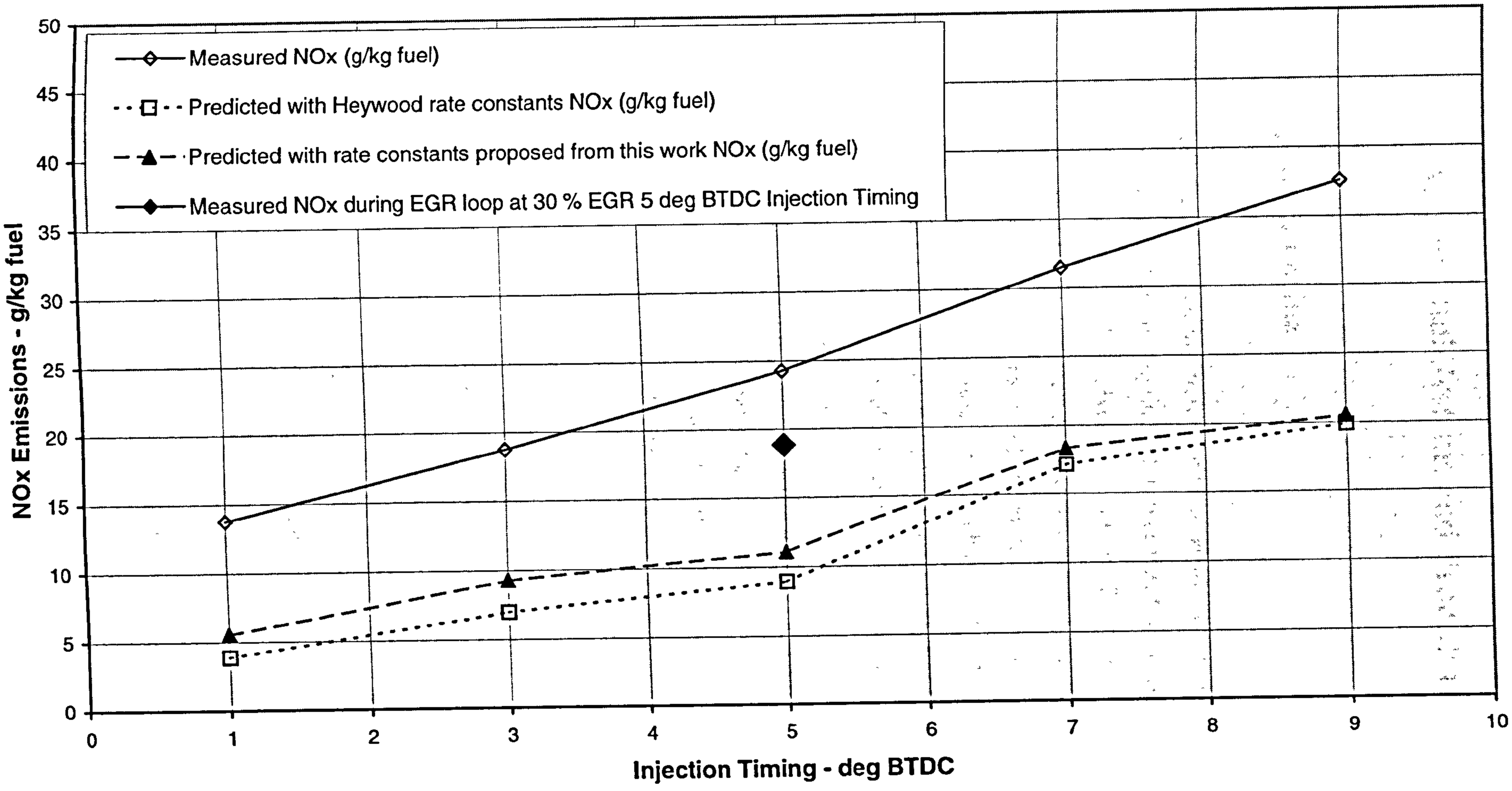

Figure 5.19 Comparison of experimental results and predicted NOx emissions using Heywood and proposed rate constants, versus injection timing at 2700 rpm 8.0 bar BMEP

Chapter 6

Experimental Systems and Procedures

6.1 Description of Engine

The engine used for the experimentation was a Ford "Lynx Upgrade" advanced prototype 16-valve inline 1.8 litre 4 cylinder turbo-charged high speed DI diesel. The aluminium cylinder head featured 4-valves per cylinder, 2 intake and 2 exhaust and a central vertical Bosch 17 mm diameter 2-spring injector. Separate intake ports, one helical and one directed were cast in the head to provide the in-cylinder swirl to support air-fuel mixing and combustion. The re-entrant combustion bowl was centrally located in the piston crown. Fuel was injected through 6 hole nozzles by a Bosch electronically controlled high-pressure rotary VP30 fuel injection pump. Exhaust gas flowed through the 2 valves to a Siamese exhaust port. A Garrett GT15 turbocharger was attached to a compact exhaust manifold for the standard configuration. For the "additional" EGR experimentation a Garrett GT17V variable nozzle turbine turbocharger was used. A single overhead camshaft, driven by a timing belt from the crankshaft, operated pairs of intake and exhaust valves via master and slave rockers; each rocker contacted its valve with a hydraulic tappet. The master rocker had a roller to follow the cam lobe to minimise friction.

The grey iron cylinder block was from the production 1.8 litre 4 cylinder diesel used in the Fiesta, Escort and Mondeo cars, having the same cylinder bore diameter of 82.5 mm, and cylinder bore and head bolt spacing, as the current production 1.8. The crankshaft was forged steel with a carry-over throw of 41 mm and had the same bearing journal diameters as the current 1.8 litre diesel. Mahle pistons were used with modified "wedged" small end, current production con-rods.

The general dimensions and specification for this engine are shown in **Table 6.1** and a power curve is shown in **Figure 6.1.**

Table 6.1 Lynx Upgrade General Dimensions and Specification

Configuration / no. of cylinders	Inline 4
Bore - mm	82.5
Stroke - mm	82.0
Cubic capacity - cc	1753
Con-rod length – mm	130.0
L/R ratio	3.17
Rated Power - kW	74
Rated speed - rpm	4500
Mean piston speed at max power - m/s	12.3
Max torque - Nm	225
Max torque speed	2000
Firing order	1,3,4,2
Compression ratio	19:1
Peak cylinder pressure - bar	135
Valve-train	SOHC & rockers, 4-valves/cyl
Intake valve diameter – mm	27.7 (2)
Exhaust valve diameter – mm	25.0 (2)
Intake valve opens - deg BTDC	9
Intake valve closes - deg ABDC	37
Exhaust valve opens - deg BBDC	49
Exhaust valve closes - deg ATDC	9

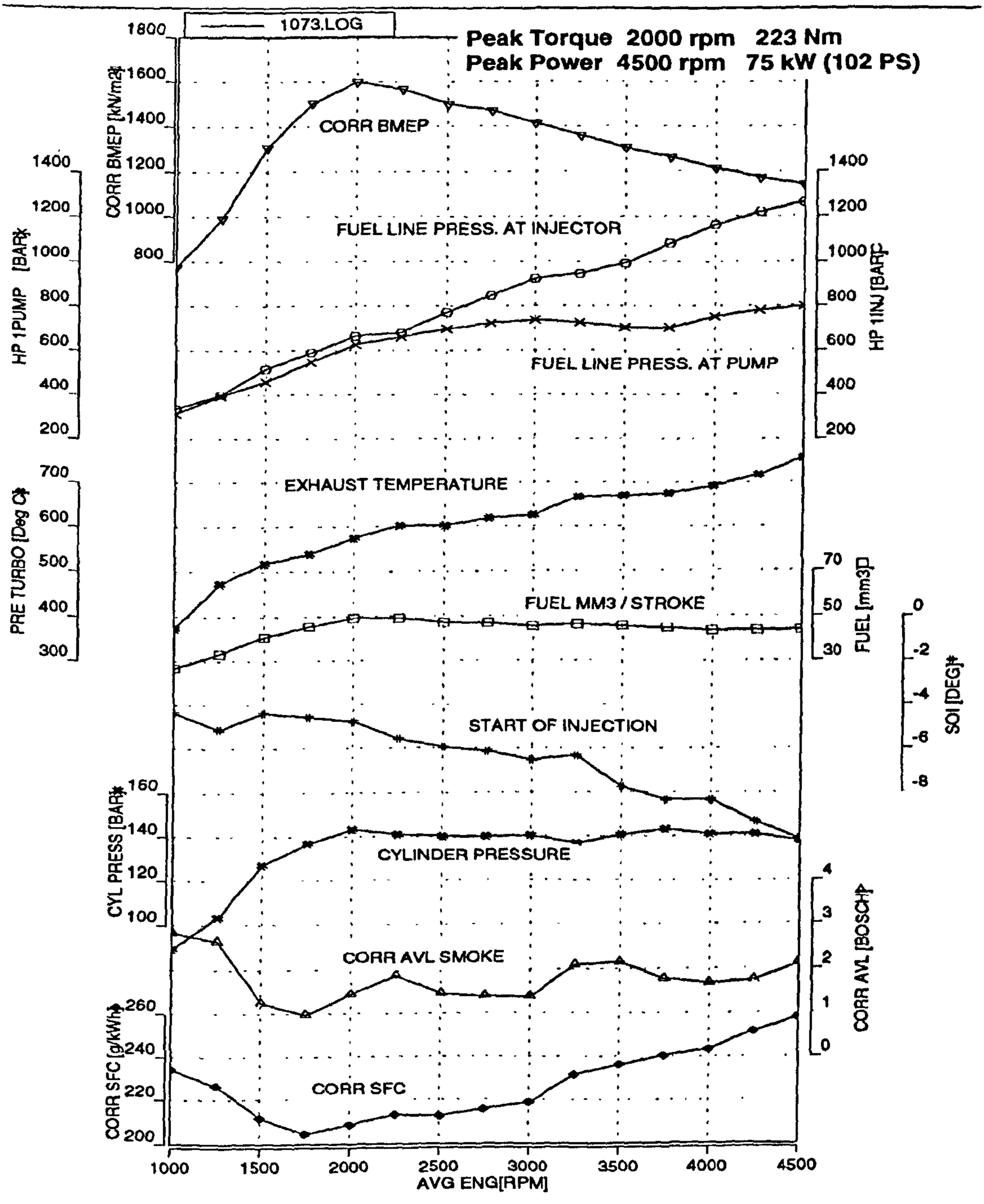

Figure 6.1 Power curve for "Lynx Upgrade" advanced prototype 16-valve inline 1.8 litre 4 cylinder turbo-charged inter-cooled high speed DI diesel

6.2 Description of Engine Intake, Exhaust and EGR Systems

Air was draw through the rotary airflow meter and then through a filter before entering the turbocharger compressor. The outlet of the compressor was connected to a Bowman water to air heat exchanger for inter-cooling. The charge air then entered the engine throttle body and passed into the plenum of the intake manifold.

The exhaust gas from the cylinder head ports entered a compact cast iron manifold and flowed into the turbocharger turbine. The turbine housing and manifold were integrated in one casting. The standard Lynx Upgrade engine had a fixed geometry Garrett GT15 turbocharger.

The standard EGR system comprised of a vacuum operated EGR valve that was attached to the rear end of the exhaust manifold. The outlet side of the valve was bolted directly to the cooler, which took the gas across the back of the engine to the intake side. From the outlet of the cooler, a thin walled stainless steel EGR pipe connected the re-circulated exhaust gas to the throttle body, where it mixed with the charge air from the inter-cooler. The throttle, upstream of the EGR entry, was also vacuum operated and restricted the charge airflow when necessary to assist EGR flow into the intake manifold plenum. **Table 6.2** gives the supplier and description of the EGR system components.

Table 6.2 EGR System Components

Component	Supplier	Description
EGR Valve	Pierburg	Vacuum operated poppet valve, 24 mm diameter, cast iron body
Cooler	Serck	Stainless steel tube and plate cooler, 37 tubes 6.35 diameter by 156 mm long.
Throttle Valve	Pierburg	"Butterfly" type swivelling throttle valve, 52mm diameter, aluminium body

For the "additional" EGR experiments a Garrett GT17V variable nozzle turbine (VNT) turbocharger was fitted to the engine. This was accomplished by sawing off the turbine housing from a spare manifold, and attaching a flange suitable for the VNT unit. Compressed air was used to operate the pneumatic motor to move the turbine vanes. A diagram of a variable nozzle turbine turbocharger is shown in **Figure 6.4**. This shows the operation and movement of the vanes, and illustrates how the nozzle area is changed from the open to closed positions. During the early "additional" EGR testing, two sizes of venturi were used in place of the throttle body for the introduction of EGR into the charge air stream; these are shown in **Figures 6.2 and 6.3**. **Figure 6.5** shows photographs of a venturi and the EGR connection pipe.

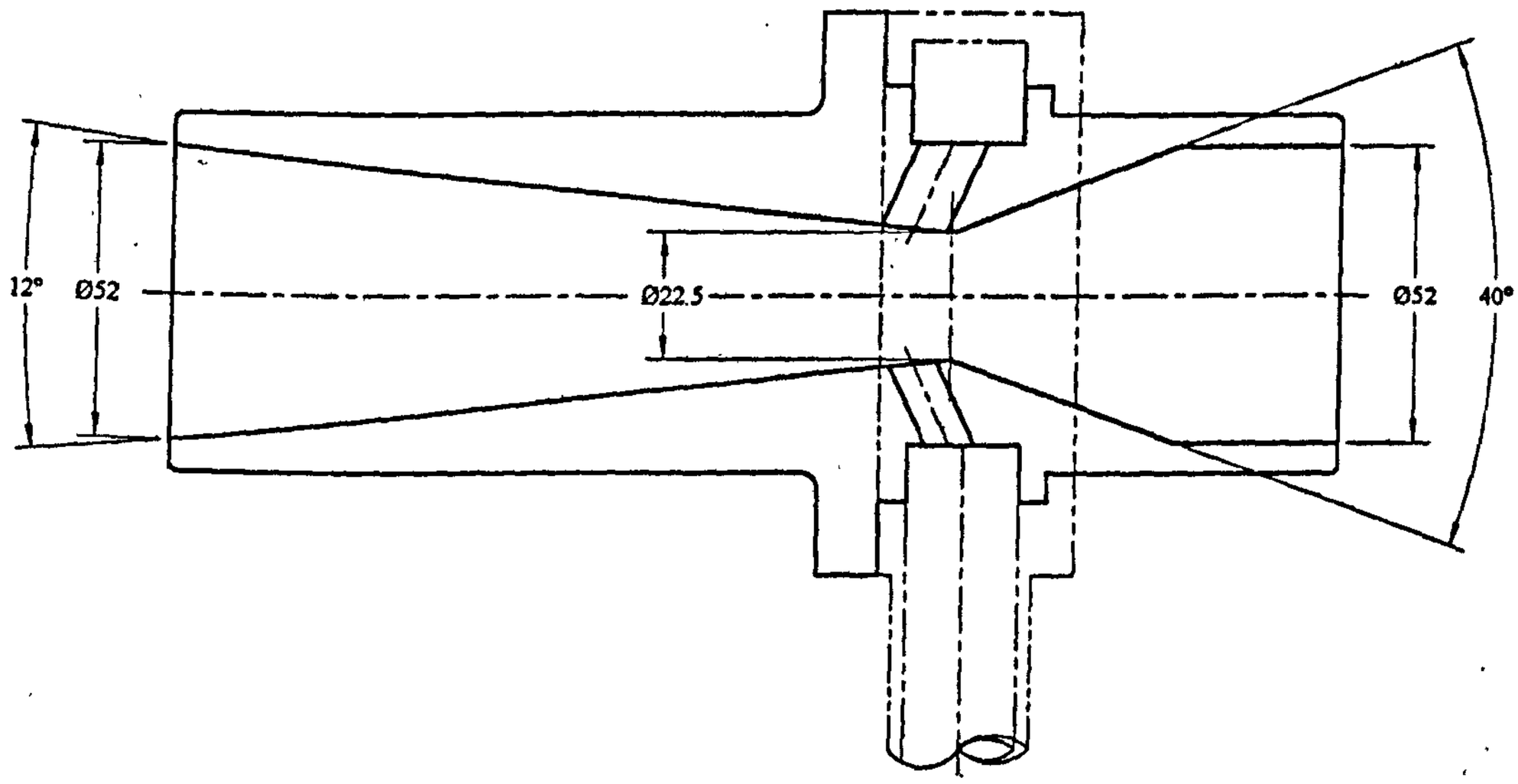

Figure 6.2 Diagram of venturi 1 with throat diameter of 22.5 mm

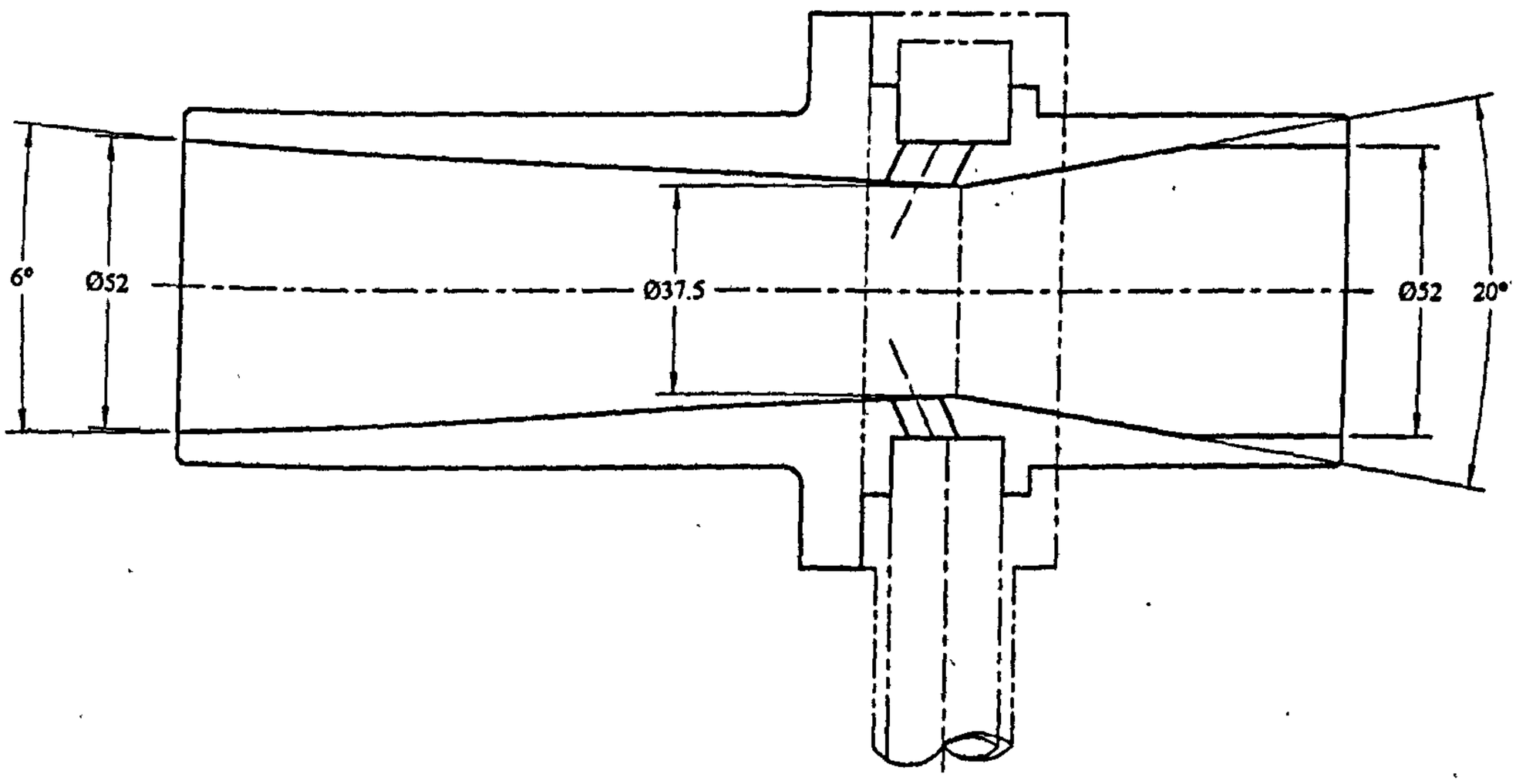

Figure 6.3 Diagram of venturi 2 with throat diameter of 37.5 mm

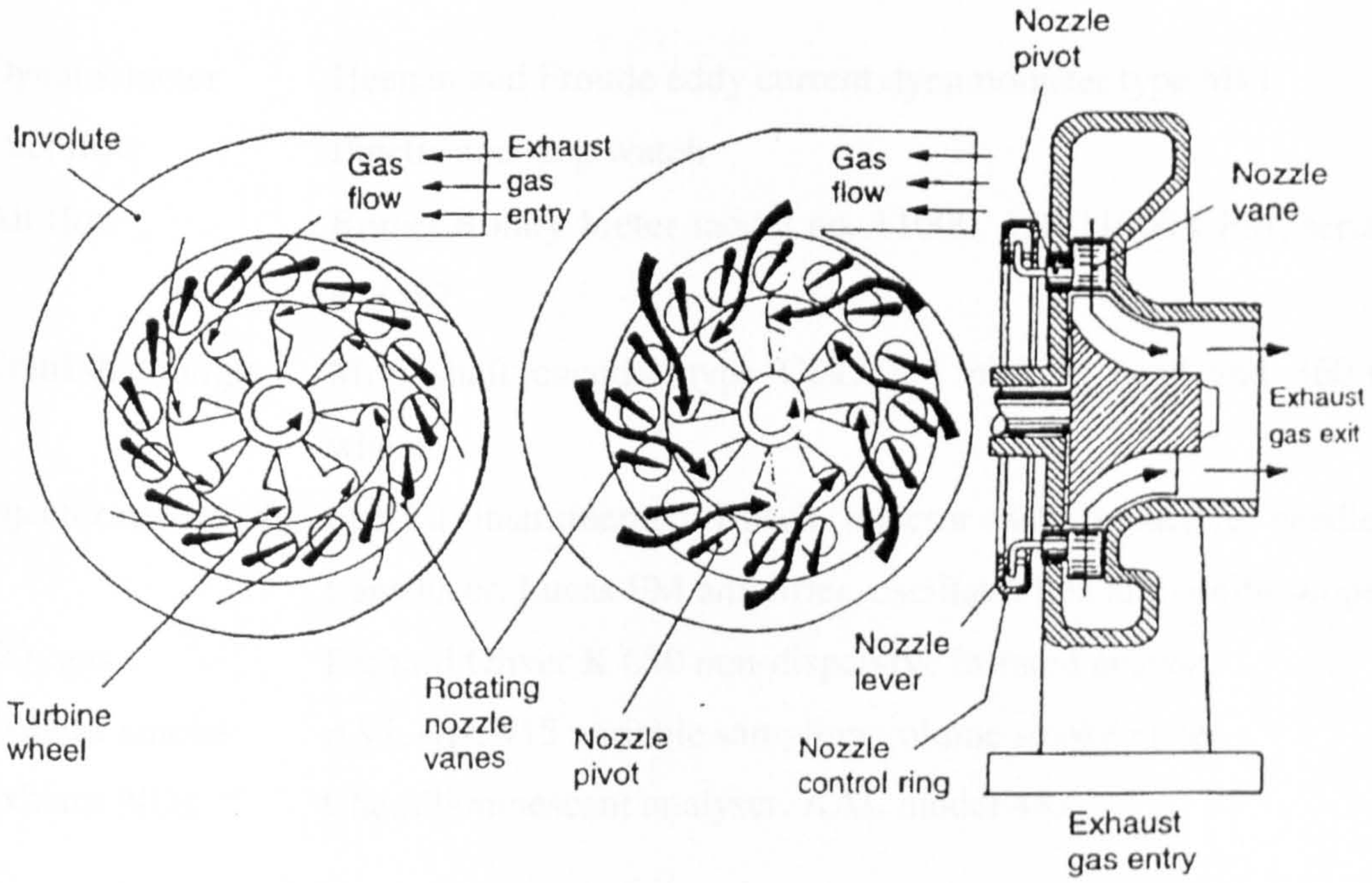

Variable nozzle geometry turbocharger

Figure 6.4 Diagram of a variable nozzle turbine turbocharger

(Heisler, 1997 Fig 6.68 p 342)

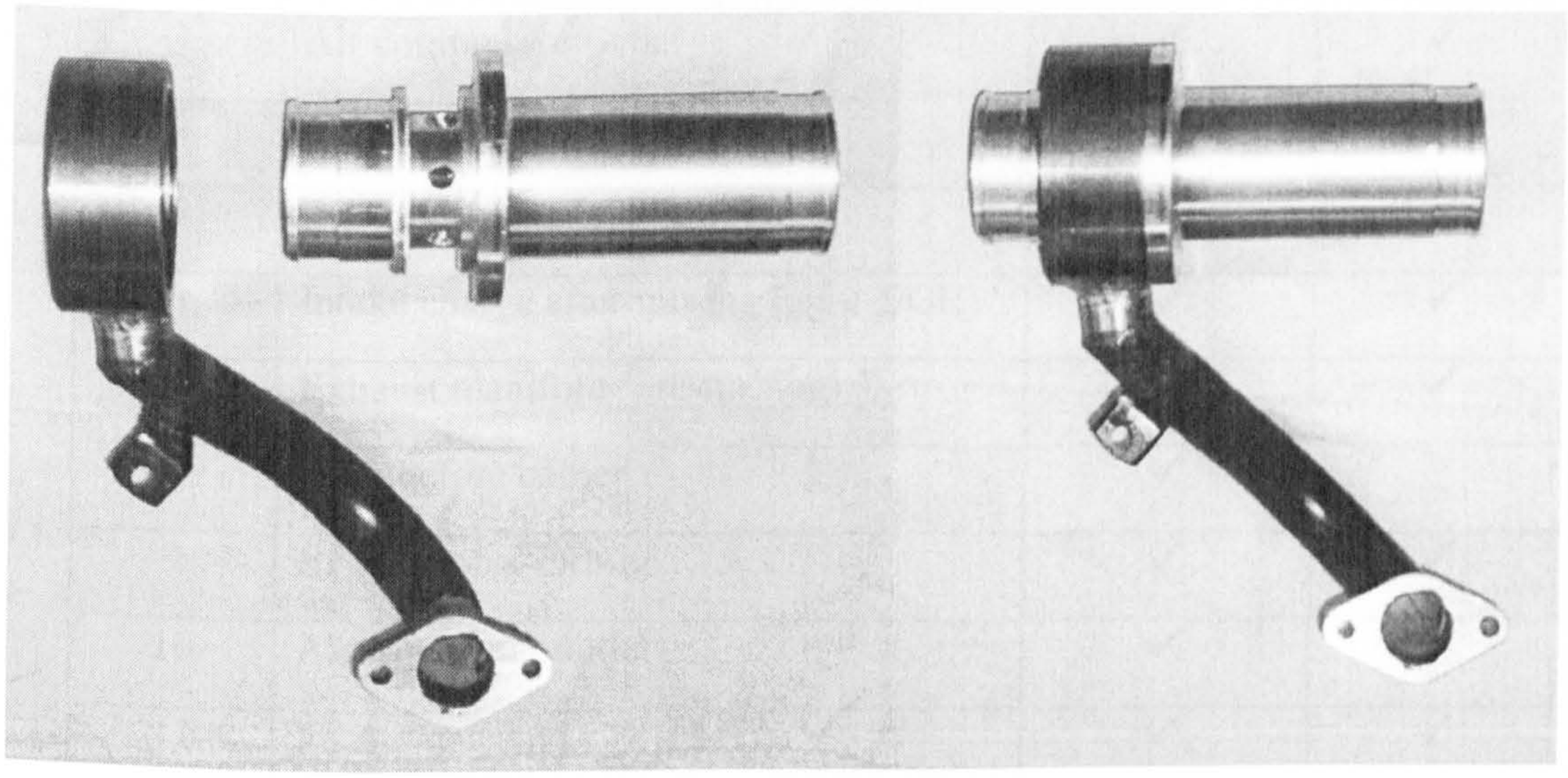

Figure 6.5 Photographs of a venturi, showing EGR tube connection.

6.3 Instrumentation

Dynamometer	Heenan and Froude eddy current dynamometer type Mk1
Fuel flow	Pipette and stop watch
Air flow	Romet Rotary Meter model no. 11000, 550-11000 CFM, serial no. 873487
Crankshaft angle	Mini shaft encoder type GEL 244 pick-up head and 360-tooth wheel
Injector needle lift	Special instrumented Bosch injector with inductive needle lift transducer, Lucas FM amplifier, oscillator box and oscilloscope
CO_2 gas	Richard Oliver K 650 non-dispersive infrared analyser
Exhaust smoke	AVL type 415 variable sampling volume smoke meter
Exhaust NOx	Chemiluminescent analyser, AAL model 443

Table 6.3 Temperature and Pressure Instrumentation

Location No.	Location	Temperature	Pressure
1	Air filter inlet	✓	✓
2	Air filter outlet	✓	✓
3	Air compressor outlet	✓	✓
4	Air intercooler outlet	✓	✓
5	EGR cooler outlet	✓	✓
6	Intake charge after mixing (air + EGR)	✓	✓
7	Exhaust manifold (pre-turbine)	✓	✓
8	EGR before cooler	✓	–
9	Exhaust post-turbine	✓	✓
10	Airflow meter outlet	✓	✓
11	Intake manifold	✓	✓
12	Cooling water outlet	✓	–
13	Fuel at measuring pipette	✓	–
14	In-cylinder (pressure) at glow plug	–	✓

Temperature and pressure measurements around the engine are listed in **Table 6.3** and the locations are shown in **Figure 6.7.**

The thermocouples used were of the "K" type. Cylinder pressure was measured with a Kistler type 6055B80 minature piezoelectric transducer, which was installed in a special glow plug adaptor.

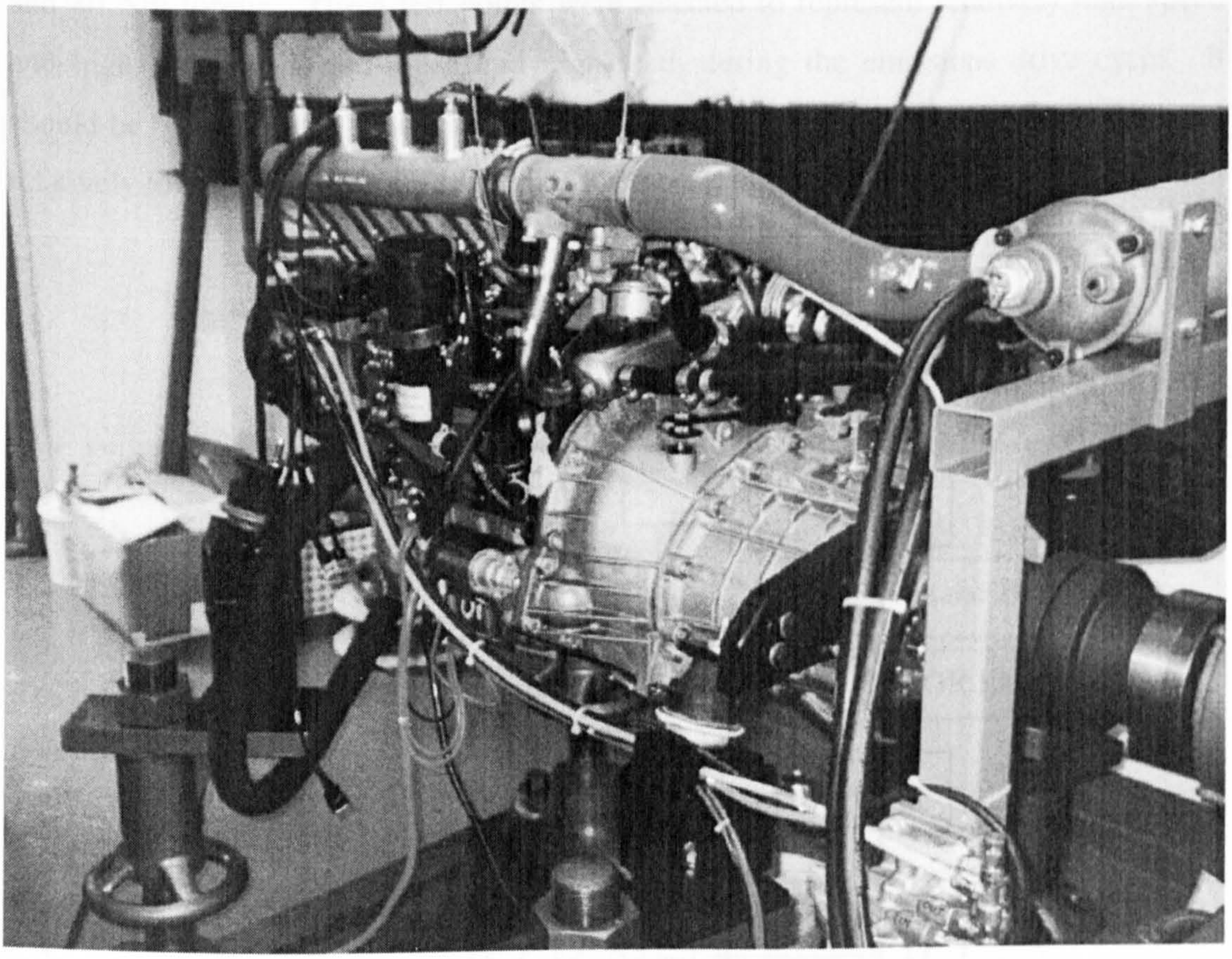

Figure 6.6 Photograph of the engine installation in the test cell.

6.4 Experimental Procedure

Figure 6.6 is a photograph of the engine set-up in the dynamometer test cell for the experimentation. This shows the intake side of the engine. The charge air pipe from the Bowman heat exchanger can be clearly seen connected to the standard throttle body. The EGR tube from the EGR cooler can be seen connecting to the underside of the

throttle body. The intake manifold with the instrumentation tappings sticking up from the plenum is also clearly visible.

For the experimental phase of the work two modes were chosen from the 14-mode steady-state emissions mapping points used at Ford to simulate the European driving cycle for the 1.8 litre 'Lynx' DI diesel Focus. The engine conditions chosen are shown in **Table 6.4**, and these were 2700 rpm speed and 111.7 Nm torque, and 1900 rpm speed and 80 Nm torque. These test points were selected to represent relatively high speed and high load and a mid-speed and high load, during the emissions drive cycle. It should be noted that the speeds and loads experienced during the vehicle drive cycle are relatively low compared to the rated speed and peak torque of the engine.

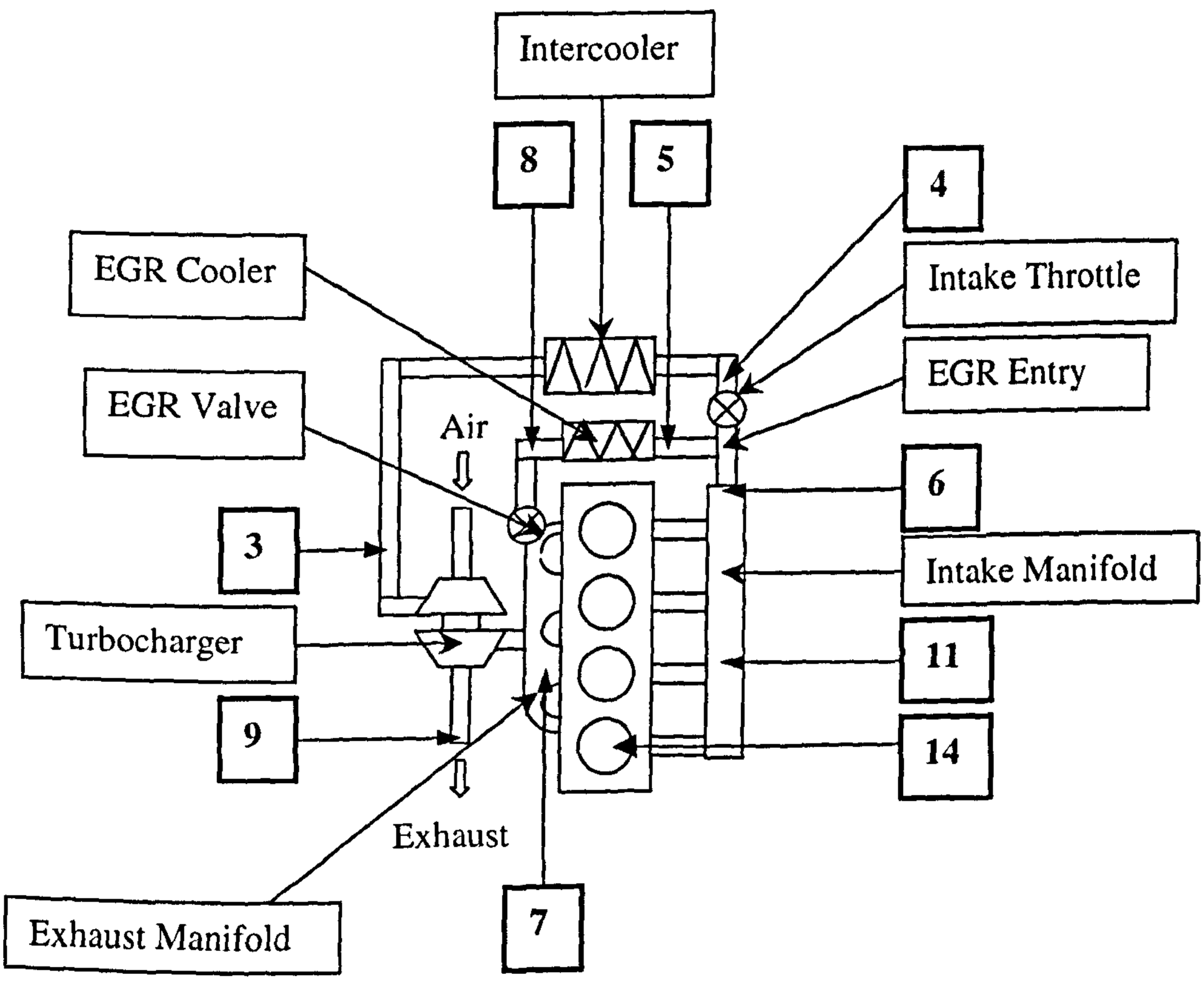

Figure 6.7 Schematic diagram of engine, showing instrumentation locations.

Table 6.4 Engine Test Conditions

Test Condition No.	Speed rpm	Torque Nm	BMEP bar	Injection Timing
1	2700	111.7	8.0	5deg BTDC
2	1900	81	5.8	4deg ATDC

The experiments were started at the 2700 rpm speed and 111.7 Nm torque, 8 bar BMEP; engine test condition 1. Testing was concluded in five stages.

1. A variable geometry turbocharger was installed on the engine to replace the original fixed geometry unit. EGR was introduced at the standard throttle body, as the original engine set-up.
2. A venturi (1) with a throat diameter of 22.5 mm was installed in place of the original throttle body unit, to introduce EGR to the charge air stream.
3. An alternative second venturi (2) of throat diameter 37.5 mm was tested.
4. The original throttle body was refitted to introduce EGR, without use of the throttle. This was a repeat of the first test above.
5. A number of tests were carried with the same engine build, at the test condition 2 (1900 rpm, 81 Nm).

At each of the test conditions, for each engine build configuration described above, EGR loops were run, by progressively opening the EGR valve from closed to fully open, each loop was run with the VNT turbine vanes in the fully open, mid-position and fully closed.

As discussed in more detail in chapter 7, following all the tests at the first test condition, it was concluded from the results that venturi 1 and 2 did not offer any advantage over the simple EGR entry point from the original engine configuration, although the throttle was not required. For this reason the second mode was tested with the throttle body installed and neither venturi was used for the experiments at the slower speed.

An analysis of the diesel test fuel is shown in **Appendix 2** on page 266.

6.5 Emissions Calculations - NOx and Soot

During the experimentation, readings of NOx and smoke emissions were recorded. This section shows the post processing calculations to convert NOx from ppm to g/h, and Bosch smoke units to soot emissions in g/h. The equations used in this section come from the standard post processing used in the Engine Laboratory at the Ford Dunton Engineering Centre.

The calculated NOx and soot results were normalised according to the procedure given in **Appendix 3** on page 268.

6.5.1 NOx emissions mass flow (g/h):

$$Mass, NOx = \frac{46\times10^{-3}(1+AFR)(Fuel)(NOx)}{EMW} \quad \text{(g/h)} \qquad 6.1$$

Where:

Mass NOx (g/h)

AFR (Ratio)

Fuel (kg/h)

NOx (ppm)

EMW = Exhaust Gas Molecular Weight

$$EMW = 34.67 - \frac{83.33}{AFR} \qquad 6.2$$

(Note: If AFR > 14.7 then *EMW* = 29.0)

6.5.2 Soot emissions (g/h) from Bosch smoke measurements:

$$Soot = 982(Smoke)\left(10^{(0.1272(Smoke)-1.66)}\right) \quad \text{(g/m}^3\text{)} \qquad 6.3$$

$$Soot = \left(\frac{GAH \times Soot}{1204.2} \right) \quad \text{(g/h)} \qquad 6.4$$

Where:

Soot = Soot emissions (g/h)

Smoke = Measured Smoke (Bosch)

GAH = Total Mass Flow (Air + Fuel) (kg/h)

6.6 EGR Flow Calculations

6.6.1 Mass flow rate of EGR

Treating the intake charge and EGR gases as *perfect gases*, the characteristic equation of state may be used, whereby;

$$pV = mRT$$

and $$pV = \frac{m}{M_{wt}} R_o T$$

where R_o is the Universal Gas Constant, 8.3144 kJ/kmol K and M_{wt} is the molar mass.

$$\frac{V}{m} = \frac{R_o}{M_{wt}} \frac{T}{p}$$

Intake Charge Stream

Sp volume of O_2 in intake charge $= [R_o/M_{wtO2}] \cdot [T_{ic}/P_{ic}]$ (m^3/kg)

Sp volume of N_2 in intake charge $= [R_o/M_{wtN2}] \cdot [T_{ic}/P_{ic}]$ (m^3/kg)

Sp volume of CO_2 in intake charge $= [R_o/M_{wtCO2}] \cdot [T_{ic}/P_{ic}]$ (m^3/kg)

Sp mass of O_2 in intake charge $= [\text{Int charge } O_2 \text{ vol frac}]/[R_o/M_{wtO2}][T_{ic}/P_{ic}]$ (kg/m^3)

Sp mass of N_2 in intake charge $= [\text{Int charge } N_2 \text{ vol frac}]/[R_o/M_{wtN2}][T_{ic}/P_{ic}]$ (kg/m^3)

Sp mass of CO_2 in intake charge $= [\text{Int charge } CO_2 \text{ vol frac}]/[R_o/M_{wtCO2}][T_{ic}/P_{ic}]$(kg/$m^3$)

Where subscript "ic" refers to "intake charge"

Total specific mass of intake charge

$= \sum$ {Specific mass of O_2, N_2, CO_2 in intake charge}

Mass fraction of O_2 in intake charge

= Specific mass of O_2 in intake charge / Total specific mass of intake charge

Mass fraction of N_2 in intake charge

= Specific mass of N_2 in intake charge / Total specific mass of intake charge

Mass fraction of CO_2 in intake charge

= Specific mass of CO_2 in intake charge / Total spec mass of intake charge

EGR Stream

Sp volume of O_2 in EGR stream = $[R_o/M_{wtO2}] \cdot [T_{EGR}/P_{EGR}]$ (m^3/kg)

Sp volume of N_2 in EGR stream = $[R_o/M_{wtN2}] \cdot [T_{EGR}/P_{EGR}]$ (m^3/kg)

Sp volume of CO_2 in EGR stream = $[R_o/M_{wtCO2}] \cdot [T_{EGR}/P_{EGR}]$ (m^3/kg)

Sp mass of O_2 in EGR stream = [Int charge O_2 vol fract]/$[R_o/M_{wtO2}][T_{EGR}/P_{EGR}]$ (kg/m^3)

Sp mass of N_2 in EGR stream = [Int charge N_2 vol fract]/$[R_o/M_{wtN2}][T_{EGR}/P_{EGR}]$ (kg/m^3)

Sp mass of CO_2 in EGR stream = [Int charge CO_2 vol fract]/$[R_o/M_{wtCO2}][T_{EGR}/P_{EGR}]$ (kg/m^3)

Total specific mass of EGR stream = $\sum$ {Specific mass of O_2, N_2, CO_2 in EGR stream}

Mass fraction of O_2 in EGR stream

= Specific mass of O_2 in EGR stream / Total specific mass of EGR stream

Mass fraction of N_2 in EGR stream

= Specific mass of N_2 in EGR stream / Total specific mass of EGR stream

Mass fraction of CO_2 in EGR stream

= Specific mass of CO_2 in EGR stream / Total spec mass of EGR stream

Taking a CO_2 Mass Balance

$(M_{air\ flow} + M_{EGR})\ (CO_2\ mass\ fraction_{\ int\ chg}) = (M_{EGR})(CO_2\ mass\ fraction_{\ EGR})$

$M_{EGR} = M_{air\ flow} / \{ [(CO_2\ mass\ frac_{\ EGR}) - (CO_2\ mass\ frac_{\ int\ chg})] / [CO_2\ mass\ frac_{\ int\ chg}] \}$

6.6.2 EGR mass flow based on mass balance of CO_2:

$$M_{EGR} = \{M_{air\ flow}\ (CO_2 mass\ frac_{int\ chg})\} / \{(CO_2 mass\ frac_{EGR}) - (CO_2 mass\ frac_{int\ chg})\}$$

6.6.3 EGR proportion based on volumetric fraction of CO_2 in intake manifold and exhaust:

$$EGR(\%) = \frac{CO_2(inlet \sim manifold) - CO_2(ambient)}{CO_2(exhaust)} x100$$

6.6.4 EGR proportion based on reduction in air flow:

$$EGR(\%) = \frac{M_{\ withoutEGR} - M_{\ withEGR}}{M_{\ withoutEGR}} x100$$

From the experimental readings, EGR per cent was calculated using the above three methods for a range of test conditions. Comparisons of the three calculation methods are shown in **Figures 7.30 to 7.35** and a discussion of the results is made in **Section 7.3,** in **Chapter 7.**

Chapter 7

Experiments with "Additional" EGR

7.1 "Additional" EGR Systems

The conventional EGR systems that are in wide use today on automotive diesel engines, re-circulate exhaust gases into the intake charge in place of fresh air. The intake airflow thus reduces as the level of EGR increases. This is known as "substitutional" or "replacement" EGR and results in dilution of oxygen from the intake charge. The air/fuel ratio thus reduces, for the same engine speed and load, as the level of EGR is increased. These give rise to the classic NOx/particulates trade-off, over an EGR loop, where EGR is increased at constant engine speed and load conditions. The particulate characteristic response is for a gradual increase as the air/fuel ratio reduces until around 20:1, where there is a sudden dramatic increase in particulate emissions, owing to the lack of oxygen. The actual air-fuel ratio where this rapid increase in particulate emissions occurs, as the EGR is increased, will depend on the combustion and fuel injection systems. Modern 4-valve central vertical injector designs with high pressure injection systems will burn cleanly down to lower air-fuel ratios than older 2-valve designs with angled injectors, because of better fuel distribution around the combustion chamber and therefore better air-fuel mixing.

"Additional" EGR is a concept, as the name implies, where EGR is added to the intake charge on top of the normal airflow. Thus the total flow into the engine is increased with the re-circulated exhaust gas. This can only be achieved by the use of a variable geometry turbocharger, so that boost pressure and pre-turbine exhaust pressure, in other words the pressure drop across the engine, can be modulated by the turbine vane position.

The work carried out at the TNO Road-Vehicles Research Institute, reported by Baert et al (1996, 1999), was focused on reducing heavy-duty diesel NOx emissions. Since heavy-duty engines operate predominantly at full load or near full load, and the ECE

R49 13-mode emissions cycle is dominated by peak torque and maximum power conditions, the engineers at TNO studied the potential of EGR to reduce NOx formation at full load. They came to the position that to reduce NOx by EGR at high load conditions, with a low air/fuel ratio, the EGR system had to enable "additional" rather than "replacement" EGR to be used, to avoid an increase in particulate emissions. When applying "additional" EGR at full load, the original air mass flow through the engine has to be maintained at its baseline level, in order to maintain the same air-fuel ratio and hence particulates level. This can pose a problem under full load conditions, since the mean exhaust manifold pressure can be lower than the intake manifold pressure. This was overcome by the use of a venturi to locally reduce the intake system pressure at the EGR entry point. In order to flow the added mass of the original air mass flow and "additional" EGR into the engine charge, the turbine flow area has to be reduced to increase the boost pressure, which has the effect of increasing re-turbine pressure, but at a faster rate. As soon as the pre-turbine pressure exceeds the pressure at the venturi throat, EGR flows into the intake system. The downside to this is that as the turbine flow area is reduced, the turbine efficiency drops off.

The TNO researchers found that, not surprisingly, the simplest system of a VGT turbocharger only, without a venturi or backpressure valve, offered the least resistance to flows, provided the highest airflow and lowest BSFC and particulates for a given NOx emission. However, this simple system could not achieve the highest EGR level at maximum power conditions, where a venturi enabled 15 per cent EGR and the best trade-off between NOx and BSFC.

As far as the author is aware, there is no published work on the application of "additional" EGR to a small high-speed automotive diesel engine.

7.2 "Additional" EGR System Layout

As already stated, a variable geometry turbocharger is necessary for this EGR system, in order that boost and pre-turbine pressures can be varied at any given engine condition. The Garrett GT15 fixed geometry turbocharger was therefore replaced with a GT17V swivelling turbine nozzle guide vane type, variable geometry turbocharger. The vane

angle was adjusted by modulating external air pressure, acting on a linear diaphragm type motor.

Following the work at TNO on a heavy-duty diesel engine, it was anticipated that a venturi would be required to assist in the "additional" flow of EGR in order to minimise the increase in pre-turbine pressure and to provide the best boost pressure recovery after mixing. Two venturis were designed, one with a throat diameter of 22.5 mm and one with a larger throat diameter of 37.5 mm. These were designed to be the same length as the standard throttle body unit used for the Lynx Upgrade engine, such that they could be inter-changed without significant modification of the total intake system. A diagram of the system is shown below in **Figure 7.1**.

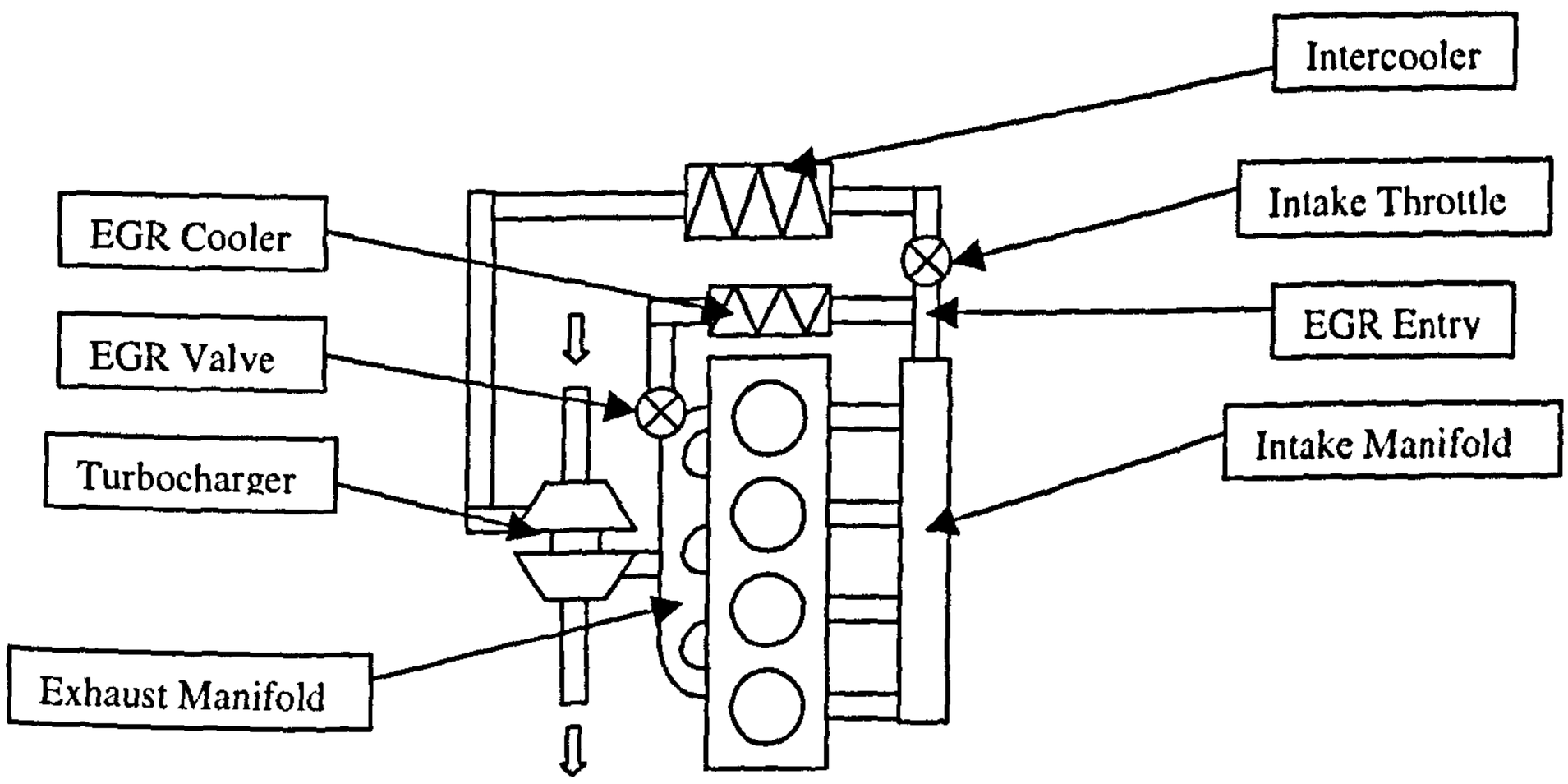

Figure 7.1 Schematic diagram of engine intake, exhaust and EGR systems.

7.3 Experimental Results

The Lynx Upgrade 1.8 litre 16-valve DI diesel engine was operated at two test conditions, at a speed of 2700rpm at 8.0bar BMEP a torque of 111.7Nm and 1900rpm at 5.8bar BMEP a torque of 81Nm. A number of EGR loops were run, each at a fixed turbine vane position, ranging from fully open to fully closed. Applying air pressure to the linear actuator operated the turbine vanes. A pressure of 30, 35 and 40 psi, acting on the linear motor, corresponded to the vanes being fully open, at mid-position and fully

closed. EGR flow was increased by progressively opening the EGR valve from shut to fully open.

EGR loops are shown in **Figures 7.2, 7.3 and 7.4**, for the 2700rpm at 8.0 bar BMEP (111.7Nm torque) operating condition, with the variable nozzle turbine vanes in the fully open, mid-position and fully closed positions, respectively. The data plotted covers the two sizes of venturi, the EGR tube connected to the standard throttle body, which forms a "T" joint with the charge air duct (but without use of the throttle) and the results with the original system using a fixed geometry turbocharger and EGR throttle as the engine was supplied from Ford.

With the turbine vanes fully open, as can be seen from **Figure 7.2**, all the modified systems gave a better NOx/particulates trade-off, getting nearer to the origin, compared to the standard arrangement. The use of a venturi was shown not to be necessary at this engine condition, and in fact, did not provide the best NOx/particulates, or the lowest BSFC. This was achieved without the use of a venturi, simply by fitting the existing EGR tube to the original throttle body. This system provided significant benefits of lower NOx and particulates as well as improved BSFC. The optimum calibration would be without a venturi, with an airflow of 39 g/s, with the EGR valve almost fully open to give an EGR flow of 11 g/s. At this condition the engine emitted 53.5 g/h NOx and 3.8 g/h particulates and gave a specific fuel consumption of 219 g/kWh.

At the mid-vane position, shown in **Figure 7.3**, an improved NOx/particulates trade-off was achieved at lower emissions values, but at this vane setting, the BSFC was worse at the lower NOx values. This indicates that there were higher pumping losses to achieve the desired flow of air and EGR into the engine. At this vane position, the optimum calibration would be with the smaller venturi number 1, an air flow of 44 g/s, with the EGR valve almost fully open, at an EGR flow of 11 g/s, giving 88 g/h NOx, 4.1 g/h particulates at a BSFC of 226 g/kWh.

It is of interest to compare these last two results. At this engine condition of 2700 rpm 8.0 bar BMEP, in moving the turbine vanes from fully open to the mid-position, the airflow increased by 13 per cent, the EGR flow remained the same at 11 g/s, which

meant in percentage terms it fell a small amount from 28 to 25 per cent of the airflow, but the NOx emissions increased by a substantial 65 per cent. Even though the airflow increased, giving a higher air/fuel ratio, particulates increased 8 per cent. The cost of higher turbocharger work was a 3 per cent increased in fuel consumption. Clearly the higher airflow was not required.

At the fully closed vane position, shown in **Figure 7.4**, the turbocharger was creating the highest boost pressure with the highest pre-turbine pressure, in other words it was working hard, which was reflected in the higher BSFC figures compared to the standard fixed geometry set-up. With the vanes fully closed, the turbine efficiency would have been lower than on a standard fixed geometry unit. Under these conditions the venturis did not offer any advantages, except at very high EGR levels. Using the standard EGR connection did offer a superior NOx/particulates trade-off at high EGR levels, but because of the high pumping work, the BSFC was significantly worse.

Overall, the best condition to run the engine at 2700 rpm and 8.0 bar BMEP (111.7 Nm), for the lowest emissions of NOx and particulates and with lowest fuel consumption for this level of NOx, was with the turbine vanes fully open as shown in **Figure 7.2**, without a venturi. The calibration would be as listed above, ie airflow of 39 g/s, with the EGR valve almost fully open, at an EGR flow of 11 g/s, giving 53.5 g/h NOx, 3.8 g/h particulates at a BSFC of 219 g/kWh.

Since there is not a requirement to operate a light-duty automotive engine with EGR under full load conditions to meet the emissions standards, the use of a venturi was not pursued any further in this work. The EGR tube was connected to the standard throttle body, where the exhaust gas was introduced and mixed with the charge air. The throttle was not used with the variable geometry turbocharger.

The Lynx Upgrade engine was operated at an alternative test condition of 1900rpm and 5.8 bar BMEP (81Nm torque). Following the results from the earlier test at 2700rpm and 8bar BMEP, the EGR was connected to the intake system without a venturi. Like the earlier tests, a number of EGR loops were run, each at a fixed turbine vane position, ranging from fully open to fully closed. EGR flow was increased by progressively

opening the EGR valve from shut to fully open.

Figure 7.5 shows the NOx versus particulates and BSFC characteristics during the EGR loops for the turbocharger turbine vane positions of fully open, mid-position and fully closed, at the 1900 rpm/5.8 bar BMEP (81Nm) operating condition. It is immediately apparent from this plot that the use of the VGT turbocharger gave a large benefit for the NOx versus particulates trade-off, as well as superior engine efficiency demonstrated by the lower BSFC, compared to the standard set-up of the fixed geometry turbocharger and conventional EGR system. The fully open to mid-position of the turbine vanes gave the best NOx/particulates trade-off and best efficiency at this engine operating condition.

Figures 7.6 and 7.7 show air/fuel ratio (AFR) and soot versus NOx emissions for the two test conditions. In these figures the characteristic relationship of increasing soot and reducing NOx emissions as air/fuel ratio reduces can be clearly observed. Increasing EGR flow reduced the air fuel ratio in these tests. At the 2700 rpm 8.0 bar BMEP test condition shown in **Figure 7.6**, the reduction in NOx emissions is almost linear with the fall in air/fuel ratio, and the increase in soot emissions becomes very steep with an air/fuel ratio much below 30:1, but with the sensitivity becoming greater as the turbine vanes were closed down. At this operating condition it is clear that the best NOx/soot trade-off was achieved with the turbine vanes in the fully open position. The 1900 rpm 5.6 bar BMEP operating point is shown in **Figure 7.7**, here a similar picture is presented; a very steep reduction in NOx emissions and a dramatic increase in soot as the air/fuel ratio was reduced. Similarly, at this test condition the sensitivity to air/fuel ratio becomes greater as the turbine vanes were closed; an AFR of 25:1 giving a soot level of less than 2 g/h with the vanes fully open, but an AFR of 30:1 being required with the vanes fully closed to achieve the soot level of 2 g/h. This will be due to the increased pumping work required with the vanes fully closed. At this operating condition there was less difference between the vane settings in terms of the best NOx/soot trade-off. It was achieved with the turbine vanes in the fully open position, but there was not a big difference between fully open and the mid-position.

Figures 7.8 and 7.9 show intake charge oxygen volume fraction and soot emissions

versus NOx emissions for the two engine test conditions. The strong relationship between reducing intake charge oxygen volume fraction and reducing NOx emissions is clear to see in both figures. As is the characteristic increase in soot emissions as the oxygen content falls. However, it is interesting to compare the two test conditions. At 2700 rpm the load was greater at 8.0 bar BMEP and so both NOx and particulate emissions were higher. Particulate emissions started to rise significantly when the oxygen content fell to around 18 per cent. Generally, the scatter of results was greater at this engine test condition. At the lower speed of 1900 rpm and light load of 5.6 bar BMEP, there was a close non-linear correlation between intake charge oxygen proportion and NOx emissions, with a nice tight grouping of results at the three vane positions. The particulate turn-up occurred at a lower oxygen content, around 17 per cent, again with a tighter grouping of the results.

The term "additional EGR" is used loosely to infer that EGR flow is in addition to the normal intake charge airflow, as has been discussed earlier. Thus an analysis of the flow into the engine should show that the total charge flow into the cylinders, under conditions where EGR is flowing, is greater than without EGR. **Figures 7.10 to 7.12** illustrate the split of mass flow into the cylinders of the 1.8 litre 16-valve DI diesel, showing air mass flow, EGR mass flow and total mass flow into the cylinders plotted against NOx emissions, for the engine condition of 2700rpm 112Nm with the turbine vanes in the fully open, mid position and fully closed, respectively. Similar plots for the 1900rpm 81Nm engine operating condition are shown in **Figures 7.13 to 7.15**. The flow characteristics shown in these graphs demonstrate similar trends, for each engine operating condition and for each of the turbine settings, of air mass flow reducing as the EGR mass flow increases, giving the characteristic reduction in NOx emissions. Although the total mass flow remained fairly constant until the highest EGR flow levels, it was initially thought that "additional EGR" had not been achieved, since the total mass flow did not increase with the flow of EGR. However, there were two other considerations that needed to be taken into account: firstly, an engine is a "volumetric" machine, in other words it displaces half its cubic capacity per revolution (for a 4-stroke engine), and secondly the introduction of EGR increased the charge temperature, thus reducing its density. To increase the mass flow into the engine the intake charge density would need to be increased, but in practice, as the amount of relatively hot EGR

increases, the total charge temperature increases thus reducing the total charge density. Charge density for the EGR loops at the three vanes settings is plotted in **Figure 7.16** for the 2700rpm 112Nm engine condition and in **Figure 7.17** for 1900rpm 80Nm operating point. These graphs clearly illustrate the reduction in charge density as the NOx emissions are reduced by the introduction of EGR. The plots also effectively demonstrate how the charge density increased as the turbine vanes are closed.

The analysis of the flow into the cylinders was then calculated on a volumetric basis, assuming the specific gas constant for EGR was the same as that for air. **Figures 7.18 to 7.20** illustrate volumetric efficiency based on airflow and airflow plus EGR flow for 2700rpm 112Nm. Similar plots for the 1900rpm 80Nm engine operating condition are shown in **Figures 7.21 to 7.23**. These plots show an exciting characteristic; the total volumetric flow into the engine did increase as EGR was introduced. The peak volumetric efficiency occurred at the lowest NOx emission level, that is, with the maximum flow of EGR. The level of volumetric efficiency depended on the turbine vane setting, the highest level being achieved with the vanes fully closed. Thus the "additional" EGR concept has been realised on a volumetric flow basis. However, this could not be reflected as increased total mass flow rate into the engine because of the reduction in inlet charge density caused by the EGR heating the intake charge.

Graphs of EGR mass flow versus NOx emissions are shown in **Figure 7.24** for 2700rpm 112Nm and in **Figure 7.25** for 1900rpm 81Nm. This is plotted as per cent of air mass flow in **Figures 7.26 and 7.27** for the two engine conditions. These show the level of EGR flow for each of the turbine vane positions. As the earlier graphs have shown, the highest EGR flow was achieved with the vanes fully closed, this of course gave the highest pre-turbine pressure. However, the highest level of EGR did not produce the lowest NOx emissions. The most efficient use of EGR, in other words the lowest level of EGR for a given NOx level, was achieved with the vanes in the fully open position.

Hawley et al (1997, 1999) conducted similar comparisons between fixed and variable nozzle turbochargers on a 1.8 litre 8-valve DI TCI diesel engine, sponsored by Ford Motor Company. They came to the same conclusion that variable geometry turbochargers (VGT) have the potential to enhance EGR flow rates over what can be

achieved with fixed geometry turbochargers (FGT) and then current EGR schedules. But the concept of "additional" EGR was not considered. EGR mass and volumetric flow rates were not reported. Their results confirmed that it was possible to greatly enhance EGR flow rates at light load, which had a high tolerance to nominal air/fuel ratio without compromising the baseline BSFC and smoke.

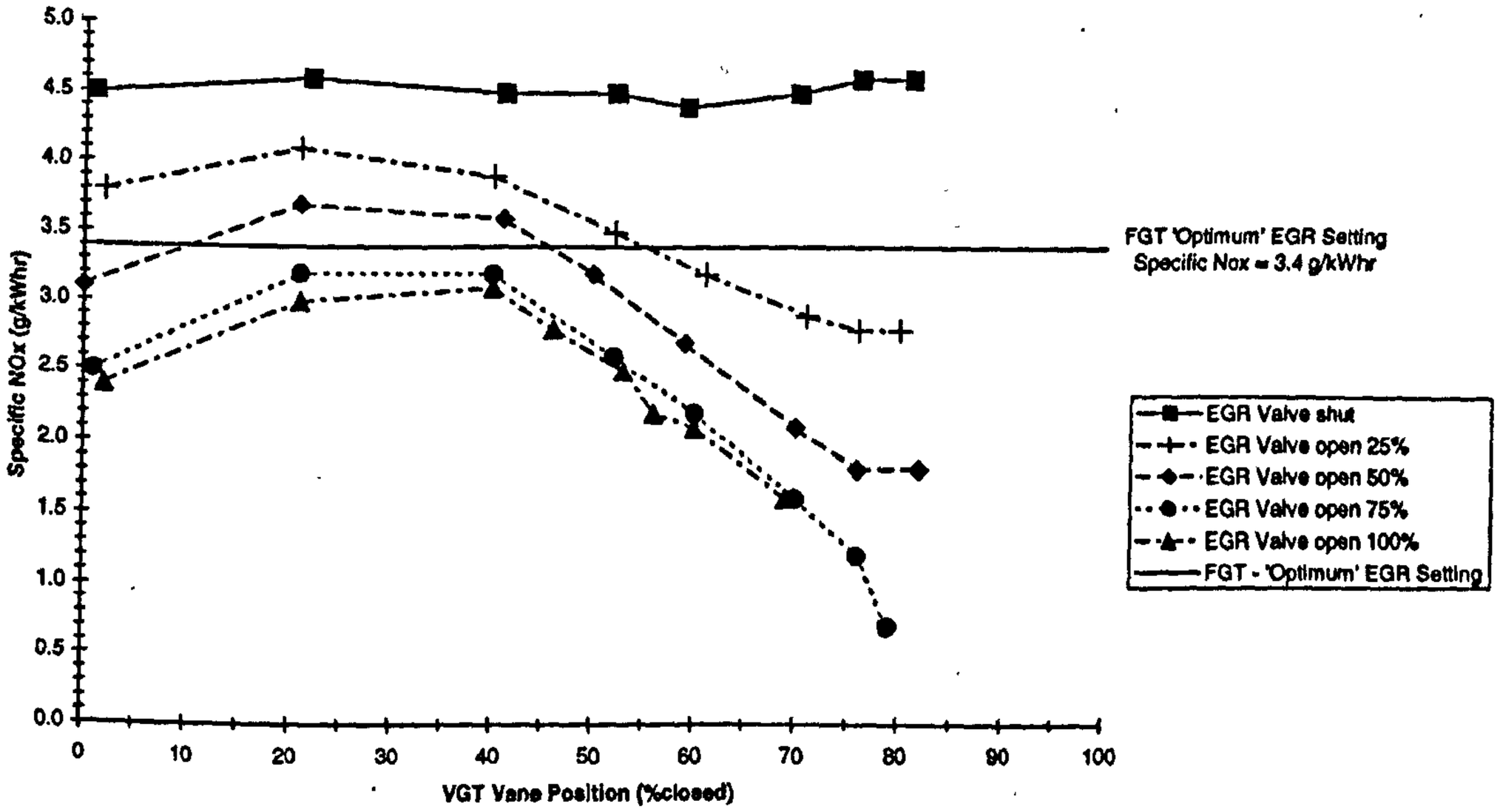

Figure 7.28 Specific NOx versus VGT vane position at 60 per cent rated speed and 56 per cent peak torque (Hawley et al, 1999)

Hawley et al considered 2 operating modes, their Mode 10, which was 60 per cent rated speed and 56 per cent peak torque corresponds very closely with the 2700 rpm 112Nm test point used in this exercise. **Figure 7.28** shows a plot of specific NOx versus VGT vane position for this operating point. Clearly this result is similar to that found in this work, showing at this condition a vane setting nearly fully open with a fully open EGR valve provides a lower NOx emission level. **Figure 7.29** shows an optimisation plot for BSFC and specific NOx, illustrating the best operating quadrant.

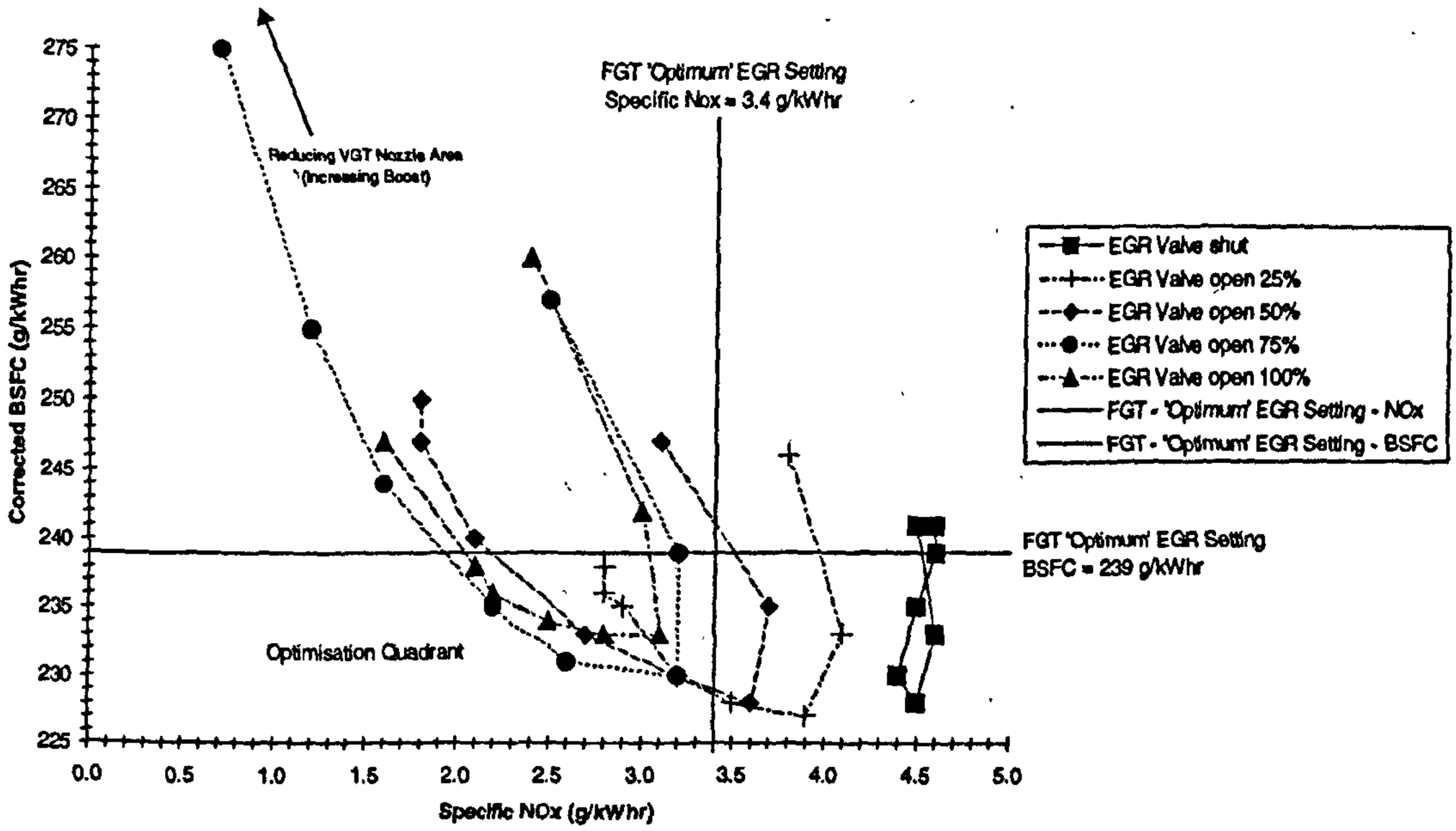

Figure 7.29 Optimisation plot for BSFC and specific NOx at 60 per cent rated speed and 56 per cent peak torque (Hawley et al, 1999)

7.3 Methods of calculating EGR flow

The substance of this chapter, that is the effect of additional EGR on emissions and BSFC, has been dealt within section 7.2 above. Before ending this chapter it would be useful to consider briefly a technical issue of some practical importance. This concerns the different ways in which researchers define and estimate the amount of EGR flow into an engine, both in absolute terms and as per cent of intake charge.

As discussed in the literature survey in **Chapter 2**, there are a number of ways of calculating EGR flow, even though it is usually expressed as per cent. A common practice, owing to its simplicity, is to base it on the reduction in airflow, referenced against the airflow for the same engine condition without EGR. This gives a true measurement on a volumetric basis, at the airflow meter conditions, for naturally aspirated engines. It is not correct for turbocharged engines owing to the reduction in charge airflow as EGR is introduced because of the lower exhaust energy transfer to the turbine. Another common method is based on the ratio of CO_2 measurements taken as ppm, between the intake manifold (allowing for the very low ambient level) and

exhaust. It is not usual to calculate EGR on a mass flow basis because of the additional number of measurements and more complex calculations required, although this is not a major task with modern instrumentation and computers for post-processing.

During this exercise, EGR flow was calculated by the three methods described above, using the equations detailed in Chapter 6. The results are plotted in **Figures 7.30 to 7.32** for the engine condition of 2700rpm/8.0bar BMEP (112Nm) at the three turbine vane settings, respectively. Similar plots for 1900rpm/5.8bar BMEP (81Nm) are shown in **Figures 7.33 to 7.35**. In all cases it can be seen that the calculation using CO_2 ppm readings gave a very close correlation to the true mass calculation. The accuracy of the method using reduction in airflow varied depending on the engine operating condition and the VNT turbine vane setting. This is because, as stated above, the change in airflow will also be affected by the reduction in exhaust flow to the turbine. In addition there is the difference in temperature between the charge air and EGR gas. These factors are illustrated when comparing the results at 2700rpm/8.0bar BMEP in **Figures 7.30 to 7.32**, to those at 1900rpm/5.8bar BMEP in **Figures 7.33 to 7.35.** At the higher speed and load, the difference between the reduction in airflow and EGR mass calculations was large, and got larger as the turbine vane setting was closed. This is because the reduction in airflow was considerably higher, owing to the lower efficiency of the turbocharger as the vanes were closed, than the increase in EGR mass flow, since the exhaust gas got considerably hotter as the vanes were closed. These effects were less at the lower speed and lighter load condition.

7.4 Conclusions

- At the two part-load engine conditions tested, 1900rpm/5.8bar BMEP and 2700rpm/8.0bar BMEP, the use of a variable geometry turbocharger and a modern EGR system with an EGR cooler, gave lower NOx and particulate emissions at an improved level of fuel consumption, compared to a traditional fixed geometry turbocharger and similar EGR system with an intake throttle.

- The use of a venturi to assist the flow of EGR into the charge air was found to be less efficient than a simple EGR entry, for these part load engine-operating conditions.

- "Additional" EGR did occur, in that the total volumetric flow into the engine did increase with the flow of EGR.

- The highest EGR mass flow, achieved by closing the turbine vanes, was not the most efficient method of reducing NOx emissions, since additional pumping work was required, which increased the in-cylinder NOx formation.

- Potentially, further improvements in emissions and fuel consumption could be achieved with a reduction in the flow losses of the EGR system.

- Calculation of EGR flow from exhaust and manifold CO_2 readings gives a close correlation to true EGR mass flow calculations. Use of reduction in airflow is not an accurate method for calculating EGR mass flow for turbocharged engines.

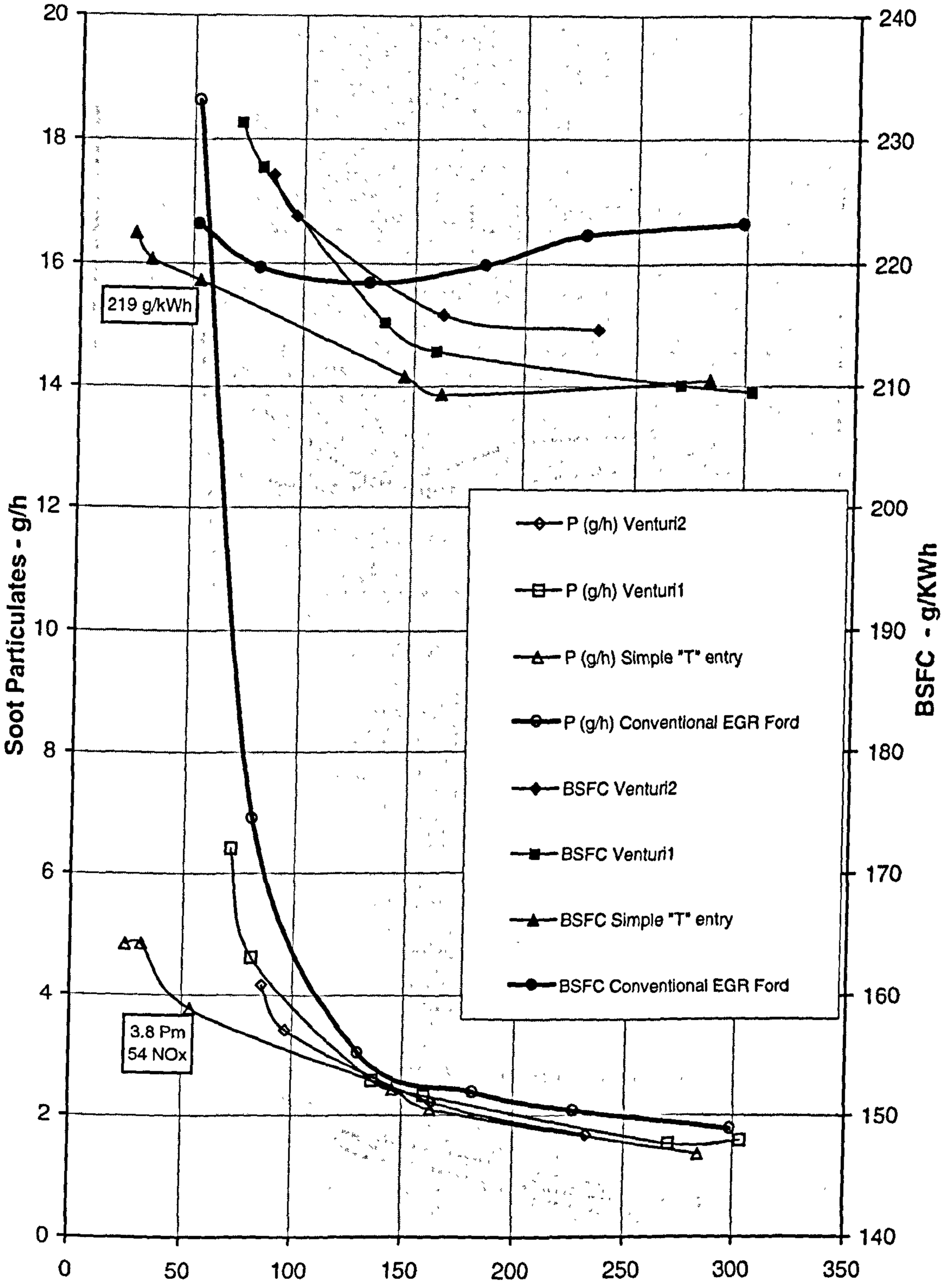

Figure 7.2 Soot and BSFC versus NOx at 2700 rpm 8.0 bar BMEP (112Nm) with VNT vanes fully open

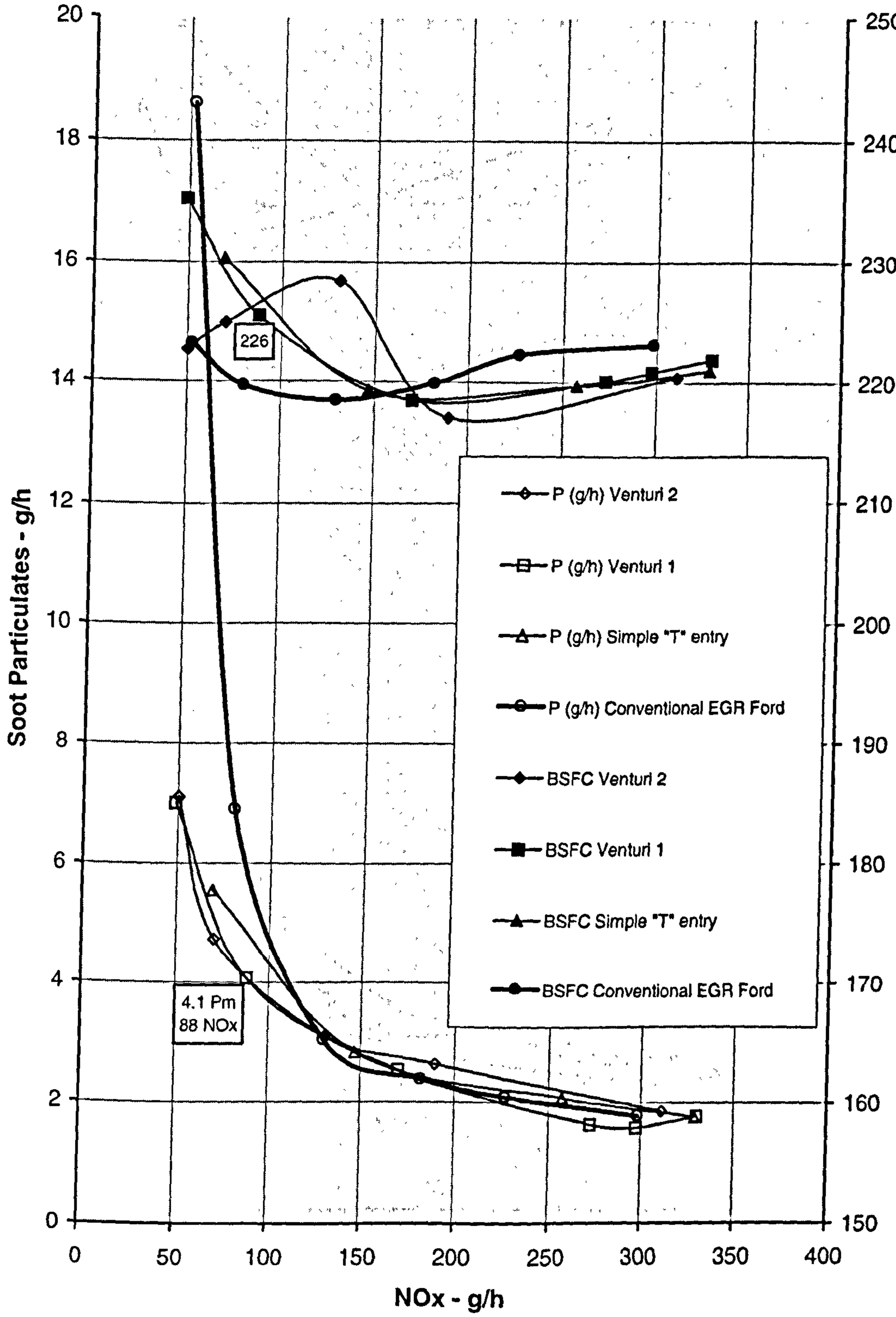

Figure 7.3 Soot and BSFC versus NOx at 2700 rpm 112Nm with VNT vanes in mid-position.

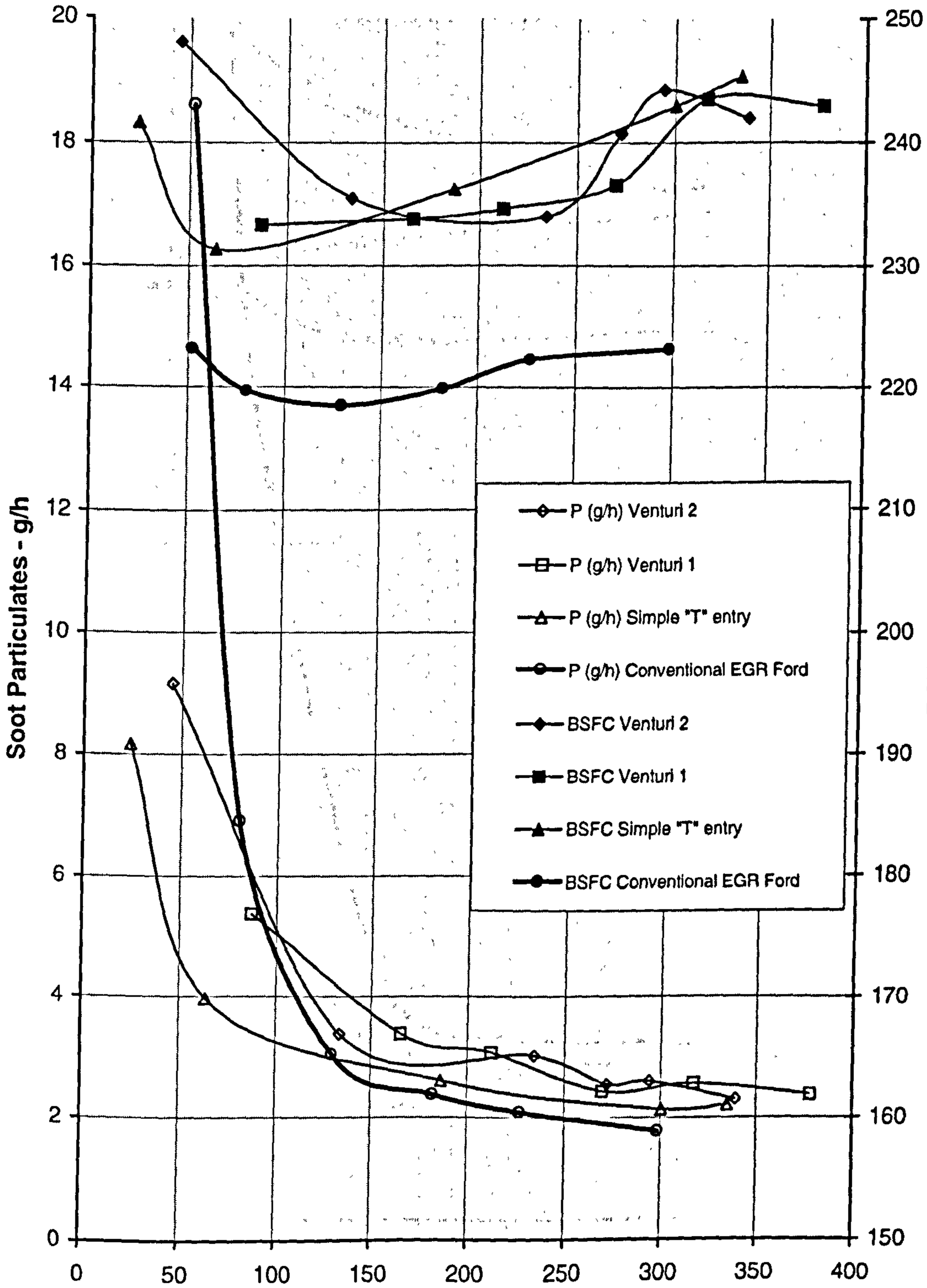

Figure 7.4 Soot and BSFC versus NOx at 2700rpm 112Nm with VNT vanes fully closed

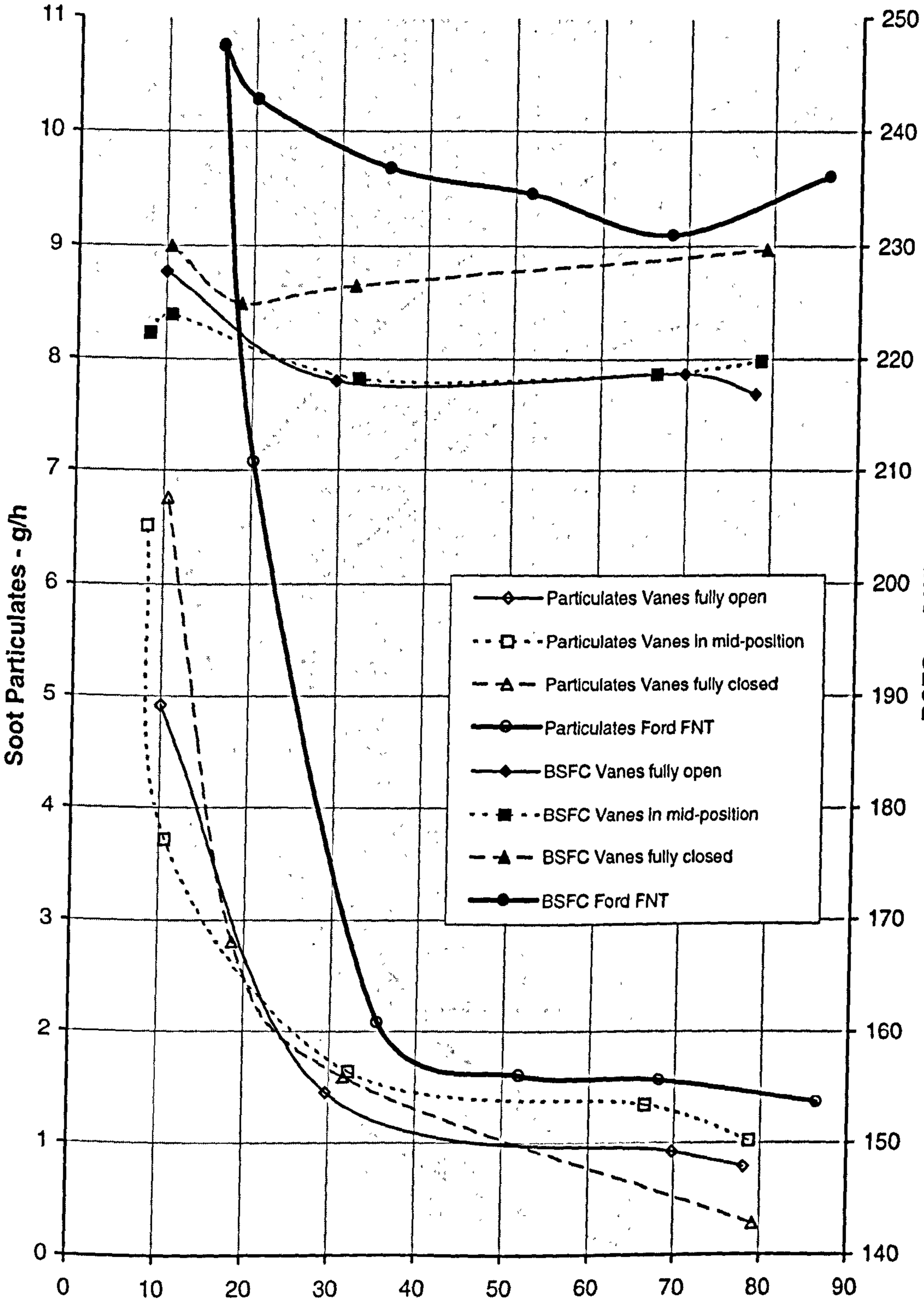

Figure 7.5 Soot and BSFC versus NOx for 1900 rpm 5.6 bar BMEP

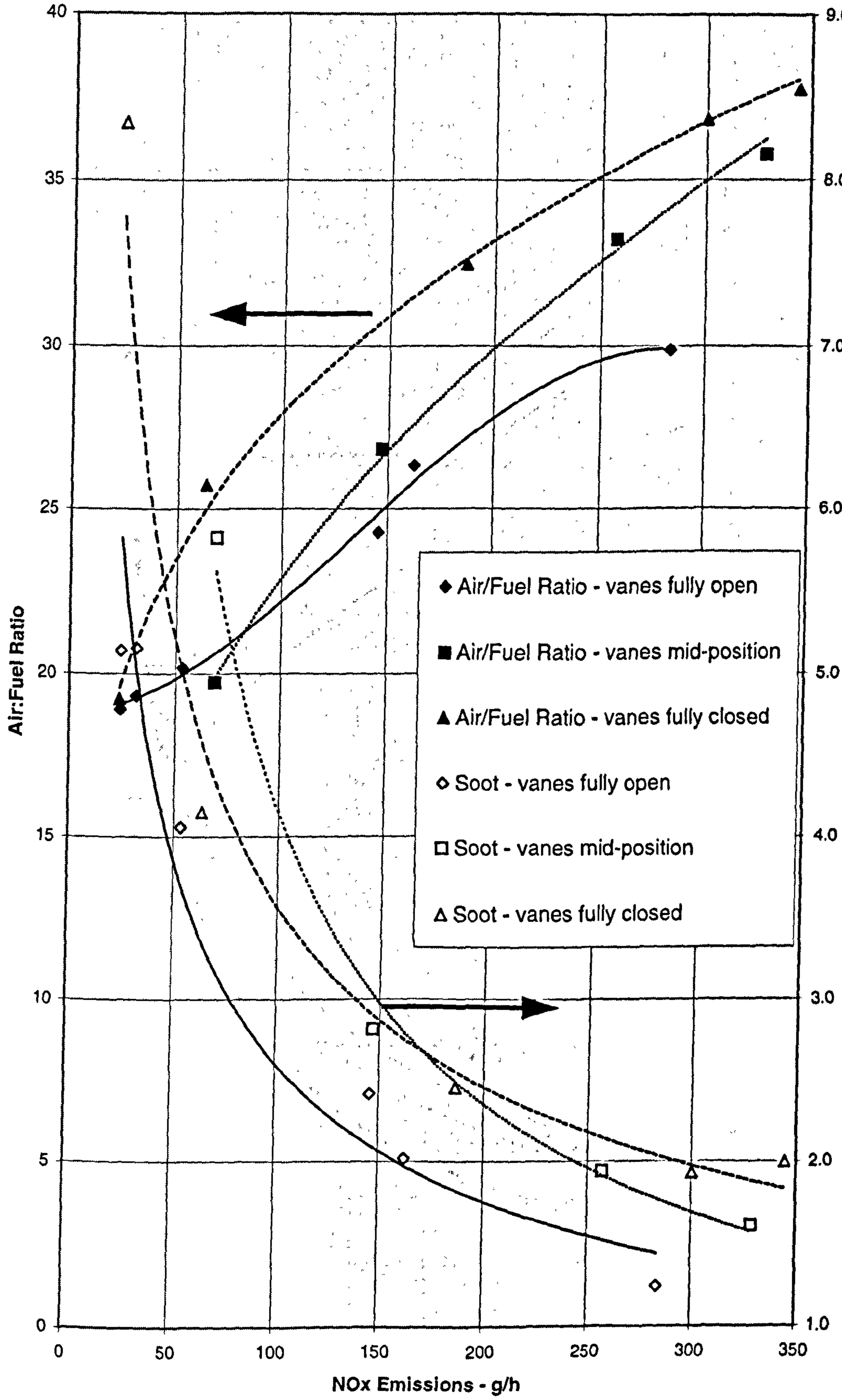

Figure 7.6 Air/fuel ratio and soot emissions versus NOx emissions at 2700 rpm 8.0 bar BMEP (112Nm).

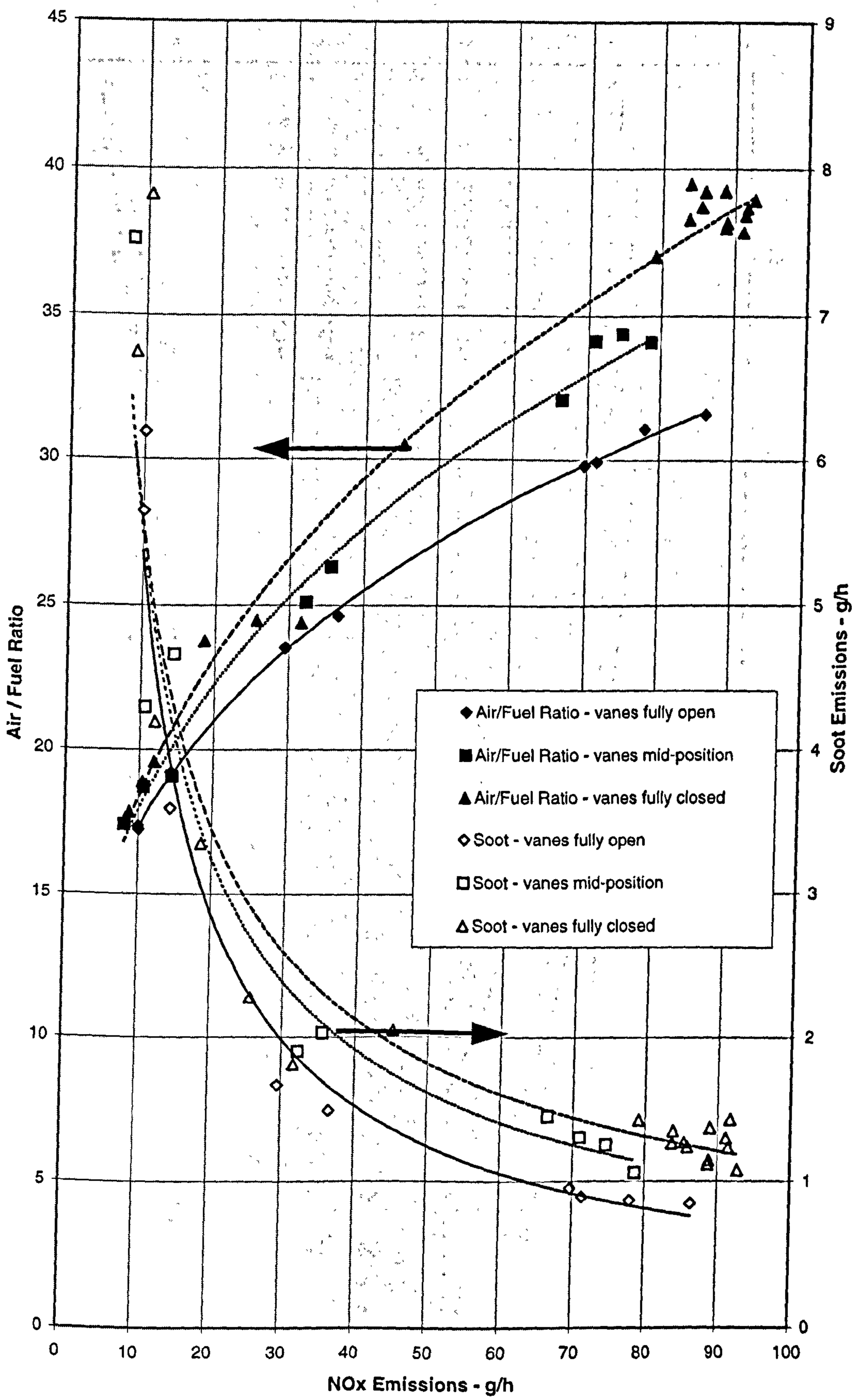

Figure 7.7 Air/fuel ratio and soot emissions versus NOx emissions at 1900rpm 5.6 BMEP (80Nm).

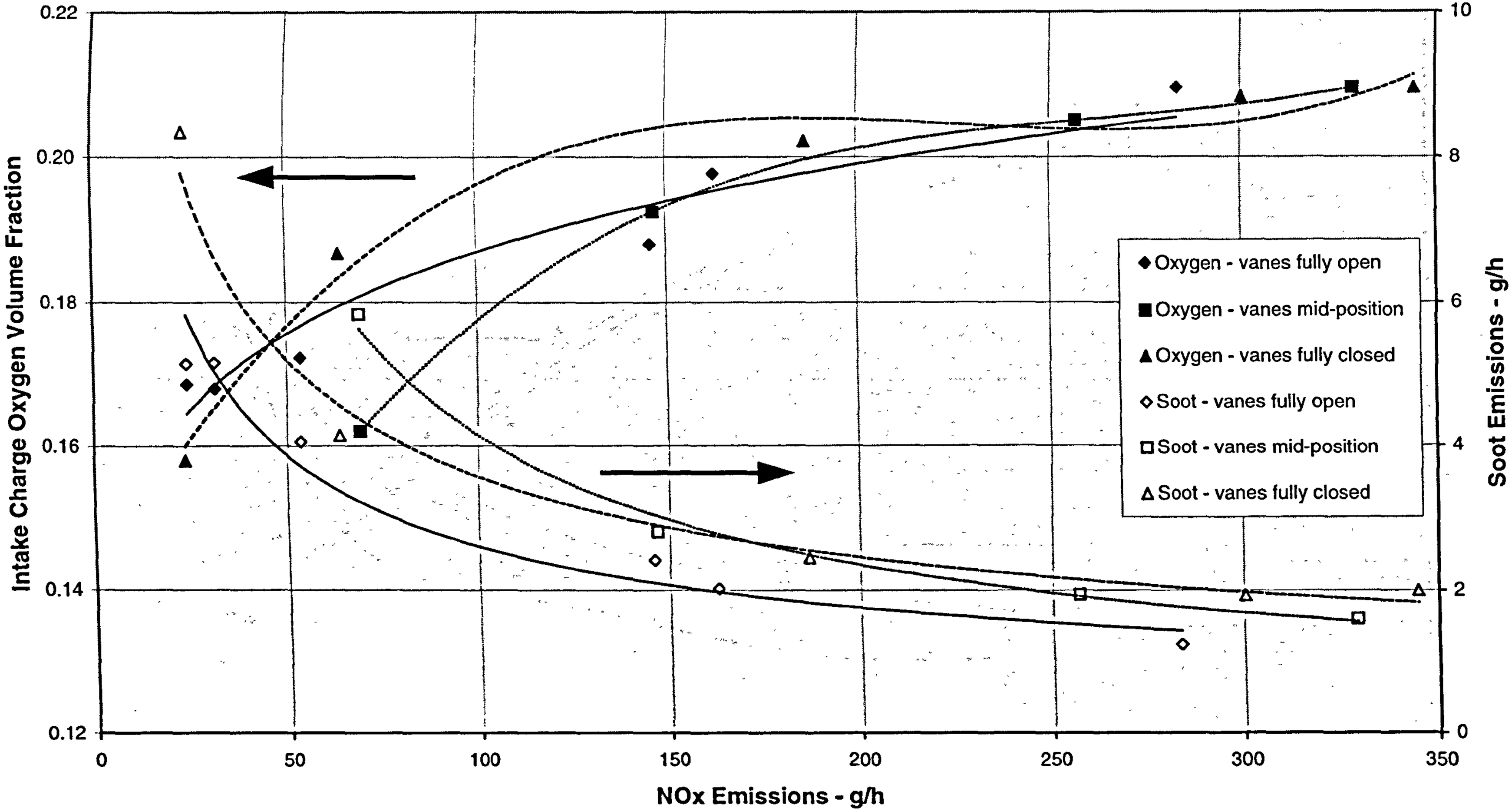

Figure 7.8 Intake charge oxygen volume fraction and soot emissions versus NOx emissions at 2700 rpm 8.0 bar BMEP (112Nm)

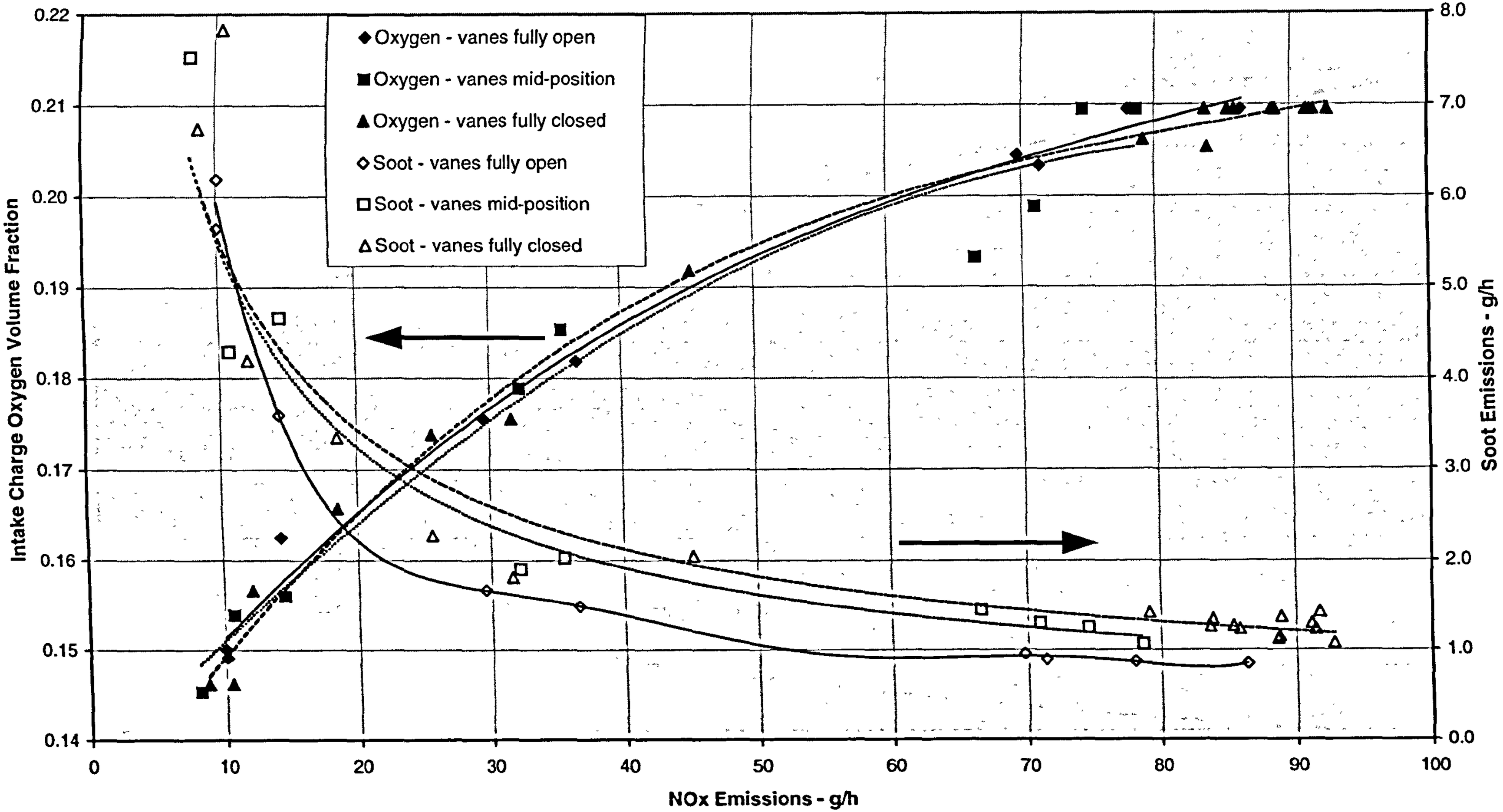

Figure 7.9 Intake charge oxygen volume fraction and soot emissions versus NOx emissions at 1900 rpm 5.6 bar BMEP (80 Nm).

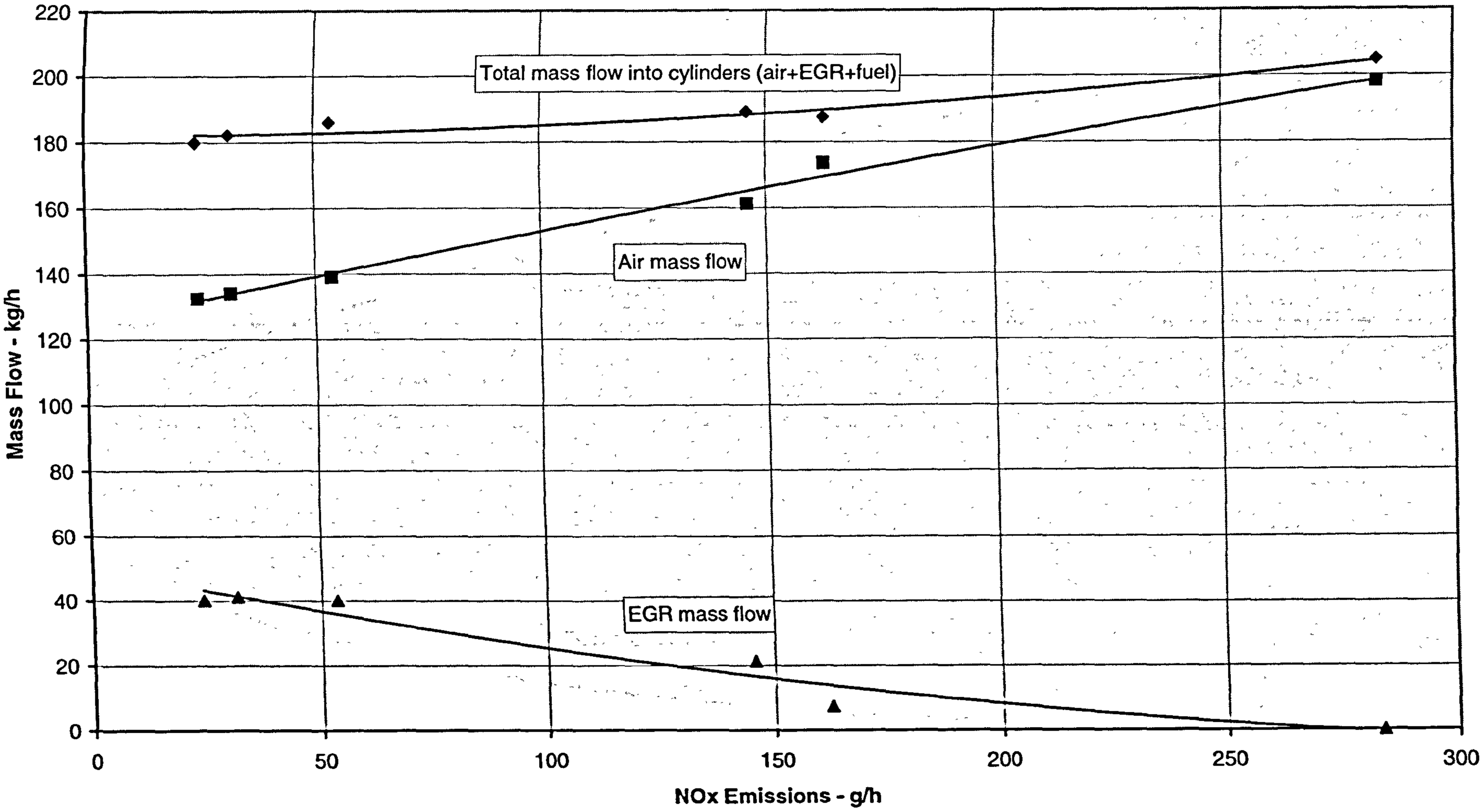

Figure 7.10 Mass flow into engine at 2700 rpm 8.0 bar BMEP (112Nm) with VNT vanes fully open.

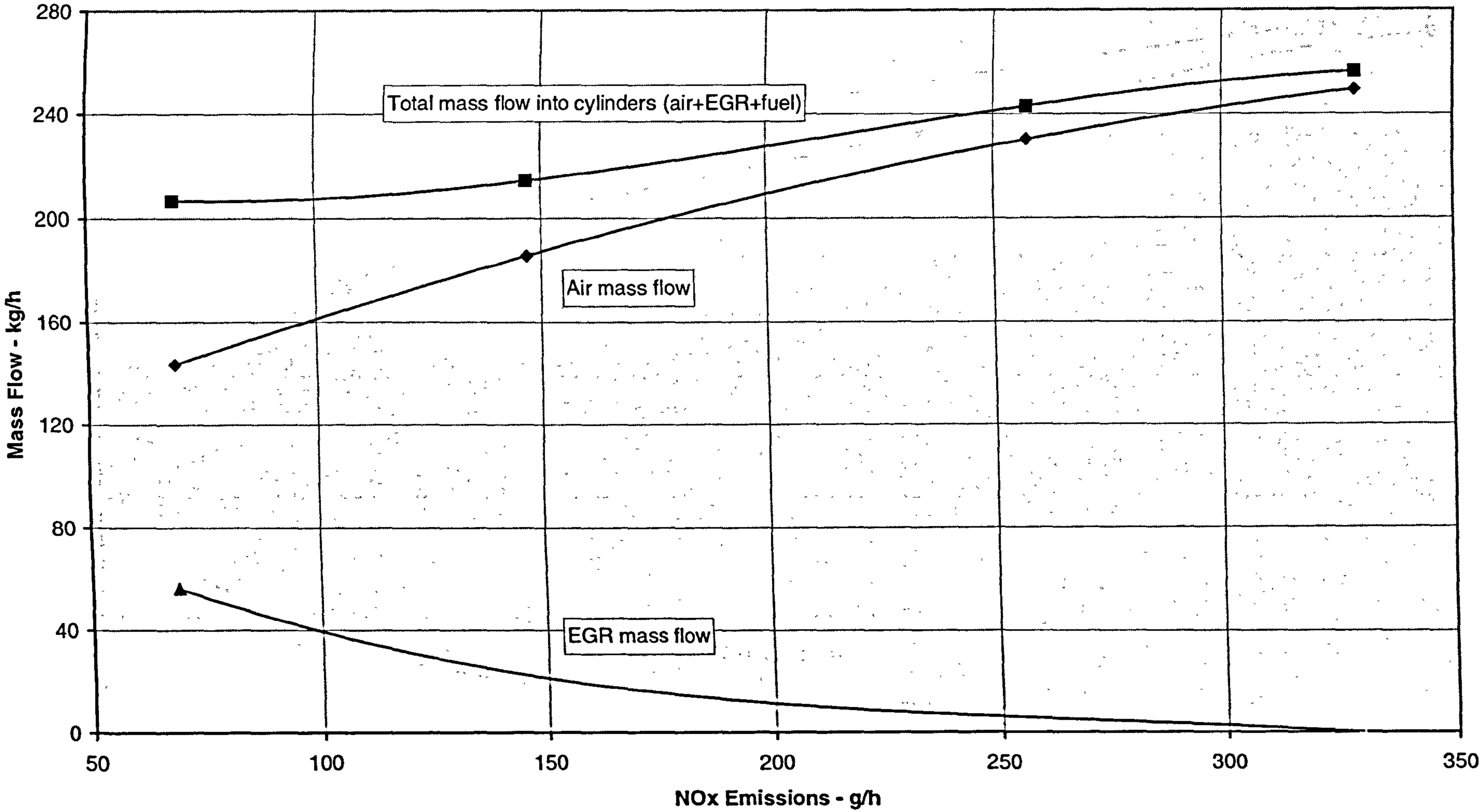

Figure 7.11 Mass flow into engine at 2700 rpm 8.0 bar BMEP (112Nm) with VNT vanes in mid-position.

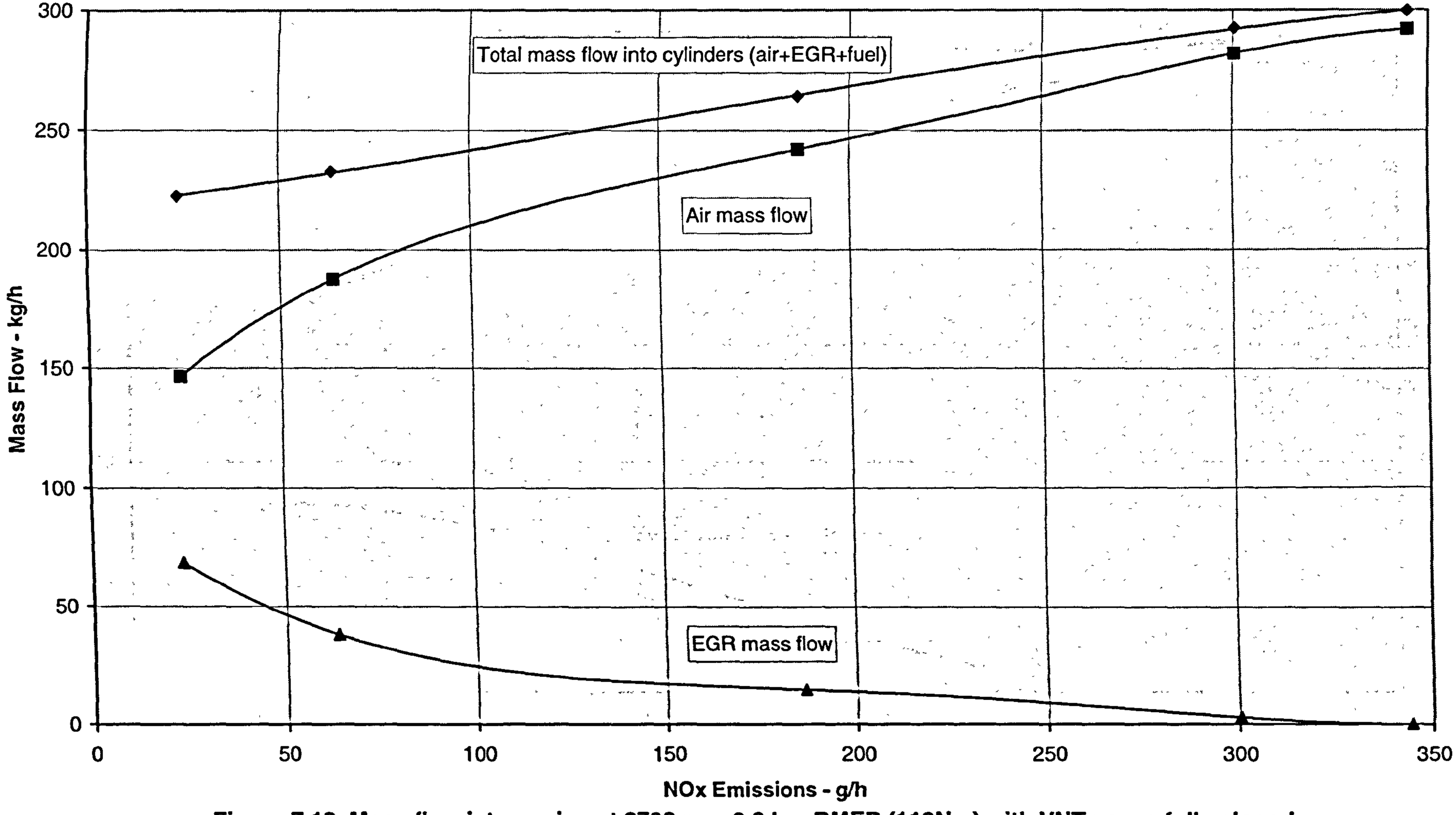

Figure 7.12 Mass flow into engine at 2700 rpm 8.0 bar BMEP (112Nm) with VNT vanes fully closed.

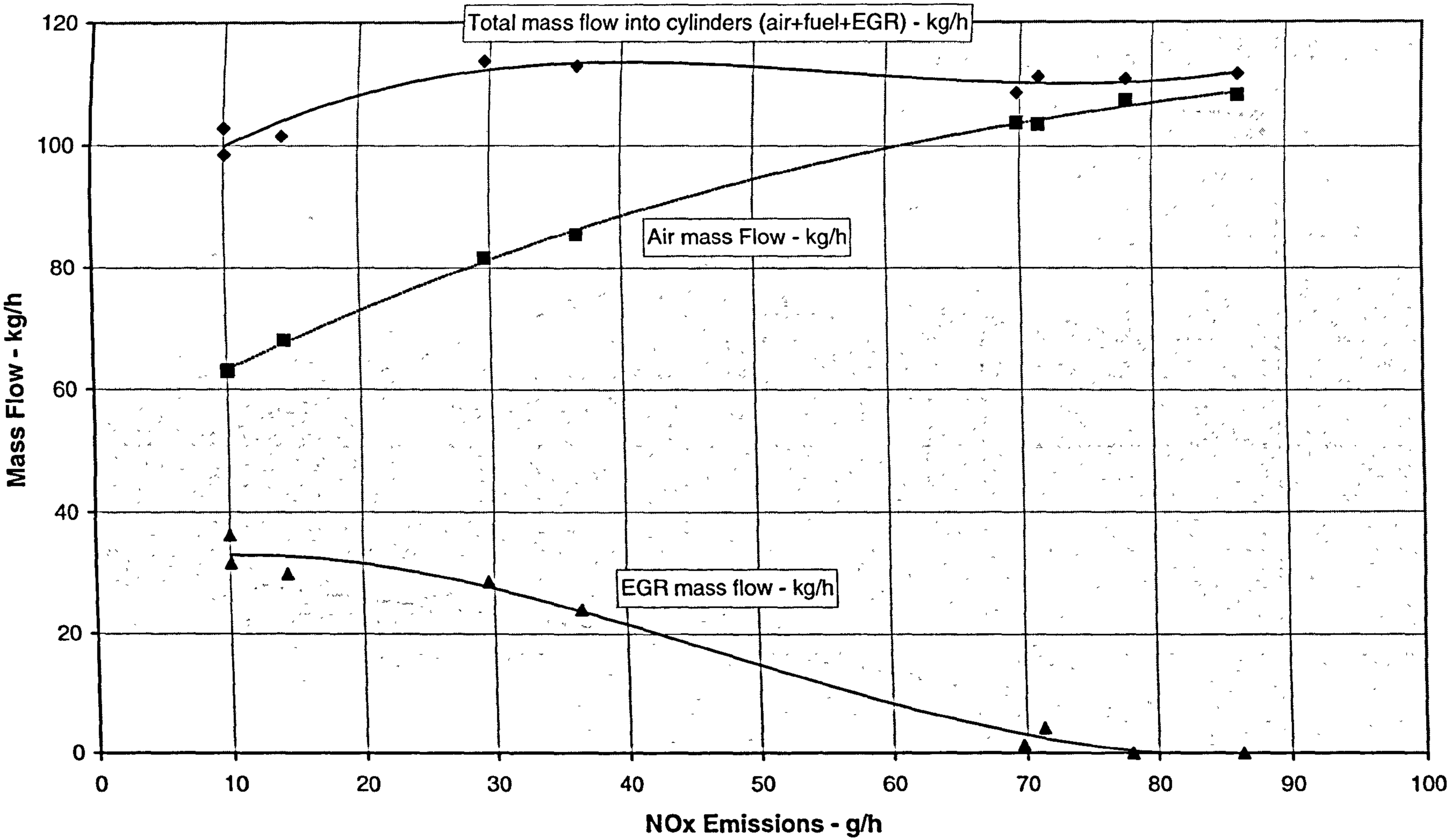

Figure 7.13 Mass flow into engine at 1900 rpm 5.7 bar BMEP with VNT vanes fully open.

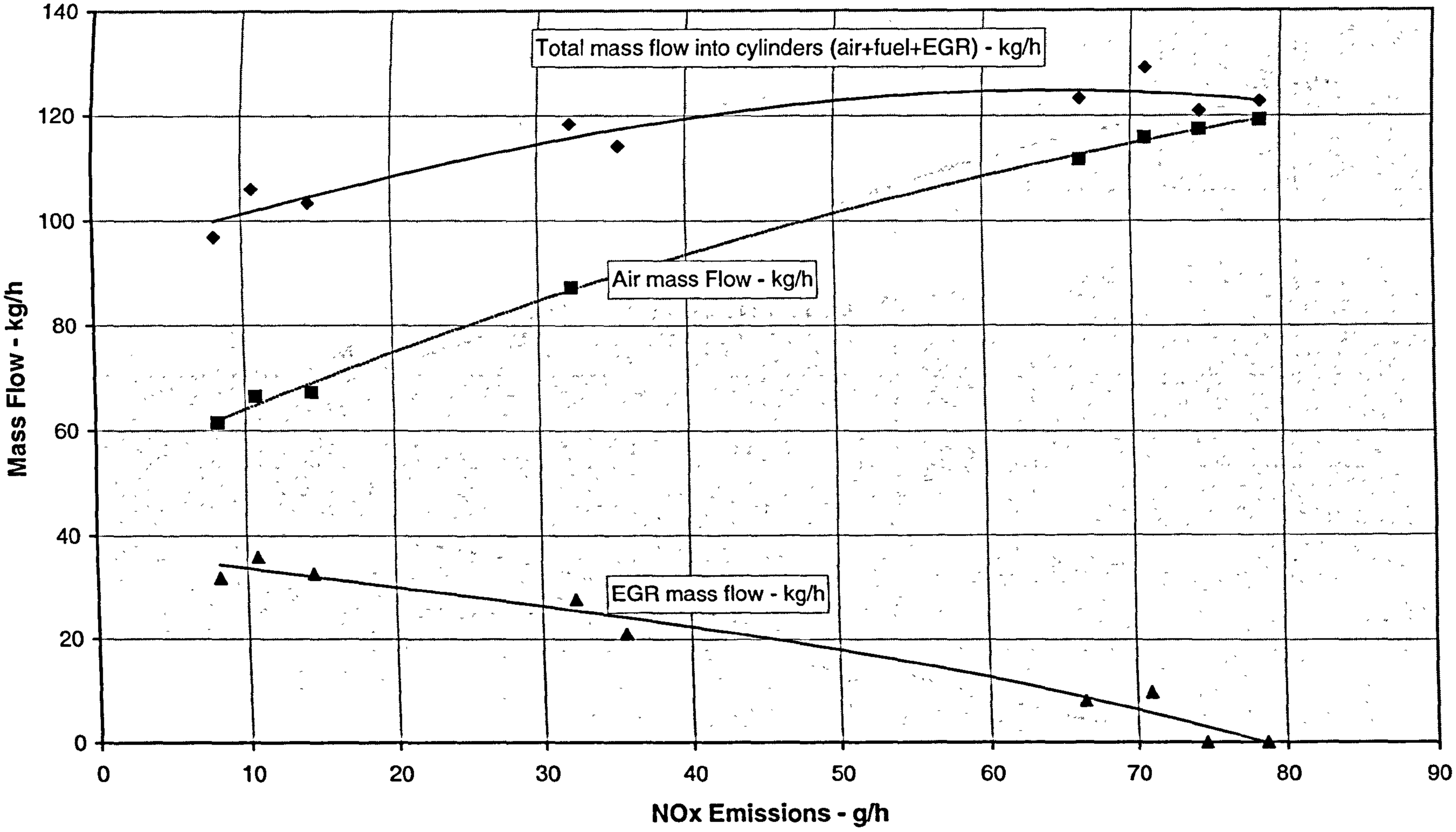

Figure 7.14 Mass flow into engine at 1900 rpm 5.7 bar BMEP (80Nm) with VNT vanes in mid-position.

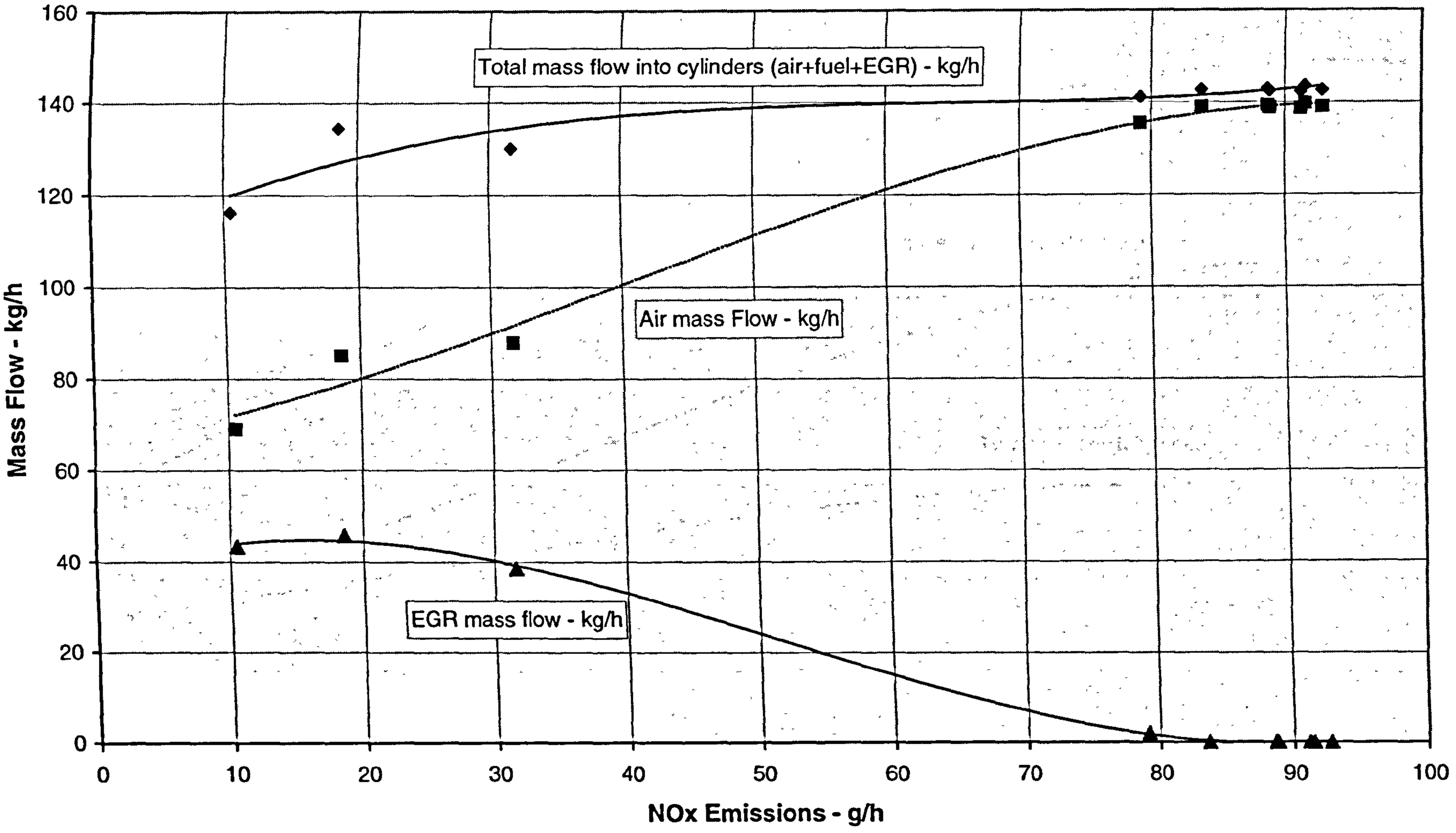

Figure 7.15 Mass flow into engine at 1900 rpm 5.7 bar BMEP (80Nm) with VNT vanes fully closed.

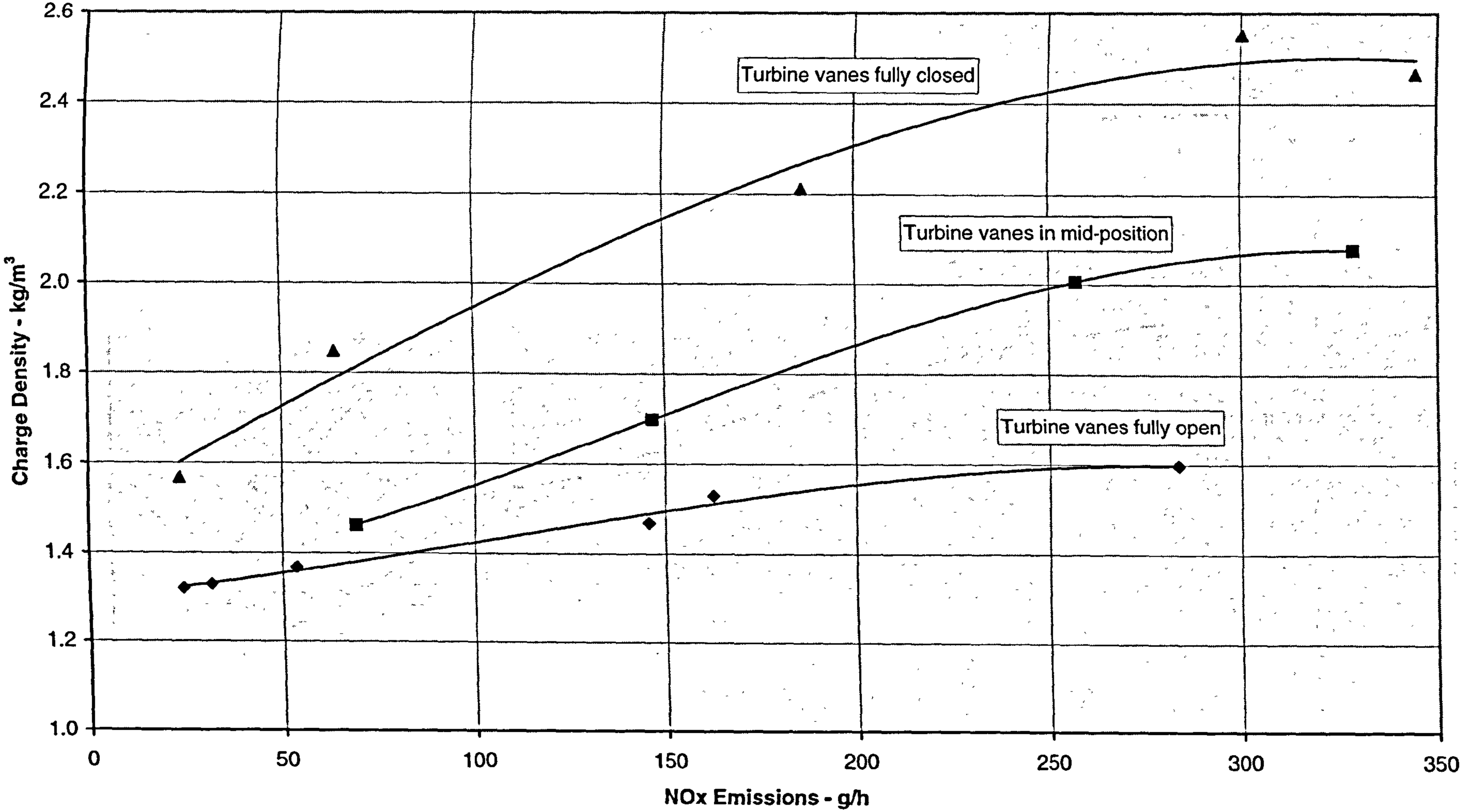

Figure 7.16 Charge density at 2700 rpm 8.0 bar BMEP (112Nm).

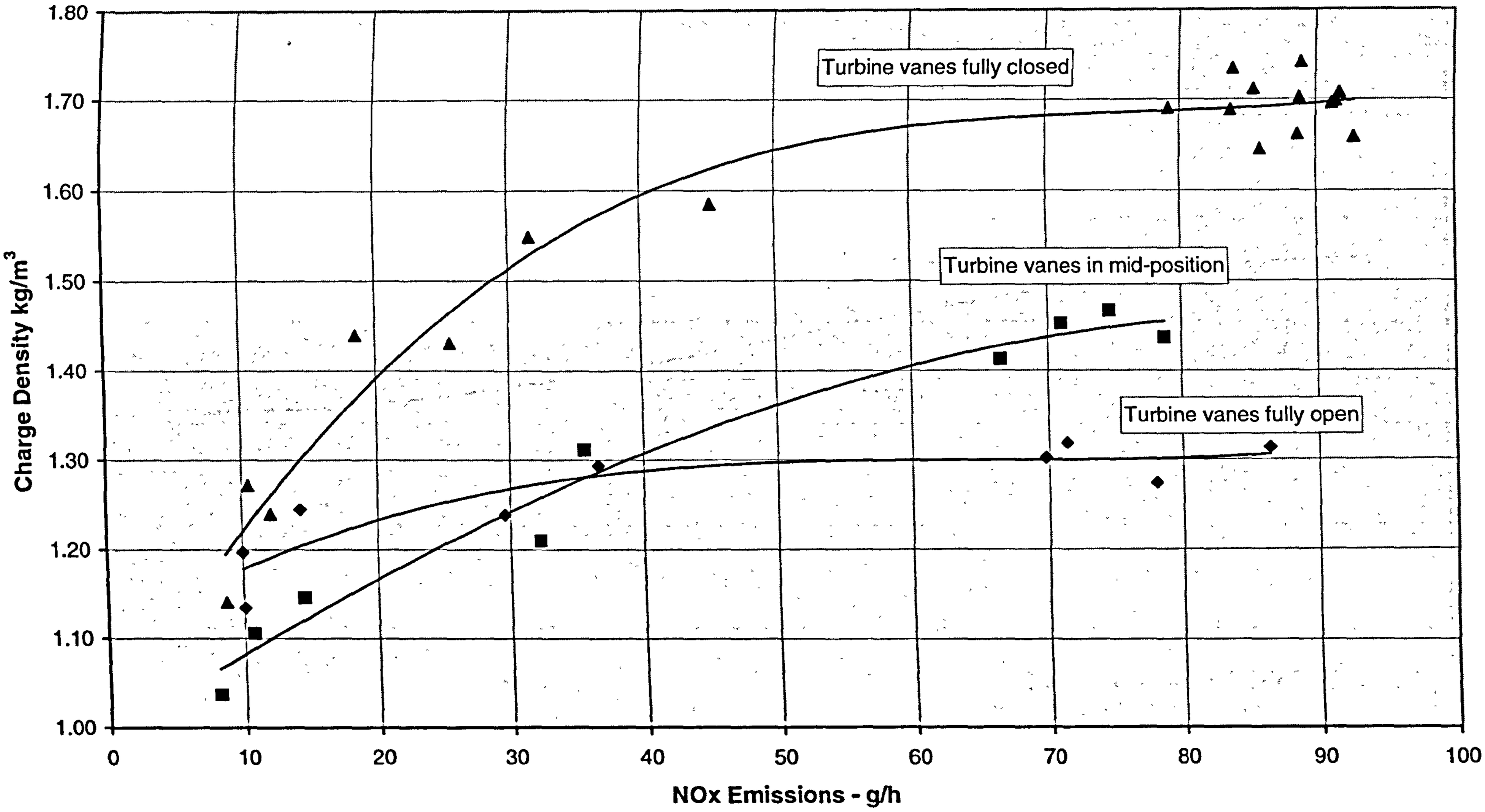

Figure 7.17 Charge density at 1900 rpm 5.7 bar BMEP (80Nm).

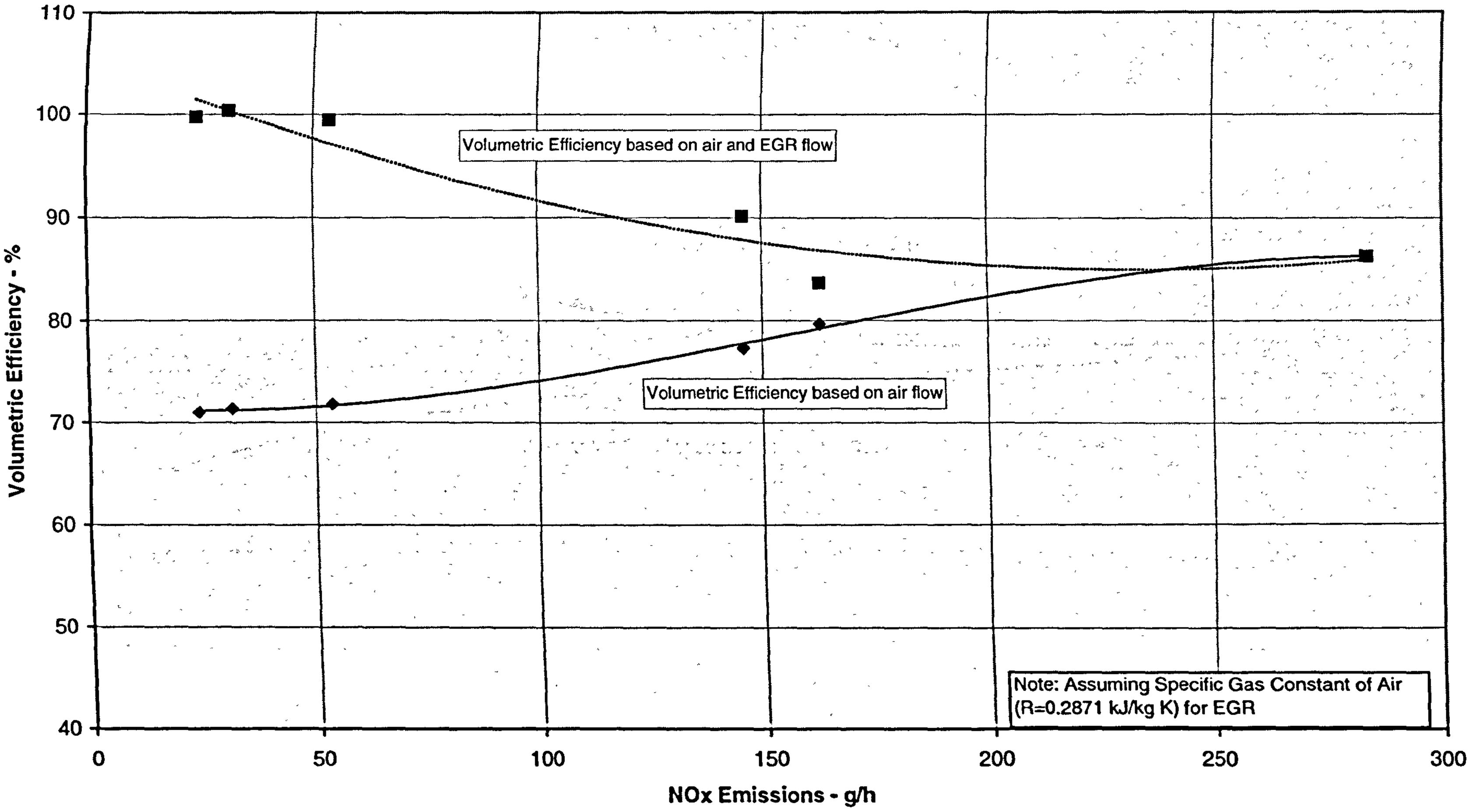

Figure 7.18 Volumetric efficiency at 2700 rpm 8.0 bar BMEP (112Nm) with VNT vanes fully open.

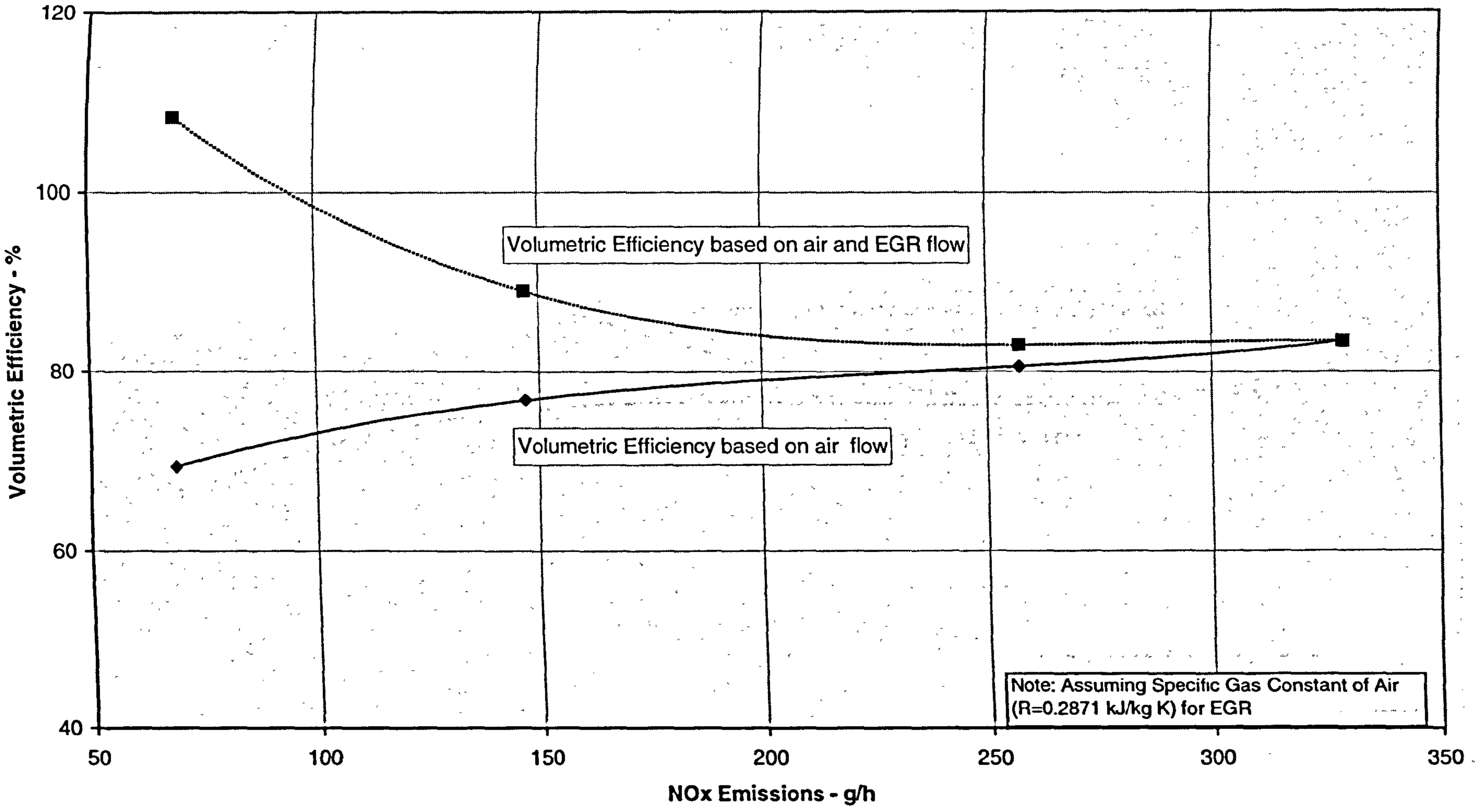

Figure 7.19 Volumetric efficiency at 2700 rpm 8.0 bar BMEP (112Nm) with VNT vanes in mid-position.

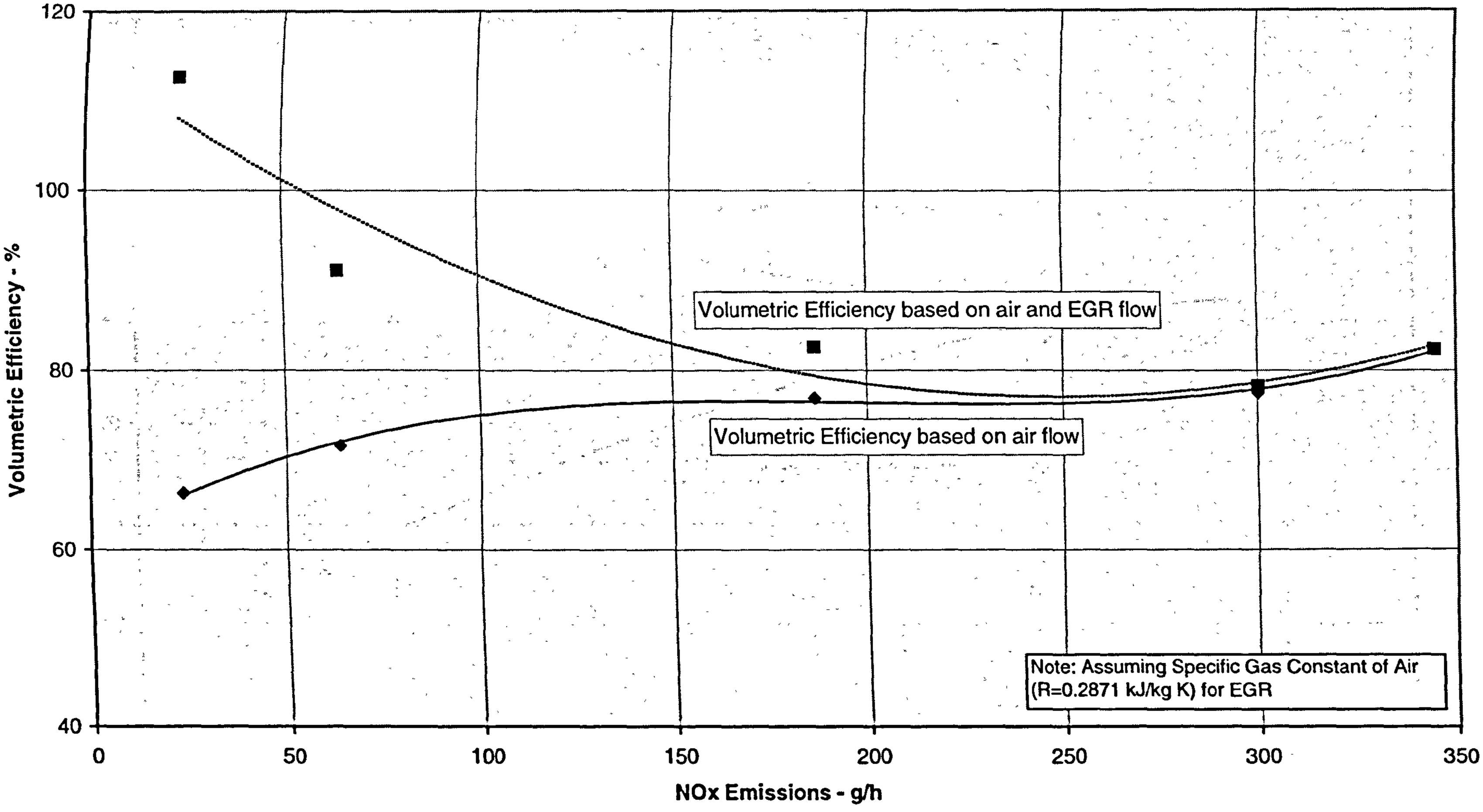

Figure 7.20 Volumetric efficiency at 2700 rpm 8.0 bar BMEP (112Nm) with VNT vanes fully closed.

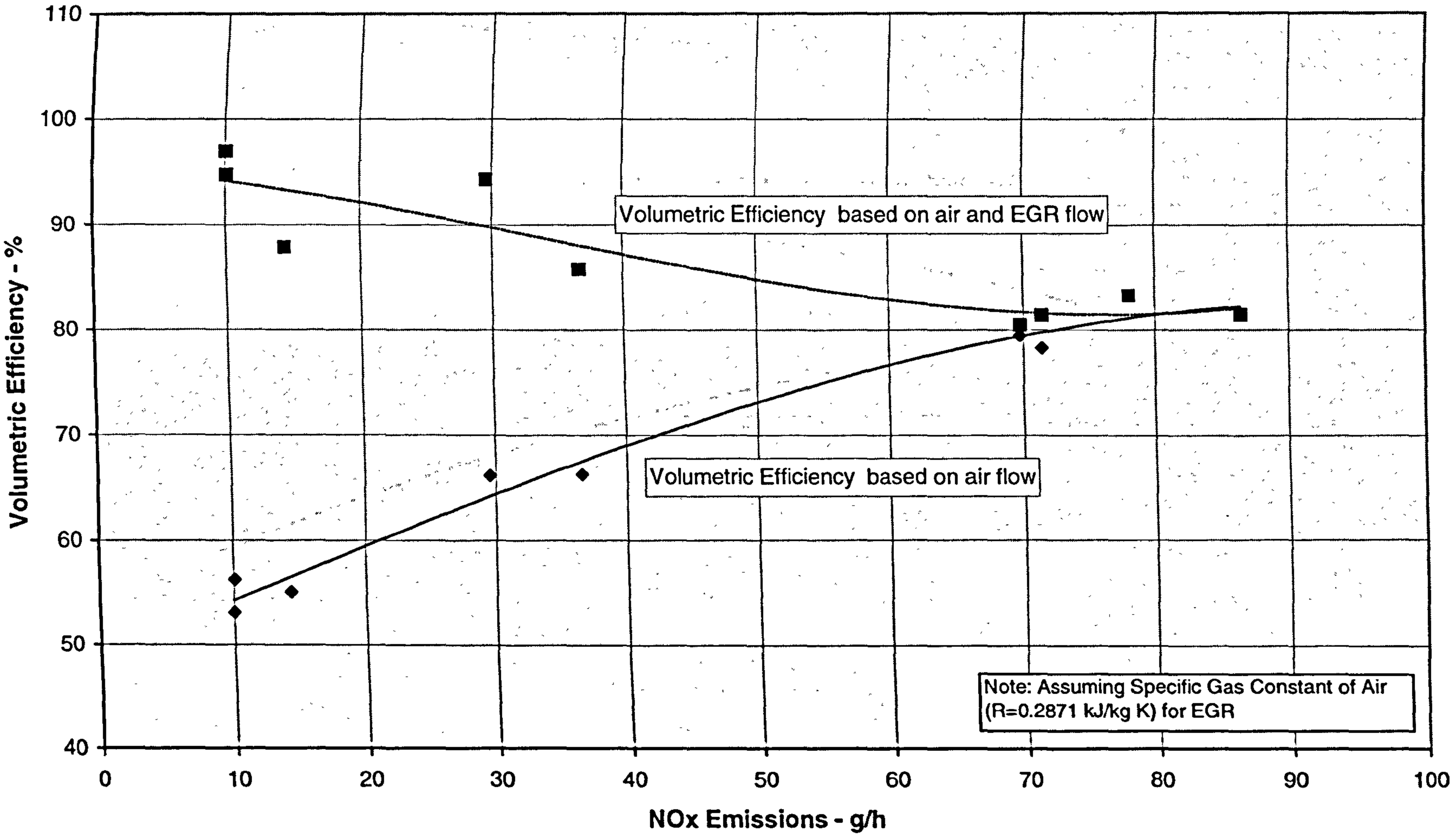

Figure 7.21 Volumetric efficiency at 1900 rpm 5.7 bar BMEP (80Nm) with VNT vanes fully open.

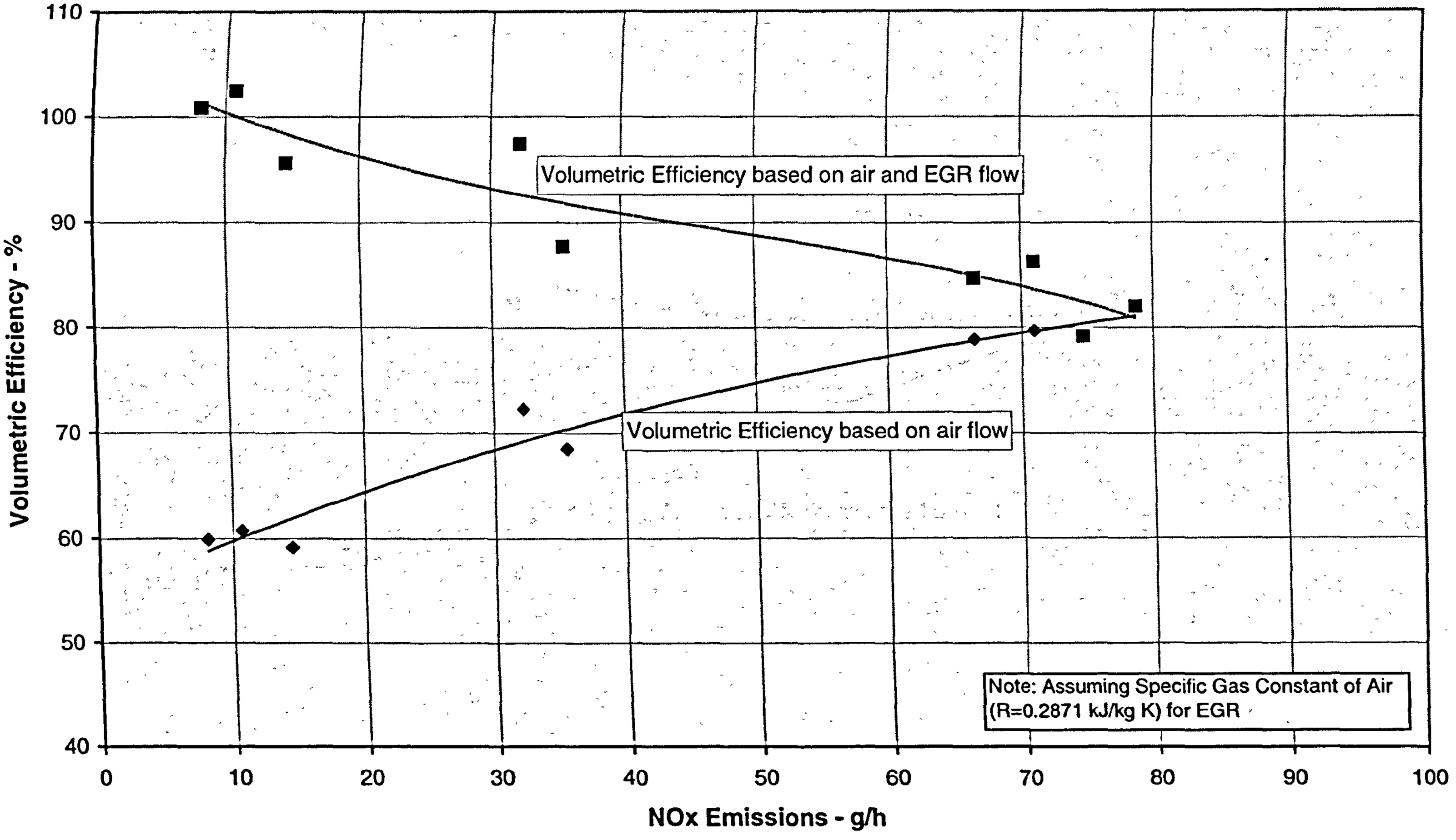

Figure 7.22 Volumetric efficiency at 1900 rpm 5.7 bar BMEP (80Nm) with VNT vanes in mid-position.

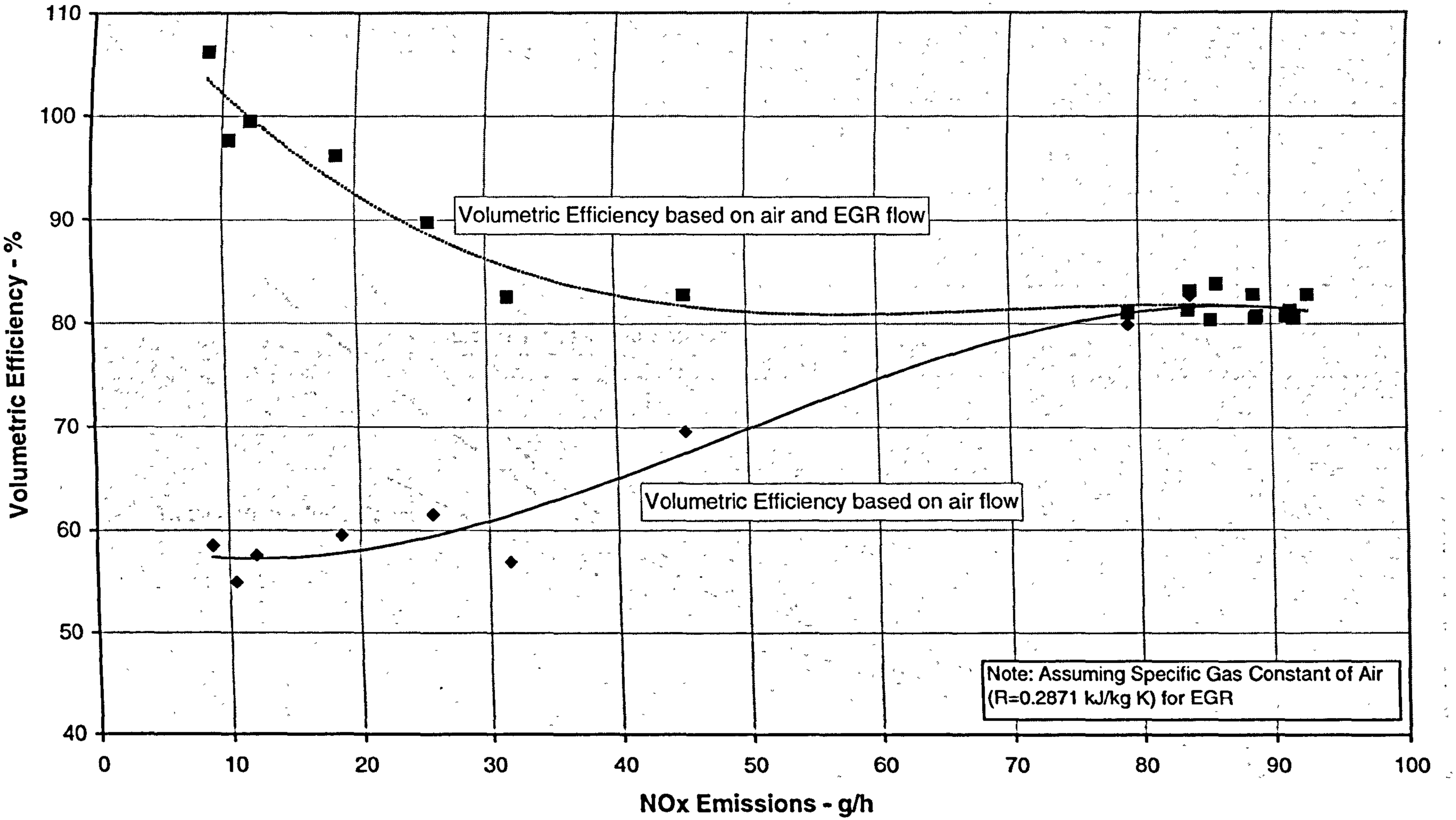

Figure 7.23 Volumetric efficiency at 1900 rpm 5.7 bar BMEP (80Nm) with VNT vanes fully closed.

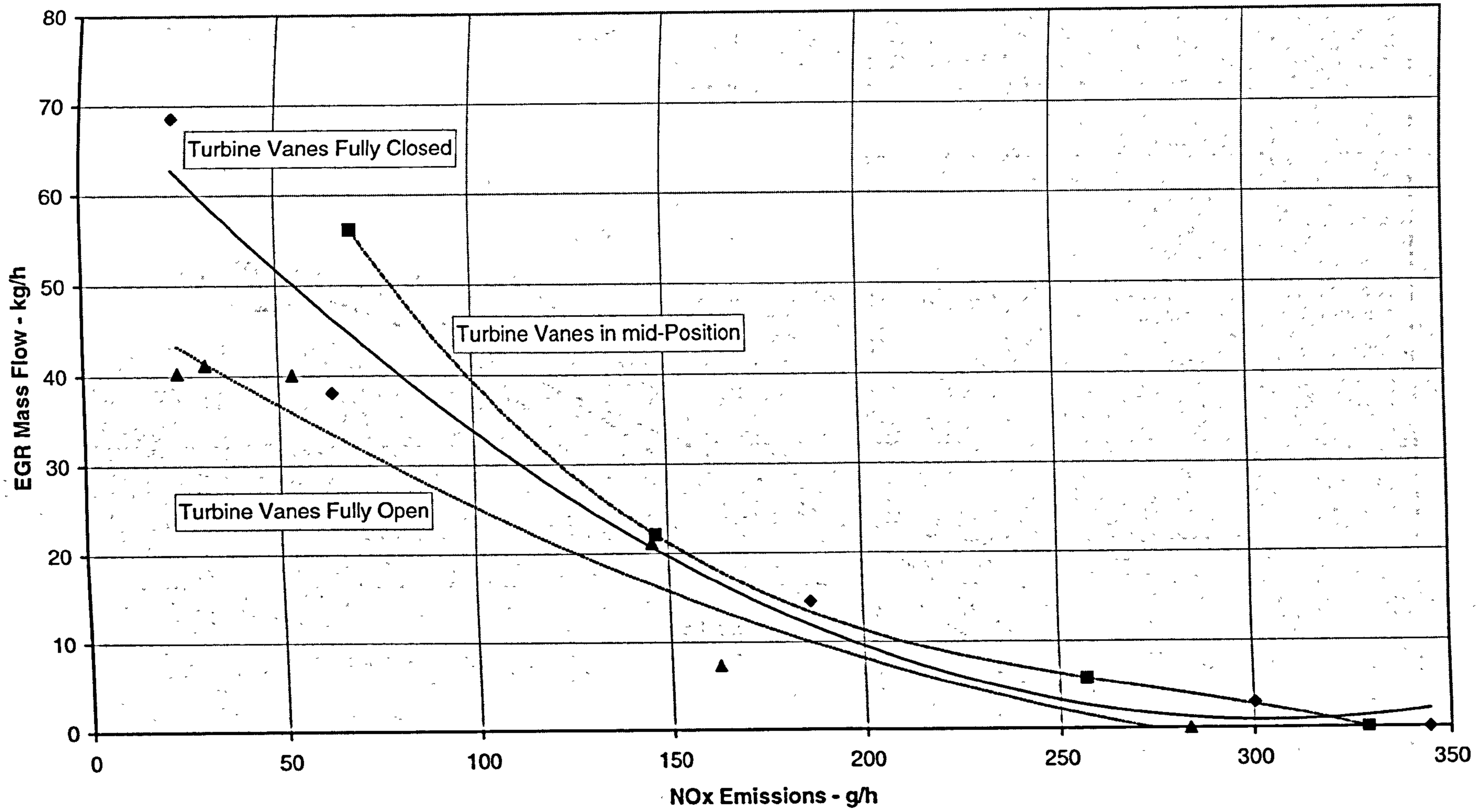

Figure 7.24 EGR mass flow at 2700 rpm 8.0 bar BMEP (112Nm).

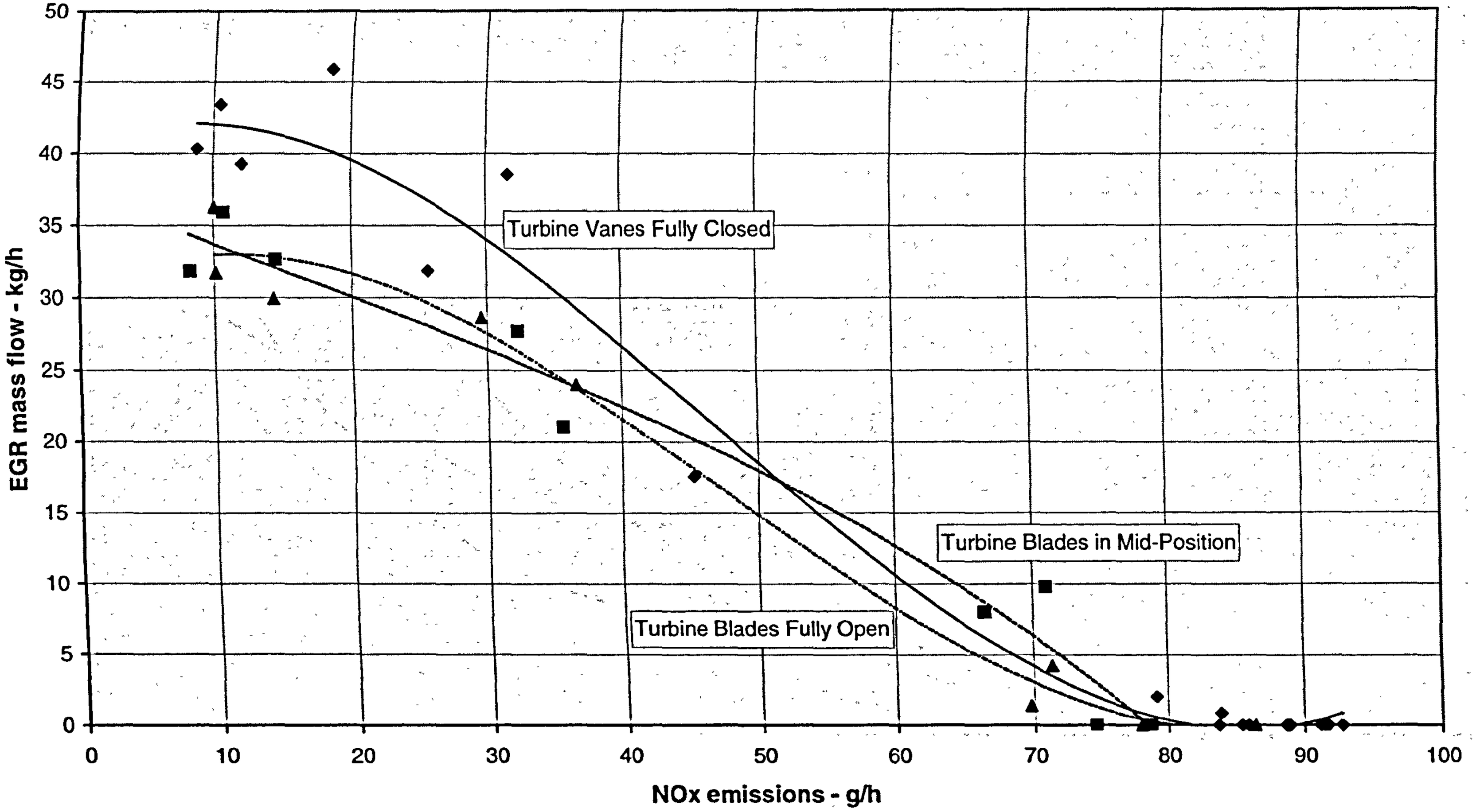

Figure 7.25 EGR mass flow at 1900 rpm 5.7 bar BMEP (80Nm).

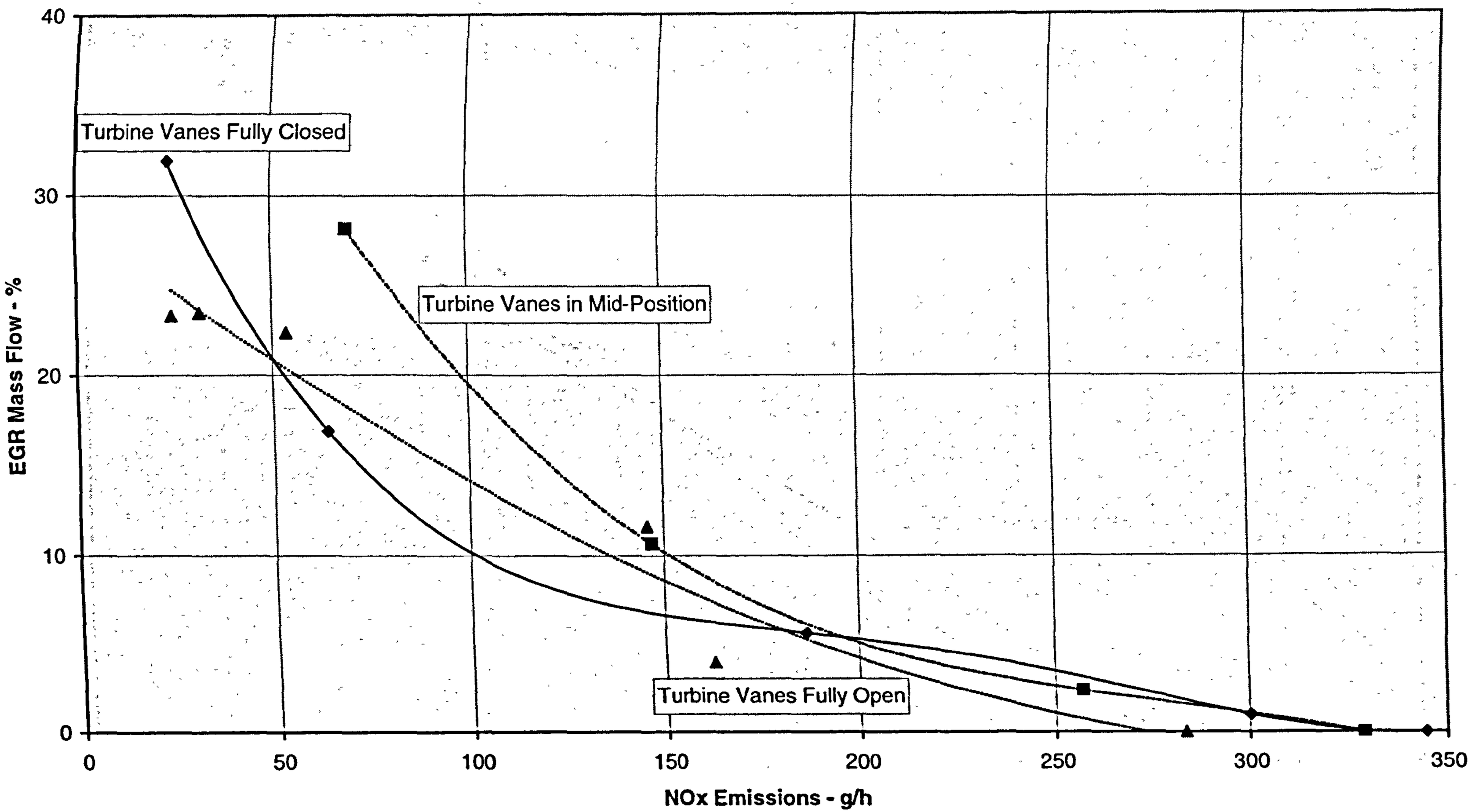

Figure 7.26 EGR mass by per cent at 2700 rpm 8.0 bar BMEP (112Nm)

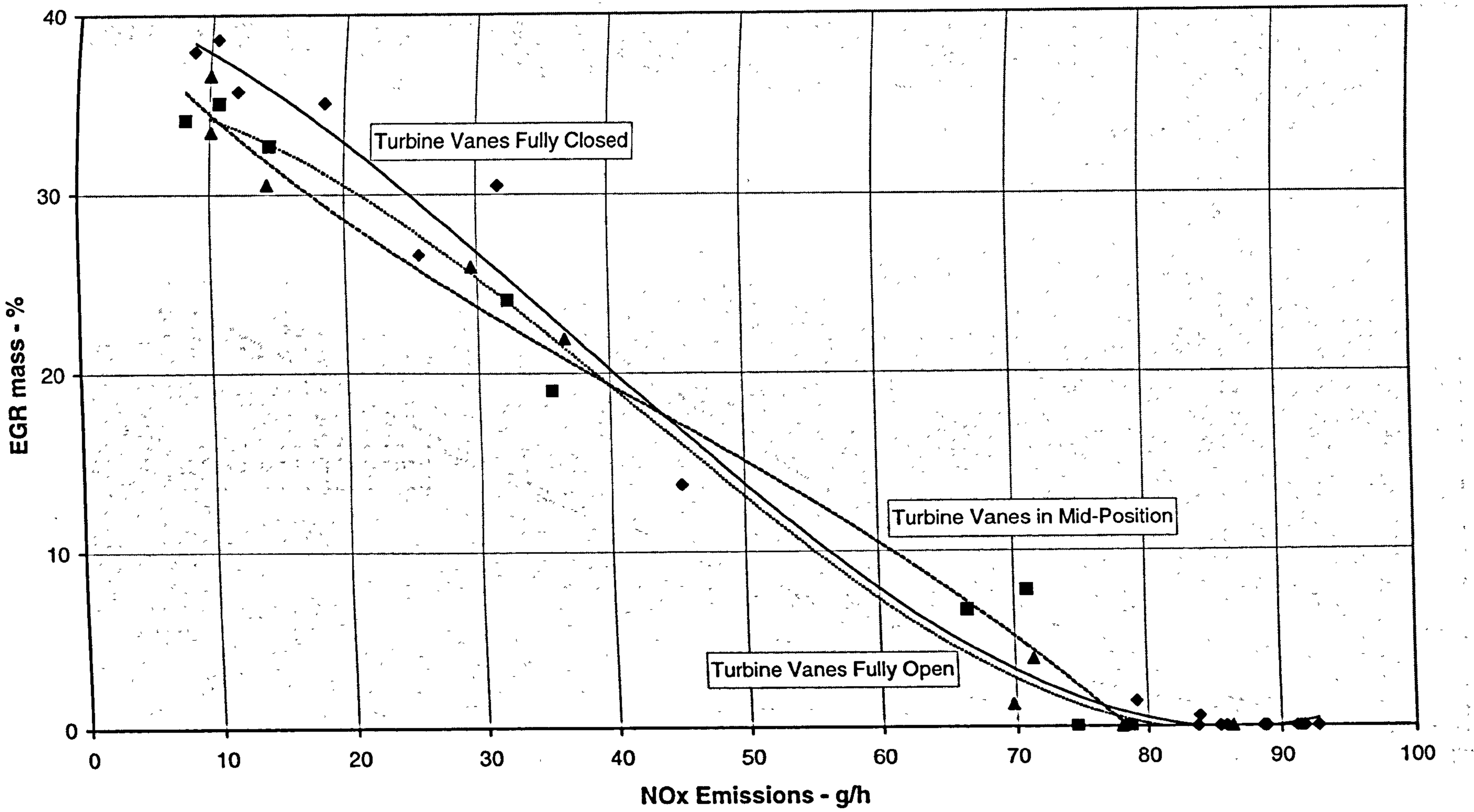

Figure 7.27 EGR mass by per cent at 1900 rpm 5.7 bar BMEP (80Nm).

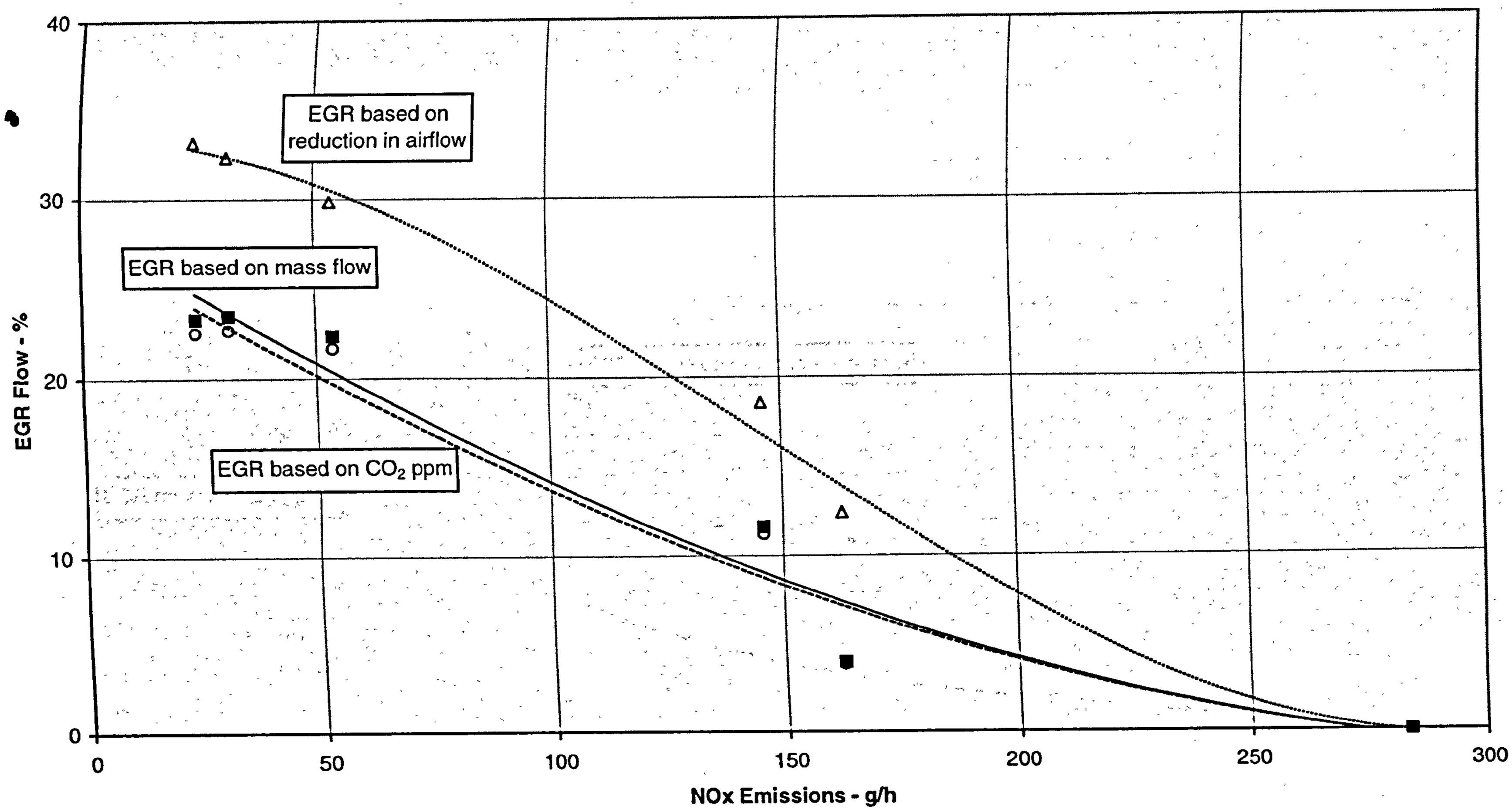

Figure 7.30 Comparison of methods for calculating EGR flow at 2700 rpm 8.0 bar BMEP (112Nm) with VNT vanes fully open.

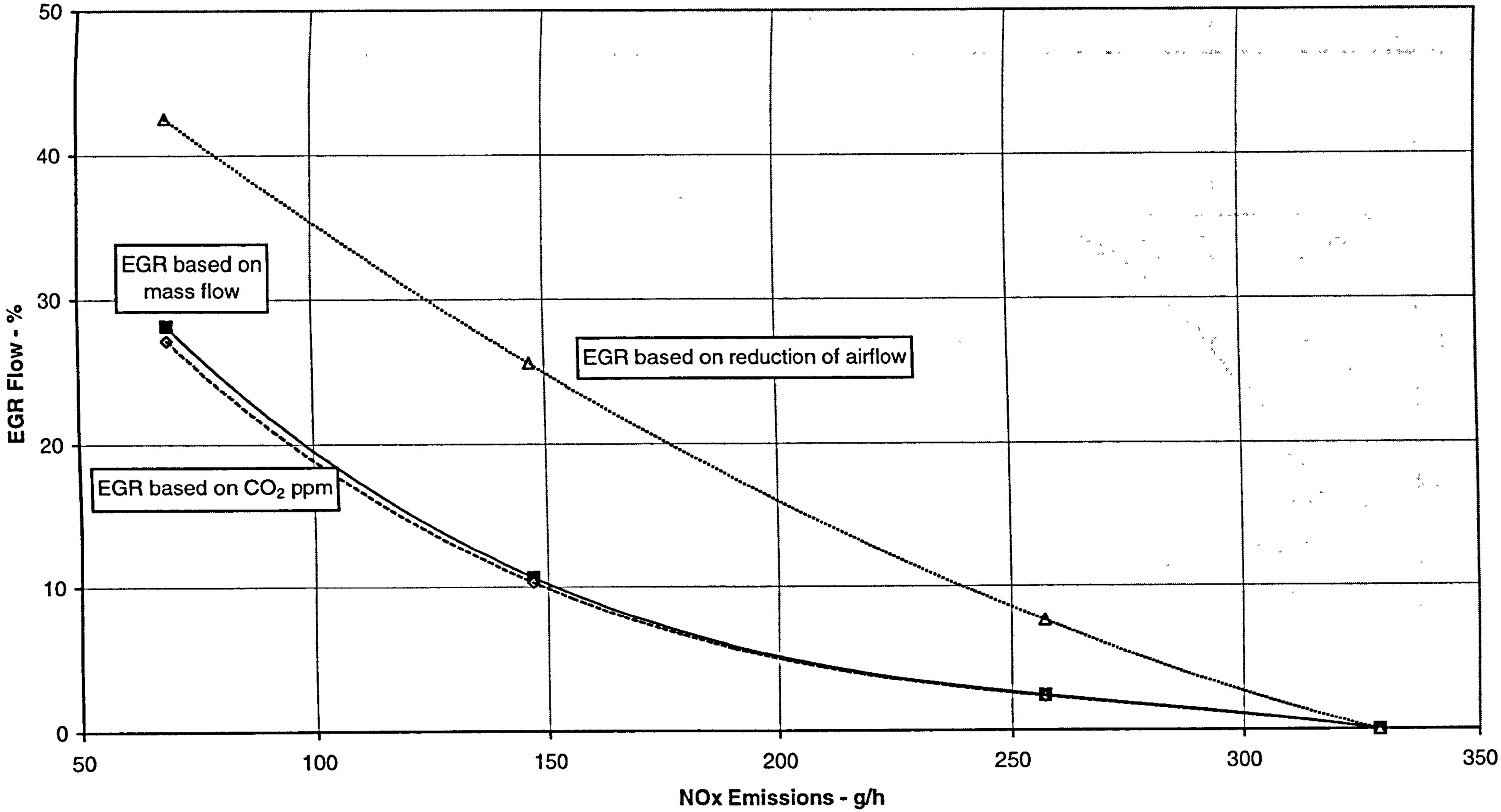

Figure 7.31 Comparison of methods of calculating EGR flow at 2700 rpm 8.0 bar BMEP (112Nm) with VNT vanes in mid-position.

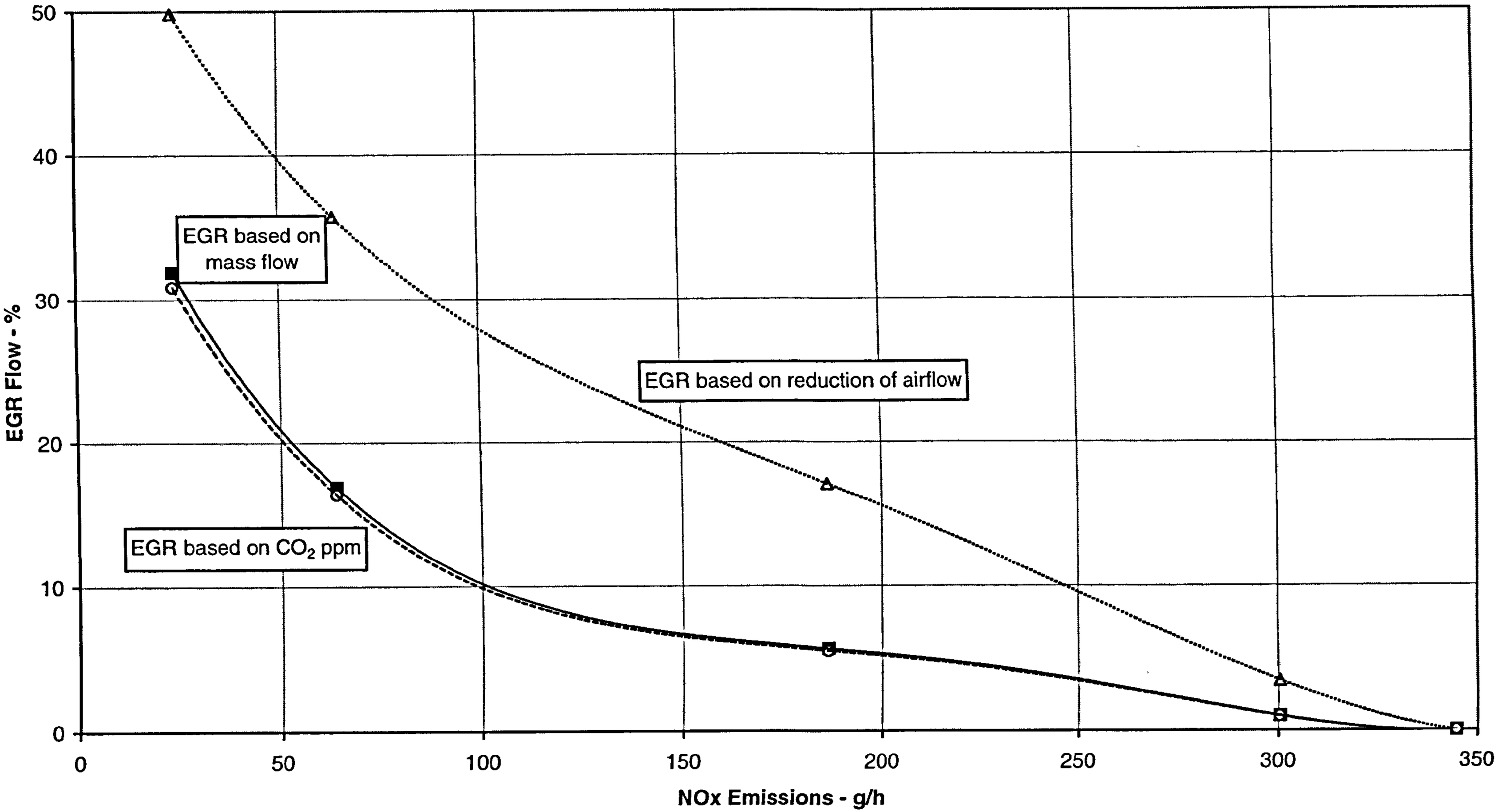

Figure 7.32 Comparison of methods of calculating EGR flow, at 2700 rpm 8.0 bar BMEP (112Nm) with vanes fully closed

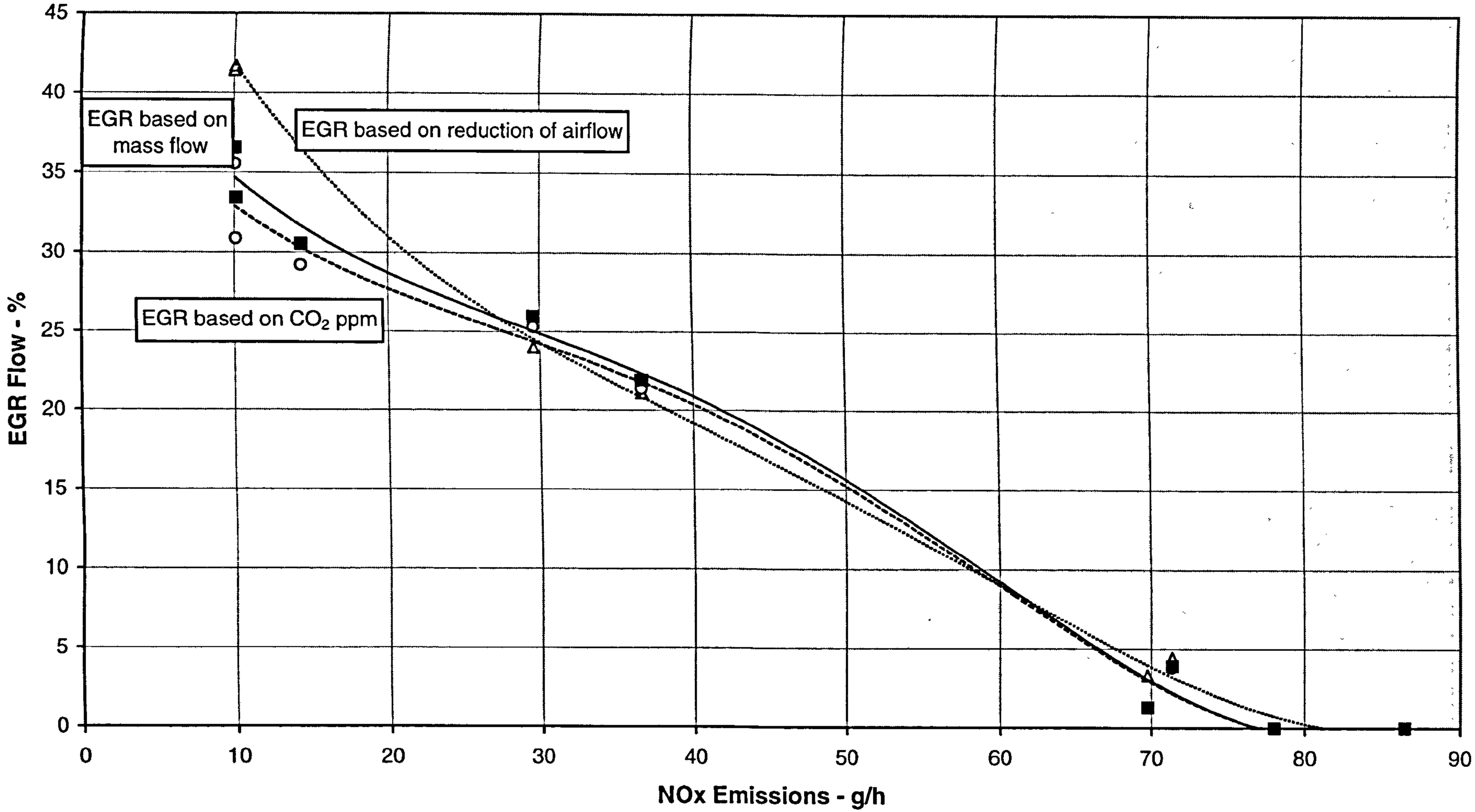

Figure 7.33 Comparison of methods of calculating EGR flow at 1900 rpm 5.7 bar BMEP (80Nm) with vanes fully open.

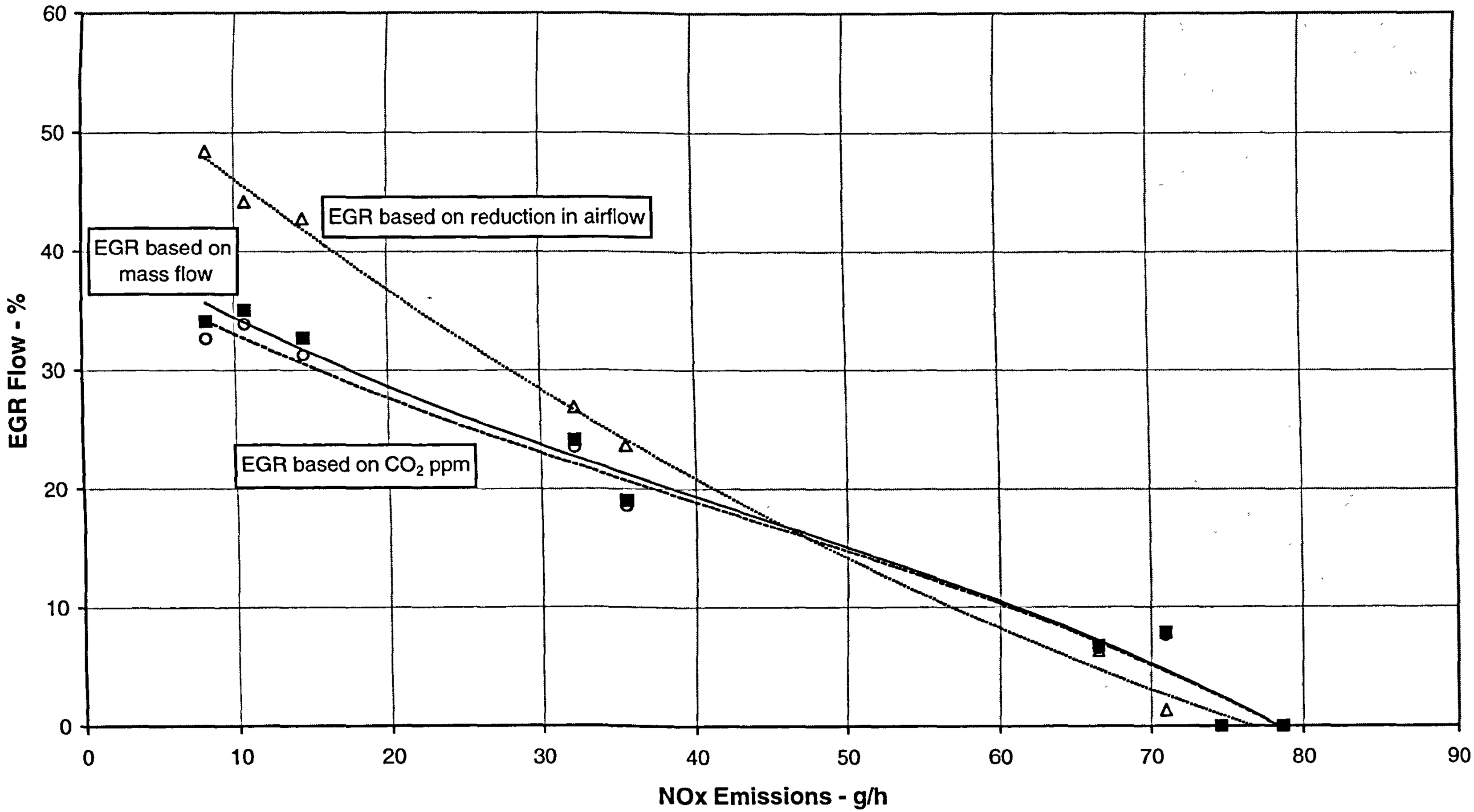

Figure 7.34 Comparison of methods of calculating EGR flow at 1900 rpm 5.7 bar BMEP with VNT vanes in mid-position.

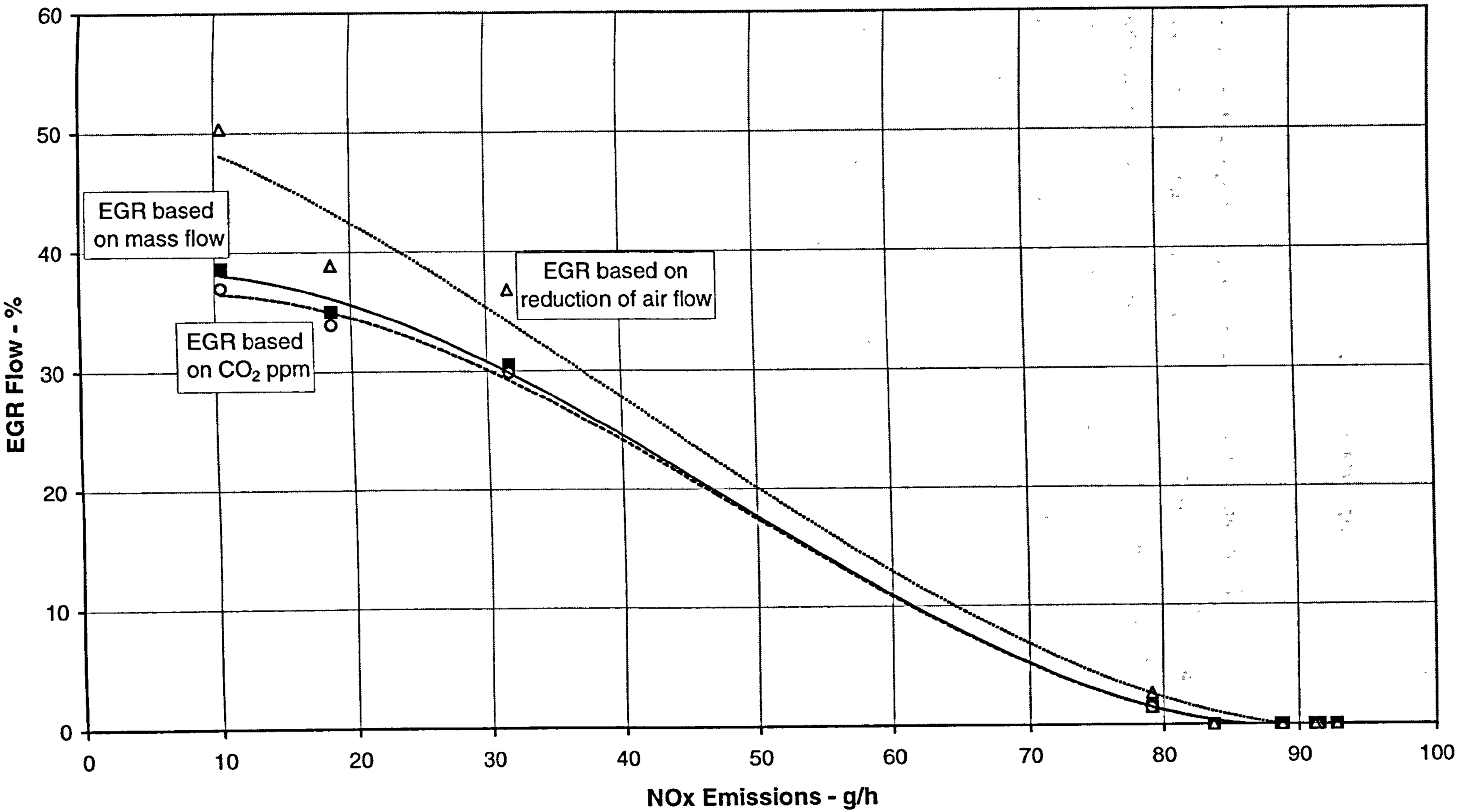

Figure 7.35 Comparison of methods of calculating EGR flow at 1900 rpm 5.7 bar BMEP (80Nm) with VNT vanes fully closed.

Chapter 8

Conclusions

This study has been undertaken to investigate the mechanisms by which oxides of nitrogen are formed during diesel combustion and to review the current methods of controlling their emissions, such as fuel injection timing retard, EGR and exhaust after-treatment. Experimentation on a 1.8 litre inline 4-cylinder 4-valve/cylinder DI diesel with a variable nozzle turbine (VNT) turbocharger, has demonstrated the concept of "additional" EGR on this small automotive engine. The reasons for achieving lower NOx emissions when using a VNT turbocharger and EGR have been explained.

There is wide consensus that the extended Zeldovich mechanism for thermal NO formation is the mechanism responsible for the vast majority of NO formed in premixed and diffusion combustion of hydrocarbon fuels at elevated pressures and temperatures.

$$O + N_2 \Leftrightarrow NO + N$$

$$N + O_2 \Leftrightarrow NO + O$$

$$N + OH \Leftrightarrow NO + H$$

From the Zeldovich mechanism rate constants, it is evident that the rate of NO formation rises exponentially with temperature. According to the Zeldovich mechanism, NO is formed by atomic oxygen, which is the result of a 2-step thermal dissociation of the primary reaction products CO_2 and H_2O. The 2-step thermal dissociation is the reason for the temperature sensitivity of NO formation.

Additionally, there are a number of other reactions responsible for the formation of NO during diesel combustion. These are, 'prompt NO' formation, conversion of N_2O to NO, and NO formed from fuel bound nitrogen. These reactions, however, only contribute a small proportion of the total NOx formation.

Oxidation of NO to NO_2 does occur in diesel engines, NO_2 emissions can be as high as 30 to 50 per cent of the total nitrogen oxides from a DI diesel at low load and speed

conditions.

Retarding fuel injection timing will reduce NOx formation by lowering combustion temperatures; this may also cause an increase in HC and smoke emissions, as well as an increase in fuel consumption. Pilot injection delays the development of high-temperature regions and can facilitate injection retard while maintaining fuel consumption, to provide beneficial reductions in NOx emissions.

EGR has been used on production automotive diesel engines since the mid- to late-1980s and remains the most effective way of controlling NO formation. EGR is currently used on all automotive high-speed DI diesel engines for reduction of NOx emissions in order to meet European Stage 2, Stage 3 and Stage 4 standards. A review of the key features of most production EGR systems is included in Chapter 3. EGR reduces NOx formation and emissions by lowering the flame temperature through two effects; by dilution, reducing the oxygen mass fraction, and by a thermal effect, increasing the specific heat capacity of the charge. The dilution effect is by far the greater of the two. Cooling EGR prior to mixing with the intake charge provides further reductions of NOx emissions and is generally beneficial for particulates. The higher volumetric efficiency with cooled EGR leads to an improvement in fuel economy. The use of an EGR cooler is becoming more widespread, in order to meet the stricter emissions standards.

Vacuum operation of the EGR valve and throttle, where fitted, is the most widespread actuation method at present, but electric operation is being introduced to improve the response time.

Early EGR control was by simple on-off schedules. Today on automotive high speed DI diesels, EGR control is electronic, with pre-set maps contained in the ECU. EGR level is set either by feedback from an air mass flow sensor, or from an EGR valve lift transducer.

Water addition, either injected with the intake air charge, or as a water-in-fuel emulsion, will reduce NOx emissions and is more effective in combination with EGR. However it

is impractical for automotive use owing to the relatively large amount of water required and problems with internal corrosion of engine components.

NOx simulations, using the extended Zeldovich mechanism in the Merlin-DEEPC code for an EGR loop, over-predicted NOx emissions at zero and low levels of EGR and under-predicted at high EGR rates. Modified rate constants gave a small improvement in accuracy. Despite these inaccuracies in the absolute levels, the correct trends were predicted for increasing EGR and for changes in injection timing.

For the experimental work, two part load engine conditions were tested, 1900rpm/5.8bar BMEP and 2700rpm/8.0bar BMEP. Using a variable nozzle turbine turbocharger and a modern EGR system with a cooler, lower NOx and particulate emissions at an improved level of fuel consumption were demonstrated, compared to a traditional fixed geometry turbocharger and similar EGR system with an intake throttle. This was achieved by "additional" EGR, whereby the flow of EGR was greater than with the traditional set-up, causing the total volumetric flow into the engine to increase. However, the highest EGR mass flow, achieved by closing the turbine vanes, was not the most efficient method of reducing NOx emissions, since additional pumping work was required, which increased the in-cylinder NOx formation.

The use of a venturi to assist the flow of EGR into the charge air was found to be less efficient than a simple EGR entry, for these part load engine-operating conditions. But further improvements in emissions and fuel consumption could potentially be achieved with a reduction in the flow losses of the EGR system.

Calculation of EGR flow from exhaust and manifold CO_2 readings gives a close correlation to true EGR mass flow calculations. Use of reduction in airflow is not an accurate method for calculating EGR mass flow for turbocharged engines.

New exhaust after-treatment technologies such as selective catalytic reduction (SCR) NOx catalyst systems offer important additional scope that will help engine manufacturers meet emission legislation during the next five to ten years and bring the diesel NOx emissions closer to those of gasoline engines fitted with 3-way catalysts. The highest conversion efficiencies have been demonstrated with urea injection and a

vanadium-titanium catalyst, 65 and 83 per cent have been achieved on the European and FTP-75 cycles, respectively. However, this system requires an additional storage tank for the reactant, which would need replenishing over the life of the vehicle.

References

Abramovich G N, The Theory of Turbulent Jets, MIT Press, 1963, 269.

Ahmad T and Plee S L, Application of Flame Temperature Correlations to Emissions from a Direct-Injection Diesel Engine, SAE paper 831734, October 1983.

Ahmad T and Plee SL, Application of Flame Temperature Correlations to Emissions from a Direct-Injection Diesel Engine, SAE paper 831734, November 1983.

Ambs JL and McClure BT, The Influence of Oxidation Catalysts on NO2 in Diesel Exhaust, SAE paper 932494, 1993.

Amsden A A, Butler T D and O'Rourke P J, The KIVA-II computer program for transient multidimensional chemically reactive flows with sprays, SAE paper 872072, 1987.

Amsden A A, Butler T D, O'Rourke P J and Ramshaw J D, KIVA - A comprehensive model for 2-D and 3-D engine simulations, SAE paper 850554, 1985.

Ando H and Asaba T, Int J Chem Kinet, **8,** 259-275, 1976.

Andrews G E and Nurein A M, A non-metallic diesel fuel additive for the reduction of particulate emissions, I Mech E Seminar on Fuels for Automotive and Industrial Diesel Engines, MEP, November 1990.

Andrews G E and Salih F M, Ethanol/diesel mixtures for reduced NOx and particulate emissions, I Mech E Seminar on Fuels for Automotive and Industrial Diesel Engines, MEP, November 1990.

Anisits F and Kratochwill H, The new BMW 6 Cylinder Diesel Engine, 7. Aachener Kolloquium Fahrzeug- und Motorentechnik 1998.

Anisits F, Borgmann K, Kratochwill H and Steinparzer F, Der erste Achtzylinder-Dieselmotor mit Direktinspritzung von BMW (The First Direct-Injection Eight-Cylinder Diesel Engine from BMW), MTZ Motortechnische Zeitschrift 60 (1999) 6.

Anisits F, Borgmann K, Kratochwill H and Steinparzer F, Der neue BMW Vierzylinder-Dieselmotor (The New BMW Four-Cylinder Diesel Engine, ATZ/MTZ-Sonderausgabe, 1998.

Anisits F, Borgmann K, Kratochwill H and Steinparzer F, Der neue BMW Sechszylinder-Dieselmotor (BMW's New Six-Cylinder Diesel, MTZ Motortechnische

Zeitschrift 59 (1998) 11.

Anon, MAN trucks first to opt for EGR, Auto Industry, p 6, December 1999.

Anon, No end to the diesel boom, Automobile International Management, 4/2000, pp 34-35, December 2000.

Anon, Stricter than Californians, Automobile International Management, pp 20-22, January 1998.

Arcoumanis C, Bae C, Nagwaney A and Whitelaw J H, Effect of EGR on Combustion Development in a 1.9 L DI Diesel Optical Engine, SAE paper 950850, 1995.

Arcoumanis C, Nagwaney A, Hentschel W and Ropke S, Effect of EGR on Spray Development, Combustion and Emissions in a 1.9 L Direct-Injection Diesel Engine, SAE paper 952356, October 1995.

Aoyagi Y, Kamimoto T, Matsui Y and Matsuoka S, A Gas Sampling Study on the Formation Processes of Soot and NO in a DI Diesel Engine, SAE paper 800254, SAE Trans vol 89, 1980.

Aoyama T, Mizuta J and Oshima Y, NOx Reduction by Injection Control, SAE paper 900637, 1990.

Ayoub N S and Reitz R D, Multidimensional modelling of fuel composition Effects on combustion and cold starting in diesel engines, SAE paper 952425 (SP-1123), 1995.

Bach M, Jablonski J, Bauder R, Hoffmann H, Endres H and Poelzl, H-W, Der neue V8-TDI-Motor von Audi, Teil 2: Konstruktion und Mechanik, 10 Jahre TDI-Motor von Audi, ATZ/MTZ-Sonderausgabe, 10 Jahre TDI-Motor von Audi, September 1999.

Baert R S G, Beckman D E and Veen A W M J, Efficient EGR Technology for Future HD Diesel Engine Emissions TargetsSAE Paper 1999-01-0837, March, 1999.

Baert R, Beckman D E and Veen A W M J, EGR technology for lowest emissions, paper C517/034/96, I Mech E International Seminar on Application of Powertrain and Fuel Technologies to Meet Emissions Standards, 24-26 June 1996.

Balian R A, In-Cylinder and Exhaust Emissions Analysis with EGR, Project Report for Ford Motor Company, Brunel University, December 1995.

Balian R A, In-Cylinder NOx Sampling of a 2.5 litre DI/TC Ford diesel engine, End of Year Report, Project Report for Ford Motor Company, Brunel University, June 1992.

Bartlett et al, Diesel fuel aromatic content and its relationship with emissions from

diesel engines, COCAWE report no. 92/54, June 1992.

Bartok W and Sarofim A F, Fossil Fuel Combustion, A Source Book, John Wiley and Sons Inc, 1991.

Bauder R, Dorsch W, Endres H, Franke G, Jablonski J, Reuss T und Staehle H, Der Audi V6-TDI-Motor schadstoffarm und leistungsgesteigert, ATZ/MTZ-Sonderausgabe, 10 Jahre TDI-Motor von Audi, September 1999.

Bauder R, Dorsch W, Poelzl H-W and Mikulic L, The New Audi V6 Turbo-Diesel Engine with Direct Injection and Four Valves per Cylinder, Part1: General concept and thermodynamics, 18th International Vienna Engine Symposium 1997, Vol 1, pp48-69.

Baulch D L, Drysdale D D and Horne D G, Evaluated Kinetic Data for High Temperature Reactions, Vol 2, Butterworths, London, 1973.

Baulch D L, Drysdale D D and Horne D G, Report No 5, Dept of Physical Chemistry, The University of Leeds, 1969.

Bazari Z and French BA, Performance and Emissions Trade-Offs for a HSDI Diesel Engine - An Optimization Study, SAE paper 930592, 1993.

Bazari Z, A DI Diesel Combustion and Emission Predictive Capability for use in Cycle Simulation, SAE Paper 920462, February 1992.

Bazari Z, Diesel Exhaust Emissions Prediction Under Transient Operating Conditions, SAE paper 940666, February 1994.

Benjamin S F, Weaving J H, Glynn D R, Markatos N C and Spalding D B, Development of a mathematical model of flow, heat transfer and combustion in a stratified charge engine, I Mech E Stratified Charge Automotive Engine Conference, C403/80, p91, 1980.

Berger H, Eichlseder H and Steinmayr T, Das EU-3 Abgaskonzept fur den neuen Vierzylinder-Dieselmotor von BMW (The EU-3 Exhaust Concept for the New Four-Cylinder Diesel Engine), MTZ Motortechnische Zeitschrift 59 (1998) 5.

Bird GL, Duffy K A and Tolan LE, Development and application of the Stanadyne new slim tip pencil injector. I Mech E Seminar on Diesel fuel systems, 10-11 October 1989, p 133 (Mechanical Engineering Publications, London).

Bittker D A and Scullin V J, GCKP84-General Chemical Kinetics Code for Gas Phase Flow and Bench Processes Including Heat Transfer Effects, NASA Technical Paper 2320, 1984.

Blauwens J, Smets B and Peeters J, 16th Int Symp Combust, Combustion Institute, Pittsburgh, 1055-1064, 1977.

Bostock PG and Cooper L, Turbocharging the Ford 2.5 HSDI diesel engine. I Mech E Seminar on Diesel fuel injection systems, 14-15 April 1992 (Mechanical Engineering Publications, London).

Bower GR and Foster DE, The Effect of Split Injection on Soot and NOx Production in an Engine-Fed Combustion Chamber, SAE paper 932655, 1993.

Bowman C T, Control of combustion-generated nitrogen oxide emissions: technology driven by regulation, Twenty-Fourth Symposium (International) on Combustion, The Combustion Institute, pp 859-878, 1992.

Bowman C T, Kinetics of Pollutant Formation and Destruction in Combustion, Prog Energy Combust Sci, vol 1, pp 33-45, 1975.

Bradley J N and Craggs X, 15th Int Symp Combust, Combustion Institute, Pittsburgh, 833-842, 1975.

Broering LC and Holtman L W, Effect of Diesel Fuel Properties on Emissions and Performance, SAE paper 740692, September, 1974.

Broering LC and Wulfhurst DE, Design Factors That Affect Diesel Emissions, Bascom RC, SAE paper 710484, 1971.

Bromly J H, Barnes F J and Little L H, The effect of low levels of CO, H2 and hydrocarbons on NO2/NO ratios in heated gases, Journal of the Institute of Energy (89) 1988.

Bromly J H, et al, An experimental investigation of the mutually sensitised oxidation of nitric oxide and n-butane, Twenty-fourth Symposium (Int) on Combustion, The Combustion Institute, 1992, pp 899-907.

Brown A J and Heywood J B, A fundamentally-based stochastic mixing model method for predicting NO and soot emissions from direct-injection diesel engines, Calculations of Turbulent Reactive Flows-AMD- Vol 81 (Book Number H00350) The ASME pp 293-312, 1987.

Brueggemann H, Arbeiter E and Reifenrath, The New V8 CDI, Lightweight Design by DaimlerChrysler: Diesel Engines with Common Rail Injection – State of the Development and Forecast, 8. Aachener Kolloquium Fahrzeug- und Motorentechnik 1999.

Brueggemann H, Arbeiter E, Fausten H, Reifenrath H P, Roth H and Weisbarth, M, Der neue V8-Pkw-Dieselmotor von Mercedes-Benz (The New Mercedes-Benz V-8 Passenger Car Diesel Engine), MTZ Motortechnische Zeitschrift 61 (2000) 6.

Brueggemann V H and Wamser M, Die neuen Dieselmotoren OM 668 mit Common-Rail-Direkteinspritzung fur die Mercedes-Benz-A-Klasse, Teil 1: Motorkonstruktion und mechanischer Aufbau, Sonderausgabe ATZ und MTZ, 1997.

Burgler L, Herzog P L and Zelenka P, Strategies to meet US 1994/5 diesel engine Federal emission legislation for HSDI diesel engine powered vehicles, Proc Instn Mech Engrs Vol 206, 1992.

Burley H A and Rosebrock T L, Automotive Diesel Engines - Fuel Composition vs Particulates, SAE paper 790923, October 1979.

Campbell I M and Thrush B A, Reactivity of Hydrogen to Atomic Nitrogen and Atomic Oxygen, Trans Faraday Soc, 1968, Vol 64, Part 5 pp 1265-1274.

Carnochan WA and Horrocks RW, The Ford 1.8 IDI TCI Diesel in Mondeo and future developments, Aachen Colloquium, 1993.

Caton J A and Siebers D L, Combustion & Flame 79:31-46, 1990

Caton J A and Siebers D L, *Comparison of Nitric Oxide Removal by Cyanuric Acid* and by Ammonia, Combust Sci and Tech, 1989 Vol 65, pp 277-293.

Charlton S J, Control Technologies for Compression-Ignition Engines, Handbook of Air Pollution from Internal Combustion Engines, Ed E Sher, Academic Press, 1998.

Chigier N, Energy, Combustion and Environment, McGraw-Hill Book Company, 1981.

Chikahisa T, Konno M and Murayama T, Analysis of NO Formation Characteristics and Control Concepts in Diesel Engines from NO Reaction-Kinetic Considerations, SAE paper 950215, 1995.

Chikahisa T, Konno M, Murayama T and Kumagai T, Analysis of NO formation characteristics and its control concepts in diesel engines from NO reaction kinetics, 948047, Proceedings 941, JSAE Technical Paper No 9432985 (JSAE).

Chmela F G, Werlberger P and Cartellieri W P, Parameters Affecting In-Cylinder Soot and NOx Formation in a Direct Injection Diesel Engine, FISITA-Congress; 7-11 June 1992, London England.

Clark T C, Garnett S H and Kistiakowsky G B, J Chem Phys **51,** 2885-91, 1969.

Clyne M A A and Thrush B A, Proc Royal Society, London, A261, 259, 1961.

Cook DH and Law CK, A Preliminary Study on the Utilization of Water-in-Oil Emulsions in Diesel Engines, Combustion Science and Technology 1978, Vol 18 pp217-221.

Cooper BJ and Thoss J E, Role of NO in Diesel Particulate Emission Control, SAE paper 890404, 1989.

Corcione F E, Fusco A, Valentino G and Papetti F, Numerical and Experimental Analysis of Diesel Air Fuel Mixing, SAE paper 931948, 1993.

Curtis E W, Uludogan A and Reitz R D, A new high pressure droplet vapourization model for diesel engine modelling, SAE paper 952431 (SP-1123), 1995.

Davies CP, personal communication, March 2001.

Dec J E, A Conceptual Model of DI Diesel Combustion Based on Laser-Sheet Imaging, SAE paper 970873, February 1997.

Deeba M et al, Catalytic Abatement of Nox from Diesel Engines: Development of Four Way Catalyst, SAE paper 952491, October, 1995.

Dent J C and Metha P S, Phenomenological Combustion Model for a Quiescent Chamber Engine, SAE paper 811235, 1981.

Dent J C, Metha P S and Swan J, A Predictive Model for Automotive DI Diesel Engine Performance and Smoke Emission, I Mech E paper C 126/82, 1982.

Desai R R, Gaynor E, Watson H C and Rigby G R, Giving Standard Diesel Fuels Premium Performance Using Oxygen-Enriched Air in Diesel Engines, SAE paper 932806, 1993.

Dietz M, Lambert L Nester U and Brueggemann H, The New Common-Rail Direct-Injection Diesel Engine for the Smart, Part 2: Combustion and Engine Management, MTZ Motortechnische Zeitschrift 60 (1999) 12.

Duernholz M, Eifler G and Endres H, Exhaust-gas recirculation - a measure to reduce exhaust emissions of a DI diesel engine, SAE paper 920725, 1992.

Duernholz M, Eifler G and Endres H, Reducing Emissions of DI Diesel Engines by Exhaust Gas Recirculation, 3rd Aachen Seminar "Vehicle and Engine Technology," Aachen, 1991.

Duggal V K, Kuo T W, Mukerjee T, Przekwas A J and Singhai A K, Three-dimensional modelling of in-cylinder processes in DI diesel engines, SAE paper 840227, 1984.

Duggal V K, Priede T and Khan I M, A Study of Pollutant Formation within the Combustion Space of a Diesel Engine, SAE paper 780227, SAE Trans vol 87, 1978.

Dunne M and Frost B, Vehicle Emission Standards Past, Present and Future, 21st century emissions technology conference, I Mech E, London, 4-5th December, 2000.

Duxbury J and Pratt N H, 15th Int Symp Combust, Combustion Institute, Pittsburgh, 843-855, 1975.

Elsaesser A, Braun R and Jensen H, Air Supply Modules for DaimlerChtysler's New Common Rail Diesel Engines OM611 and OM612, MTZ Worldwide, MTZ Motortechnische Zeitschrift 61 (2000) 3.

Engler B H, Leyrer J, Lox E S and Ostgathe K, Catalytic Reduction of NOx with Hydrocarbons under Lean Diesel Exhaust Gas Conditions, SAE paper 930735, 1993.

Fetterman P and Shank G, Cool running for clean diesels, Infineum Insight, Issue number 5, March 2000.

Flanigan C, Litzinger T A and Graves R L, The Effect of Aromatics and Cycloparaffins on DI Diesel Emissions, SAE paper 892130, 1989.

Flower W L, Hanson R K and Kruger C H, Combust Sci Technol, **15,** 115-128, 1977.

Ford Motor Company, Competitive Analysis and Teardown, BMW 320 2.0L TD Diesel Board Pictures, Dunton, England, May 1999.

Ford Motor Company, Competitive Analysis and Teardown, Mercedes-Benz 1.7 CDI Diesel Board Pictures, Dunton, England, March 1999.

Fourth Report of the Photochemical Oxidants Review Group, 1997, Ozone in the United Kingdom, published 1997, ISBN: 1-870 303-30-9.

Fraser B, Regulation Review, European Union, 98/69/EC, 1999/102/EC and 2001/1/EC St III, updated 22 February 2001, Ford Motor Company internal report.

Fusco A, et al , An experimental and numerical study of air-fuel mixing and combustion of a divided-chamber diesel engine system, SAE paper 952427, 1995.

Gardiner W C, Combustion Chemistry, Springer-Verlag New York Inc, 1984

Garo A, Hilaire C and Puechberty D, Combust Sci Technol, 86:87-103, 1992.

Glarborg P, Lilleheie N I, Byggstoyl S, Magnussen B F, Kilpinen P and Hupa M, 24th Symp (Int) on Combustion, Sydney, 889, 1992.

Glarborg P, Miller J A and Kee R J, Kinetic Modeling and Sensitivity Analysis of

Nitrogen Oxide Formation in Well-Stirred Reactors, Combustion and Flame 65:177-202, 1986.

Glassman I, Combustion, Third Edition, Academic Press, 1996.

Gosman A D and Marooney C J, Development and Validation of Computer Models of In-Cylinder Flow and Combustion in Diesel and Spark Ignition Engines, I Mech E , Auto Tech 89 C399/19, November, 1989.

Gosman A D, Krali C, Marooney C and Theodossopoulos P, The development of the SPEED code for Diesel combustion simulation, Proc 3rd Int Conf Innovation and Reliability in Automotive Design and Testing, ATA and DMTI (1992) 653-662.

Gosman A D, Krali C, Marooney C J and Theodopossopoulos P, Development strategies for diesel combustion simulation using the SPEED code, I Mech E, C448/035 (1992) 21-27.

Hammerle R H et al, Emissions from Diesel Vehicles with and without Lean Nox and Oxidation Catalysts and Particulate Traps, SAE paper 952391, October 1995.

Handbook on Air Pollution and Health, The Stationery Office, published 1997, ISBN: 011 322096 0.

Hansen R K, Flower W L and Kruger C H, Combust Sci Technol, **9,** 79-86, 1974.

Hanson RK and Salimian S, Survey of Rate Constants in the N/H/O System, Combustion Chemistry (W C Gardiner, Jr, ed), pp361-421, Springer-Verlag, New York, 1984.

Harrington J A and Shishu R C, A Single-Cylinder Engine Study of the Effects of Fuel Type, Fuel Stoichiometry and Hydrogen-to-Carbon Ratio and CO, NO and HC Exhaust Emissions, SAE paper 730476, 1973.

Harris R J, Nasralla M and Williams A, Combust Sci Technol **14,** 85-94, 1976.

Havenith C, Needham J R, Nicol A J and Such C H, Low Emission Heavy Duty Diesel Engine for Europe, SAE paper 932959, 1993.

Havenith C, Verbeek R P, Heaton D M and van Sloten P, Development of a Urea DeNOx Catalyst Concept for European Ultra-Low Emission Heavy-Duty Diesel Engines, SAE paper 952652, November 1995.

Haverinth C, Such CH, Porter BC and Nicol AJ, Demonstration of a Euro 3 Heavy-Duty Diesel Engine using Exhaust Gas Recirculation, 18th International Vienna Motor Symposium, 24-25 April 1997.

Hawley J G, Wallace F J, Pease A C, Cox A, Horrocks R W and Bird G L, Comparison of variable geometry turbocharging (VGT) over conventional wastegated machines to achieve lower emissionsI Mech E Autotech Conference, Paper No. C524/070/97, Birmingham, 1997.

Hawley J G, Wallace F J, Pease A C, Cox A, Horrocks R W and Bird G L, Reduction of Steady State NOx Levels from an Automotive Diesel Engine Using Optimised VGT/EGR Schedules, SAE paper 1999-01-0835, March 1999.

Hawley JG, Brace CJ, Wallace FJ and Horrocks RW, Combustion-Related Emissions in CI Engines, Handbook of Air Pollution from Internal Combustion Engines, edited E Sher, Academic Press 1998, ISBN: 0-12-639855-0

Heap M P, Chen S L, Kramlich J C, McCarthy J M and Pershing D W, An advanced selective reduction process for NOx control, Nature Vol 335 13 October 1988 pp 620-622.

Heaton D M, Martin B, Bertoli C and Giavazzi F, Fuel Composition Efects on Diesel Engine Emissions - a Joint European Study, Inst Mech Engrs, April 1993.

Heck R M, Chen J M and Speronello B K, Operating Characteristics and Commercial Operating Experience with High Temperature SCR NOx Catalyst, Environmental Progress (Vol 13 No 4), November 1994.

Heimrich M J and Deviney M L, Lean NOx Catalyst Evaluation and Characterization, SAE paper 930736, 1993.

Heisler H, Advanced Engine Technology, pub Arnold, 1997, ISBN 0 340 56822 4.

Held W, Konig A, Richter T and Puppe L, Catalytic NOX Reduction in Net Oxidizing Gas, SAE paper 900496, Febrary 1990.

Hentschel W, Schindler K-P and Haahtela O, European Diesel Research IDEA-Experimental Results from DI Diesel Engine Investigations, SAE paper 941954, 1994.

Herron J T, J Chem Phys, **35,** 1138, 1961

Herron J T, J Res Nat Bur Stand, **65A,** 411, 1961.

Hewson J C and Bollig M, Reduced Mechanisms for NOx Emissions from hydrocarbon diffusion flames, 26th Symposium (Int) on Combustion, The Combustion Inst, Pittsburg, 1996.

Heywood J B, Internal Combustion Engine Fundamentals, McGraw-Hill Book Company, McGraw-Hill Book Company 1988, ISBN: 0-07-100499-8.

Hilliard J C and Wheeler R W, Nitrogen Dioxide in Engine Exhaust, SAE paper 790691, June 1979.

Hiroyasu H and Kadota T, Models for Combustion and Formation of Nitric Oxide and Soot in Direct Injection Diesel Engines, SAE paper 760129, 1976.

Hiroyasu H, Diesel Engine Combustion and Its Modeling, in Proceedings on International Symposium on Diagnostics and Modeling of Combustion in Reciprocating Engines, COMODIA 85, pp 53-75, Tokyo, September 4-6, 1985.

Hori M et al, The effect of low-concentration fuels on the conversion of nitric oxide to nitrogen dioxide, Twenty-Fourth Symposium (Int) on Combustion, The Combustion Institute, 1992, pp 909-916

Horrocks R W and Robertson P, Light-duty diesel developments for low emissions and low fuel consumption, 4th International Conference and Exhibition, Brussels, Belgium, September, 1996.

Horrocks R W, Developments in high speed direct injection Diesel engines, 6. Aachener Kolloquium, Aachen, 20-22 October, 1997.

Horrocks R W, Light-duty diesels - an update on the emissions challenge, Proc Instn Mech Engrs, Part D, **208**, 289 - 298, 1994.

Horrocks R W, Light-duty diesels - the emissions challenge, Proc Instn Mech Engrs, Part D, **206**, 249 - 255, 1992.

Horrocks R W, Robertson P S, Brohmer A M and Heuser G, Entwicklung schnellaufender 4-Ventil-Direkteinspritz-Dieselmotoren, Pkw-Dieselmotoren Haus der Technik, Essen, Germany, June 1995.

Hosier C, European Emissions Stage V Forecast, VRD EU/M/216, issued 12 July 2000, Ford Motor Company Ltd internal report.

Iida N and Watanabe J, Surrounding Gas Condition Effects on NOx and Particulate, COMODIA 90, Proc Int Sym Diagnostics and Modeling of Combustion in Internal Combustion Engines, Sept 1990.

Iida N, and Sato G T, Temperature and Mixing Effects on NOx and Particulate, SAE paper 880424, 1988.

Ikegami M, Shioji M and Koike M, A stochastic approach to model the combustion process in direct-injection diesel engines, 20th Symp (Int) Combust pp 217-224, The Combustion Institute, 1984.

Ishida M and Chen Z L, An Analysis of the Added Water Effect on NO Formation in DI Diesel Engines, SAE paper 941691, 1994.

Ishida M and Chen Z-L, An analysis of the added water effect on NO formation in DI diesel engines SAE paper 941691, SP-1050, 1994.

Ishida M and Chen Z-L, An Analysis of the Added Water Effect on NO Formation in DI Diesel Engines, SAE paper 941691, September 1994.

Ishida M, Chen Z L, Veki H and Sakguchi D, Combustion analysis by Two-Zone Model in a DI Diesel Engine, Proc of Int Symposium COMODIA 94 (1994)

Ishiguro J, Kidoguchi Y and Ikegami M, Three-dimensional simulation of the diesel combustion process, JSME Int J, Series II, 31 (1), 158-165, 1988.

Johnson G M and Smith M Y, Emissions of Nitrogen Dioxide from a Large Gas Turbine Power Station, Combust Sci Technol. **19**, 67 1978.

Jost K, A diesel in your future? Editorial, Automotive Engineering International, January 2001, Volume 109, No 1, pp 6.

Jost K, New Diesel V8 for S-Class, Automotive Engineering International, January 2001, Volume 109, No 1, pp 78-80.

Kamimoto T and Kobayashi H, Combustion Processes in Diesel Engines, Prog Energy Combust Sci 1991 Vol 17 pp 163-189, 1991.

Kamimoto T, Aoyagi Y, Matsui Y and Matsuoka S, The Effect of some Engine Variables on Measured Rates of Air Entrainment and Heat Release in a DI Diesel Engine, SAE paper 800253, 1980.

Kaneko Y, Kobayashi H and Komagome R, The Effects of Exhaust Gas Recirculation and Residual Gas on Engine Emissions and Fuel Economy, SAE paper 750414, 1975.

Kato S, Onishi S, Tanabe H and Sato G T, Development of Low Emission Diesel Engine by Impingement of Fuel Jet, SAE paper 921645, 1992.

Kato S, Onishi S, Tanabe H and Sato G T, Development of OSKA-DH Diesel Engine Using Fuel Jet Impingement and Diffusion Investigation of Mixture Formation and Combustion, SAE paper 940667, 1994.

Kaufman F and Decker L J, 7th Int Symp Combust, Butterworths, London, 57-60, 1959.

Ketcher D, Status of passive diesel lean NOx catalyst tests, internal Ford report, February 1997.

Khan I M and Wang C H T, Factors affecting emissions of smoke and gaseous pollutants from direct injection diesel engines, I Mech E, C151/71, 1971.

Khan I M, Greeves G and Probert D M, Prediction of soot and nitric oxide concentrations in diesel engine exhaust, Instn Mech Engrs, C142/71, 1971.

Kistiakowsky G B and Volpi G G, J Chem Phys, **27,** 1141, 1957.

Klingmann R, Fick W and Brueggemann H, The New Common Rail Direct Injection Diesel Engines for the Updated E-Class, Part 1: Engine Design and Mechanical Layout, MTZ World wide, MTZ Motortechnische Zeitschrift 60 (1999) 7/8.

Kong S C and Reitz R D, Multidimensional Modeling of Diesel Ignition and Combustion Using a Multistep Kinetics Model, paper 93-ICE-22 ASME Transactions, Journal of Engineering for Gas Turbines and Power, Vol 115 No 4 pp 781-789, 1993.

Kong S-C, Han Z and Reitz R D, The Development and Application of a Diesel Ignition and Combustion Model for Multidimensional Engine Simulation, SAE paper 950278 (SP-1101), 1995.

Kong S-C, Ricart LM and Reitz R D, In-Cylinder Diesel Flame Imaging Compared with Numerical Computations, SAE paper 950455 (SP-1090), 1995.

Konno M, Chikahisa T and Murayama T, An Investigation on the Simultaneous Reduction of Particulate and NOx by Controlling Both the Turbulence and the Mixture Formation in DI Diesel Engines, SAE paper 932797, 1993.

Konno M, Chikahisa T, Murayama T and Iwamoto M, Catalytic Reduction of NOx in Actual Diesel Engine Exhaust, SAE paper 920091, 1992.

Kretschmer C B and Peterson H L, J Chem Phys, **39,** 1772, 1963.

Kyriakides S C, Dent J C and Mehta P S, Phenomenological Diesel Combustion Model Including Smoke and NO Emissions, SAE paper 860330, February 1986.

Ladommatos N, Abdelhalim S M, Zhao H and Hu Z, The Dilution, Chemical and Thermal Effects of Exhaust Gas Recirculation on Diesel Engine Emissions - Part 1: Effect of Reducing Inlet Charge Oxygen, SAE paper 961165, May 1996.

Ladommatos N, Abdelhalim S M, Zhao H and Hu Z, The Dilution, Chemical and Thermal Effects of Exhaust Gas Recirculation on Diesel Engine Emissions - Part 2: Effect of Carbon Dioxide, SAE paper 961167 May 1996.

Ladommatos N, Abdelhalim S M, Zhao H and Hu Z, The Effects of Carbon Dioxide in EGR on Diesel Engine Emissions, Proceedings of International Seminar on

Application of Powertrain and Fuel Technologies to Meet Emissions Standards, pp.157-174, Institution of Mechanical Engineers, 1996.

Ladommatos N, Balian R, Horrocks R and Cooper L, The Effect of Exhaust Gas Recirculation on Combustion and Nox Emissions in a High-Speed Direct-Injection Diesel Engine, SAE paper 960840, February 1996.

Ladommatos N, Parsi M and Knowles A, The effect of fuel cetane improver on diesel pollutant emissions, Fuel 1996 Vol 75 No 1.

Ladommatos N, Rubenstein P and Bennett P, Some effects of molecular structure of single hydrocarbons on sooting tendency, Fuel 1996 Vol 75 No 2.

Lange W W et al, The Influence of Fuel Properties on Exhaust Emissions from Advanced Mercedes Benz Diesel Engines, SAE paper 932685, October 1993.

Lapuerta M, Salavert J M and Domenech C, Modelling and Experimental Study about the Effect of Exhaust Gas Recirculation on Diesel Engine Combustion and Emissions, SAE paper 950216, February 1995.

Lavoie G A, Heywood J B and Keck J C, Experimental and Theoretical Study of Nitric Oxide Formation in Internal Combustion Engines, , Combustion Science and Technology, 1970, Vol 1 pp 313-326.

Lawrence PJ and Evans R W, The Ford 1.8L Four Cylinder Turbocharged Diesel Engine for Passenger Car Applicationn, SAE paper 901716, September 1990.

Lawrence PJ, Knight D and Carnochan WA, The development of a 1.8 L diesel engine for passenger car application, I Mech E paper C382/070, 1989.

Lawrence PJ, Lake P, Turtle D, Taylor T, Carnochan W, Finch J, Gellett T and Woelfle M, The All New Duratorq Direct Injection Diesel Engines in the Ford Transit, MTZ Motortechnische Zeitschrift 61 (2000) 1.

Lawrence PJ, The New 1.8L Endura – DI Diesel Engine for the Ford Focus, 7 Aachener Kolloquium, Aachen 5-7 October, 1998.

Lenner M, Linqvist O, Ljungstrom, Lundgren I and Rosen A, Catalysis of the Low Temperature Oxidation of Nitric Oxide by Diesel Particulates, SAE paper 821037, 1982.

Lenner, M, Nitrogen dioxide in exhaust emissions from motor vehicles, Atmospheric Environment Vol 21 No 1, pp 37-43, 1987.

Leyrer J, Lox ES and Strehlau W, Design Aspects of Lean Nox Catalysts for

Gasoline and Diesel Engine Applications, SAE paper 952495, October 1995.

Liotta F J and Montalvo D M, The Effect of Oxygenated Fuels on Emissions from a Modern Heavy-Duty Diesel Engine, SAE paper 932734, (SP-994), 1993

Lipkea W H and DeJoode A D, A model of a direct injection diesel combustion system for use in cycle simulation and optimization studies, SAE paper 870573, 1987.

Lueders H et al, An Urea Lean NOx Catalyst System for Light Duty Diesel Vehicles, SAE paper 952493, October 1995.

Lyon R K, Thermal DeNOx, Controlling nitrogen oxides emissions by a noncatalytic process, Environ Sci Technol Vol 21 No 3 1987 pp231-235, 1987.

Magnussen B F and Hjertager B H, On mathematical modelling of turbulent combustion with special emphasis on soot formation and combustion, 16th Symp (Int) Combust pp 719-729, The Combustion Institute, 1976.

Malte P C and Pratt D T, The role of energy-releasing kinetics in NOx formation: fuel lean, jet_stirred CO-air combustion, Combust Sci Tech 9, 221-231, 1974.

Mansouri S H, Heywood J B and Radhakrishnan K, Divided-Chamber Diesel Engine, Part I: Cycle-Simulation Which Predicts Performance and Emissions, SAE paper 820273, SAE Trans vol 91, 1982.

Marshall WF and Hurn RW, Modifying Diesel Engine Operating Parameters to Reduce Emissions, Bu Mines RI 7579, 1971.

Martin B and Bigeard P H, Hydrotreatment of Diesel Fuels - Its Impact on Light-Duty Diesel Engine Pollutants, SAE paper 922268, October 1992.

Mase Y, Kawashima J and Sato T, and Eguchi M, Nissan's New Multivalve DI Diesel Engine Series, SAE paper 981039, February 1998.

Mavroyannis C and Winkler C A, Chemical Reactions in the Lower and Upper Atmosphere, Proc Int Symo, Stanford, 1961, 287, Interscience, New York, 1961.

McCarthy et al, Diesel Fuel Property Effects on Exhaust Emissions from a Heavy Duty Diesel Engine that Meets 1994 Emissions Requirements, SAE paper 922267, October 1992.

McConnell G, Oxides of Nitrogen in Diesel Engine Exhaust Gas: Their Formation and Control, Proc Inst Mech Engrs 178, 1963.

McCullough R W, Kruger C H and Hansen R K, Combust Sci Technol, **15,** 213-223, 1977.

Mellor A M et al, Skeletal Mechanism for NOx Chemistry in Diesel Engines, SAE paper 981450, 1998.

Menne R J, Lawrence P J, Horrocks R W and Robertson P S, Ford 4-Valve Light-Duty DI Diesel Developments, SAE paper 941926, October 1994.

Mikulic L, Kuhn M, Schommers J and Willig E, Exhaust Emision Optimization of DI Diesel Passenger Car Engine with High Pressure Fuel Injection and EGR, SAE paper 931035, 1993.

Miller J A , Branch M C and Lee R J, A Chemical Kinetic Model for the Selective Reduction of Nitric Oxide by Ammonia, Combustion and Flame 43:81-98, 1981.

Miller J A and Bowman C T, Mechanism and modelling of nitrogen chemistry in combustion, Proc Energy Combust Sci Vol 15, pp 287-338, 1989.

Miller J A, Branch M C, McLean W J, Chandler D W, Smooke M D and Lee R J, The Conversion of HCN and N2 in H2-O2-HCN-Ar Flames at Low Pressure, Twentieth Symposium (Int) on Combustion, The Combustion Institute, 1984, pp 673-684.

Miller R, Davis G, Lavoie G, Newman C and Gardner T, A Super-Extended Zel'dovich Mechanism for NOx Modeling and Engine Calibration, SAE paper 980781, February 1998.

Mitchell D L, Pinson J A and Litzinger T A, The Effects of Simulated EGR via Intake Air Dilution on Combustion in an Optically Accessible DI Diesel Engine, SAE paper 932798, 1993.

Miyamoto N et al, Description of Diesel Emissions by Individual Fuel Properties, SAE paper 922221, October 1992.

Monat J P, Hanson R K and Kruger C H, 17th Int Symp Combust, Combustion Institute, Pittsburgh, 543-552, 1979.

Monroe D R, Dimaggio C L, Beck D D and Matekunas FA, Evaluation of a Cu/Zeolite Catalyst to Remove NOx from Lean Exhaust, SAE paper 930737, 1993.

Montreuil C N and Gandhi H S, Selective catalytic reduction of NO in a lean environment by copper exchanged type ZSM5 zeolites, Ford Technical Report no. SR-92-35, March, 1992.

Montreuil C N, An investigation into the NO decomposition characteristics of copper exchanged type ZSM5 zeolite, Ford Technical Report no. SR-92-07, January, 1992.

Muramatsu G, Abe A, Furuyama M and Yoshida K, Catalytic Reduction of NOx in

Diesel Exhaust, SAE paper 930135, (SP-943), 1993.

Nagase K and Funatsu K, A Study of NOx Generation Mechanism in Diesel Exhaust Gas, SAE paper 901615, Sept 1990

Nandi M, Jacobs D C Liotta F J Jr and Kesling H S Jr, The Performance of a Peroxide-Based Cetane Improvement Additive in Different Diesel Fuels, SAE paper 942019, 1994.

Nefischer P, Steinparzer F and Stuetz W, Der Ladungswechsel des neuen BMW V8 Dieselmotors (Gas Exchange System of the New BMW V8 Diesel Engine), 8. Aachener Kolloquium Fahrzeug- und Motorentechnik 1999.

Neumann K-H, Neyer D and Steht H, The new 3-cylinder diesel engine with high pressure injection from Volkswagen,

Newhall H K and Shahed S M, Kinetics of Nitric Oxide Formation in High-Pressure Flames, Proceedings of Thirteenth International Symposium on Combustion, pp 381-390, The Combustion Institute, 1971.

Odaka M, Koike N, Tsukamoto Y and Narusawa K, Optimizing Control of Nox and Smoke Emissions from DI Engine with EGR and Methanol Fumigation, SAE paper 920468, 1992.

Odaka M, Koike N, Tsukamoto Y, Narusawa K and Yoshida K, Effects of EGR with a Supplemental Manifold Water Injection to Control Exhaust Emissions from Heavy-Duty Diesel Powered Vehicles SAE paper 910739, 1991.

Ohigashi S et al, Heat Capacity Changes Predict Nitrogen Oxides Reduction by Exhaust Gas Recirculation, SAE paper 710010, 1971.

Olikara C and Borman GL, A Computer Program for Calculating Properties of Equilibrium Combustion Products with some Applications to I.C. Engines, SAE paper 750468, February 1975.

Parker RF and Walker JW, Exhaust Emission Control in Medium Swirl Rate Direct Injection Diesel Engines, SAE paper 720755, 1972.

Paterson M A, Kong S C, Hampson G J and Reitz R D, Modeling the Effects of Fuel Injection Characteristics on Diesel Engine Soot and NOx Emissions, SAE paper 940523, 1994.

Patterson D J and Henein N A, Emissions from Combustion Engines and Their Control, Ann Arbor Science Publishers Inc, 1972.

Perez J, Current status and development prospects for passenger-car diesel engines in Europe, Global Powertrain Congress 2000, Detroit, USA, June 6, 2000.

Perry R A and Siebers D L, Rapid reduction of nitrogen oxides in exhaust gas streams, Nature Vol 324 18/25 December 1986.

Perry R A, Kinetics of the reactions of NCO radicals with H2 and NO using laser photolysis-laser induced fluorescence, J Chem Phys 82 (12), 15 June 1985.

Pershing D W and Berkau E E, The Chemistry of Nitrogen Oxides and Control through Combustion Modifications, Advan Chem Ser 1973, 127.

Peters A and Puetz W, The New Four Cylinder Diesel Engine OM611 with Common Rail Injection, Part 2: Combustion and Engine Management, MTZ Worldwide, MTZ Motortechnische Zeitschrift 58 (1997) 12

Phillips L F and Schiff H I, J Chem. Phys., **36,** 1509, 1962.

Piccone A and Rinolfi R, Fiat Third Generation DI Diesel Engines, I Mech E Seminar, Euro IV Challenge, Future Technologies and Systems, London, December 1997.

Pierpont D A, Montgomery D T and Reitz R D, Reducing Particulate and NOx Using Multiple Injections and EGR in a *DI Diesel, SAE paper 950217, 1995.*

Pinchon P, Three dimensional modelling of combustion in a prechamber diesel engine, SAE paper 890666, 1989.

Pipho M J, Kittelson D B and Zarling D D, NO_2 Formation in a Diesel Engine, SAE paper 910231, 1991.

Pischinger R and Cartellieri W, Combustion System Parameters and Their Effect Upon Diesel Engine Exhaust Emissions, SAE paper 720756, 1972.

Pittermann, R, Hinz M and Kauert L, Einfluss von Abgas rueckfuehrung und Kraftstoff-Wasser-Emulsion auf Verbrennungsablauf und Schadstoffbildung im Dieselmotor, (Effect of Exhaust Gas Recirculation and Fuel-Water Emulsion on Combustion and Pollutant in a Diesel Engine), MTZ Motortechnishe Zeitschroft 60 (1999) 12, translation in MTZ worldwide.

Plee S L, Ahmad T and Myers J P, Diesel NOx Emissions - A Simple Correlation Technique for Intake Air Effects, Proceedings of Nineteenth International Symposium on Combustion, pp 1495-1502, The Combustion Institute, Pittsburgh, 1982.

Plee S L, Ahmad T, Myers J P and Siegla D C, Effects of Flame Temperature and Air-Fuel Mixing on Emission of Particulate Carbon from a Divided-Chamber Diesel Engine,

Particulate Carbon - Formation During Combustion, ed Siegla D C and Smith G W, Plenum Press, New York, pp 423-487, 1981.

Plee S L, Ahmad T, Myers J P, Faeth G M and Faeth G M, Diesel NOx emissions - a simple correlation technique for intake air effects, Nineteenth Symposium (International) on Combustion, The Combustion Institute, pp 1495 - 1502, 1982.

Plee SL, Myers JP and Ahmed T, Flame Temperature Correlation for the Effects of Exhaust Gas Recirculation on Diesel Particulate and NOx Emissions, SAE paper 811195, SAE Trans vol 90, 1981.

Polifke et al, A NOx prediction scheme for lean-premixed gas turbine combustion based on detailed chemical kinetics, ASME paper 95-GT-108, 1995.

Pundir B P, Zvonow V A and Gupta C P, Nitric oxide formation in spark-ignition engines with in-cylinder charge non-homogenity of a random nature, Proc Inst Mech Engrs Vol 199 No D3, 1985.

Raine R R, Stone C R and Gould J, Modelling of nitric oxide formation in spark ignition engines with a multizone burned gas, Combustion and Flame 102: 241-255, 1995.

Reitz R D and Rutland C J, 3-D Modeling of Diesel Engine Intake Flow Combustion and Emissions, SAE paper 911789, 1991.

Reitz R D et al, Improvements in 3-D Modeling of Diesel Engine Intake Flow and Combustion, SAE paper 920463, 1992.

Reitz R D et al, Progress in Diesel Engine Intake Flow and Combustion Modeling, SAE paper 932458, 1993.

Rhode W and Weib M, A direct injection turbodiesel engine, Automotive Design Engineering, 1993.

Rhode W, Goekesme S, Liang J R and Schmitt J L, Der nue directinspritzende 1,9 l Dieselmotor von Volkswagen, Volkswagen's new 1.9 DI Diesel engine, 3. Aachener Kolloquium Fahrzeug- und Motorentechnik 1991.

Ropke S, Schweimer G W and Strauss T S, NOx Formation in Diesel Engines for Various Fuels and Intake Gases, SAE paper 950213, February 1995

Rutland C J et al, Progress towards diesel combustion modelling, SAE paper 952429 (SP-1123), 1995.

Rutland C J et al, Toward Predictive Modeling of Diesel Engine Intake Flow,

Combustion and Emissions, SAE paper 941897, 1994.

Sawter RF et al, Factors of Controlling Polutant Emissions from Gas Turbine Engines, Atmospheric Pollution by Aircraft Engines, AGARD CP-125, Paper No 22, 1973.

Schiller R and Ruegheimer U, The new Audi V8 TDI, Audi AG Product and Technology Communication, Ingolstadt, May 1999.

Schofield K, Evaluation of Kinetic Rate Data for Reactions of neutrals of Atmospheric Interest, Planet Space Sci, 1967, Vol 15, pp 643-670.

Seery D J and Zablielski M F, Laser Probes for Combustion Chemistry, American Chem Society, Washington DC, 375-380, 1980.

Seko T et al, Performance of Lean Nox Catalyst Applied to a Heavy- Duty Methanol Engine Exhaust, SAE paper 952494, October 1995.

Shahed S M, Chiu W S and Yumlu V S, A Preliminary Model for the Formation of Nitric Oxide in Direct Injection Diesel Engines and its Application in Parametric Studies, SAE paper 730083, 1973.

Shahed SM and Waszkiewicz W, Diesel Cleans Up, Engine Technology International issue 1/100, March 2000.

Shiozaki T, Nakajima H, Kudo Y, Miyashita A and Aoyagi Y, The Analysis of Combustion Flame Under EGR Conditions in a DI Diesel Engine, SAE 960323, February 1996.

Shundoh S, Komori M, Tsujimura K and Kobayashi S, NOx Reduction from Diesel Combustion Using Pilot Injection with High Pessure Fuel Injection, SAE paper 920461, 1992.

Sienicki E J, et al, Diesel Fuel Aromatic and Cetane Number Effects on Combustion and Emissions from a Prototype 1991 Diesel Engine, SAE paper 902172, 1990.

Slone R J and May D F, Early Engine Emission Reduction Test Results with RAPRENOX, Proceedings of the Automotive Technology Development Contractors' Coordination Meeting, Dearborn, Michigan, USA, October 22-25, 1990, Report No. SAE-P-243.

Spreen K B, Ullman T L and Mason R L, Effects of Cetane Number, Aromatics, and Oxygenates on Emissions from a 1994 Heavy-Duty Diesel Engine with Exhaust Catalyst, SAE paper 950250, 1995.

Stawsky A, Lawson A, Vergeer H C and Sharp F A, Diesel exhaust emissions

control using EGR and particulate filters,Presented at the 86th Annual General Meeting of CIM, Ottawa, April 1984, Heavy Duty Diesel Emission Control: A Review of Technology pp 261-290.

Stephenson P W and Rutland C J, Modelling the effects of valve lift profile on intake flow and emissions behaviour in a DI diesel engine, SAE paper 952430 (SP-1123), 1995.

Studzinski W M et al, A Computational and Experimental Study of Combustion Chamber Deposit Effects on NOx Emissions, SAE paper 938215, 1993.

Takenaka Y, Aoyagi Y, Tsuji Y and Joko I, 3D numrical simulation of fuel injection and combustion phenomena in DI diesel engines, SAE paper 890668, 1989.

Tamanouchi M and Akasaka Y, Effect of Fuel Composition on Exhaust Gas Emissions from DI and DI Impingement Diffusion Combustion Diesel Engines, SAE paper 941016, 1994.

Taylor P H, Cheng L and Dellinger B, The Influence of Nitric Oxide on the Oxidation of Methanol and Ethanol, Combustion and Flame, 115:561-567 (1998).

Thiemann W, Brueggemann H, Wawra H and Bakaj L, The New Diesel Engine for the Smart, 8. Aachener Kolloquium Fahrzeug- und Motorentechnik 1999.

Third Report of The United Kingdom Review Group on Acid Rain, Acid Deposition in the United Kingdom 1986-1988, Warren Spring Laboratory, published 1990, ISBN: 0 85624 6506.

Timoney D J and Smith W J, Correlation of Injection Rate Shapes with DI Diesel Exhaust Emissions, SAE paper 950214, 1995.

Torpey P M, Whitehead M J and Wright M, Experiments in the control of diesel emissions, I Mech E, C124/71, 1971.

Tosaka S, Fujiwara Y and Murayama T, The Effect of Fuel Properties on Diesel Engine Exhaust Particulate Formation, SAE paper 890421, 1989.

Tree D, Bower G , Donahue R, Shamis D and Foster D, Emission Tests of Diesel Fuel with NOx Reduction Additives, SAE paper 932736 (SP-994), 1993.

Tsuchi H, Hamada H et al, Catalytic Performance of Alumina for NOx Control in Diesel Exhaust, SAE paper 940242, 1994.

Turns S R, An Introduction to Combustion: Concepts and Applications, McGraw-Hill Inc, 1996.

Uchida N, Daisho Y, Saito T and Sugano H, Combined Effects of EGR and Supercharging on Diesel, SAE paper 930601, 1993.

Ullman TL et al, Effects of Fuel Aromatics, Cetane Number, and Cetane Improver on Emissions from a 1991 Prototype Heavy-Duty Diesel Engine, SAE paper 902171, 1990.

Uyehara O, A Method to Estimate H_2 in Engine Exhaust and Factors that Affect Nox and Particulate in diesel Engine Exhaust,SAE paper 910732, 1991.

Uyehara O, Factors that Affect Nox and Particulates in Diesel Engine Exhaust - Part II,SAE paper 920695, 1992.

Uyehara OA, Reducing NOx in ICE, SAE paper 940896, 1994.

Vioculescu I A and Borman G L, An Experimental Study of Diesel Engine Cylinder-Averaged NOx Histories, SAE paper 780228, SAE Trans vol 87, 1978.

Wade W R, Hunter C E, Trinker F H and Cikanek H A, Reduction of NOx and particulate emissions in the combustion process, Trans ASME J Engng for Gas Turbines and Pwr 109, 426-434, 1987.

Wahab E, Description of the DEEPC Multizone Combustion-Emissions model capabilities and limitations, Ford Motor Company internal report, February 1998.

Walder C J, Reduction of Emissions from Diesel Engines, SAE paper 730214, 1973.

Williams A, Combustion of Liquid Fuel Sprays, Butterworths, 1990.

Wilson R P, Muir E B and Pellicciotti F A, Emissions Study of a Single-Cylinder Diesel Engine, SAE paper 740123, 1974.

Wolfer H H, Der Zuenderzug im Dieselmotor, CDI-Forschungsheft 392, 15-24, 1938.

Wray K L and Teare J D, J Chem Phys, **36,** 2582, 1962.

Xiaobin Li and Wallace J S, A phenomenological model for soot formation and oxidation in direct-injection diesel engines, SAE paper 952428 (SP-1123), 1995.

Yoshikawa H, Ikeda T, Haraguchi K, Kawamura T, Tanaka M and Yamaguchi T, Simultaneous Reduction of Nox and Soot Exhausted from Diesel Engine, SAE 940457, (SP-1020), 1994.

Yu R C and Shahed S M, Effects of Injection Timing and Exhaust Gas Recirculation on Emissions from DI Diesel Engine, SAE paper 811234, SAE Trans vol 90, 1981.

Zeldovich Y B, The Oxidation of Nitrogen in Combustion Explosions, Acta Physicochimica USSR, 21, 577-628, 1946.

Appendix 1

Merlin Model Block Diagram

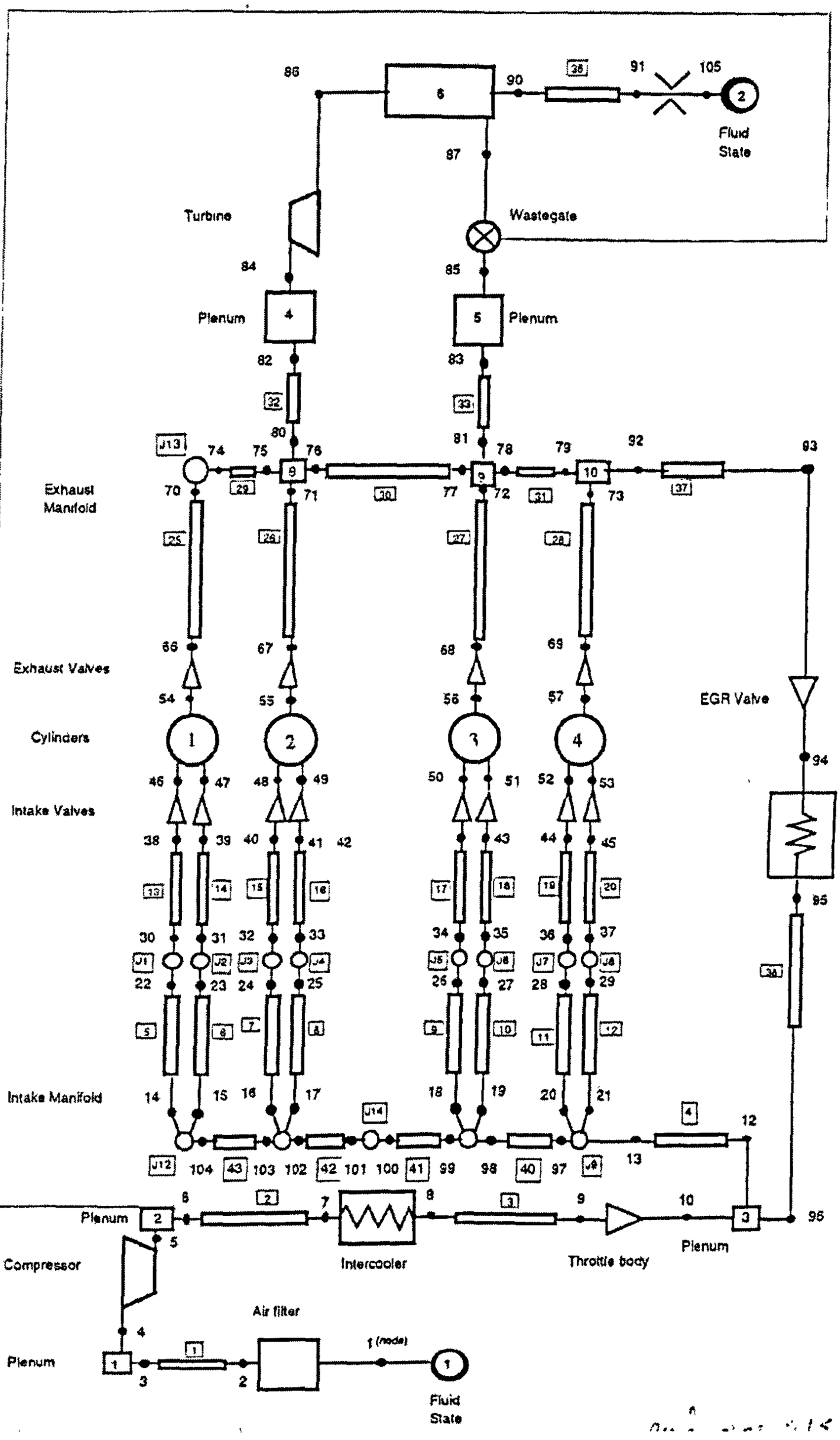

Appendix 2

Diesel Fuel Analysis

SAYBOLT UNITED KINGDOM LTD.

A Member of Saybolt-Van Duyn BV
Eastern Hemisphere Group
Independent Inspectors
Quality Assurance Services
Chemical Laboratories
Metrology/Calibration Engineers
Members ASTM/IP

SAYBOLT
A Core Laboratories Company

CERTIFICATE OF QUALITY

Client : Ford Motor Company Limited,
Central Accounts Payable,
Room 40/327 Trafford House,
Station Way,
Basildon, Essex. SS16 5XX

NAMAS
TESTING
No. 123

Date : April 30, 1998

ANALYSIS REPORT No. 0498-361 Ref No. 105063/98

Sample submitted as : Diesel Site development diesel
Received : 17.4.98
Marked : Sample as supplied by Ford Motor, Dunton
Tracking No. SA 1157
Place/Date Sampling : As supplied
Analysis Completed : 5.5.98
Page Number : 1 of 3

Test	Units	Method	Result
Appearance		SIHM 89/3	C & B
Ash	% Wt	IP 4	LT 0.001
Accelerated Stability	mg/100ml	IP 388	0.7
Colour		Visual	Red
Colour-ASTM		ASTM D1500	LT 4.5
Cloud Point	oC	IP 219	MINUS 14 6.8°F
Cold Filter Plugging Point	oC	IP 309	MINUS 20 -4°F
Copper Corrosion (3 hrs @ 100oC)		IP 154	1A
Conradson on 10% Bottoms	% Wt	IP 13	0.08
Cetane Index		ASTM D976	52.8
Cetane Number		ASTM D613	51.5
Density at 15 oC	g/ml	IP 160	0.8365
Flash Point-P M(Closed)	oC	IP 34	67
Neut No-Total Acid	mgKOH/g	IP 139	0.007
Odour		SIHM 89/2	Marketable
Pour Point	oC	IP 15	BELOW MINUS 30
Sulphur Content	% Wt	IP 336	0.03
Viscosity at 40 oC (104°F)	cst	IP 71	2.574
Water Content	mg/kg	ASTM D1744	0.007
Particulate Contamination	mg/kg	DIN 51 419	5
Calorific Value-Gross	MJ/kg	IP 12	45.67
-Nett	MJ/kg	IP 12 (calc)	42.83
Silicon Content	ppm	IP 377	LT 1
Carbon/Hydrogen Ratio		♦	1.87
Carbon			86.14
Hydrogen			13.40
Carbon Weight Fraction			0.861

♦ Carried out by an outside contractor (not NAMAS accredited)

Authorised Signatories - S. J. Sullivan, T. Richardson

Postal address : Oliver Close, Riverside Estate, West Thurrock, Grays, Essex RM20 3EE
Tel : 01708 862611 Telex : 8956078 Fax : 01708-867401

SAYBOLT UNITED KINGDOM LTD.

A Member of Saybolt-Van Duyn BV
Eastern Hemisphere Group
Independent Inspectors
Quality Assurance Services
Chemical Laboratories
Metrology/Calibration Engineers
Members ASTM/IP

SAYBOLT
A Core Laboratories Company

NAMAS
TESTING
No. 123

CERTIFICATE OF QUALITY

Client : Ford Motor Company Limited,
Central Accounts Payable,
Room 40/327 Trafford House,
Station Way,
Basildon, Essex. SS16 5XX

Date : April 30, 1998

ANALYSIS REPORT No. 0498-361 Ref No. 105063/98

Sample submitted as : Diesel
Received : 17.4.98
Marked : Sample ex. Ford Motor, Dunton
Tracking No. SA 1157
Place/Date Sampling : As supplied
Analysis Completed : 5.5.98
Page Number : 2 of 3

Test	Units	Method	Result
Viscosity @ Zero °C	32 cst	IP 71	7.060
(Minus 5°C)	23		8.343
(Minus 10°C)	14		10.05
(Minus 15°C)	5		12.65
(Minus 20°C)	-4		17.68
(Minus 25°C)	-13		24.61
(Minus 30°C)	-22		35.86
(Minus 35°C)	-31		Solid
Distillation		IP 123	
Initial Boiling Point	°C		170
5 %	°C		194
10 %	°C		206
20 %	°C		229
30 %	°C		248
40 %	°C		262
50 %	°C		272
60 %	°C		280
70 %	°C		290
80 %	°C		302
90 %	°C		318
95 %	°C		327
Final Boiling Point	°C		341
Recovered %			99
Residue %			1
Loss %			Nil

Authorised Signatories - S. J. Sullivan, T. Richardson

Postal address : Oliver Close, Riverside Estate, West Thurrock, Grays, Essex RM20 3EE
Tel : 01708 862611 Telex : 895807A Fax : 01708-867401

Appendix 3

Normalisation Process

During engine testing it is normal to find that there are invariably differences in results from day to day for the same engine due to variations in ambient conditions and test equipment resolution. There are standards for correcting power, torque and smoke emissions to standard atmospheric testing conditions, however not all standards correct turbocharged engines. There may also be variations in results between engine to engine and test facility to test facility. This may be due to a whole range of reasons ranging from tolerances of engine build, to different measuring systems. This is particularly true for exhaust emissions readings. In order to minimise this effect, a normalisation process was used for smoke and NOx emissions, to enable a meaningful comparison of results taken at Brunel with the original Ford results obtained at the Dunton Engineering Centre.

In order to offset the day-to-day variations in test conditions, at the start of testing with the VNT turbocharger a number of tests were conducted to establish an average baseline at Brunel. Because the engine had been equipped with the VNT turbocharger, the baseline testing was conducted at the two test conditions, by adjusting the vane positions until the air mass flow equated to the respective Dunton measurement of airflow. The average NOx and smoke measurement during this exercise became the Reference Baseline.

At the start of each day's testing, a baseline test was repeated, and the normalised result was calculated as follows.

Normalised Daily Result = [Reference Baseline / Day's baseline] x [test result]

This normalised day-to-day variations. This result was then normalised a second time for the facility-to-facility variations in order to make a comparison with the original Ford result as follows.

Normalised Ford Result = [Ford Result / Reference Baseline] x [Normalised Daily Result]

Appendix 4

A Brief History of Variable Nozzle Turbochargers

Variable geometry (VGT) or variable nozzle turbochargers (VNT) first went into production at Garret Turbochargers in 1989 for a commercial vehicle application.

The first passenger car application was at Fiat for the 1.9 litre DI diesel for the Croma car in 1991. The Garrett VNT 25 variable nozzle turbocharger was used to increase torque from 190 Nm at 2500 rpm to 200 Nm at the lower speed of 2000 rpm, and power was raised from 68 to 69 kW, compared to the earlier engine with a fixed geometry turbocharger.

The next passenger car application came in 1995 when VW applied the newly developed scaled down VNT15 machine from Garrett, to the 1.9 litre DI diesel engine. This development of the 1.9 engine increased torque from 182 Nm at 2300 rpm, to 235 Nm at the lower speed of 1900 rpm and maximum power was increased from 66 kW at 4000 rpm to 81 kW at the slightly higher speed of 4150 rpm. This development was really the starting point for high power diesel engines, giving comparable performance to gasoline engines. It also marked the start of the dramatic increase in diesel engine power that has been seen over the next 5 years, which has largely been due to VNT turbochargers and higher-pressure fuel injection systems. The ubiquitous Audi/VW 1.9 diesel now produces up to 110 kW and 320 Nm with electronic unit injectors and the VNT turbocharger.

Most manufacturers of diesel passenger cars now offer high power output engines using VNT turbochargers. The most notable are the new premium V8 engines from Audi, BMW and Mercedes, which produce power in the range of 165-175 kW. These engines are fitted with twin VNT Garrett turbochargers that have electric actuators to enable the electronic engine management system to control the turbine vane position.

The demand for VNT turbochargers has risen dramatically over the last 5 to 6 years. Garrett produced over 1.8 million VNT turbochargers in the year 2000. Other manufacturers like 3K Warner Turbosystems, Mitsubishi and IHI are all developing similar VNT units.